



Fakultät Maschinenwesen
Lehrstuhl für Flugsystemdynamik

Flight Control with Large Time Delays and Reduced Sensory Feedback

Tim Moritz Julius Fricke

Vollständiger Abdruck der von der Fakultät für Maschinenwesen der Technischen Universität München zur Erlangung des akademischen Grades eines

Doktor-Ingenieurs

genehmigten Dissertation.

Vorsitzender: Univ.-Prof. Dr.-Ing. Hans-Jakob Kaltenbach
Prüfer der Dissertation: 1. Univ.-Prof. Dr.-Ing. Florian Holzapfel
2. Univ.-Prof. Dr. phil. Klaus Bengler

Die Dissertation wurde am 02.11.2016 bei der Technischen Universität München eingereicht und durch die Fakultät für Maschinenwesen am 06.03.2017 angenommen.

“Flying is done largely with one’s imagination!”

— Wolfgang Langewiesche, *Stick and Rudder: An Explanation of the Art of Flying*, 1944

ACKNOWLEDGEMENTS

The present thesis was formed, developed and finalized during my time as research assistant at the Institute of Flight System Dynamics of the Technical University of Munich. First and foremost, I would like to thank the institute chair, professor Florian Holzapfel, for his support, his technical inputs, his confidence and the great freedom he gave me during these last years. Furthermore, I want to thank professor Klaus Bengler for kindly assuming the role of second examiner reviewing this thesis and professor Hans-Jakob Kaltenbach for chairing the thesis committee.

As a great part of this thesis is based on flight simulator experiments, I am in debt to all those who facilitated them or participated in them. Therefore, I would like to express my thanks to Dr. Rui Costa, Dr. Vítor Paixão and Nuno Loureiro, who enabled multiple interesting experimental sessions by travelling with their equipment to Munich and by welcoming me in Lisbon. For the first tests with BMI control in our simulator, I have to thank Dr. Thorsten Zander, Jonas Brönstrup and professor Klaus Gramann. Moreover, I want to thank all (former) colleagues who set up or even built the flight simulators and thereby allowed experiments to be conducted in the first place. Last but not least, I want to express my thanks to all experiment subjects, who devoted their time, their sweat and sometimes even their hairstyle, flying in the simulators. Without the commitment of the above people, my research would have been not as insightful – and fun!

Several other people supported my research on a theoretical-technical level. The numerous discussions with Fubiao Zhang have sparked some of the thoughts presented in this thesis and I would like to cordially thank him for that. Most notably, he once asked me to perform a simulator flight with a time delay of several seconds. To cope with the situation, I quickly resorted to a characteristic behavior that was new to me then, but which turned out to be one pillar of this thesis. Human behavior in general was among the most important aspects of my research. Therefore, Dr. Anna Jaworek's inputs from the point of view of a psychologist, especially those concerning experiment design and analysis, were extremely valuable. Furthermore, I want to thank my institute colleagues for the supportive atmosphere and their help with day-to-day scientific and technical problems.

With their humor, these very same institute colleagues, along with all my friends, also lightened up the more stressful times. Thank you! Finally, I want to express very special thanks to my parents and my partner Anna for their unconditional support, which was a key ingredient in the writing of this thesis and on my way there.

Munich, October 2016

Tim Fricke

ZUSAMMENFASSUNG / ABSTRACT

Flugsteuerung mit großen Totzeiten und eingeschränkter sensorischer Rückmeldung ist kennzeichnend für zwei Beispielfälle: Flugfernsteuerung über Funkverbindungen mit großer Latenz sowie Flugsteuerung mittels einer Gehirn-Maschine Schnittstelle (brain-machine interface, BMI). Diese Arbeit beschreibt und modelliert zunächst das bei großen Totzeiten typische, pulsartige Pilotenverhalten und stellt weiterhin ein darauf zugeschnittenes Flugsteuerungssystem vor. Zum Abschluss werden einige Flugsimulator Experimente beschrieben, in denen die Modelle und das Flugsteuerungssystem evaluiert und Methoden aus der Luftfahrt in der BMI Steuerung angewandt werden.

Flight control with large time delays and reduced sensory feedback is characteristic for two example applications: remote flight control via high-latency radio links and on-board flight control using brain-machine interfaces (BMI). This thesis first describes and models the characteristic, pulse-like pilot behavior associated with large time delays. It then presents a flight control system tailored to this behavior. It concludes with the description of several flight simulator experiments, in which the models and the flight control system were evaluated and aerospace methods were applied to BMI control.

TABLE OF CONTENTS

Zusammenfassung / Abstract	i
Table of Contents	iii
List of Figures	vii
List of Tables	xiii
Nomenclature	xv
1 INTRODUCTION.....	1
1.1 Problem.....	1
1.2 State of the Art	5
1.3 Goals and Contributions.....	12
1.3.1 Research Goals	12
1.3.2 Contributions of this Thesis	13
1.4 Outline	15
2 HANDLING QUALITIES PRELIMINARIES	17
2.1 Reference Configuration, Mission and Flight Phases.....	17
2.1.1 Aircraft, Measurements and Estimations	17
2.1.2 Mission and Flight Phases.....	20
2.2 Flight Mechanics and Flight Control	22
2.2.1 Equations of Motion	22
2.2.2 Flight Control Systems and Handling Qualities Implications.....	26
2.2.3 Handling Qualities Criteria and Requirements	30
2.2.4 Pilot-Induced Oscillations.....	33
3 ANALYSIS AND MODELING OF HUMAN FLIGHT CONTROL BEHAVIOR	37
3.1 Pilot Modeling Basics and Quasi-Linear Behavior.....	37
3.1.1 Physiological and Sensory Pilot Models.....	37
3.1.2 Linear Control-Theoretic Models.....	43
3.2 Time Delays and Existing Models of Nonlinear Behavior	48
3.2.1 The Effects of Large Time Delays	48
3.2.2 Highly Nonlinear Pilot Behavior	51

Table of Contents

3.2.3	Models of Pulse-Like Control Behavior	55
3.3	New Pilot Models Describing Control with Large Time Delays	57
3.3.1	Compensatory Tracking of a Stationary Target	57
3.3.2	Implications on Flight Control System Design	65
3.3.3	A Dual-Mode Pursuit Tracking Model.....	67
3.4	BMI Modeling.....	77
3.4.1	An Introduction to BMIs	77
3.4.2	A Simple BMI Model.....	80
4	FLIGHT CONTROL SYSTEM DESIGN	87
4.1	Design Goals, Basic Design Choices and Implications	88
4.2	Controller Design	94
4.2.1	Command Variables	94
4.2.2	Limitations, Protection Mechanisms and Supporting Functions	96
4.2.3	Controller Implementation	99
4.3	Human Control Input Interfaces	102
4.3.1	Inceptor Characteristics.....	102
4.3.2	Brain-Machine Interface Characteristics	104
4.4	Sensory Feedback	105
5	EXPERIMENTAL EVALUATION OF BMI CONTROLLED FLIGHT	109
5.1	Experimental Setup	110
5.1.1	Participants	110
5.1.2	Flight Simulator and Brain-Machine Interface	110
5.1.3	Displays	112
5.2	Tasks and Briefing	115
5.2.1	Task 0 – Training	115
5.2.2	Task 1 – Turns.....	116
5.2.3	Task 2 – Heading Bug Tracking	116
5.2.4	Task 3 – Approach	118
5.3	BMI Control System Tuning.....	119
5.3.1	Motor Imagery BMI	119
5.3.2	Operant BMI.....	120
5.4	BMI Flight Control Performance.....	123

5.4.1	Performance Metrics and Baseline Performance	123
5.4.2	Comparison of Different Configurations	125
5.5	Experimental BMI Model Validation	137
6	EXPERIMENTAL EVALUATION OF MANUAL REMOTE FLIGHT CONTROL.....	145
6.1	Hypotheses	145
6.2	Experimental Setup	148
6.2.1	Participants	148
6.2.2	Flight Simulator and Inceptor.....	150
6.2.3	Displays	151
6.2.4	Data Collection	154
6.3	Tasks and Briefing	155
6.3.1	Task A – Generic Tracking.....	156
6.3.2	Task B – Flight Path Tracking.....	158
6.3.3	Task C – Approach	160
6.3.4	Task D – Approach with Predictors.....	161
6.4	Experiment Evaluation	162
6.4.1	Initial Exposure and Learning.....	163
6.4.2	Tracking and the Influence of Control Sensitivity	172
6.4.3	Operational Context and Predictors.....	177
6.4.4	Conclusion on Hypotheses.....	188
6.4.5	Pilot Opinion.....	189
6.5	Experimental Pilot Model Validation	197
6.5.1	Pure Pursuit Tracking	197
6.5.2	Pursuit and Pre-Cognitive Tracking.....	208
7	CONCLUSIONS AND PERSPECTIVE.....	221
	References	229
	APPENDIX	241
A.	Flight Controller Layout.....	243
B.	Handbook for Experiments on Manual Remote Flight Control	249

LIST OF FIGURES

Figure 1.1 – Illustration of possible forms of remote piloting activities	2
Figure 1.2 – Relation of the two problems stated to traditional flight control	4
Figure 1.3 – The spectrum of automation [15] related to flight control	5
Figure 1.4 – Illustration of remote haptic teleoperation	7
Figure 1.5 – Illustration of remote flight control	8
Figure 2.1 – Sketch of the DA42, based on the maintenance manual [64]	18
Figure 2.2 – Illustration of the reference flight mission.....	22
Figure 2.3 – Signal flow chart of the longitudinal motion, adapted from [66]	24
Figure 2.4 – Signal flow chart of the lateral-directional motion, adapted from [66]	25
Figure 2.5 – Illustration of conventional airplane responses, as in [73].....	29
Figure 2.6 – Illustration of the Bandwidth Criterion’s bandwidth and phase rate	34
Figure 2.7 – Bandwidth Criterion diagrams of handling qualities levels, as in [67].....	34
Figure 2.8 – Bandwidth Criterion diagram of PIO susceptibility, as in [83].....	35
Figure 2.9 – APR Criterion diagram of handling qualities levels, as in [71]	35
Figure 3.1 – Bode plot comparison of different neuromuscular system models.....	38
Figure 3.2 – Illustration of the sensory channels most relevant to flight control	39
Figure 3.3 – A control-theoretic model for visual perception, derived from [86]	40
Figure 3.4 – Basic dual-loop pilot model, adapted from Gibson [71].....	43
Figure 3.5 – Illustration of different tracking strategies.....	44
Figure 3.6 – Illustration of some of the Neal-Smith Criterion parameters, as in [92]....	46
Figure 3.7 – Neal-Smith Criterion diagram of handling qualities levels, as in [92].....	46
Figure 3.8 – Hess’ revised structural model as in [94].....	47
Figure 3.9 – Crossover Model evaluation for different time delays	48
Figure 3.10 – Bode plot comparison of simple gain pilot and lead-lag pilot	49
Figure 3.11 – Time history plot of pulse-like control activity from [96]	51
Figure 3.12 – Time history plot of pulse-like control activity, redrawn from [88].....	52
Figure 3.13 – Bimodal distribution evidencing pulse-like control, redrawn from [88]...	52
Figure 3.14 – Comparison between piloting techniques, redrawn from [43]	53
Figure 3.15 – Time history plot of pulse-like control activity, redrawn from [98].....	53
Figure 3.16 – Maneuver comparison between continuous and pulse-like control.....	54
Figure 3.17 – Hess’ pulsive control model as in [97].....	56
Figure 3.18 – Generic form of the proposed compensatory pilot model	58

Figure 3.19 – Simplified generic form of the proposed compensatory pilot model	59
Figure 3.20 – Characteristics of the nonlinear decision mapping element.....	59
Figure 3.21 – Proposed compensatory control loop with pilot and aircraft.....	59
Figure 3.22 – Compensatory control loop: example trajectory in the phase plane.....	61
Figure 3.23 – Compensatory control loop: limit cycle in the phase plane	62
Figure 3.24 – Influence of pilot lead on phase plane switching lines	63
Figure 3.25 – Influence of aircraft lags on the phase portrait, derived from [100]	65
Figure 3.26 – State machine of the dual-mode pursuit tracking model	68
Figure 3.27 – Illustration of time delay values in the system’s step response	69
Figure 3.28 – Dual-mode pursuit tracking model, on-off control system.....	71
Figure 3.29 – Effects of the proposed pilot model’s neuromuscular system	71
Figure 3.30 – Inceptor mapping function	72
Figure 3.31 – Dual-mode pursuit tracking model, continuous control system	74
Figure 3.32 – The effect of control system type on neuromuscular noise rejection.....	76
Figure 3.33 – Afferent and efferent pathways and the BMI pathway.....	78
Figure 3.34 – Steps of BMI signal processing	78
Figure 3.35 – Block diagram of the proposed BMI model.....	82
Figure 3.36 – Relation between SNR and STR	83
Figure 4.1 – Pilot and controlled system. Pilot and aircraft are considered given.....	87
Figure 4.2 – Operating point for controller gains tuning.....	99
Figure 4.3 – Step responses of the nonlinear augmented airplane	101
Figure 4.4 – Inceptor force-deflection characteristic.....	103
Figure 4.5 – Sensory feedback design proposed for the example applications	107
Figure 5.1 – Cockpit of the DA42 simulator as set up for the experiments	111
Figure 5.2 – Signal processing for Motor Imagery and Operant BMI	112
Figure 5.3 – Photo of the DA42 simulator cockpit setup with custom display.....	113
Figure 5.4 – Custom DA42 display: basic version, BMI- and task-related elements... 114	
Figure 5.5 – Time history plot of the forcing function of Task 2	117
Figure 5.6 – Sketch of the approach flown in task 3.....	118
Figure 5.7 – Comparison of command filters: task 1, subject M1.....	120
Figure 5.8 – Tasks 0 and 1, flown by subject O1 during system tuning	121
Figure 5.9 – Task 0 flown with a suitable configuration of command filter B	122
Figure 5.10 – Frequency-domain comparison of filters and a pure time delay.....	123
Figure 5.11 – Time history plots of tasks 1 and 2, manual control	125

Figure 5.12 – Evolution of tracking errors during task 3, manual control.....	125
Figure 5.13 – Exemplary time history plots of subject M2.....	126
Figure 5.14 – Time history plots of subject M3 in task 1	127
Figure 5.15 – Time history plots of subject M7 in task 1	127
Figure 5.16 – Time history plots of subjects M3 and M7 in task 2.....	128
Figure 5.17 – Evolution of tracking errors during task 3, subject M3, configuration B	128
Figure 5.18 – Horizontal trajectories during task 3, subjects M3 and M7	129
Figure 5.19 – Time history plots of subject O1 in tasks 0 and 1	130
Figure 5.20 – Time history plot of subject O1 in task 2	130
Figure 5.21 – Horizontal trajectories during task 3, subject O1.....	131
Figure 5.22 – Task 1 TRI comparison of different configurations.....	131
Figure 5.23 – Task 1 overshoot comparison of different configurations	132
Figure 5.24 – Task 1 RMSE comparison of different configurations.....	133
Figure 5.25 – Task 1 maximum error comparison of different configurations	134
Figure 5.26 – Task 1 EVAR comparison of different configurations.....	134
Figure 5.27 – Task 2 RMSE comparison of different configurations.....	135
Figure 5.28 – Task 2 maximum error comparison of different configurations	135
Figure 5.29 – Task 2 EVAR comparison of different configurations.....	136
Figure 5.30 – Exemplary Operant BMI output amplitude distributions	138
Figure 5.31 – Variations in measured STR for subject O1	139
Figure 5.32 – Exemplary output amplitude distributions of subject M3.....	141
Figure 5.33 – Exemplary output amplitude distributions of subject M7.....	141
Figure 5.34 – Exemplary output amplitude distributions of subject M6.....	142
Figure 5.35 – Estimated PSDs of BMI outputs.....	143
Figure 6.1 – Expected workload and performance for different configurations	147
Figure 6.2 – Distribution of age and experience across all subjects.....	148
Figure 6.3 – Cockpit of the Research Flight Simulator as set up for the experiments .	151
Figure 6.4 – Tracking display (black and white colors inverted)	152
Figure 6.5 – HUD with tracking target (no background shown).....	152
Figure 6.6 – HUD with compass rose, target altitude, target heading and predictors .	153
Figure 6.7 – Photo illustrating the visual cues during task C.....	154
Figure 6.8 – Construction of the γ forcing function.....	159
Figure 6.9 – Sketch of the approach flown in tasks C and D.....	160
Figure 6.10 – Box plots of TLX ratings and control energy in task A	164

List of Figures

Figure 6.11 – Box plots of normalized completion time and completion time (task A)	165
Figure 6.12 – Time history plots of run Ac, subject 1	166
Figure 6.13 – TBI in run Ac, subject 1	167
Figure 6.14 – Time history plots of run Ao, subject 6	168
Figure 6.15 – TBI in run Ao, subject 6	168
Figure 6.16 – Time history plots of run Ao, subject 5	169
Figure 6.17 – TBI in run Ao, subject 5	170
Figure 6.18 – Box plots of time until strategy change in task A	170
Figure 6.19 – Self-assessments on piloting strategy	171
Figure 6.20 – Self-assessments on latency estimation	172
Figure 6.21 – Pilot ratings on control system support	172
Figure 6.22 – Box plots of TLX ratings in task B	173
Figure 6.23 – Box plots of control energy in task B	174
Figure 6.24 – Box plots of tracking RMSE in task B	175
Figure 6.25 – Box plots of tracking EVAR in task B	176
Figure 6.26 – Box plots of TLX ratings in tasks C and D	177
Figure 6.27 – Box plots of control energy in tasks C and D	178
Figure 6.28 – Box plots of performance in altitude tracking	180
Figure 6.29 – Box plots of performance in heading tracking	181
Figure 6.30 – Box plots of performance in localizer tracking	182
Figure 6.31 – Box plots of performance in centerline tracking, runway 05R	183
Figure 6.32 – Centerline tracking errors during the swing-over maneuver	184
Figure 6.33 – Box plots of performance in glide slope tracking, runway 05R	185
Figure 6.34 – Glide slope tracking errors during final approach (with swing-over)	186
Figure 6.35 – Mean pilot ratings for predictors	187
Figure 6.36 – Mean subjective amount of attention on the HUD	187
Figure 6.37 – Qualitative differences in actual workload and performance	189
Figure 6.38 – Pilot ratings of the altitude hold function	190
Figure 6.39 – Pilot ratings of the path straightener function	190
Figure 6.40 – Pilot ratings of the standard rate turn hold function	191
Figure 6.41 – Pilot ratings of the protections	191
Figure 6.42 – Pilot preference for either control system type	192
Figure 6.43 – Pilot model simulation: task A, on-off control, minimum noise	199
Figure 6.44 – Pilot model simulation: task A, continuous control, minimum noise	200

Figure 6.45 – Pilot model simulation: task A, continuous control, extreme noise ny .	201
Figure 6.46 – Pilot model simulation: task A, on-off control, extreme noise ne	202
Figure 6.47 – Metrics of pilot model simulations, task A, on-off control	203
Figure 6.48 – Averaged metrics of pilot model simulations, task A, on-off control	204
Figure 6.49 – Comparison of pilot model simulation and experimental run Ao.....	205
Figure 6.50 – Metrics of pilot model simulations, task A, continuous control.....	206
Figure 6.51 – Comparison of pilot model simulation and experimental run Ac.....	207
Figure 6.52 – Metrics of pilot model simulations, task B2, on-off control	209
Figure 6.53 – Comparison of pilot model simulation and experimental run B2o.....	210
Figure 6.54 – Comparison of pilot model simulation and experimental run B2c.....	212
Figure 6.55 – Comparison of pilot model simulation and experimental run B3o.....	213
Figure 6.56 – Comparison of pilot model simulation and experimental run B3c.....	214
Figure 6.57 – Comparison of pilot model simulation and experimental run B4o.....	215
Figure 6.58 – Comparison of pilot model simulation and experimental run B4c.....	216
Figure 6.59 – Comparison of pilot model simulation and experimental run B1o.....	217
Figure 6.60 – Comparison of alternative model simulation and experimental run B1o	218
Figure 6.61 – Comparison of pilot model simulation and experimental run B1c.....	219
Figure A.1 – Altitude hold mode structure	243
Figure A.2 – Longitudinal outer control loop structure.....	244
Figure A.3 – Longitudinal inner control loop structure	244
Figure A.4 – Autothrottle structure	245
Figure A.5 – Turn rate hold mode structure	246
Figure A.6 – Lateral outer control loop structure.....	246
Figure A.7 – Lateral inner control loops structure	246
Figure A.8 – Directional inner control loops structure.....	247
Figure A.9 – Lateral-directional control allocation structure	247

LIST OF TABLES

Table 1.1 – Latency estimates for RPAS communication links, from [7]	3
Table 2.1 – Parameters assumed available from onboard sensor fusion	18
Table 3.1 – Values for parameters of the neuromuscular system transfer function	38
Table 3.2 – Independent parameters of the dual-loop pursuit tracking model	76
Table 4.1 – Example implementations of different control system types in spacecraft ..	90
Table 4.2 – Relevant paragraphs from EASA CS-23	92
Table 4.3 – DA42 characteristic speeds from [72] and chosen transition speeds	96
Table 4.4 – Possible limit cycle characteristics in γ	101
Table 5.1 – List of participants of the experiments with Motor Imagery BMI control ..	110
Table 5.2 – Sequence of heading target steps for task 0	115
Table 5.3 – Sequence of heading target steps for task 1	116
Table 5.4 – Task 2 forcing function components	117
Table 5.5 – Some quantitative statistical results for BMI model validation	139
Table 5.6 – Comparison of measured STR, model STR and model SNR	140
Table 6.1 – List of subjects and sequence of experimental runs	149
Table 6.2 – List of task A tracking target steps	157
Table 6.3 – Control sensitivity levels in task B	159
Table 6.4 – List of positions and announcements during tasks C and D	161
Table 6.5 – Factors and factor levels for statistical analysis	162
Table 6.6 – Quantitative statistical results for TLX ratings and control energy, task A	164
Table 6.7 – Quantitative statistical results for (normalized) completion time in task A	166
Table 6.8 – Quantitative statistical results for time until strategy change in task A	171
Table 6.9 – Quantitative statistical results for TLX ratings in task B	173
Table 6.10 – Quantitative statistical results for control energy in task B	174
Table 6.11 – Quantitative statistical results for RMSE in task B	175
Table 6.12 – Quantitative statistical results for EVAR in task B	176
Table 6.13 – Quantitative statistical results for TLX ratings in tasks C and D	178
Table 6.14 – Definition of evaluation segments for tasks C and D	179
Table 6.15 – Quantitative statistical results for altitude tracking	181
Table 6.16 – Quantitative statistical results for heading tracking	182
Table 6.17 – Quantitative statistical results for localizer tracking	183
Table 6.18 – Quantitative statistical results for centerline tracking	183

List of Tables

Table 6.19 – Quantitative statistical results for glide slope tracking..... 185

Table 6.20 – Quantitative statistical results for amount of attention on the HUD 188

Table 6.21 – Summary of hypotheses outcome 188

Table 6.22 – Rewritten pilot comments related to predictors and workload..... 193

Table 6.23 – Rewritten pilot comments related to latency, precision and flight phase 194

Table 6.24 – Rewritten pilot comments related to other aspects 195

Table 6.25 – Rewritten pilot remarks and suggestions..... 196

NOMENCLATURE

Latin Symbols

Symbol	Description	Unit
A	Amplitude	
C	Command variable	
c	Control intention of the pilot	–
c_{CL}	Closed-loop control intention of the pilot	–
D	Drag	N
d	Differential displacement	
	Disturbance	
E_{ctl}	Control Energy	
e	Error	
e_{tol}	Tolerated error, desired accuracy	
F	F-distribution	–
f	Blending function	–
g	Gravitational acceleration	m/s^2
H	Discrete transfer function	–
h	Altitude	m
h_B	Barometric altitude	m
h_R	Height above terrain	m
i	Index	–
j	Imaginary unit	–
K	Gain	
K_{agg}	Pilot control input aggressiveness	–
k	Constant coefficient, parameter or index	
L	Lift	N
	Dimensional derivative: roll moment	
M	Rotation matrix	–
	Dimensional derivative: pitch moment	
m	Mass	kg
N	Dimensional derivative: yaw moment	
	Number of samples	–

Latin Symbols (continued)

Symbol	Description	Unit
n	Load factor	–
	System order	–
	Noise	
	Number of elements	–
p	Roll rate	rad/s
	p-value	–
q	Pitch rate	rad/s
r	Yaw rate	rad/s
S	Power spectral density	–
s	Laplace variable	–
T	Time constant	s
	Period	s
	Thrust	N
t	Time	s
	Student's t-distribution	–
t_{bt}	Time between target step changes	s
t_{ch}	Time of target step change	s
t_m	Duration of the move phase or of a control input	s
t_s	Sampling time	s
t_w	Duration of the wait phase	s
u	System input	
V	Velocity	m/s
V_{climb}	Normal climb speed	kt
V_{IAS}	Indicated airspeed	kt
V_R	Takeoff rotation speed	kt
V_{REF}	Reference approach speed	kt
V_{S1}	Stall speed in landing configuration	kt
V_T	Transition speed	kt
X	Dimensional derivative: longitudinal force	
x	Coordinate system axis	–
Y	Transfer function	
	Dimensional derivative: lateral force	

Latin Symbols (continued)

Symbol	Description	Unit
Y_{act}	Transfer function: actuator	
Y_{cf}	Transfer function: command filter	
Y_d	Transfer function: display	
Y_{dm}	Decision mapping element	
Y_{fs}	Transfer function: feel system	
Y_i	Inceptor dynamics	
Y_{pf}	Transfer function: proprioceptive feedback	
y	Coordinate system axis	—
	System output	
Z	Dimensional derivative: vertical force	
z	Coordinate system axis	—
	Z-transform variable	—

Greek Symbols

Symbol	Description	Unit
α	Angle of attack	<i>rad</i>
β	Angle of sideslip	<i>rad</i>
γ	Flight path climb angle	<i>rad</i>
Δ	Random BMI output variable	—
δ	Control input (e.g., inceptor displacement/force or BMI output)	—
$\hat{\epsilon}_{GG}$	Estimation of sphericity according to Greenhouse and Geisser	—
$\hat{\epsilon}_{HF}$	Estimation of sphericity according to Huynh and Feldt	—
ζ	Rudder deflection	<i>rad</i>
	Damping ratio	—
η	Elevator deflection	<i>rad</i>
θ	Pitch angle	<i>rad</i>
μ	Mean value	
μ_K	Kinematic bank angle	<i>rad</i>
ξ	Aileron deflection	<i>rad</i>
σ	Standard deviation	

Greek Symbols (continued)

Symbol	Description	Unit
τ	Time delay	<i>s</i>
τ_{sp}	Signal processing time delay	<i>s</i>
τ_v	Time delay of the visual system	<i>s</i>
Φ	Bank angle	<i>rad</i>
φ	Phase angle	$^\circ$ (or <i>rad</i>)
φ_{pc}	Pilot compensation parameter	$^\circ$
χ	Flight path course angle	<i>rad</i>
Ψ	Heading	<i>rad</i>
ω	Frequency	<i>rad/s</i> (or <i>Hz</i>)
ω_c	Crossover frequency	<i>rad/s</i>
$\tilde{\omega}$	Normalized frequency	<i>rad</i>

Subscripts

Subscript	Description
0	Initial, reference or trim value
<i>a</i>	Aircraft
<i>att</i>	Attitude-related
<i>B</i>	Body-fixed coordinate system
<i>BW</i>	Bandwidth (Criterion)
<i>cmd</i>	Command
<i>dem</i>	Demand
<i>filt</i>	Filter
<i>K</i>	Kinematic (coordinate system)
<i>L</i>	Lower
<i>lat</i>	Lateral (motion)
<i>LC</i>	Limit Cycle
<i>lim</i>	Limit
<i>lon</i>	Longitudinal (motion)
<i>max</i>	Maximum
<i>min</i>	Minimum

Subscripts (continued)

Subscript	Description
<i>N</i>	Negative user intention
<i>nm</i>	Neuromuscular system
<i>opt</i>	Optimum
<i>P</i>	Positive user intention
<i>p</i>	Pilot
<i>ss</i>	Steady-state
<i>t</i>	Total
<i>tgt</i>	Target
<i>U</i>	Upper
<i>Z</i>	Zero (neutral) user intention

Acronyms

Acronym	Description
ANOVA	Analysis Of Variance
APR	Average Phase Rate
BMI	Brain-Machine Interface
CHR	Cooper-Harper Rating
CNS	Central Nervous System
EASA	European Aviation Safety Agency
EEG	Electroencephalography
EVAR	Error Variability
EVS	External Visual System
FAA	Federal Aviation Administration
FSD	Full-Scale Deflection
FTD	Flight Training Device
HSS	Half-Screen Size
HSI	Horizontal Situation Indicator
HUD	Head-Up Display
IAS	Indicated Airspeed
LPD	Landing Point Designator
LOES	Low-Order Equivalent System

Acronyms (continued)

Acronym	Description
NASA	National Aeronautics and Space Administration
PIO	Pilot-Induced Oscillation
PSD	Power Spectral Density
RMSE	Root Mean Square Error
RPA	Remotely Piloted Aircraft
RPAS	Remotely Piloted Aircraft System
SIDM	Système Intérimaire de Drones de Moyenne altitude longue endurance
SMA	Simple Moving Average
SNR	Signal-to-Noise Ratio
STR	Single-Trial Reliability
TBI	Time Between Inputs
TLX	Task Load Index
TRI	Turn Rate Index
TUM	Technical University of Munich
UAV	Unmanned Aerial Vehicle

1 INTRODUCTION

1.1 Problem

Humans may have mastered the art of flight about a century ago, but we are still designed by nature to stay on the ground. Only by using a complex technical apparatus can we safely lift our bodies off the soil and roam the atmosphere and space above. Apart from their ability to fly itself, aircraft also need to accommodate the pilots' skills and limits. Considering the intricate nature of human flight, it is not surprising that advances in control and automation technology have been used to teach machines how to fly. Tasks that require an aircraft, but not a human pilot, can be accomplished by Unmanned Aerial Vehicles (UAVs). A UAV does not need any cockpit or life support systems and can therefore be constructed at a lighter weight and lower costs as compared to a manned aircraft [1]. Moreover, UAVs can operate for long periods of time without interruption and they can enter airspaces that are dangerous to humans. The loss of a UAV does not necessarily entail the loss of a human life, which makes UAVs more expendable than manned aircraft.

Even though UAVs are unmanned, they are most often controlled by a remote human pilot. Fully autonomous systems are rare, and for many missions there will always be an interest to keep a human operator in the loop. In particular, missions where the unique human skill of obtaining situational awareness in an unknown or unpredicted environment and taking appropriate decisions is needed, cannot be accomplished by autonomous flying machines. One example for such a situation is flight testing, which is usually accomplished by a human pilot, even for UAVs that are designed for autonomous operation [2]. To emphasize the human-in-the-loop nature of a certain UAV, it is common to use the term Remotely Piloted Aircraft (RPA). A Remotely Piloted Aircraft System (RPAS) encompasses not only the aircraft itself, but also the ground control station, signal transmission links and other system elements associated with the operation of the remote aircraft. RPA pilots are often called, or even call themselves, operators, especially when the level of RPA autonomy is high, to distinguish them from pilots who fly manned aircraft. As one desired outcome of this thesis is to enable RPA control with low vehicle autonomy, the terms pilot and operator are used interchangeably, at least when referring to aircraft. As Figure 1.1 indicates, an RPA can either be controlled by an external pilot who has direct visual contact with the vehicle, or by an internal pilot who operates the aircraft from within a ground control station.

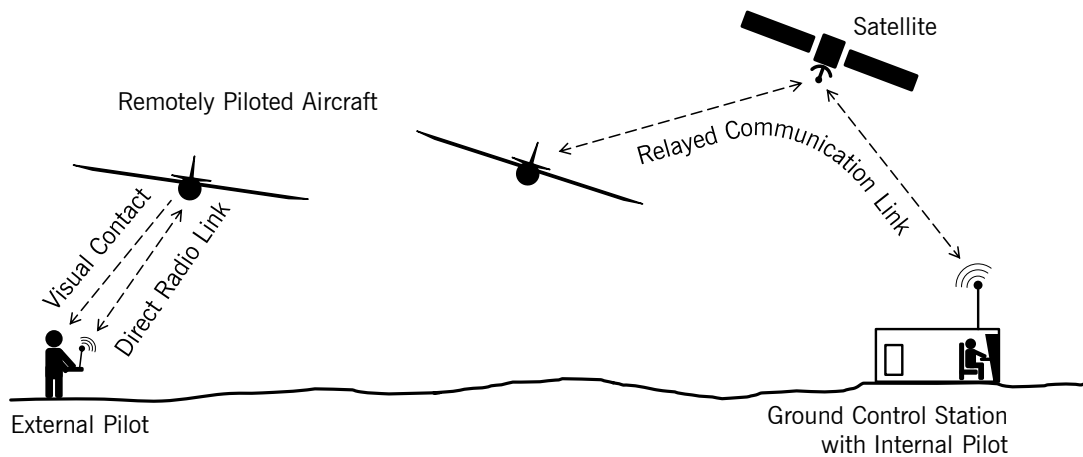


Figure 1.1 – Illustration of possible forms of remote piloting activities

One problem inherent to remote operation is that the pilot receives only reduced sensory feedback from the vehicle. In the case of RPA, visual feedback is often limited to outside observation of the vehicle, as long as it flies within the visual line-of-sight of an external pilot, or, in the case of long-distance remote operation, to the field of view of a camera mounted on the aircraft [3]. A major issue faced by external pilots which has caused several accidents is the reversal of lateral-directional controls when the aircraft is approaching the operator, as compared to the aircraft flying away from the operator [4]. Internal pilots, on the other hand, cannot simply turn their head to visually scan the surroundings of the RPA and they cannot rely on their ability to detect attitude variations through peripheral vision [5]. Visual cues may be limited, but vestibular feedback is even completely missing in RPA control, thus leading to an increased possibility of flight envelope excursions [5]. The olfactory, thermal and auditory channels, which contribute more to the pilot's general situational awareness than to his flight control capabilities, are disconnected as well. Although proprioceptive feedback is felt when handling the inceptor of the ground control station, some characteristics of this feedback may be affected by time delay introduced by the communication link. It therefore exhibits minor differences to the proprioceptive feedback from onboard fly-by-wire control systems and major differences to that of mechanical control systems, as can be seen in Figure 1.5 and section 2.2.2. Another major issue with remote aircraft control is that RPA operators tend to take more or higher risks than pilots of manned airplanes when maneuvering the vehicle and when making operational decisions, because they do not share the fate of the aircraft [6]. The operators' impoverished sensory environment is a contributing factor to this excessive risk-taking behavior.

Remote operation furthermore necessitates a communication link that enables uplink transmission of control signals and downlink transmission of feedback signals. While RPA control from within the visual line-of-sight can be accomplished with a direct radio link, remote control over larger distances requires more elaborate communication links that may comprise one or more satellites or ground-based relay stations [7]. These signal transmission paths often exhibit a significant amount of latency, caused not only by the large distances, but also by datalink electronics, encryption, compression, error correction, synchronization and computations [7]. The resulting round trip time delays can range from

under a second to values as high as six or eight seconds [8–10]. Most over-the-horizon RPA operations are handled with a geostationary satellite link, for which, according to Table 1.1, a total round trip time delay of at least 674.0 *ms* is estimated [7]. A subject of the experiments presented in chapter 6 of this thesis, who has experience in operating RPA, explained that he usually experienced 3.2 *s* round trip latency when controlling the Harfang UAV (also known as système intérimaire de drones de moyenne altitude longue endurance or SIDM) [11] via satellite link. Values approaching six seconds have been reported for the low earth orbit, when multiple up-down links are employed [9]. When pilot-vehicle communication channels or some of their characteristics change during operation, time delays may vary. This is typically the case during control of fast travelling spacecraft or when communication is established via the internet. If this variation is large enough, it constitutes an additional nuisance for the human operator.

Table 1.1 – Latency estimates for RPAS communication links, from [7]

Source of Latency	Line-of-Sight Communication		Geostationary Satellite Relay	
	Minimum [<i>ms</i>]	Maximum [<i>ms</i>]	Minimum [<i>ms</i>]	Maximum [<i>ms</i>]
Transceiver	40.0	300.0	80.0	300.0
Transport	0.2	3.3	239.0	281.0
Encryption	0.0	4.0	0.0	4.0
Compression	0.0	375.0	0.0	375.0
Error correction	0.0	1.5	0.0	1.5
Synchronization	8.0	32.0	8.0	32.0
Computations	10.0	30.0	10.0	30.0
Uplink	58.2	370.8	337.0	648.5
Downlink	58.2	745.8	337.0	1023.5
Round trip total	116.4	1116.6	674.0	1672.0

It is known that time delays degrade the performance of closed-loop control systems, reduce stability margins and can lead to instability. In combination with the impoverished sensory environment, they constitute a major cause for RPA incidents and accidents, which occur at much higher rates than in the domain of manned aircraft [4]. In a way, the delayed presentation of airplane reactions itself can be considered a form of sensory feedback reduction. Hence, time delays are usually avoided or at least reduced to an acceptable level. In RPA control, for example, it is quite common to have a local pilot within visual line-of-sight perform takeoff and landing with very little time delay and to operate the vehicle from afar with large time delays only during non-terminal flight phases that require less tracking precision (cf. section 2.1.2), or during ground movements, where terrain or buildings obstruct the direct line-of-sight. As a result, it is necessary to hand over control between operators. These handover procedures are associated with some risks, as vividly described in [12].

However, avoidance or reduction of signal transmission time delays may not always be possible. In some cases, like long-range flights into remote, dangerous or hostile areas, it may be difficult to deploy a local pilot and/or a local ground control station. Furthermore, system failures may prevent a successful handover from remote pilot to local pilot. If, in

this case, the flight control system is not laid out for operation through large time delays and with missing sensory feedback channels, a safe continuation of the flight is at risk. The ability of an RPAS to be safely and efficiently controlled in spite of large time delays and reduced sensory feedback would therefore constitute a major advantage over other systems. Established means to accomplish this goal as well as their shortcomings are outlined in the following section 1.2.

Aviation evolves, however, not entirely towards unmanned systems. For some missions, a human pilot aboard the aircraft is irreplaceable. In many respects, human performance still is unmatched by computers. Moreover, flying is too much fun to leave it to the machines and be a mere spectator or passenger. Interestingly though, the future of manned aviation as envisioned by the European research project BRAINFLIGHT [13] holds similar challenges as those of RPA control pointed out above. The project’s long term vision was to enable control of aircraft via brain activity only, i.e., without the need for physical interaction with control inceptors. This would enable physically disabled people to fly and thereby enlarge access to aviation [14]. Not needing their hands to control the aircraft also means that pilots could manually operate other systems in flight. The whole concept could also be applied to other dynamic systems, facilitating different activities of work or daily life for all kinds of people. Needless to say, the prospect of using a so-called Brain-Machine Interface (BMI) to control aircraft or other machines and devices is certainly enticing for many in today’s technophile era.

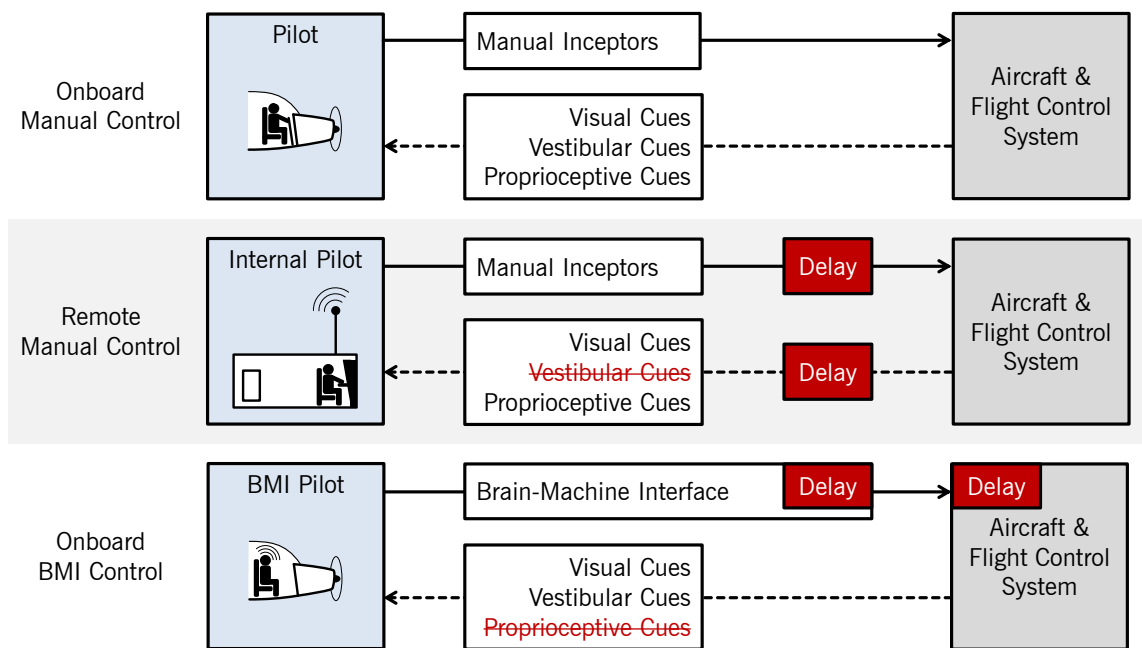


Figure 1.2 – Relation of the two problems stated to traditional flight control

An obvious problem with BMI control is that the user does not perceive any haptic, tactile or proprioceptive feedback from control inceptors. Why proprioceptive inceptor feedback is of great importance in (flight) control is discussed in section 3.1.1 of this thesis. Furthermore, the algorithms that identify the user’s intent from his brain activity only do this with a certain degree of reliability. This translates to a very noisy control signal.

Filtering of the control signal introduces lags that add to the time delay caused by processing of the raw brain activity signals. Successful BMI control therefore requires a control system designed to make large time delays and missing proprioceptive feedback tolerable.

The two examples of long-distance RPA control and BMI control discussed above show that flight control with large time delays and missing sensory feedback channels is an emerging, if not already immediate, problem. Figure 1.2 illustrates the two examples and relates them to conventional, onboard manual flight control. Note that the time delay of the BMI control system is split up into a signal processing delay within the BMI and a BMI output filtering delay, which is considered a part of the flight control system.

1.2 State of the Art

Tools and machines have been conceived and used by humans for millennia, but with the advent of digital computers and the following increase in computing power, the possible level of involvement of machines in control tasks has skyrocketed. Today, machines can have far more states than merely on and off and each and every state can be designed for a different distribution of tasks between human and machine. This fact led to the definition of several discrete levels of automation, into which systems or system states can be categorized. At a high level of automation, most tasks are accomplished by the machine, whereas at a low level of automation, the human operator is responsible for the majority of tasks. More generally, one could speak of a continuous, one-dimensional spectrum of automation degrees [15]. For the following analyses, Figure 1.3 has been derived from [15], locating different approaches to flight control within this spectrum.

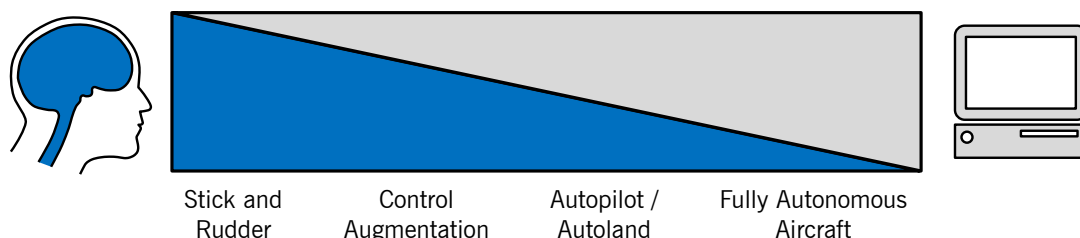


Figure 1.3 – The spectrum of automation [15] related to flight control

The so-called stick and rudder flying is done without any assistance of the machine: pilots actuate the control surfaces with their hands and feet through inceptors and mechanical linkages. If a flight control computer is installed, the machine can provide various degrees of assistance. Control augmentation, for example, can be considered a rather low degree of automation, because it merely improves some manual handling characteristics. Autopilots, on the other hand, relieve human pilots from performing manual flight control. The degree of automation is therefore higher, with humans playing only a supervisory role. On the far right end of the spectrum, we find fully autonomous aircraft that accomplish a predefined mission without constant supervision.

A common strategy to deal with time delays in human-closed control loops is to increase vehicle automation or autonomy, i.e., to move right in the spectrum of Figure 1.3. Instead

of resorting to a local pilot during terminal flight phases, it is possible to rely on an automatic takeoff and landing system. Nonterminal flight phases, too, are regularly flown at higher degrees of automation. RPA operators then merely state high-level goals – waypoints to follow or an area to observe – that are accomplished autonomously by the aircraft. The presence of time delays and the absence of some sensory feedback is less critical when higher-level goals are communicated instead of low-level control inputs, as section 2.2.1 explains.

The strategy of increasing vehicle automation to mitigate issues associated with time delays and reduced sensory feedback, however, has its limitations. One problem with highly automated aircraft that has already been apparent for some years now is that pilots increasingly rely on automation and thereby become complacent and less and less proficient in low-level (manual) flight control [16, 17]. This may be acceptable as long as the automation systems function nominally. However, as soon as component failures occur in the automation systems that cause the control system to revert to a lower level of automation, the human pilots' ability to fly the aircraft at this lower level of automation is needed. Similarly, spontaneous changes in the flight mission, such as evasive maneuvers, may require pilots to deliberately bypass any automated systems to react in an adequate timespan while maintaining situational awareness. Not only do pilots need to be able to perform low-level flight control, but the airplane's control system must enable them to do so in the first place. It is exactly in the abovementioned, sudden non-normal situations that the flight control system must exhibit adequate handling qualities to support the pilot, who experiences great stress. A control system that is designed to operate at a high degree of automation to mitigate excessive time delays and missing feedback channels, however, may not even provide controllable handling qualities for a safe continuation of the flight or a safe landing once its functionality is degraded to lower degrees of automation.

There are more disadvantages of high vehicle autonomy. Highly automated RPA control can prevent pilots from rapidly intervening when necessary [3] and it can produce degraded situational awareness as, for instance, pilots would not notice changes in handling qualities due to icing. Furthermore, the use of automation to compensate for human shortcomings does not completely solve the problem, as the automation itself can fail or introduce other problems for the crew, such as complicated and extremely time consuming flight planning processes [4]. Several accidents in which automation performed as designed, but failed to carry out the desired task because of imperfect implementation or an undetected malfunction, were due to the fact that developers were unable to predict all possible contingencies [12]. Indeed, handling rare or unplanned events and appropriately incorporating risk-based decision-making using uncertain and incomplete information still constitute challenges for UAV automation [18].

Automation also affects the freedom of movement of a vehicle. Non-automated systems already exhibit certain physical limits, but as soon as some automation is introduced, the operator's freedom is additionally limited to a certain space designed by control engineers. In systems with high degrees of automation, excessive restrictions may occur. This may be the case in some RPAS and it is a major issue in BMI control. Consider the following method to cope with high uncertainties in BMI, proposed in [19] for BMI control of a

wheelchair. Instead of commanding the movement itself of the wheelchair via a BMI, only the desired destination is communicated and the wheelchair moves on its own towards that destination. Obviously, destinations that have not been preprogrammed cannot be reached.

All these examples show that the common approach of resorting to higher degrees of automation is, although successful in many respects, unsatisfactory. The experienced test pilot and engineer Rogers Smith claims that the best pilot-vehicle performance in manned aviation is attained through the balanced and synergetic use of skilled manual flight control together with automation systems [20]. Likewise, mixed or hybrid control approaches to UAV control are deemed favorable by other researchers [8]. It is certainly prudent to employ automation in situations where pilot errors easily result in accidents or significantly reduce operational performance. This already is common practice in manned aviation and it should be for unmanned aviation as well. Tasks that require high bandwidth and high precision, too, may need to be performed by automatic systems or a local pilot. Takeoff and landing are examples of such tasks. However, giving human pilots the ability to perform (flight) control at lower degrees of automation, even with large time delays and reduced sensory feedback, improves safety and effectiveness at least in some situations like automation failure and in unforeseen or rapidly changing environments. This is why this ability should be developed and advanced.

Most of the research on large time delays in human-closed control loops with low automation degrees is done in the domain of haptic teleoperation. In haptic teleoperation, humans close the control loop in remote object manipulation tasks, sending haptic command signals and receiving haptic feedback signals [21]. Usually, a remote slave manipulator mimics the behavior of the master manipulator, which in turn takes into account the input torques from the slave [22]. This is illustrated by Figure 1.4.

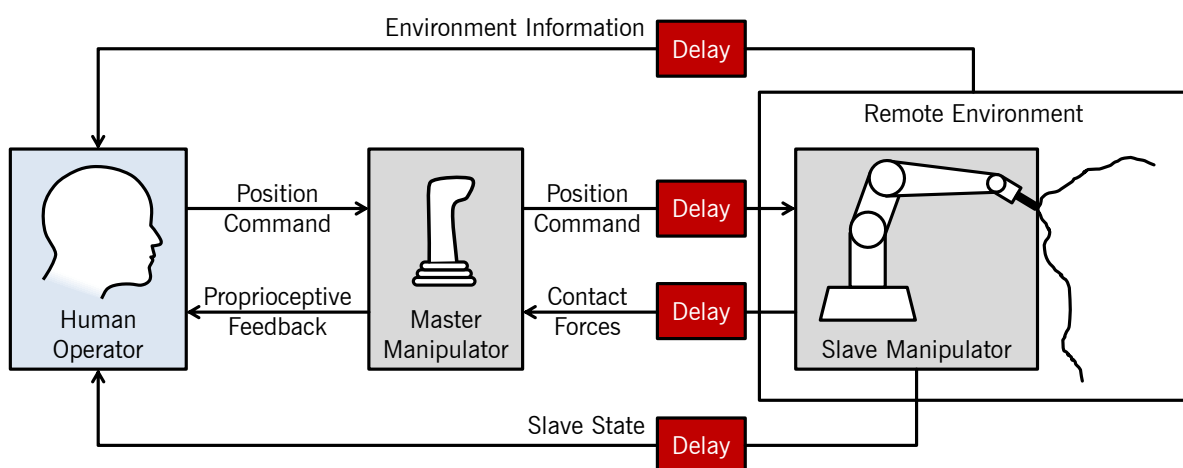


Figure 1.4 – Illustration of remote haptic teleoperation

Here, the proprioceptive feedback loop, which is the fastest control loop involving the human operator (cf. section 3.1.2), comprises both master and slave manipulator. Time delays in the fast position/force control loop between master and slave manipulator easily destabilize the system. Part of haptic teleoperation research therefore aims at providing

stable master-slave control loops with high-bandwidth force feedback to accurately return the environment's haptic characteristics, i.e., the shape and hardness of objects, to the user. The fact that haptic teleoperation is categorized into bilateral, shared and semiautonomous schemes [21] illustrates that in this domain, too, an increase in automation is considered a possible remedy for time delays. Of those three categories, bilateral teleoperation resembles the considered types of non-autonomous flight control most. It is important, however, to note the differences between haptic teleoperation and (remote) flight control with time delays. The aim of haptic teleoperation is to enable haptic interaction between the operator and the remote environment. Flight control with time delays, on the other hand, is not about interaction with the environment and does not involve a master-slave pair of control inceptors. As indicated by Figure 1.5, it is a kind of free-motion teleoperation. A known plant – the aircraft – is controlled such that the deviation from certain target parameters, like attitude or flight path, is minimized. In this case, control loops are either closed onboard the aircraft, or by the human pilot. The problem of finding a stable master-slave control loop is thus avoided and corresponding methods are inapplicable. Instead, previous research on human-closed control loops and free-motion teleoperation with large time delays is highly relevant.

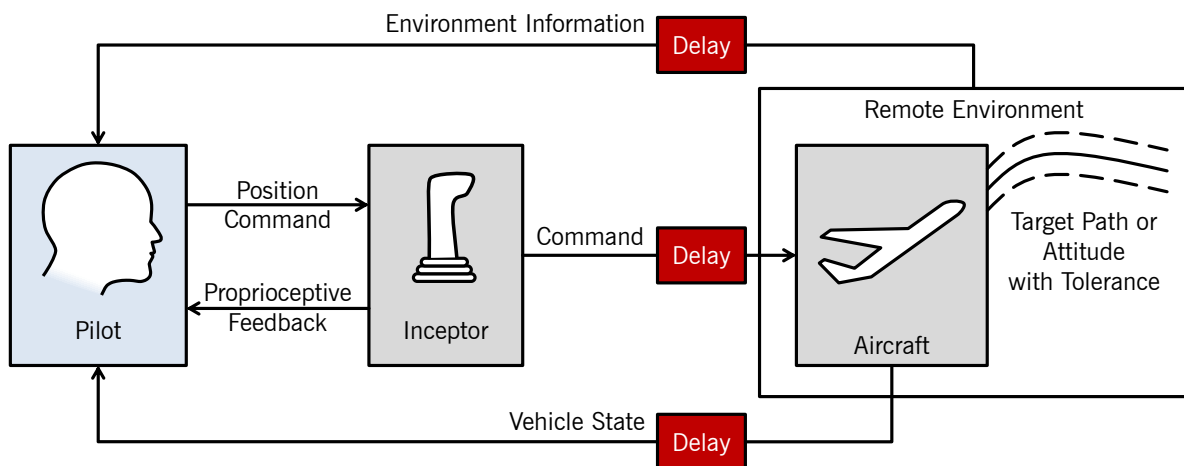


Figure 1.5 – Illustration of remote flight control

An overview of about five decades of research in bilateral teleoperation is given in [22]. Initial experiments by Sheridan and Ferrell [23] and by Ferrell [24] identified and described a distinct operator behavior that is adopted in control tasks with time delays. This behavior, which they called move-and-wait strategy, is extensively described in section 3.2.2 of this thesis. Subsequent research in haptic teleoperation focused on introducing supervisory control with increasing autonomy of the remote system, but also led to the development of predictor displays [25, 26]. Such displays present a prediction of the remote system's response before the delayed feedback of the actual system response and thereby reduce the apparent time delay. Predictor displays have been described for both visual and force feedback [9, 27], but their usage in teleoperation is often limited to free motion, due to the complexity of dynamic force and torque modeling during contact [28]. In parallel to the research on predictor displays, a function called "software jig" was

proposed [29] that implements movement constraints imposed by the task and thereby reduces the degrees of freedom the user needs to control.

Those applications of bilateral teleoperation presented in [22] which are most relevant to the topic of this thesis are underwater vehicle operations, where the time delay problem is tackled by relying on supervisory control, and mobile robots that provide haptic feedback about real or virtual obstacles [30, 31]. A similar approach that uses haptic aids to support obstacle avoidance or gust rejection in UAV flight, but that neglects the time delay problem, is described in [32, 33]. The methods for obstacle avoidance force feedback could be used in flight control, either for actual obstacle avoidance, or as a type of flight director that directs the pilot's control inputs during tracking tasks. However, obstacle avoidance tasks are rare in aviation and therefore not within the scope of this thesis, and the use of a flight director requires autopilot functionality or, in other words, a higher degree of automation. A flight director is indeed nothing else than a display of those command inputs that an autopilot would make to lower-level flight control loops. The only difference to actual autopilot control is that the human pilot makes those inputs, is thereby more involved in the flight control task, and retains the freedom to disregard the autopilot commands.

Comparably few research activities take place in the domain of remote air- and spacecraft control or, more precisely, remote manual control of aerial or orbital vehicle movements. Although some propositions have been published on desirable UAV or RPA dynamic characteristics [1, 34, 35], none of them addresses the main issues of this thesis. Elsewhere, it has been shown that the abovementioned concept of predictor displays can be applied to remote spacecraft rendezvous and docking maneuvers to effectively increase success rate while reducing time and fuel required [36]. In [37], a predictive factor has been defined that indicates how well a spacecraft operator can cope with time delays. This factor depends on operator skill and time delay and is positively influenced by predictor displays. In aircraft control with negligible time delay, perspective flight path displays with a predictive capability have been shown to improve manual control performance [38, 39]. Such displays visualize the target flight path as a so-called tunnel in the sky and also feature a flight path predictor symbol that indicates the future position of the aircraft at a specified time ahead. Moreover, the cross section of the tunnel that the aircraft shall pass at that time is marked. The task of the pilot is to align the predictor symbol with the center of the marked tunnel cross section. By implementing an appropriate predictor law, near-optimal transfer characteristics from control input to predictor position can be achieved. Such a predictor law does not necessarily constitute a highly elaborate model of the aircraft's dynamics. It can be as simple as a linear or quadratic Taylor polynomial approximation. However, when more states need to be predicted, like in the case of teleoperation with six or more degrees of freedom, the predictor model is necessarily more complex. The combination of flight path predictor and tunnel in the sky contributes to minimizing the predicted as well as the current path error, but it obviously requires a priori knowledge about the target flight path. If such knowledge is not available, target prediction cannot be provided. State prediction on its own, however, is already generally quite effective in supporting human performance, since it replaces a cognitive task with a simpler perceptual one [40].

For RPA control with large time delays, a full state predictor relying on a virtual visual environment comparable to that of a flight simulator has been proposed [41], enabling compensation of the downlink latency. It is also possible to compensate the entire round trip latency [2], although it needs to be stressed that prediction inaccuracies due to disturbances and model errors increase with prediction time. An important limitation of predictor displays is the need for synchronization between predictor model and real system. When the real system did not exactly follow the prediction, as is usually the case due to various disturbances, and the prediction model is updated to the actual system state, transient movements of the predictor can occur. Depending on their magnitude, such transient movements can be quite confusing for the operator, as they do not conform with the expected, physical behavior of the system.

In research on hypersonic aircraft control [42, 43], the problem of path-attitude decoupling was encountered, which manifests itself in lags as high as 20 s or more between attitude and flight path. For altitude tracking tasks, this problem was addressed by displaying vertical speed and vertical acceleration and instructing pilots to perform flight path control by immediately counteracting changes of these variables. This piloting technique is different from the conventional technique of adjusting the airplane's attitude to produce the desired flight path changes (cf. section 3.1.2). By reducing the attention pilots devote to pitch attitude, the significance of path-attitude decoupling was reduced. Moreover, a predictor display proposed as additional mitigation strategy was shown to be an appropriate and efficient means to support the pilots' control efforts [44].

Indeed, new control strategies may have to be found for flight control with large time delays [18]. Investigations into the capture of satellites using a remotely piloted orbital maneuvering vehicle [45] came to the conclusions that a lower control authority is desirable for remote operations due to the pilot's reduced situational awareness. Since pilots controlled vehicle accelerations, control authority can be understood as the maximum translational and rotational acceleration producible with the inceptors. Moreover, "direct" acceleration control was preferred over "proportional" acceleration control as time delays increased from 2 s to 6 s. Here, proportional control enabled pilots to command different levels of acceleration by varying inceptor deflection, whereas direct control simply caused appropriate thrusters to fire when the inceptor was moved out of detent [46]. Direct control thus effectively gave operators a choice of only three distinct control inputs: positive acceleration, negative acceleration and no acceleration.

The problem of reduced sensory feedback in RPA control has already been identified by the aerospace research community [3, 18]. Different strategies have been proposed to either reintroduce or substitute selected sensory channels and thereby enhance the feeling of shared fate and improve flight control performance. One strategy to reinstate vestibular feedback is to put pilot (and ground control station) on a motion platform and use measurements from the real RPA to replicate the linear accelerations and rotations on the ground [6]. Like in a moving-base simulator, the motion feedback needs to be well synchronized with the visual feedback to prevent vertigo. Evidently, this approach results in a considerable increase in ground control station complexity, cost and maintenance effort.

Instead of reintroducing a certain feedback modality, it is well possible to substitute it with another. Information that cannot be transmitted in a non-visual sensory channel is often displayed visually, with the disadvantage of cluttering up the visual channel. An alternative way to compensate for the reduced sensory feedback in RPA control is the use of new presentation options [18] or multimodal information displays [3]. Such displays, which may comprise auditory and tactile cues, do not necessarily compensate the loss of one certain feedback channel. They more generally reduce cognitive-perceptual workload levels and thereby compensate for the increased workload associated with establishing situational awareness in an impoverished sensory environment. The method of distributing information on multiple sensory channels may increase the maximum overall information rate, but it comes with the risk of different channels competing with each other. Coning of attention can still occur – either onto one channel or onto one information within one channel. The examples of multimodal displays given in [3] only comprise event based alerts and annunciations, but continuous multimodal feedback for the flight control task is also possible. The use of tactile displays for onboard manual flight control has been investigated by several studies [47–50]. Their application to remote UAV control is deemed to potentially improve the operators' situational awareness [51]. A more detailed analysis of sensory feedback channels and multimodal displays is provided in sections 3.1.1 and 4.4.

The state of the art in BMI control is that some systems enable users to select one item out of a given set, whereas others allow to communicate binary decisions. With such binary commands, one degree of freedom of a vehicle's movement can be controlled. As mentioned earlier, BMI output signals are quite noisy, which is why extensive filtering is required to make the signals usable for communication or control. This generally makes continuous low-level control impractical and leaves high-level decision taking as the only option. So-called synchronous or cue-paced BMIs constitute an extreme case, since they only allow for communication in well-defined time frames [52]. Consider the BMI controlled car presented in [53] as an example. Upon reaching a crossroads, the user is prompted to decide on the direction to take. He then has a few seconds to communicate his intention via the BMI. The BMI neither considers the possibility that the user does not want to communicate at that moment, nor does it allow the user to communicate during the time between two crossroads. The P300 speller [54], too, is a synchronous BMI. It allows to spell a letter by focusing visual attention on it in a table of multiple letters, while each letter (or each group of letters) is intensified for a short time in random order. The time required to spell one single letter is fixed by the system and can be as high as 21.6 s [54]. Asynchronous or self-paced BMIs, on the other hand, leave the decision on when and when not to communicate to the user [52]. They continuously monitor the user's brain activity and look for certain intentions. An example application of an asynchronous BMI is the control of a quadcopter's movement described in [55]. Here, binary decisions could be made in two degrees of freedom. Subjects had continuous low-level control of the quadcopter, commanding left/right and up/down movements as it slowly moved forward. This is the most similar approach to what is presented in this thesis. Another study related to BMI control of aircraft relied on the same basic BMI approach that enables binary decisions in one degree of freedom, but used it to successively specify segments of a

two-dimensional target path that a UAV would then automatically follow [56, 57]. A more detailed introduction to BMIs follows in section 3.4.1.

The issues arising when proprioceptive feedback is missing have not yet been addressed. It exists in cases like BMI or speech control that are usually employed for higher-level, semiautonomous control. In such control systems, human-machine communication resembles verbal communication, so it does not necessarily require proprioceptive feedback, even if manual means of control are used, like the command line interface of a computer. BMIs mainly rely on visual displays, although some also provide tactile or auditory feedback [52].

1.3 Goals and Contributions

1.3.1 Research Goals

In one sentence, the aim of the research leading up to this thesis was to make low level, closed-loop flight control by a human pilot in the presence of large time delays and with missing sensory feedback channels safer, more effective and more efficient. The following paragraphs concretize this mission statement and provide some explanation.

Low-level flight control is the act of controlling an airplane's movement, i.e., flight path or, whenever necessary, attitude, throughout an exemplary reference flight mission. Closed-loop control is to be understood in the sense that the pilot continuously modifies his control input depending on the sensory feedback received to pursue his objectives. During open-loop control, on the other hand, control inputs are made entirely without relying on sensory perception of the target parameter. Driving a car along a winding road is an example of closed-loop control, whereas selecting a target altitude on an autopilot mode control panel constitutes open-loop control. Note that during closed-loop control, pilots may nevertheless use an open-loop control strategy. In this case, the result of each open-loop control input is assessed and, if necessary, corrected by another control input.

It is assumed that the signal transmission or processing characteristics in the case of RPA or BMI control, respectively, do not noticeably change during one flight and that the time delay therefore is constant. A minimum time delay of 1 s is considered realistic given the state of the art in both RPA and BMI control. It corresponds, for instance, to a geostationary satellite link with at least some compression. Considering the maximum values in Table 1.1 and the reports from the RPA-experienced experimental subject, a maximum time delay of about 3 s is considered, representing ultra-long-range remote control or extensively filtered BMI outputs. During RPA control, vestibular feedback is missing, and BMI control does not provide proprioceptive feedback.

The time delay is considered to be effectively present in the control loop. This means that no efforts were made to reduce or eliminate the apparent time delay by introducing predictor displays or entire virtual environment displays. Although the implementation of predictors may be challenging, their effectiveness in mitigating time delay (by apparently reducing it) is quite straightforward. It has been proven in many studies and is therefore

not under scrutiny here. Instead, the effect that such predictor displays have on the pilots' distribution of attention was investigated.

It was clear from the beginning that an eventual handling improvement is necessarily limited in its extent. Conventional flight control will never be matched in performance when large time delays are present and sensory feedback channels are missing, much like a telephone conference around the globe will never adequately replace a face-to-face meeting. The research focus therefore was to make flying under these adverse circumstances safe. This means that a departure from a safe flight regime must be prevented, notably by ensuring stability of the control loop closed by the human pilot. Operational performance is important as well, but only the second priority. It is inevitably degraded with respect to that of onboard manual flight control. In the mission statement, the term effectiveness refers to the ability to accomplish operational goals, whereas efficiency is a measure of resources needed to accomplish those goals, such as pilot workload or time. Attempts were made to establish operational effectiveness and to improve operational efficiency by minimizing the additional pilot workload introduced by time delays and reduced sensory feedback. The first priority, however, was to provide safety.

1.3.2 Contributions of this Thesis

Throughout the thesis, remote flight control with large signal transmission latencies and BMI controlled flight serve as example applications. By working towards the goals described above, this thesis contributes to an increased independence from automation and/or local pilots in RPA control and to more application-driven BMI research. It also promotes a better understanding of human operator behavior when confronted with large time delays. The following paragraphs list and explain in detail the particular contributions of this thesis.

Novel representations of the dynamic behavior of pilots

The first major contribution is the analysis and modeling of the nonlinear pilot behavior that occurs during control of systems with large time delays. Although this specific, pulse-like behavior has been observed by many researchers, few efforts were made to describe or even model it. Section 3.2 of this thesis provides a survey of previous research on this issue which shows, that pulse-like behavior is long known as a strategy to control higher-order systems. In the control of systems with large time delays, a very similar behavior occurs and a hybrid open- / closed-loop control strategy is applied by operators. This thesis pieces these insights together to form an integral description of both the characteristic control strategy and the characteristic control activity of human operators in control tasks with large time delays.

Established pilot models do not satisfyingly describe this behavior, since they are applicable either to flight control without time delays, where pilots behave quasi-linearly, or to control of higher-order systems, where they can still perform pure closed-loop control. Therefore, novel representations of the dynamic behavior of pilots are derived in section 3.3. First, a control-theoretic model is presented that describes pure closed-loop tracking

of a stationary target in the presence of large time delays. Since it contains a nonlinear element, classical linear methods cannot be applied. A novel approach of pilot behavior analysis is therefore presented which makes use of the phase plane method. Based on this model, the implications of the characteristic pilot behavior on flight control system design are discussed. Furthermore, a second model is presented that extends the first model and thereby describes the hybrid open- / closed-loop control strategy observed during pursuit control with large time delays. This second model is validated by comparison with experimental data in section 6.5.

A flight control system concept tailored to the pilots' natural behavior

Pilot models only constitute a mean to analyze the problem, or a tool in the process of finding a solution to it. Going one step further, chapter 4 of this thesis proposes a flight control system design that applies the insights gained from pilot modeling to address the problem of flight control with large time delays and reduced sensory feedback. The major innovation in this design is the decision to deliberately restrict pilot inputs by implementing an on-off control system. In a pilot-centered approach, this decision is derived from the characteristic behavior described and modeled in sections 3.2 and 3.3. It is furthermore shown in section 4.1 that similar control systems have already been implemented in various spacecraft, albeit for onboard manual control.

Although some previous studies indicate that an on-off control system may indeed be better suited for control tasks with time delay than a value-continuous control system, a detailed experimental evaluation has not yet been done. Hence, in the research leading up to this thesis, a large-scale experimental comparison between the two control system types has been set up and conducted to gain quantitative insights into the advantages and disadvantages of each approach. Its results, presented in section 6.4, constitute another core contribution of this thesis. They shed light on how far pilot workload and task performance differ between continuous and on-off control. Moreover, the influence of varying control sensitivities was investigated for both types of control systems. Since most of the experiment's subjects had never been exposed to the problem of (flight) control with large time delays before, insights were also advanced concerning the initial learning phase and the natural strategy to cope with the problem.

As indicated in section 1.2, automation should be employed in situations where pilot errors significantly reduce operational performance or easily result in accidents. With the flight control approach proposed in this thesis, however, remote RPA pilots can take over control if system failures cause the control system to revert to a lower level of automation or if deemed necessary due to unanticipated circumstances, like, for instance, an impending collision. Even if the proposed control system type will not enable picture-perfect landings, it will at least enable the remote pilot to end the flight in a desired area and thereby avoid harm to persons or damage to objects on the ground. With a conventional control system, on the other hand, pilots may more easily lose control in flight. Apart from RPA flight control, the findings of this thesis also contribute to RPA payload control and to teleoperation in general.

Application of methods from the aerospace domain in the realm of BMI

BMI controlled flight is very far from actual application. Research activities on BMI control mainly focus on improving the algorithms that identify the user's intention from the measured electromagnetic brain signals. Indeed, significant advances in this area are required to mature the technology. To implement suitable algorithms, traditional BMI research relies on neuroscience and, more rarely, on signal theory. Moreover, control schemes are usually open-loop. This thesis gives examples of how to employ tools and methods from the aerospace domain to closed-loop BMI control. Considering that controllability has been a major issue in aviation since its dawn, it seems foolish not to translate this hard-earned know-how to other problems of control.

The experiments presented in chapter 5 are an example for how handling qualities research can be done in the field of BMI control. Instead of fixing a single BMI system design and then determining in an open-loop task how often the algorithm correctly classifies the users' intention, various configurations were set up and the dynamic characteristics of the entire, closed control loop were systematically adapted to the subjects' needs. Another substantial difference with respect to many BMI control studies is, that apart from objective performance metrics, subjective user comments were taken into account. Finally, experiment subjects were immersed in a highly realistic environment, namely a flight simulator, as opposed to the typical, rather functional laboratory environment. Human users behave differently whether they operate a desktop-computer simulation, a highly realistic simulator or the real system. A more application-driven approach therefore constitutes an important step from BMI research towards actual BMI products.

Aerospace methods cannot replace neuroscience and signal theory in BMI research, but they complement the scientific toolbox. They cannot be used to improve the brain signal classification accuracy itself, but they are helpful in identifying suitable dynamic characteristics of the controlled system. In this regard, this thesis constitutes a starting point that hopefully acts as impetus towards the combined application of neuroscience, signal theory and aerospace engineering methods to the problem of BMI control.

1.4 Outline

Following this introductory chapter 1, some basic information about flight mechanics, flight control systems and handling qualities is provided in chapter 2. Then, chapter 3 presents existing and novel pilot models and gives an introduction to BMIs. Chapter 4 describes the flight control system design. Chapters 5 and 6 then compile results from several flight simulator experiments on BMI control and RPA control, respectively. Finally, concluding remarks and an outlook are given in chapter 7. A more detailed outline of the core chapters of this thesis is given by the following paragraphs.

Chapter 2 starts off with the definition of a reference aircraft as the flight controller environment with certain sensors and control effectors. Furthermore, a flight mission and its different flight phases are outlined in section 2.1.2. They, too, serve as a reference for flight control system design. A brief analysis of flight mechanics follows in section 2.2.1,

as well as a look on the historic evolution of flight control systems and the resulting implications on aircraft handling and requirements in section 2.2.2. Then, methods for quantifying handling qualities and the concept of handling qualities criteria are presented in section 2.2.3. Chapter 2 concludes by outlining pilot-induced oscillations as manifestation of a major handling deficiency that is very relevant to the topic of this thesis and by describing two handling qualities criteria that aim at identifying this deficiency in a given control system.

Chapter 3 begins with an introduction to the pilots' input (sensor) and output (motor) channels and their characteristics relevant to flight control. Next, several established quasi-linear physiological and control-theoretic pilot models are presented in section 3.1.2. In section 3.2.1, the effects of large time delays are examined, based on previous research in this field and using the pilot models presented before. A hybrid open- / closed-loop control strategy is described as natural operator behavior in section 3.2.2. The shortcomings of the quasi-linear models in describing this behavior are identified and a survey of alternative models is given in section 3.2.3. Then, in section 3.3.1, a new model is derived that describes closed-loop compensatory tracking of a stationary target with fixed-amplitude control inputs. This model is expanded in section 3.3.3 to describe pursuit tracking and the hybrid open- / closed-loop control strategy observed. In the last part of chapter 3, a more detailed introduction to BMIs is given and some challenges of BMI control are characterized using a control-theoretic BMI model. This model also serves as an illustration for the source and the level of time delays in BMI control.

Based on the information collected in the first three chapters, a flight control system is designed in chapter 4 that addresses the given problem. The design process encompasses the entire chain from the inceptor or BMI through the flight control algorithms to the feedback mechanisms or displays. After delineating some design goals and basic design choices in section 4.1, section 4.2 describes the flight controller with its functions and shows the behavior of the implemented system. Then, suitable inceptor characteristics are identified and minimum and desired BMI performance outlined. Thoughts on displays relying on different possible sensory modalities conclude chapter 4.

Chapters 5 and 6 describe the experimental evaluation of BMI control and manual remote flight control, respectively. They cover multiple human subject studies that have been conducted in flight simulators, each highlighting a different part of the problem or the proposed solution. BMI control and manual remote flight control were split up in separate experiments as well as in separate chapters of this thesis because the goals, the setup and the outcome of the experiments differed drastically. Although both example applications do have some similarities, BMI control is still in its infancy. Therefore, the experimental setup, the tasks and the results discussed in chapter 5 are of a more explorative nature. Chapter 6, on the other hand, starts off by listing several a-priori hypotheses that were tested in the experiments. After a description of the experimental setup and the tasks, the experiment results are discussed and related to the hypotheses. The BMI model defined in section 3.4.2 is validated in section 5.5, whereas section 6.5 determines whether the new pilot model from section 3.3.3 well describes the pilot behavior observed in the experiments on manual remote flight control.

2 HANDLING QUALITIES PRELIMINARIES

2.1 Reference Configuration, Mission and Flight Phases

According to Cooper and Harper [58], “handling qualities are those qualities or characteristics of an aircraft, that govern the ease and precision with which a pilot is able to perform the tasks required in support of an aircraft role.” As a result, a concise understanding of the aircraft and its role is required to conceive a flight control system that provides adequate handling qualities. The reference airplane and flight mission of this thesis are described in this section.

2.1.1 Aircraft, Measurements and Estimations

For several reasons, a light airplane is considered a suitable reference configuration for RPA and BMI control. First, it is similar in size and weight to many existing and possible future RPA which could benefit from the proposed approach. Second, BMI flight control could first find its application in light general aviation airplanes, since agile airplanes in military missions require a very high control system bandwidth that BMIs will not provide in a foreseeable future and airline operations with large transport aircraft extensively rely on automation. The reference airplane chosen is the Diamond DA42 [59]. A drawing of this twin piston engine airplane with four seats and a maximum takeoff mass of 1900 *kg* is shown in Figure 2.1. This airplane can be flown under visual and instrument flight rules by a single pilot. The certification basis is JAR-23, the predecessor document of CS-23 [60]. The fact that an optionally piloted version of the DA42, which can be operated either as a manned aircraft or as an RPA, is available [61] emphasizes that this airplane is a suitable reference configuration for this thesis.

The infrastructure of the Institute of Flight System Dynamics of the Technical University of Munich (TUM), where the research for thesis has been conducted, not only includes dynamic models of the DA42 implemented in MATLAB and Simulink [62, 63], but also a DA42 Flight Training Device (FTD) or – simply said – simulator. Details of the DA42 simulator are given in section 5.1.2. The following paragraphs describe the airplane as the plant of the flight controller. The flight controller, which is presented in chapter 4, performs feedback control to shape the dynamic behavior of the entire augmented airplane, i.e., the combination of airframe and digital flight control algorithms.

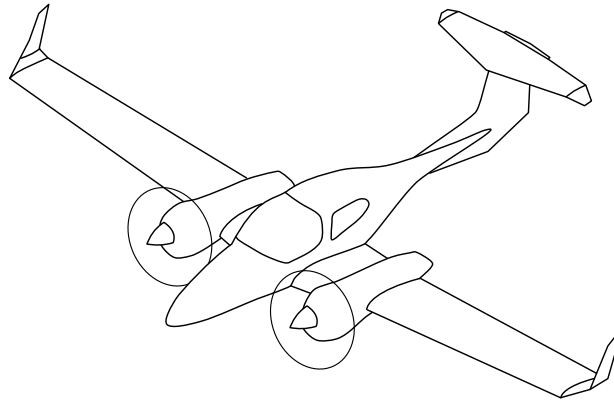


Figure 2.1 – Sketch of the DA42, based on the maintenance manual [64]

The performance attainable by feedback control not only depends on the physical characteristics of the plant, which are briefly outlined in section 2.2.1, but also to a large extent on the measurements available. As the research presented in this thesis relies on simulation rather than inflight experiments, any desired measurement could have been assumed to be perfectly available. It was, however, decided to restrict the measurements available to a realistic set that is readily available in the considered class of aircraft.

Table 2.1 – Parameters assumed available from onboard sensor fusion

Symbol	Description
p	Roll rate
q	Pitch rate
r	Yaw rate
Ψ	Heading
Θ	Pitch angle
Φ	Bank angle
$(\vec{n})_B = \begin{pmatrix} n_x \\ n_y \\ n_z \end{pmatrix}_B$	Load factor, noted in the body fixed frame
χ_K	Kinematic course angle
γ_K	Kinematic flight path climb angle
V_K	Absolute kinematic speed with respect to the rotating Earth
V_{IAS}	Indicated airspeed
\dot{h}	Kinematic vertical speed
h_B	Barometric altitude
h_R	Height above terrain

The reference airplane, for instance, is equipped by default with the Garmin G1000 avionics suite [65]. Such systems normally comprise an air data computer that processes pressure measurements from the pitot-static system and also outside temperature measurements, an inertial measurement unit that senses the specific force and angular

rate of the aircraft body, a magnetometer to obtain information on magnetic heading, and a global navigation satellite system receiver. A data fusion algorithm combines the measurements from these various sources to obtain relevant aircraft state parameters with high accuracy. If such a system is combined with a radar altimeter, which is a standard instrument in large transport aircraft, but more costly to install, the set of parameters listed in Table 2.1 can be assumed available in the considered airplane class. It is furthermore assumed that the measurement or computation of these parameters is made with a sufficiently high quality. Sensor models were therefore not implemented, but the values of these parameters were taken directly from the simulation model instead. Note that the height above terrain, which is the only measurement contributed by the radar altimeter, is only required for attitude limitation in ground proximity (cf. section 4.2.2). More challenging measurements of, for example, the flow angles α and β , are not employed.

As can be seen in Table 2.1, the load factor is assumed to be available in the body-fixed frame (subscript B). To calculate the limit flight path climb angle, however, the flight control system requires the longitudinal load factor in the kinematic frame $(n_x)_K$ (cf. section 4.2.2 and appendix A). The body-fixed frame has its origin at a reference point on the vehicle. Its x - and z -axes lie in the aircraft's plane of symmetry, pointing forward and downward, respectively. The y -axis points right to form a right-hand coordinate system. The kinematic frame's origin coincides with that of the body-fixed frame, but its x -axis is aligned with the kinematic velocity vector and its z -axis is parallel to the projection of the Earth's local surface normal onto a plane perpendicular to the x -axis. The y -axis, again, forms a right-hand coordinate system with the other axes.

An estimation of the longitudinal load factor in the kinematic frame $(\hat{n}_x)_K$, with the hat denoting estimated values, can be made based on the geometric relationship between the kinematic frame and the body-fixed frame. The rotation between these two frames is described by the three angles α_K (kinematic angle of attack), β_K (kinematic angle of sideslip) and μ_K (kinematic bank angle). According to [66], the rotation matrix from the kinematic frame to the body-fixed frame is defined by equation (2.1).

$$M_{BK} = \begin{bmatrix} 1 & 0 & 0 \\ 0 & \cos \mu_K & \sin \mu_K \\ 0 & -\sin \mu_K & \cos \mu_K \end{bmatrix} \begin{bmatrix} \cos \alpha_K & 0 & -\sin \alpha_K \\ 0 & 1 & 0 \\ \sin \alpha_K & 0 & \cos \alpha_K \end{bmatrix} \begin{bmatrix} \cos \beta_K & -\sin \beta_K & 0 \\ \sin \beta_K & \cos \beta_K & 0 \\ 0 & 0 & 1 \end{bmatrix} \quad (2.1)$$

By multiplying the inverted M_{BK} with the load factor in the body-fixed frame, the load factor in the kinematic frame can be obtained, as equation (2.2) shows.

$$\begin{pmatrix} n_x \\ n_y \\ n_z \end{pmatrix}_K = M_{BK}^{-1} \cdot \begin{pmatrix} n_x \\ n_y \\ n_z \end{pmatrix}_B \quad (2.2)$$

During the reference flight mission (cf. section 2.1.2), the airplane normally operates close to straight, coordinated flight. Hence, it can be assumed that $\beta_K, \mu_K \approx 0$. This assumption inserted into equation (2.1) and then combined with equation (2.2) leads to equation (2.3). The required parameter $(\hat{n}_x)_K$ can be read from the first line of equation (2.3), which is explicitly written down in equation (2.4).

$$\begin{pmatrix} \hat{n}_x \\ \hat{n}_y \\ \hat{n}_z \end{pmatrix}_K = \begin{bmatrix} \cos \alpha_K & 0 & \sin \alpha_K \\ 0 & 1 & 0 \\ -\sin \alpha_K & 0 & \cos \alpha_K \end{bmatrix} \cdot \begin{pmatrix} n_x \\ n_y \\ n_z \end{pmatrix}_B \quad (2.3)$$

$$(\hat{n}_x)_K = (n_x)_B \cdot \cos \hat{\alpha}_K + (n_z)_B \cdot \sin \hat{\alpha}_K \quad (2.4)$$

Note that to estimate the longitudinal load factor in the kinematic frame, an estimation of the kinematic angle of attack $\hat{\alpha}_K$ needs to be obtained in the first place. According to [66], this angle can be estimated as in equation (2.5) if θ and γ_K are small, which is the case during the considered flight mission (cf. section 2.1.2).

$$\hat{\alpha}_K = \theta - \gamma_K \quad (2.5)$$

Sensors and their measurements constitute but one interface between controller and environment. Another interface, which enables the controller to influence its environment, are the control effectors. Much like the quality of the measurements, the number, type and physical performance of the control effectors have a significant influence on the closed-loop control characteristics attainable. The flight controller presented in chapter 4 actuates elevator, ailerons, rudder and thrust lever of the DA42 simulation model. The actuators that apply the commanded deflections as well as the control effectors themselves have certain physical limitations. To model these limitations, a generic actuator model from [66] is employed for the three control surfaces. This model is defined by the second-order transfer function of equation (2.6), where s is the Laplace variable. According to [66], a frequency of 30 rad/s and a damping ratio of 0.7 are assumed.

$$Y_{act} = \frac{1}{\left(\frac{s}{30}\right)^2 + \frac{2 \cdot 0.7}{30} \cdot s + 1} \quad (2.6)$$

Control surface deflection rates are limited to an estimated value of $\pm 30^\circ/\text{s}$ and the absolute deflection limits of the actual DA42 airplane apply. They were taken from [64] and are given in equations (2.7), (2.8) and (2.9) for elevator deflection η , aileron deflection ξ and rudder deflection ζ , respectively.

$$-15^\circ \leq \eta \leq 13^\circ \quad (2.7)$$

$$-20^\circ \leq \xi \leq 20^\circ \quad (2.8)$$

$$-29^\circ \leq \zeta \leq 27^\circ \quad (2.9)$$

2.1.2 Mission and Flight Phases

While the reference aircraft is defined in the preceding section, this section is dedicated to the definition and analysis of a reference flight mission. Such a reference flight mission shall represent the normal activities of both remotely piloted UAVs and BMI controlled general aviation airplanes. All these flights either travel between two aerodromes or depart

and arrive at one single aerodrome. Note that in the case of RPA flight, an aerodrome may consist of a simple makeshift landing strip. While travel is the only purpose in some general aviation missions, other flights require the airplane to stay for an extended period in a certain target area, where activities like aerial observation or photography take place. These latter activities are similar to those of RPA missions, where cameras or other sensors are used to make observations, or where the UAV acts as an airborne relay station.

Flight missions consist of different flight phases, each of which is characterized by certain circumstances and goals (or tasks). Thus, each flight phase imposes different requirements on tracking precision of a certain tracking variable. Aerial refueling as an exemplary flight phase is characterized by close proximity to another aircraft and the goal to maintain a given relative position with high accuracy. Therefore, the pilot-aircraft system is required to track flight path-related variables with high precision. The U.S. Department of Defense's handbook "Flying Qualities of Piloted Aircraft" (MIL-HDBK-1797) [67] defines different flight phase categories that group flight phases with similar requirements. Category A flight phases are nonterminal flight phases such as air-to-air combat, aerial refueling or close formation flying "that require rapid maneuvering, precision tracking, or precise flight-path control". Note that here, the term tracking more specifically refers to attitude tracking. Category B flight phases are "nonterminal flight phases that are normally accomplished using gradual maneuvers and without precision tracking, although accurate flight-path control may be required". Examples comprise climb and cruise. Finally, category C flight phases are terminal flight phases that are "normally accomplished using gradual maneuvers and usually require accurate flight-path control." The fundamental difference between nonterminal and terminal flight phases is that the latter are characterized by ground proximity. When maneuvering close to the ground, flight path errors can easily result in a terrain collision. This is what makes accurate flight path control necessary during category C flight phases.

It has to be noted that an attempt was made to translate this concept of flight phases, which had originally been developed for manned flight, to unmanned aviation [34]. The main difference to the flight phase category definitions stated above is that terminal flight phases are divided into two categories C and D to account for certain launch and recovery methods of unmanned aircraft. Since the reference airplane performs terminal flight phases much like a manned airplane, even if remotely controlled, this subdivision of terminal flight phases brings no benefit here.

The reference flight mission inevitably includes the following terminal flight phases: takeoff, approach, landing and go-around. Furthermore, a climb phase is required to reach the operating altitude and a descent phase is required prior to commencing approach. During cruise, the airplane flies from the departure airport to the target area or the destination airport. Activities such as aerial observation are performed during a so-called loiter phase. Figure 2.2 illustrates this mission with all its flight phases and flight phase categories. Note that none of the flight phases is a category A flight phase.

Like most general aviation missions, the reference flight mission requires the pilot to perform flight path tracking throughout the entire mission. The ability to precisely track a target attitude is only required during takeoff and landing, when an incorrect attitude in

ground proximity can lead to dangerous situations and accidents like tail strikes, wing strikes or nose wheel landings. In RPA missions, it may be required to point the payload (e.g., a camera) towards a certain direction while loitering. It is assumed that this is accomplished by the payload itself and does not require the airplane to adopt a precise target attitude. Furthermore, it is assumed that there is no crosswind component during terminal flight phases. Although this is not always the case in real world operations, this assumption helps establishing an appropriate scope for this thesis without preventing an extension by subsequent research. Moreover, in the case of RPA control, terminal flight phases would be flown by a remote pilot only during non-normal operations, where the aim may be to simply bring the aircraft down without causing damage to third parties.

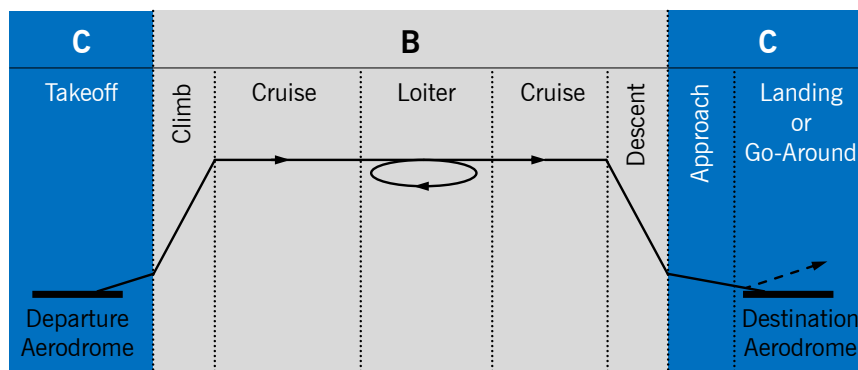


Figure 2.2 – Illustration of the reference flight mission

2.2 Flight Mechanics and Flight Control

2.2.1 Equations of Motion

Assuming that an airplane is a rigid body, its dynamic behavior in three rotational and three translational degrees of freedom can be described by a set of 12 nonlinear equations of motion. These equations are basically identical for every conventional airplane and are derived and described in corresponding literature [66, 68, 69]. Each individual aircraft then is characterized by the external forces and moments acting on it. External forces and moments originate from mass, aerodynamics and thrust. Hence, the key components of any dynamic airplane model are mass model, aerodynamic model and thrust model.

As mentioned in section 2.1.1, a nonlinear dynamic model of the Diamond DA42, implemented in MATLAB and Simulink, was available at TUM's Institute of Flight System Dynamics [70]. By determining the stationary solutions of the model and linearizing it around these trim points, the analysis of airplane dynamics and the design of (linear) control algorithms is facilitated. In this section, the linear airplane behavior around straight and level flight is examined to illustrate several basic flight dynamic characteristics. Strictly speaking, this linearization is only valid for straight and level flight, but it also well represents aircraft states that are reasonably close to this trim state. It is therefore suited to describe the aircraft's dynamic characteristics during the reference flight mission defined in section 2.1.2, which does not require large-amplitude maneuvering or extreme attitudes. When analyzing the aircraft behavior around straight and level flight, certain

assumptions can be made that facilitate linearization. In particular, it is assumed that the body angular rates p , q and r as well as the angle of attack α , the angle of sideslip β , the pitch angle Θ , the flight path climb angle γ and the bank angle Φ are small. Finally, one additional simplification is made in that wind is neglected. (This is also the case in all other parts of this thesis unless stated otherwise.) As a result, kinematic and aerodynamic frame coincide and the associated subscripts are omitted.

The linear equations of motion can, for example, be represented in the state space. It is then common to describe longitudinal and lateral-directional airplane dynamics in two separate state space representations [66], because they are normally well decoupled. Equations (2.10) and (2.11) define the state vector of the longitudinal and lateral-directional state space, respectively. The longitudinal states are velocity, flight path climb angle, angle of attack, pitch rate and altitude. Lateral states are roll rate, yaw rate, bank angle, angle of sideslip and flight path course angle. Note that the states describing horizontal position are not included here, because they are irrelevant to the subsequent analyses. Moreover, the fact that the state variables actually describe deviations from trim values is not explicitly denoted in the following equations and diagrams. For example, with trim values denoted by a subscript 0, the state variable V actually stands for $V - V_0$, which is common practice in control theory.

$$\vec{x}_{lon} = [V \quad \gamma \quad \alpha \quad q \quad h]^T \quad (2.10)$$

$$\vec{x}_{lat} = [p \quad r \quad \Phi \quad \beta \quad \chi]^T \quad (2.11)$$

Equations (2.12) and (2.13) show the state space representations of the longitudinal and the lateral-directional motion, taken from [66]. Inputs to the longitudinal dynamics are elevator deflection η and thrust lever position δ_T . Inputs to the lateral-directional dynamics are aileron deflection ξ and rudder deflection ζ . State and input matrices contain the so-called dimensional derivatives, which are related to airframe characteristics like the dimensionless aerodynamic derivatives, mass and inertia [66]. The variable g is not a derivative, but stands for the Earth's gravitational acceleration. Apart from the assumptions noted above, equations (2.12) and (2.13) furthermore assume $\Theta_0 = \alpha_0 = 0$ and neglect the very small derivatives. As a result, h is decoupled from the other longitudinal states.

$$\dot{\vec{x}}_{lon} = \begin{bmatrix} X_V & -g & X_\alpha - g & 0 & 0 \\ -Z_V & 0 & -Z_\alpha & 0 & 0 \\ Z_V & 0 & Z_\alpha & 1 & 0 \\ M_V & 0 & M_\alpha & M_q & 0 \\ 0 & -V_0 & 0 & 0 & 0 \end{bmatrix} \vec{x}_{lon} + \begin{bmatrix} X_\eta & X_{\delta_T} \\ -Z_\eta & -Z_{\delta_T} \\ Z_\eta & Z_{\delta_T} \\ M_\eta & M_{\delta_T} \\ 0 & 0 \end{bmatrix} \begin{bmatrix} \eta \\ \delta_T \end{bmatrix} \quad (2.12)$$

$$\dot{\vec{x}}_{lat} = \begin{bmatrix} L_p & L_r & 0 & L_\beta & 0 \\ N_p & N_r & 0 & N_\beta & 0 \\ 1 & 0 & 0 & 0 & 0 \\ 0 & -1 & g/V_0 & Y_\beta & 0 \\ 0 & 0 & g/V_0 & Y_\beta & 0 \end{bmatrix} \vec{x}_{lat} + \begin{bmatrix} L_\xi & L_\zeta \\ N_\xi & N_\zeta \\ 0 & 0 \\ 0 & Y_\zeta \\ 0 & Y_\zeta \end{bmatrix} \begin{bmatrix} \xi \\ \zeta \end{bmatrix} \quad (2.13)$$

Eigenvalues and eigenvectors of each state matrix correspond to the eigenmotions of the respective system, i.e., those elementary motions that can be linearly combined to describe any possible system motion. In the longitudinal motion, the DA42 exhibits the typical eigenmotions of a conventional airplane. The well damped, high frequency short period mode and the lightly damped, low frequency phugoid. Given that the airplane is certified, the characteristics of these eigenmotions necessarily provide adequate handling qualities throughout the flight envelope. Similarly, the lateral-directional motion of the DA42 is characterized by the common eigenmotions of this type of airplane: roll mode and spiral mode – both of first order – and the second-order Dutch roll, which is a coupled yaw-roll oscillation.

The physics behind the equations of motion can be well illustrated by signal flow charts, which are a graphical representation of the linearized equations of motion. Signal flow charts can also be seen as causal chains from control effector activity to corresponding aircraft reaction. Figure 2.3 shows such a chart of the constant speed approximation of the longitudinal motion. For the analysis of longitudinal handling qualities, which are primarily determined by the short period characteristics, the assumption of constant speed is often made to avoid interference of the phugoid dynamics [71]. This assumption holds for short time scales and in cases where an autothrottle system maintains airspeed with sufficiently high bandwidth. Like the linear equations of motion it is derived from, the signal flow chart of Figure 2.3 well describes operating points within a reasonable range around straight and level flight only.

It can be seen that an elevator deflection causes a pitching moment and thus a pitch angle acceleration. The pitch rate then results in a change in angle of attack, which in turn produces a vertical load factor n_z and a flight path climb angle rate $\dot{\gamma}$. The pitch angle is the sum of angle of attack and flight path climb angle. The vertical speed \dot{h} resulting from γ leads to a change in altitude.

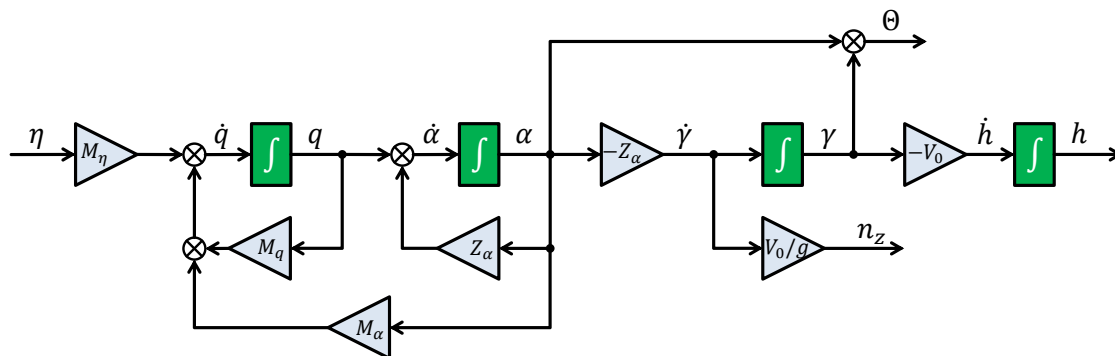


Figure 2.3 – Signal flow chart of the longitudinal motion, adapted from [66]

Each of the four integrators apparent in Figure 2.3 introduces some phase delay and some high frequency attenuation. As a result, variables on the right of the signal flow chart change on larger time scales than variables on the left. Another characteristic of longitudinal airplane dynamics, which is not immediately apparent from Figure 2.3, but that can be derived from it, is that the flight path climb angle lags pitch attitude as in equation (2.14).

$$\begin{aligned}
 \Theta &= \gamma + \alpha \\
 &= \gamma + \left(-\frac{1}{Z_\alpha}\right)\dot{\gamma} \\
 &= \left(1 - \frac{s}{Z_\alpha}\right)\gamma
 \end{aligned} \tag{2.14}$$

$$\Rightarrow \frac{\gamma}{\Theta} = \frac{1}{T_{\Theta 2} \cdot s + 1} \quad \text{with } T_{\Theta 2} = -\frac{1}{Z_\alpha}$$

Figure 2.4 shows a signal flow chart of the lateral-directional airplane motion. Again, this chart only applies to operating points within a reasonable range around straight and level flight. Moreover, the influence of Y_ζ is not shown to improve readability. It can be seen that the roll and the yaw axis are strongly coupled. For instance, aileron deflections and rudder deflections produce both a roll moment and a yaw moment. Only by coordinated deflection of both control surfaces can pure roll or yaw moments be generated. These moments then cause a build-up of roll rate and yaw rate, respectively, which in turn lead to changes in bank angle and sideslip angle. At this point, the fundamental difference between roll axis and yaw axis is that virtually any bank angle can be achieved by appropriate control inputs, whereas the possible range of sideslip angles is effectively limited by the airplane's directional stability, i.e., the weathervane effect that makes the airplane fly nose-first through the air. This effect is evidenced in Figure 2.4 by the sideslip feedback through N_β . Sideslip furthermore induces a side force, which, just like the bank angle, generates a flight path course angle rate $\dot{\chi}$, which subsequently causes flight path course angle and heading Ψ to change. Without wind, flight path course angle and airplane heading only differ by the sideslip angle.

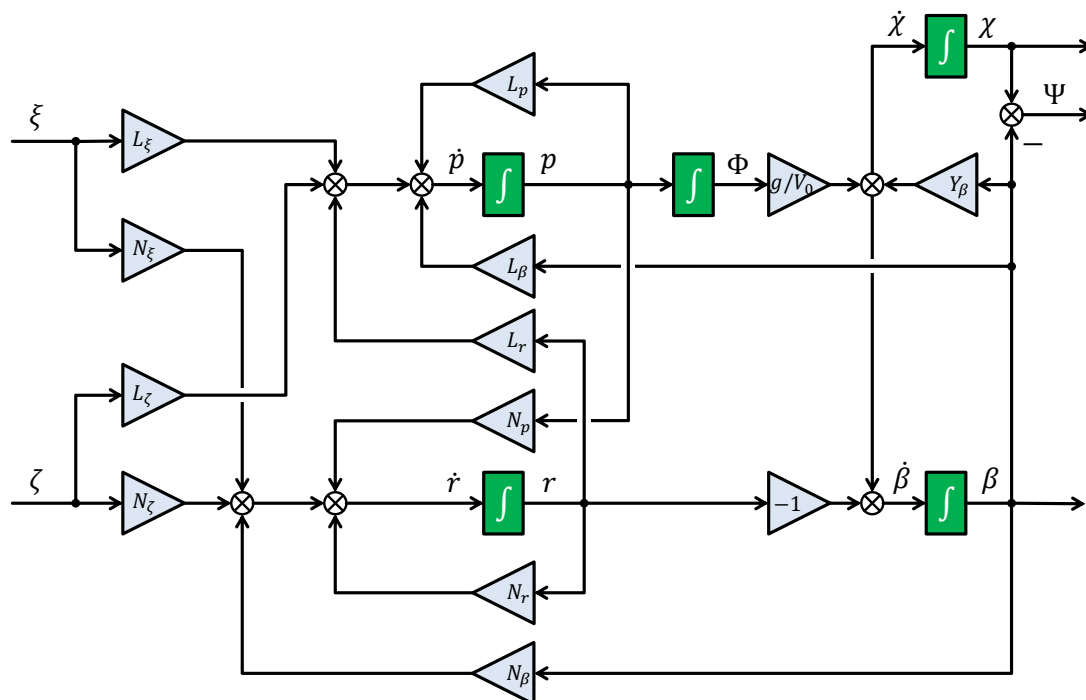


Figure 2.4 – Signal flow chart of the lateral-directional motion, adapted from [66]

Again, several integrators introduce the low-pass characteristics typical for all physical systems. A consequence of the physical low-pass in both the longitudinal and the lateral motion is that the bandwidth of a control task is a function of the controlled variable. For instance, an altitude tracking task must exhibit a lower bandwidth than a pitch angle tracking task to be accomplishable with the same airplane. This fact provides a rationale for why automation mitigates the issue of large time delays. If those control tasks that take place on smaller time scales are automated and the human operator only communicates higher level goals to the machine, his interaction with the machine is scarce. Time delay and reduced sensory feedback are thus less critical.

The analyses above provide insights into both the rotational and the translational degrees of freedom of the airplane. Sometimes, however, it is sufficient to approximate the airplane as a point mass m , which has only translational degrees of freedom. The rotational dynamics are then assumed to be fast enough to be neglected. Furthermore assuming symmetric flight, no wind, a small angle of attack and a thrust vector collinear with the speed vector, the point-mass airplane's trajectory can be described by equations (2.15), (2.16) and (2.17) [66]. Here, T denotes thrust, D drag and L lift.

$$\dot{V} = \frac{T - D}{m} + g \cdot \sin \gamma \quad (2.15)$$

$$\dot{\chi} = \frac{L \cdot \sin \Phi}{m \cdot V \cdot \cos \gamma} \quad (2.16)$$

$$\dot{\gamma} = \frac{L \cdot \cos \Phi}{m \cdot V} - \frac{g}{V} \cos \gamma \quad (2.17)$$

2.2.2 Flight Control Systems and Handling Qualities Implications

The original DA42 airplane possesses a mechanical control system [72]. Displacements of the inceptors, namely a center stick and rudder pedals in this case, are translated to control surface movements by rods and wires. This type of control system exists since the early days of aviation and is still common in light aircraft operating today. In terms of handling qualities, the distinct characteristic of a mechanical control system is that it is reversible, meaning that forces are propagated both from the inceptor to the control surfaces and vice versa. Thus, the pilot can feel the aerodynamic forces acting on the control surface.

As airplanes became faster and faster, control forces in mechanical control systems at some point became unacceptably high. Hydraulic actuators were introduced between inceptor and control surface to support the pilot, but this strategy made the flight control system irreversible. The forces that previously could be felt through a mechanical control system had to be replicated by a feel system, usually comprised of springs, dampers, added masses and other mechanical devices. The design and implementation of this sometimes complex feel system is necessary due to the importance of proprioceptive inceptor feedback, which is discussed in section 3.1.1.

Technological evolution did not stop with hydraulic control systems. Next came the introduction of digital flight control computers between inceptors and hydraulic actuators. The principal driver for this so-called fly-by-wire technology was the improvement of combat aircraft performance by reduced or even negative static stability of the airframe, but it later has also enhanced operational efficiency and safety in civil transport aviation [71]. Flight control algorithms deployed on digital flight control computers make use of various sensor feedbacks to close control loops. Pilots use their inceptors not to establish certain control surface deflections, but to generate reference values for these control loops. This type of flight control system is called maneuver demand system.

Maneuver demand systems are characterized by the command variables, i.e., those variables for which reference values are generated by inceptor inputs. In a rate command system, for instance, a given inceptor input results in a defined angular rate of the vehicle. The choice of the command variables has an immense influence on aircraft handling and thereby on the pilot's ability to safely and efficiently conduct the flight mission. As already noted in [73], a good choice enables fine tracking as well as gross maneuvering, contributes to the pilot's awareness of envelope limits and establishes an adequate workload level. Most often, however, no single command variable can satisfy all these goals in all flight phases or in the whole flight envelope. Hence, it is common to designate different command variables to different flight phases or different regions of the flight envelope [71]. If those command variables chosen produce significantly different aircraft behavior and if command variable transition is implemented by a discrete switch, one would speak of control system modes and discrete mode transitions. The presence of modes adversely affects mental workload, since pilots need to be aware of the control system mode they are operating in. So-called mode confusions can act as a trigger for aircraft incidents and accidents [74]. Moreover, aircraft dynamics transitions are known to contribute to undesired pilot-aircraft oscillations that are described in detail in section 2.2.4. For optimum handling qualities, aircraft behavior should appear consistent to the pilot. By implementing a smooth blending between command variables, it is possible to make transitions unnoticeable. The pilot is relieved from keeping track of modes and mode transitions.

In the implementation of maneuver demand systems, it seems as if engineers had almost total freedom of how to shape an airplane's response to control inputs, as long as they respect the physical constraints of the plant. However, as soon as a human pilot needs to safely fly the aircraft, some more restrictions apply. These restrictions stem from human control capabilities on the one hand, as can be seen from later sections of this thesis, and from pilot training on the other hand, as the following paragraphs explain.

Pilots need training and they always will, even though efforts continue to minimize the amount of training required. During training, pilots acquire a certain understanding of how an airplane behaves. If they later are confronted with a behavior that is different from their expectations, they are surprised at least and deemed to produce a fatal accident at worst. Pilots usually gain the first couple of hours of flying experience in light airplanes with mechanical control systems. Only afterwards, they may transition to other airplanes with hydraulic or fly-by-wire control systems. Thus, the vast majority of airplanes exhibits more

or less the same behavior, which is that of conventional airplanes with mechanical control systems. Indeed, the same or very similar handling qualities requirements normally apply for any control system, be it reversible or irreversible. Providing similar handling qualities across an entire fleet of airplanes is Airbus' strategy to minimize the training effort required to transition from one airplane type to another [75]. This does not mean that more exotic control system configurations are impractical. Such configurations, however, require different initial training or a greater amount of familiarization. Although it is perfectly valid to argue that RPA operators and also BMI pilots could be specifically trained for the control system they use, it needs to be acknowledged that this solution would produce specialists than cannot easily transition to other control system types, including the widespread mechanical type. Not knowing how an airplane behaves without digital control augmentation also results in a reduced ability to cope with control system failures.

Considering its pivotal role for pilots, conventional airplane behavior and its implications on handling qualities need to be understood prior to flight control system design. According to [66], conventional behavior is essentially characterized by

- the initial reaction to a control input,
- the short-term pseudo steady-state behavior when a control input is constant and nonzero and
- the steady-state behavior after the control input is terminated.

For both the longitudinal and lateral-directional motion, these three characteristics can be read from the signal flow charts of Figure 2.3 and Figure 2.4, respectively. Equation (2.18) summarizes the conventional initial reaction to pitch (δ_η), roll (δ_ξ) and yaw (δ_ζ) control inputs, which in mechanical control systems are equivalent to elevator, aileron and rudder deflections. These control surface deflections generate moments, which are equivalent to angular accelerations.

$$\text{Initial reaction} \begin{cases} \delta_\eta \propto \dot{q} \\ \delta_\xi \propto \dot{p} \\ \delta_\zeta \propto \dot{r} \end{cases} \quad (2.18)$$

Equation (2.19) defines the conventional short-term pseudo steady-state behavior from the pilot's point of view when a control input is constant and nonzero. In the pitch axis, the control input is proportional to the resulting pitch rate, the change in angle of attack and, equivalently, in vertical load factor and flight path climb angle rate. Note that this is only valid in the short term, under the constant speed approximation. In the roll axis, the transfer function from aileron deflection to roll rate is a first-order lag, as evidenced by Figure 2.4. In the yaw axis, a constant control input generates a proportional angle of sideslip.

$$\text{Short-term pseudo steady-state behavior} \begin{cases} \delta_\eta \propto q, \alpha, n_z, \dot{\gamma} \\ \delta_\xi \propto p \\ \delta_\zeta \propto \beta \end{cases} \quad (2.19)$$

Finally, equations (2.20), (2.21) and (2.22) reveal the idealized conventional steady-state behavior after a control input is terminated. Simply put, the airplane stabilizes at a new flight path climb angle, a new bank angle and at zero sideslip, respectively.

$$\delta_{\eta} = 0 \quad \Rightarrow \quad \begin{cases} q, \alpha, n_z = 0 \\ \gamma = \text{const.} \end{cases} \quad (2.20)$$

$$\delta_{\xi} = 0 \quad \Rightarrow \quad \begin{cases} p = 0 \\ \Phi = \text{const.} \end{cases} \quad (2.21)$$

$$\delta_{\zeta} = 0 \quad \Rightarrow \quad \beta = 0 \quad (2.22)$$

A more vivid illustration of conventional airplane behavior, similar to that given in [73], is shown in Figure 2.5. In these MATLAB-generated time history plots, it can be seen how relevant variables of the longitudinal and lateral motion evolve during and after a pitch or roll control singlet.

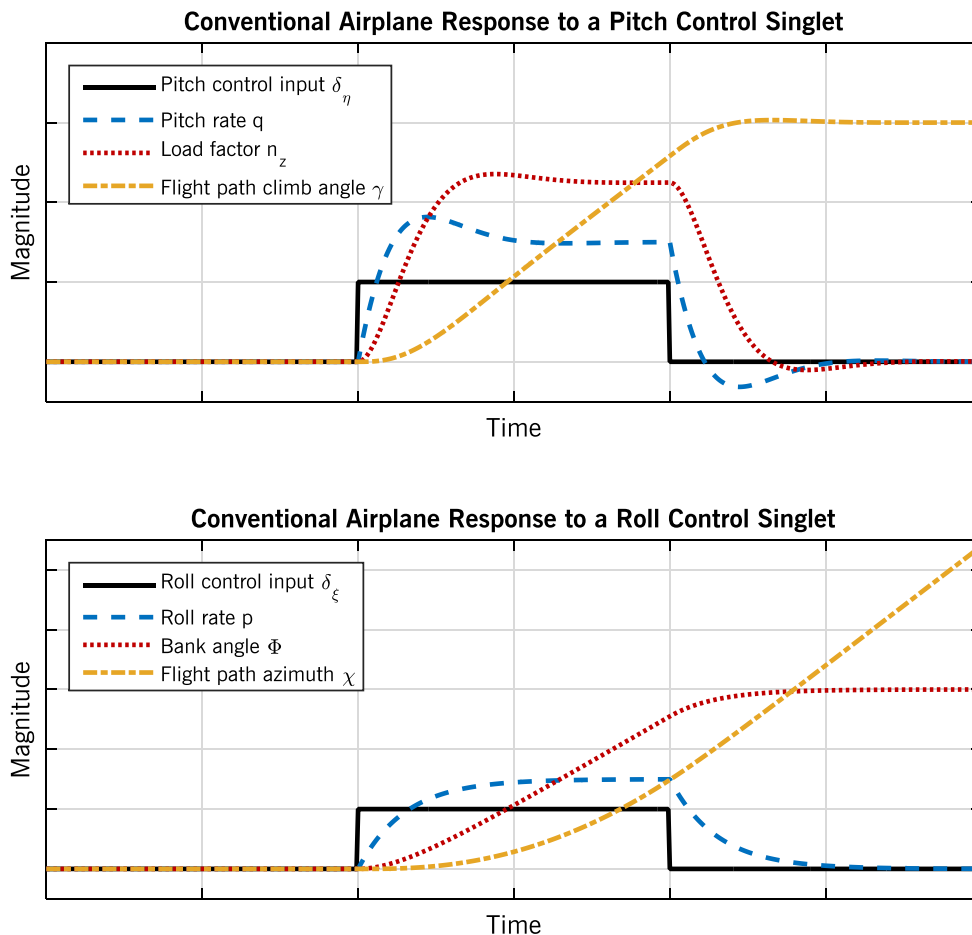


Figure 2.5 – Illustration of conventional airplane responses, as in [73]

It has to be stressed again that, like equations (2.19) and (2.20), these plots show an idealized, short-term behavior. For instance, a pitch control singlet will, in the long term, not lead to a persisting increase of the flight path climb angle, nor will in most airplanes the bank angle remain constant in the absence of lateral control inputs. To address the

sometimes rather counterintuitive long-term behavior of aircraft, suitable piloting strategies have been established. These strategies prescribe how to manage the short-term behavior to achieve a certain goal in the long term. It is shown in section 3.1.2 that this form of piloting can be seen as a cascade of control loops. The fact that the innermost loop always acts on the shortest time scale explains the importance of the (conventional) short-term dynamics described here.

Two exemplary piloting strategies for the long-term longitudinal airplane motion shall be presented here. When flying an airplane like the reference aircraft on the front side of the power curve, i.e., at velocities greater than the speed where minimum power is required for horizontal flight, vertical flight path is normally controlled by pitch control inputs, and speed is controlled by thrust control inputs. During operation on the back side of the power curve, however, flight path should be controlled by thrust and speed by pitch. This back side technique can also be applied during operation on the front side, but applying the front side technique on the back side is not recommended, because the effect of pitch control on vertical flight path is effectively reversed: a nose-up control input ultimately makes the airplane descend more steeply [76, 77]. The piloting technique of adjusting airplane attitude to obtain a desired change in flight path is also not practical in hypersonic flight, as noted in section 1.2. Indeed, the piloting technique employed needs to match the airplane dynamics. Similarly, a suitable flight control system design for flight control with large time delays and reduced sensory feedback has to be complemented by an appropriate piloting technique. In this regard, finding suitable methods of UAV control during takeoff and landing constitutes a great challenge [3], for which some ideas are presented in [78].

An airplane's long-term lateral behavior is mainly characterized, from a pilot's point of view, by its spiral stability. Positive spiral stability is the tendency of a banked airplane to return to wings level flight. As the safety benefit of this behavior is not significant, certification authorities generally permit even slightly negative spiral stability. To maintain a steady-state turn in an airplane with positive or negative spiral stability, the pilot needs to apply correcting lateral control inputs. Thus, from a handling perspective, neutral spiral stability is desirable, as no lateral control inputs are required during a turn. Turning flight is also characterized by the amount of turn compensation required. Turn compensation is the application of longitudinal control inputs in a turn to increase lift and thereby compensate the reduction of that part of lift counteracting gravity due to the tilted lift vector. Pilots need to perform turn compensation in all conventional airplanes, which is why it also constitutes a part of conventional airplane behavior. Maneuver demand systems, however, can relieve the pilot from compensating turns to some extent or even completely. The fact that less pilot inputs are required is an advantage in terms of handling qualities. However, while automatic turn compensation may remain unnoticed in small turns, it produces a noticeably unnatural behavior in steep turns: lateral control inputs produce longitudinal airplane reactions.

2.2.3 Handling Qualities Criteria and Requirements

It is evident from the previous sections that an aircraft's dynamic characteristics have enormous influence on its handling qualities. This is why control engineers, whose

perspective on aircraft handling is governed by plant dynamics, have been trying to identify those dynamic characteristics that promote good handling qualities. Various quantitative handling qualities criteria have been defined to assess or predict the handling qualities of a given aircraft or aircraft design. It has to be noted, however, that criteria suited for one case do not necessarily constitute a good model for another. This is not at all surprising, knowing that handling is intrinsically related to aircraft, mission and flight phase. The definition of flight phase and airplane categories is an attempt to account for these differences.

The problem of finding quantitative criteria starts with the problem of how to quantify handling qualities. Since they cannot be measured in a mathematical way [71], efforts were made to quantify pilot opinions. An established tool for quantitative handling qualities evaluation by pilots is the Cooper-Harper rating scale [58], ranging from 1 (excellent handling) to 10 (uncontrollable). Obviously, subjective pilot ratings vary as a function of behavior, distractions, fatigue and other factors [79]. This means that a good mean Cooper-Harper rating (CHR) indicates that the handling qualities are most probably adequate, but may also, with some probability, be deficient. Statistical methods may be used to estimate this probability.

The handbook MIL-HDBK-1797 [67], that also defines flight phase categories (cf. section 2.1.2), groups CHRs into the following three handling qualities levels:

- Level 1, “Satisfactory”, comprises CHR 1, 2 and 3. Handling qualities are clearly adequate for the mission flight phase. Desired performance is achievable with no more than minimal pilot compensation.
- Level 2, “Acceptable”, comprises CHR 4, 5 and 6. Handling qualities are adequate to accomplish the mission flight phase, but some increase in pilot workload or some degradation in mission effectiveness, or both, exists.
- Level 3, “Controllable”, comprises CHR 7, 8 and 9. Handling qualities are such that the aircraft can be controlled in the context of the mission flight phase, even though pilot workload is excessive or mission effectiveness is inadequate, or both. The pilot can transition from category A flight phase tasks to category B or C flight phases, and category B and C flight phase tasks can be completed.

Note that a CHR of 10, i.e., uncontrollable handling characteristics, is not covered by these levels. Handling qualities criteria usually relate certain quantitative aircraft characteristics to one of these three handling qualities levels. Hence, they often serve as a basis for quantitative requirements on new aircraft designs. The handbook MIL-HDBK-1797 in fact is a guideline for the definition of handling related requirements. An attempt to transfer this guideline to the domain of unmanned aviation resulted in a similar document [34], which specifically focuses on RPA as opposed to autonomously acting UAV. This first step as well as later approaches, such as dynamic scaling of handling qualities established for large, manned aircraft to smaller UAVs [35], neither take into account the reduced sensory feedback, nor do they address the issue of large time delays. The idea to tailor flying qualities to sensor requirements instead of human capabilities [1], on the other hand, is suitable mainly for UAVs that operate at high levels of autonomy and is therefore also not transferrable to the problem of this thesis.

Many existing handling qualities requirements are based on the well-known conventional aircraft behavior described in the previous section. This is partly due to the fact that the underlying handling qualities criteria were obtained in experiments with mechanical or hydraulic control systems. Today's digital flight control algorithms, however, usually introduce additional integrators and thereby increase the order of the aircraft dynamics apparent to the pilot. To apply the established criteria, especially those defined in the frequency domain, to such a higher-order flight control system, it is common to derive a low-order equivalent system (LOES), which is of the same order as the conventional airplane presented in section 2.2.1. In a LOES, higher-order system characteristics are represented by a so-called equivalent time delay. This time delay effectively lumps pure (signal processing) time delays with phase lags from additional integrators. This method can only be applied to reasonably classical designs [71]. Moreover, the differences between LOES and original higher-order system need to be smaller than the so-called maximum unnoticeable added dynamics [80], defined in the frequency domain.

With regard to the topic of this thesis, it is interesting to note that the U.S. Department of Defense's guidelines [67] only consider LOESs with an equivalent time delay of less than 0.25 s controllable. In other words, flight control systems with time delays as large as those considered in this thesis are deemed uncontrollable. The validity of the approach of grouping lags and pure delays in a single equivalent time delay, however, is much disputed, because the effects of lags and (relatively small) pure time delays on handling qualities are slightly different [71]. Moreover, it has been noted that the allowable time delay appears to be a function of the shape of the aircraft response following the initial delay time [81]. This suggests that flight control systems with more than 0.25 s time delay may indeed be controllable. Nonetheless, the maximum controllable time delay stated in [67] is a suitable reference that puts the time delays considered in this thesis into perspective.

Documents like MIL-HDBK-1797 are helpful in aircraft control system design, whether civil or military, especially because they provide guidance on how to obtain optimum handling. Apart from any requirements defined by the customer or the manufacturer itself, civil aircraft also have to comply with handling qualities requirements imposed by certifying authorities such as the European Aviation Safety Agency (EASA) or the U.S. Federal Aviation Administration (FAA) for certification. These regulations or specifications establish a certain minimum level of safety. This means that non-compliance with these requirements makes an aircraft unsafe to operate, whereas violations of more stringent customer requirements may merely compromise optimum mission performance.

In the example cases of RPA and BMI control, some handling qualities criteria and requirements that are well-established for onboard manual control are void or not applicable. These are notably those that aim at ensuring adequate vestibular or proprioceptive feedback. When such vestibular or proprioceptive feedback contributes to flight safety or good handling, this contribution needs to be adequately substituted. This is especially the case with proprioceptive feedback, as can be seen in section 3.1.1. Furthermore, existing standards, guidelines and requirements are insufficient [18], because, being designed for onboard manual control, they do not take into account the

particular challenges of RPA or BMI control, such as for example the excessive risk-taking behavior and the generally reduced situational awareness of RPA pilots.

2.2.4 Pilot-Induced Oscillations

One problem known to occur sometimes when a pilot closes the flight control loop are “sustained or uncontrollable oscillations resulting from the efforts of the pilot to control the aircraft” [67, p. 25]. These oscillations are therefore referred to as pilot-induced oscillations (PIOs), although the pilots are not to blame for this handling qualities deficiency. In fact, PIOs are a manifestation of an unstable or marginally stable closed-loop coupling of pilot and aircraft dynamics that may occur even if the aircraft itself is a stable system. The term PIO also covers biodynamic coupling phenomena like roll ratchet, where control inputs are involuntary (cf. section 3.1.1). Oscillations that are not considered PIOs include stick pumping during the flare maneuver, pitch bobble and those oscillations resulting from overcontrol when flying an unfamiliar airplane [71].

PIOs are characterized by high and possibly diverging amplitudes. As a consequence, they are quite dangerous and can cause fatal accidents. McRuer [82] proposes three categories of PIOs. Category I PIOs are essentially linear. They are characterized by a high open-loop system gain that causes a significant reduction of the phase margin. Category II PIOs are quasi-linear and involve control surface rate or position limiting. These nonlinearities introduce an amplitude-dependent lag. Category III PIOs fundamentally depend on nonlinear transitions in airplane or pilot dynamics. They may be triggered, for instance, by control system mode changes. In fact, any type of PIO is normally set off by a trigger event. Instead of evading trigger events, however, certain flight control system characteristics should be avoided to prevent PIOs.

Among the aircraft dynamic features that were found to contribute to PIOs are excessive lags, inadequate control sensitivities, control rate limiting and aircraft dynamics transitions [82]. In general, it can be said that these undesired characteristics cause aircraft and pilot dynamics to be mismatched or to easily become mismatched as pilot behavior varies. As can be seen in section 3.1.2 of this thesis, changes in pilot behavior are often accompanied by changes of the pilot-aircraft open-loop gain. Such changes cause the pilot-aircraft phase margin to vary or to be drastically reduced, especially when the phase curve is steep due to excessive phase lags. Since excessive phase lags cannot be prevented in the present case of flight control with large time delays, two corresponding handling qualities or PIO criteria are introduced in the following paragraphs.

One handling qualities criterion that accounts for the influence of excessive phase lags on PIO criticality is the Bandwidth Criterion [67]. It defines bandwidth ω_{BW} as the highest frequency at which the response of aircraft pitch attitude Θ to pilot control input (deflection δ_η or force, as applicable) has both a phase margin of at least 45° and a gain margin of at least 6 dB . In other words, this is the highest bandwidth achievable by the pilot-aircraft system without compromising stability [71]. Figure 2.6 shows an exemplary Bode plot, where $\omega_{BW,G}$ is the highest frequency with a gain margin of 6 dB and $\omega_{BW,P}$ is the highest frequency with a phase margin of 45° .

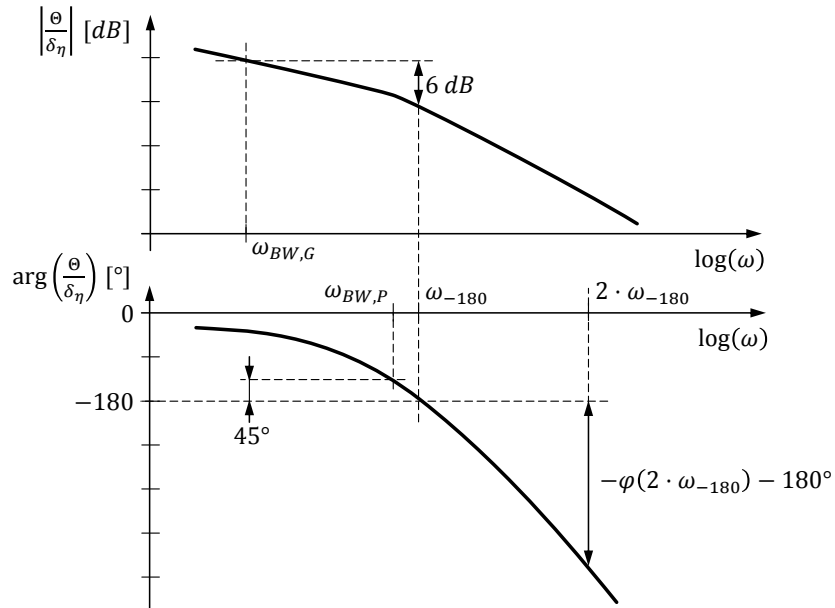


Figure 2.6 – Illustration of the Bandwidth Criterion's bandwidth and phase rate

Based on these two frequencies, bandwidth ω_{BW} is defined as in equation (2.23). The second parameter of this criterion is the time delay τ_{BW} defined by equation (2.24). It is a representation of the shape of the phase curve above the frequency ω_{-180} , i.e., the frequency where the phase angle attains -180° . Hence, the value of the numerator of equation (2.24) can also be read from Figure 2.6. Note that in equation (2.24) the unit of phase angles is $[\circ]$, the unit of frequencies is $[rad/s]$ and the unit of τ_{BW} is $[s]$.

$$\omega_{BW} = \min(\omega_{BW,G}, \omega_{BW,P}) \quad (2.23)$$

$$\tau_{BW} = \frac{-\varphi(2 \cdot \omega_{-180}) - 180^\circ}{2 \cdot \omega_{-180}} \cdot \frac{\pi}{180^\circ} [s] \quad (2.24)$$

The Bandwidth Criterion defines two diagrams, for Category A and C flight phases, respectively, that relate combinations of ω_{BW} and τ_{BW} to handling qualities levels. These diagrams are shown in Figure 2.7.

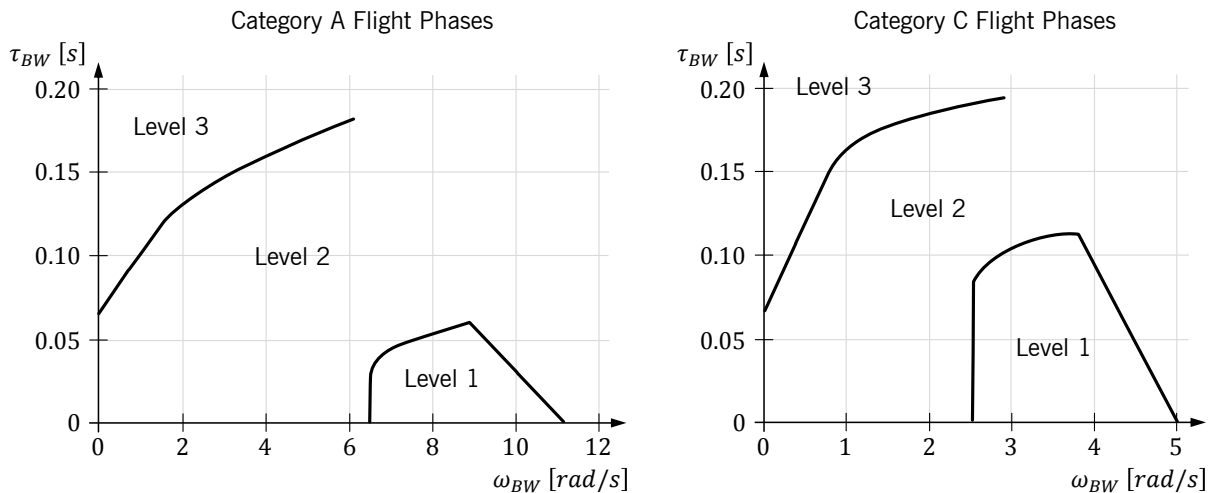


Figure 2.7 – Bandwidth Criterion diagrams of handling qualities levels, as in [67]

A third diagram for the Bandwidth Criterion has been proposed in [83]. It relates certain values of bandwidth and time delay to PIO susceptibility (Figure 2.8). Note that flight path bandwidth and pitch rate overshoot have been introduced as additional parameters.

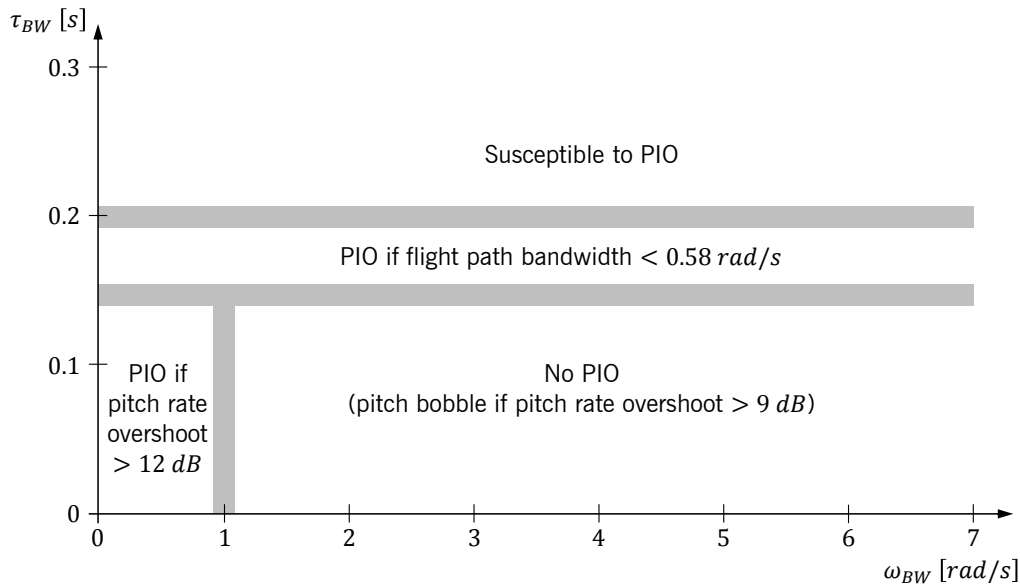


Figure 2.8 – Bandwidth Criterion diagram of PIO susceptibility, as in [83]

A similar criterion is the Average Phase Rate (APR) Criterion proposed by Gibson [71]. APR is defined as in equation (2.25) for the phase curve of the transfer function from inceptor input (force or deflection) to pitch attitude. Note that the numerator of equation (2.25) is the same as in equation (2.24), which is also visualized in Figure 2.6. Note that the unit of frequencies here is [Hz] and APR is thus measured in [°/Hz].

$$\text{APR} = \frac{-\varphi(2 \cdot \omega_{-180}) - 180^\circ}{\omega_{-180}} \cdot 2\pi \quad (2.25)$$

Again, a diagram is provided, relating combinations of ω_{-180} and APR to handling qualities levels. Figure 2.9 shows this diagram.

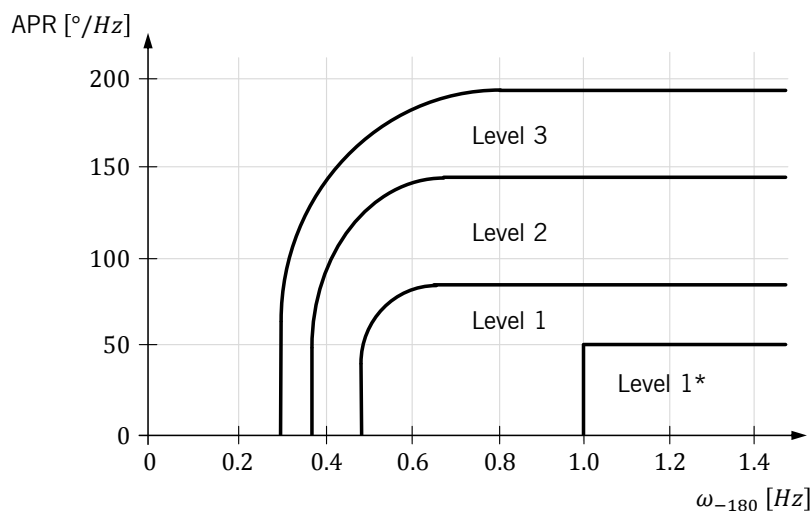


Figure 2.9 – APR Criterion diagram of handling qualities levels, as in [71]

Note that a level 1* region has been defined, which can be seen as an optimal or a design goal region.

It can be noted that the right sides of equations (2.24) and (2.25) look similar. Indeed, when combining these two equations, equation (2.26) results, evidencing a proportional relationship between APR and the time delay parameter τ_{BW} of the Bandwidth Criterion.

$$APR = 720^\circ \cdot \tau_{BW} \quad (2.26)$$

The fundamental differences between the two criteria lie in the second parameter, ω_{BW} or ω_{-180} , and in the diagrams defining desired and acceptable parameter combinations.

3 ANALYSIS AND MODELING OF HUMAN FLIGHT CONTROL BEHAVIOR

3.1 Pilot Modeling Basics and Quasi-Linear Behavior

During non-autonomous flight, the pilot constitutes an integral part of the flight control loop. Hence, efforts have been made for decades to model the dynamic behavior of pilots. Some of these efforts were driven by the need for a tool that predicts the handling qualities of an aircraft design without requiring simulator or even inflight experiments. The models that have been developed can be categorized into physiological models, sensory models and control-theoretic models. This section presents some of these models in the context of quasi-linear pilot behavior.

3.1.1 Physiological and Sensory Pilot Models

Physiological models describe how human physiology is involved in the generation of control inputs. In manual flight control, every control intention has to be translated to a body movement by the neuromuscular system. To describe this process, neuromuscular models of different levels of detail and complexity have been developed. Duane McRuer, one of the pioneers of pilot modeling, proposed a third-order linear transfer function as neuromuscular system description [84], which is given by equation (3.1).

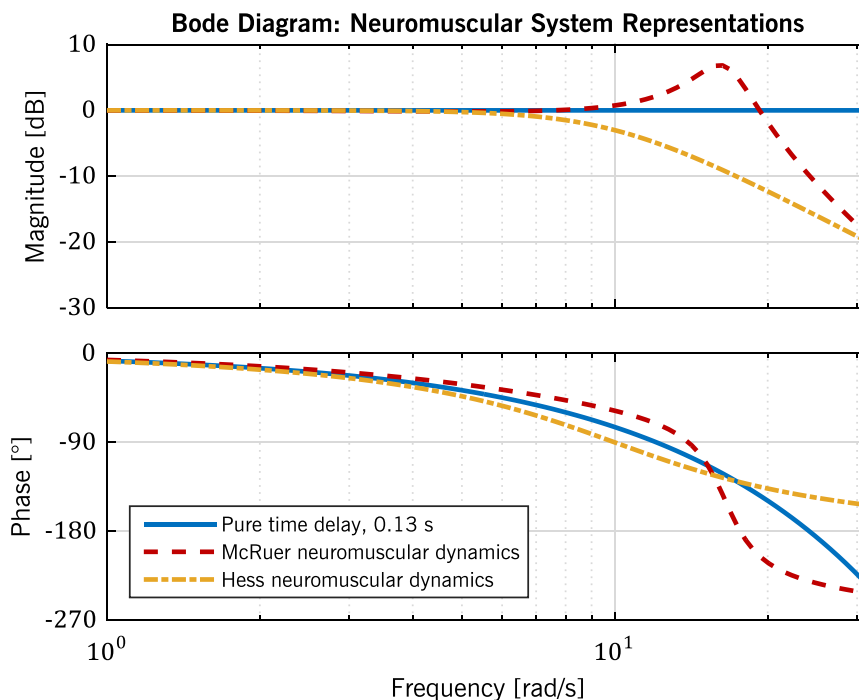
$$Y_{nm} = \frac{\omega_{nm}^2}{(1 + T_{nm}s)(s^2 + 2\zeta_{nm}\omega_{nm}s + \omega_{nm}^2)} \quad (3.1)$$

McRuer notes that this degree of model complexity is a minimum for physiological descriptions and is also often needed for the study of limb-manipulator system dynamics [85]. For other aspects of pilot-aircraft analyses, the details of the neuromuscular dynamics, which are pronounced mainly at higher frequencies, may be reduced. The result can be a first-order system or just a simple time delay [84, 85]. Ronald Hess, another early and leading pilot model researcher, models the neuromuscular system with a second-order transfer function [86]. Table 3.1 lists representative numerical values for the neuromuscular system parameters as stated in [84] and [86].

Table 3.1 – Values for parameters of the neuromuscular system transfer function

Source	T_{nm}	ω_{nm}	ζ_{nm}	System Order
McRuer [84]	0.1 s	16.5 rad/s	0.12	3 rd order
Hess [86]	0	10 rad/s	0.707	2 nd order

Based on equation (3.1) and the values from Table 3.1, Bode plots of the proposed neuromuscular transfer function can be generated using MATLAB. Figure 3.1 shows these plots along with a Bode plot of a 0.13 s pure time delay. It can be noted that all three transfer functions are in good accordance for frequencies well below 10 rad/s, which justifies the simplification to a single time delay for low frequencies mentioned above.


Figure 3.1 – Bode plot comparison of different neuromuscular system models

Apart from models of the neuromuscular system, biodynamic models constitute a type of physiological pilot models as well. They describe the human body's reaction to vehicle accelerations, which sometimes cause involuntary control inputs. One example is the roll ratchet phenomenon, where the roll acceleration following a roll control input is so high that the pilot's arm, due to its inertia, cannot follow the airplane's movement and produces a counteracting control input. The problem of biodynamic coupling occurs mainly in highly dynamic, manually controlled manned airplanes and is therefore not further discussed in this thesis.

Sensory pilot models reproduce the process of human perception of the vehicle's state. They can be used to analyze the pilot's ability to establish and maintain spatial orientation or to investigate spatial disorientation – a problem more likely to occur when sensory feedback is reduced, as is the case during RPA control [6]. Since the pilot's senses strongly influence flight control performance, it is not surprising that sensory pilot models are often

included in control-theoretic pilot models. Human perception is supported by various senses, which shall be categorized into different sensory channels. Although pilots rely on all their many senses to establish situational awareness in flight and no sensory channel is completely dispensable or easily replaceable, those sensory channels depicted in Figure 3.2 are more relevant to flight control than others. They are the visual, aural, proprioceptive and vestibular channel and they are discussed in detail in the next paragraphs.

In every channel, information is transmitted along several dimensions. For instance, two sounds are discriminable by loudness or pitch and two symbols on a visual display by shape, color, size or brightness. In human-machine interface design, both the sensory channel and the stimulus dimension can be used to code information [87]. By relying on several channels and different dimensions, more information can be displayed simultaneously. Depending on other parameters like operator attention and workload, not all of the information displayed may be properly perceived and processed.

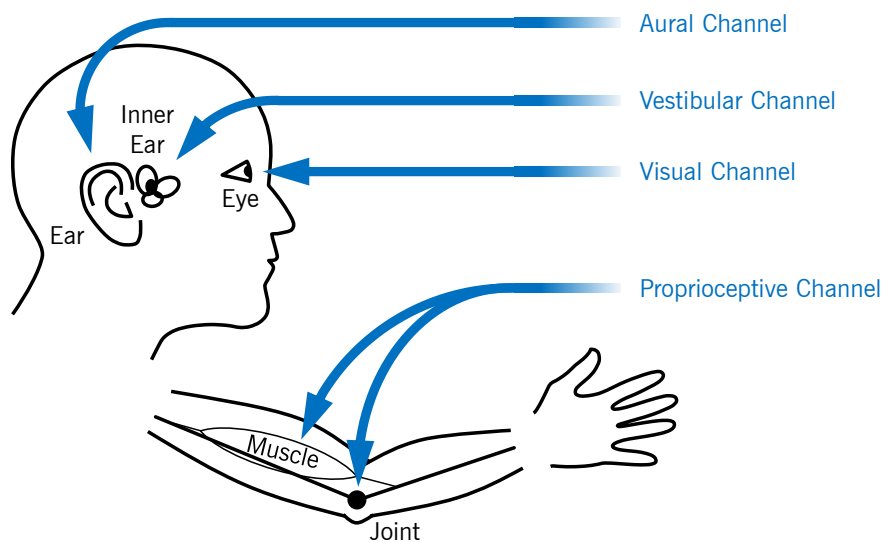


Figure 3.2 – Illustration of the sensory channels most relevant to flight control

The visual channel is very dominant in everyday life as well as during aircraft flight. Not only do pilots heavily rely on what they see, but most of the information they need is also presented visually. Visual cues can be found not only on cockpit instruments and displays, but also behind the windshield in the outside environment. The visual channel is so heavily used that pilots cannot perceive all the information presented within a reasonable amount of time. Therefore, they employ scanning techniques to gather visual information in a prioritized sequence. Coning of visual attention is obviously dangerous, as non-observed parameters may depart from a safe regime. When investigating the control-theoretic aspects of flight control, however, it is usually assumed that the pilot constantly monitors one certain parameter. The aim is to make this one task easily accomplishable, so that attention may indeed shift during actual airplane operations.

Due to the high relevance of the visual channel, models of visual perception are included in virtually every control-theoretic pilot model. The most basic model consists of a simple

gain. A more elaborate model, which is taken from Hess' structural pilot model [86], is shown in Figure 3.3. In this model, the visual perception of a parameter e is always affected by the time delay τ_2 . A switch, whose action is parameterized by the probability that it will be in the up position, separates two possible signal paths. Either the parameter e itself is perceived and multiplied by a gain K_e , or the rate of the parameter \dot{e} is derived and multiplied by a gain $K_{\dot{e}}$. Derivation of the parameter requires some additional time τ_1 . The time delay values proposed in [86] are 0.2 s for the sampling delay τ_1 and 0.075 s for the latency of the visual process τ_2 . Similar ideas have also been published in [88].

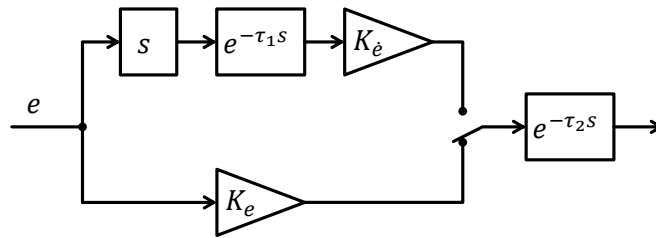


Figure 3.3 – A control-theoretic model for visual perception, derived from [86]

The aural channel, too, is heavily used in aviation. Pilots not only verbally communicate with air traffic controllers or with each other, they also hear annunciation and warning sounds and pay close attention to any change in the background noise, which might indicate a system malfunction. In military aviation, aural signals are extensively emitted by aircraft subsystems like the radar warning receiver, which indicates foreign radar sources. Gliders usually feature an aural indication of vertical speed or change in total energy, which consists of beeping sounds of varying pitch and pattern frequency. In the absence of such an indication, pilots can judge vertical speed from changes in ambient sound caused by air pressure changes [76]. This information is not used for pitch control, but to identify locations where updrafts can be used to gain energy. Aural cues for flight control are much rarer and so are control-theoretic models of aural perception. However, the simple model of visual perception given above (Figure 3.3) could also be applied to aural and tactile cues [86].

The vestibular system of the human inner ear senses linear and angular accelerations with the otoliths and the semicircular canals, respectively. Much like during inertial navigation, sensations from the vestibular system can be used to determine current linear and angular velocity, position and attitude. However, vestibular cues perceived in an aircraft can be extremely misleading, since the human vestibular system is only designed for ground operations like walking around and climbing a tree once in a while. Judging attitude or even position only from vestibular cues is practically impossible, as any passenger of a large transport airplane may notice when not seated near a window. Moreover, most sensory illusions in aviation involve the vestibular system, so one might guess that the absence of vestibular cues is not only tolerable, but even desirable. This is, however, not at all the case. The vestibular system provides valuable sensory cues to the pilot, increasing his situational awareness and the feeling of shared fate. A vivid example of how pilots rely on the sensation of vertical accelerations to judge approach speed is given in [76]. The same change in stick deflection and hence angle of attack produces different vertical accelerations at different airspeeds (cf. Figure 2.3). Instead of visually reading

their airspeed from an instrument, pilots can therefore feel for their airspeed by making small stick deflections. The perception of vertical load factor, which is required for this strategy, involves not only the vestibular system, but also the tactile feedback channel that is discussed at the end of this section.

Proprioceptive feedback plays an important role in human-machine interaction and especially in manual flight control. Proprioception is the sense of the relative position of body parts and the forces applied by muscles [40]. It enables the pilot to feel inceptor displacements and forces. These displacements and forces constitute crucial cues on aircraft behavior and thus contribute immensely to the pilot's situational awareness [73]. Proprioceptive cues from the inceptor are felt almost immediately when a control input is made, whereas any other aircraft reaction is slightly delayed due to the physical low-pass characteristics of aircraft and control system (cf. section 2.2.1). This explains why a proprioceptive feedback loop constitutes the innermost loop of some of the control-theoretic pilot models.

In airplanes with mechanical control systems, static stability of the airframe, which is the tendency of an airplane to return to pitch equilibrium after a disturbance in angle of attack, results in speed stability. An airplane is said to exhibit positive stick fixed/free speed stability if increasingly forward inceptor displacement/force is required to increase speed from trim speed, or to maintain level flight as trim speed increases. In aircraft with powered controls, the control surfaces are not free to float when the inceptor is released and thus, stick fixed and stick free speed stability are equal. A direct result of positive speed stability is the phugoid motion, which due to its low frequency is readily and naturally compensated by pilots already on their first flight. Many pilots therefore have never experienced the phugoid motion. Some fly-by-wire airplanes, including most Airbus types, provide neutral speed stability over a wide range of the flight envelope, thus suppressing the phugoid. Pilots are thereby relieved from generating corrective control inputs. This directly corresponds to an improvement in handling qualities. However, when approaching the flight envelope limits in an aircraft with neutral speed stability, important proprioceptive cues are missing: it is possible to exceed minimum or maximum speed without a change in control force or displacement.

In some airplanes that exhibit neutral speed stability in normal flight regimes, positive speed stability is introduced near the envelope borders, so that increasing force and displacement are necessary to approach or even transgress the limits. Another way to deal with this problem is to implement strong protections that actively prevent the pilot from exceeding envelope limits. The 'natural' feeling of speed stability, however, presents more intuitive cues to the pilot. The actions of a protection mechanism may not be transparent to the pilot and confusions may arise. Protection mechanisms may also be combined with proprioceptive cues. Stall protection, for example, is sometimes implemented in the form of a so-called stick pusher. Upon activation, this device generates a forward force on the inceptor, urging the pilot to make a nose-down control input. However, pilots often do the exact opposite upon their first encounter with a stick pusher event. Instinctively, they resist the force and pull the inceptor [89]. This is a vivid example for confusing or mismatched protection mechanisms or, more generally, aircraft dynamics.

Another airplane characteristic related to proprioceptive cues in flight is maneuver stability. Its definition is similar to that of speed stability. An airplane exhibits positive stick fixed/free maneuver stability if increasingly aft longitudinal inceptor displacement/force is required to increase the vertical load factor n_z . Stick free maneuver stability is also known by the name of “stick force per g”. In conventional airplanes with unpowered controls, its value varies little across the flight envelope [79]. In the case of powered controls, again, the distinction between stick fixed and stick free cannot be made. It is easy to imagine that in airplanes with low stick force per g, pilots can generate high load factors with very little physical effort. This excessive sensitivity and tendency to exceed the limit load factor is obviously undesired. High values of stick free maneuver stability, on the other hand, may lead to exaggerated physical demands on the pilot.

The final example of a proprioceptive cue in flight control is inceptor damping. Every control system has physical limits in actuation rate. Driving one or more control surfaces into their rate limit is a known cause for PIOs. (Remember McRuer’s definition of Category II PIOs presented in section 2.2.4.) Digital flight control systems usually prevent the actual control surface rate limit from being reached, but this only moves the limit to the digital control algorithms. Other physical constraints may further reduce maximum maneuverability. For instance, if the lateral controller performs feedback control of the bank angle Φ , this bank angle control loop has a certain bandwidth. If the lateral command variable is roll rate p , from which a command filter generates the bank angle reference for the Φ loop, care must be taken to prevent pilot inputs that exceed the bandwidth of the Φ controller, as the phase margin would drop and a PIO would be likely to develop. A very effective way to prevent control inputs beyond a given frequency is to introduce appropriate damping to the inceptor. From the pilot’s point of view, the inceptor damping makes the maximum actuation rates or the maximum aircraft maneuverability perceivable in the proprioceptive channel, which is why it can also be seen as a very intuitive PIO prevention scheme.

There is one sensory feedback channel that is still rarely employed for display design in aviation and therefore offers the possibility to present more information or to substitute other channels: the tactile channel. Tactile perception is the (passive) impression of touch or, more precisely, pressure and vibration. It needs to be distinguished from haptic perception, which is characterized by active exploration. A prominent example of tactile feedback in aviation is the inceptor vibration during low-speed buffeting. When airplanes approach stall and the airflow around the wings starts to separate, turbulent airflow often hits the elevator. With a reversible control system, these turbulences can be felt as vibrations in the inceptor that effectively act as a stall warning. In irreversible control systems, artificial vibrations of what is called a stick shaker are sometimes employed as a surrogate. Another sensation that can be considered a tactile cue is the feeling of being pushed down into the seat at higher load factors and of being lifted up at lower vertical load factors. In this case, tactile feedback enhances the perceptions of the vestibular system. Similarly, the pressure felt when applying a force to a control stick or yoke enhances the proprioceptive feedback perceived.

On top of these common tactile cues, tactile displays can be implemented to support flight control, flight guidance or other tasks. A tactile display is made up of several tactile actuators, so-called tactors, placed on the user's body. Tactors come in a variety of forms and sizes and rely on electrical or, more often, electro-mechanical and mechanical principles [51]. Examples include rotating eccentric masses that produce vibrations, and pneumatic tubes that exert pressure. Information can be coded by location, intensity, duration or pattern of tactile cues. Several studies have shown the potential of tactile displays for flight control [47–50]. An overview over these studies is provided in section 4.4. Finally, it has to be noted that even if the tactile channel can be used for additional information throughput, its capacity is limited as well. Effects of tactile clutter have been observed and reported for example in [49].

3.1.2 Linear Control-Theoretic Models

Control-theoretic models model the pilot as a feedback controller. They often include (simple) sensory or biodynamic models, such as the neuromuscular transfer function mentioned above in equation (3.1). The general control behavior of pilots in flight path tracking tasks can be described by Gibson's generic, dual-loop control-theoretic model [71], shown in Figure 3.4. It illustrates the piloting technique usually employed (on the front side of the power curve), which is to adjust the aircraft attitude such that a desired change in flight path results (cf. section 2.2.2). This technique is motivated by the fact that in most cases pilots can easily sense the vehicle's attitude, but most of the time need to rely on aircraft instruments to obtain information on the flight path. Moreover, attitude reactions to control inputs are more immediate than flight path reactions (cf. section 2.2.1), which facilitates closed-loop control. One challenge of flight without outside visibility is that aircraft attitude as well has to be determined with the help of instruments. This causes an increase in mental workload. When attitude tracking is performed instead of flight path control, the outer flight path loop shown in Figure 3.4 obviously is broken.

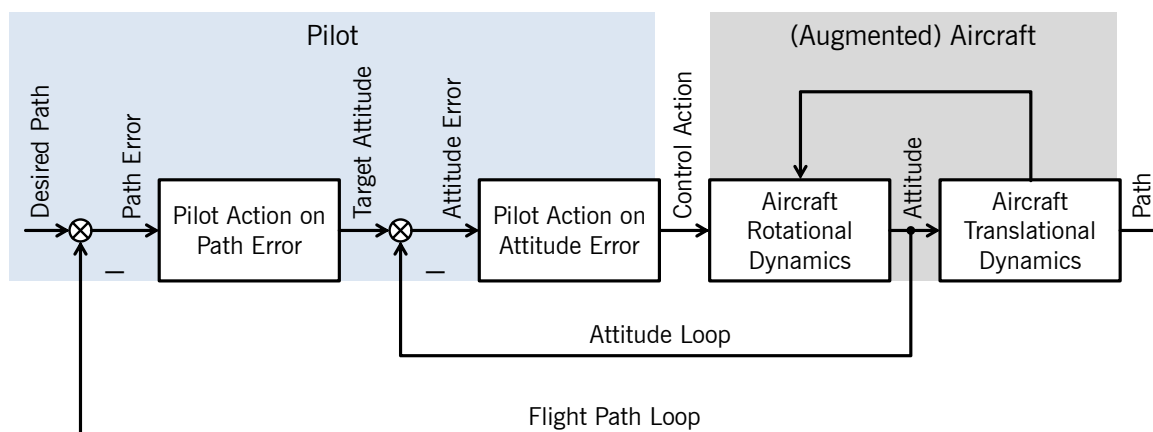


Figure 3.4 – Basic dual-loop pilot model, adapted from Gibson [71]

As already noted in section 2.2.2, flight path changes are not always accomplished by adopting a new attitude, but sometimes by varying thrust. Gibson's basic dual-loop model cannot be applied in this case. There are other pilot models relying on cascaded control

loops that could be applied in this case [90], but instead, a more detailed look shall be taken at single-loop models, since they constitute the basis for any multi-loop model.

Most control-theoretic models describe compensatory tracking, where the pilot only perceives or only focuses on the error e between tracking target u and actual system output y , as illustrated by Figure 3.5. Other forms of tracking are pursuit tracking, where the operator can distinguish between system input and system output and can therefore also include a feedforward element, and pre-cognitive tracking, where the pilot performs open-loop control, based on a high familiarity with the controlled system or with the system inputs [91]. Most pilot models describe compensatory tracking, which is justified by the fact that the other strategies also comprise it at least to some extent. Even during pre-cognitive tracking, occasional loop closures are required to eliminate residual errors. Operational flying tasks, on the other hand, rarely are purely compensatory and usually enable pilots to perform pursuit or pre-cognitive tracking.

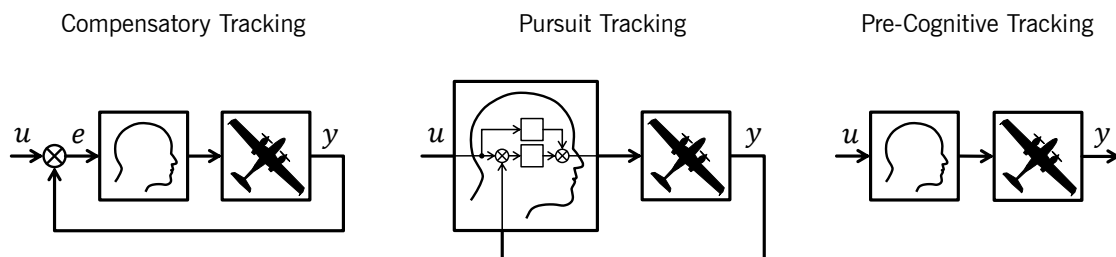


Figure 3.5 – Illustration of different tracking strategies

A very basic compensatory pilot-aircraft model that has been defined by McRuer in 1965 is the Crossover Model [84]. In his experiments, McRuer found that human operators generally adapt their behavior such that the open loop of human and machine could be described by equation (3.2) around the crossover frequency ω_c . Here, Y_p and Y_a are the transfer functions of the pilot and the aircraft, respectively. K is a simple gain, which incidentally equals ω_c , and τ is the time delay introduced by the human pilot.

$$Y_p \cdot Y_a \approx \frac{K}{s} e^{-\tau s} \quad (3.2)$$

The crossover frequency is the lowest frequency at which the open-loop gain drops below 0 dB . During closed-loop control, it becomes the pilot-vehicle system bandwidth, i.e., the upper limit frequency until which the closed pilot-aircraft loop can follow a given task. High-precision tasks require a high pilot-aircraft bandwidth and therefore a high ω_c . A low crossover frequency, on the other hand, indicates that the closed loop will be sluggish.

In terms of handling qualities, it was found that pilots experience lowest workload when they can act as a gain only [71]. By inserting this information into equation (3.2), the optimum aircraft transfer function is easily obtained. As shown in equation (3.3), it is a simple integrator. Systems that follow this optimum transfer function, which produces a slope of -20 dB per decade in the Bode magnitude plot, are often said to exhibit “ K/s -like dynamics” or “integrator-like behavior.”

$$Y_{a,opt} = \frac{K_a}{s} \quad (3.3)$$

Since the aircraft gain K_a can be assumed constant during short-term maneuvering, ω_c only depends on the pilot gain. Pilots are indeed said to be “high-gain” or “low-gain”, depending on their aggressiveness in control tasks. While high-gain pilots may achieve better performance, they also risk to destabilize the system in a PIO, unless they reduce their gain as soon as they recognize diminishing stability margins. The best PIO recovery technique is to reduce the gain momentarily to zero, i.e., to open the loop by letting go of the inceptor.

It needs to be stressed that the Crossover Model is only valid in the region around open-loop crossover. The open-loop transfer function may be very different from equation (3.2) in other frequency regions. Similarly, if the airplane transfer function differs from equation (3.3) in those other frequency regions, the airplane may still exhibit good handling qualities.

A more descriptive linear pilot model has been proposed by Neal and Smith [92]. The so-called Neal-Smith model, given by equation (3.4), explicitly contains the pilot’s abilities to correct the error (gain K_p) and to quicken or smoothen the system response (lead T_{p1} and lag T_{p2}). It also accounts for the delay introduced by perception, decision and actuation.

$$Y_p = K_p \frac{T_{p1}s + 1}{T_{p2}s + 1} e^{-0.3s} \quad (3.4)$$

The model is designed for compensatory pitch attitude tracking tasks with conventional airplane dynamics. Its applicability to other tasks and other dynamic characteristics is therefore limited. The three model parameters K_p , T_{p1} and T_{p2} are tuned according to the following two rules.

- The closed loop (pilot and aircraft) must have a bandwidth ω_{-90} greater than 1.5 rad/s for flight phase categories B and C and 2.5 rad/s for landing. Bandwidth ω_{-90} is defined as the frequency where the phase angle first reaches -90° (cf. Figure 3.6).
- Closed-loop droop may not exceed 3 dB . Droop is the low-frequency drop in system gain (cf. Figure 3.6). This means that the closed-loop Bode magnitude plot may not cross the -3 dB line before the first resonance peak.

No limits are imposed on the model parameters. The model is intimately connected with a handling qualities criterion. The Neal-Smith Criterion’s parameters are the magnitude of the resonance (cf. Figure 3.6) and the pilot compensation defined by equation (3.5).

$$\varphi_{pc} = \arg\left(\frac{T_{p1}j\omega_{-90} + 1}{T_{p2}j\omega_{-90} + 1}\right) \quad (3.5)$$

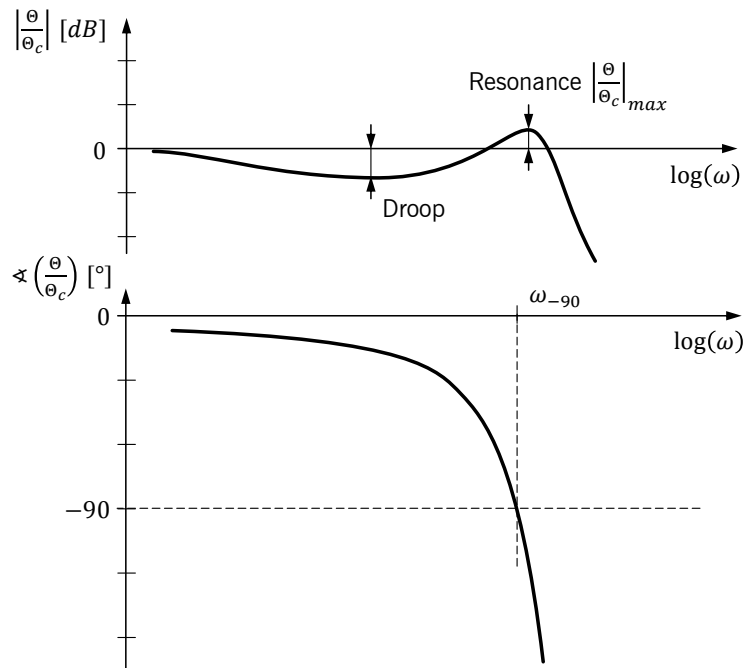


Figure 3.6 – Illustration of some of the Neal-Smith Criterion parameters, as in [92]

Figure 3.7 relates combinations of resonance and pilot compensation to handling qualities levels. It can be noted that small (absolute) values of both parameters are favorable.

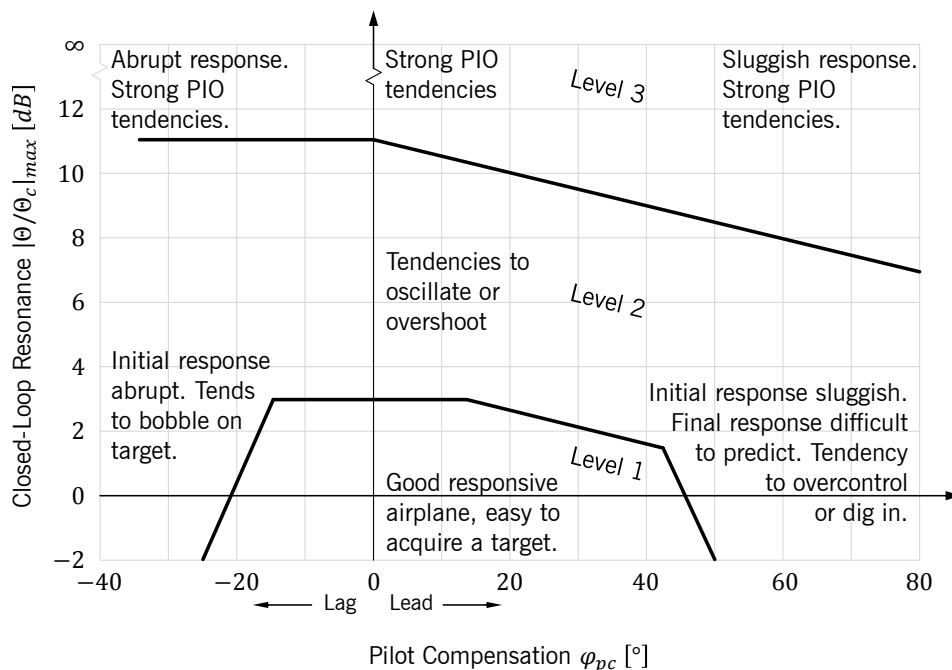


Figure 3.7 – Neal-Smith Criterion diagram of handling qualities levels, as in [92]

Several modifications and extensions of the Neal-Smith pilot model and criterion have been proposed [67, 93], a further analysis of which is left out as it would not provide more insight to the problem of this thesis. Instead, another pilot model shall be discussed. While the previously presented models approach the problem top-down, Hess’s structural pilot model can be considered a bottom-up approach. Each relevant component of the

human pilot – most notably each relevant sensory channel – also constitutes a distinct part in the model. A first version of the model has been presented in [86]. The result of a later revision of the model [94] is shown in Figure 3.8.

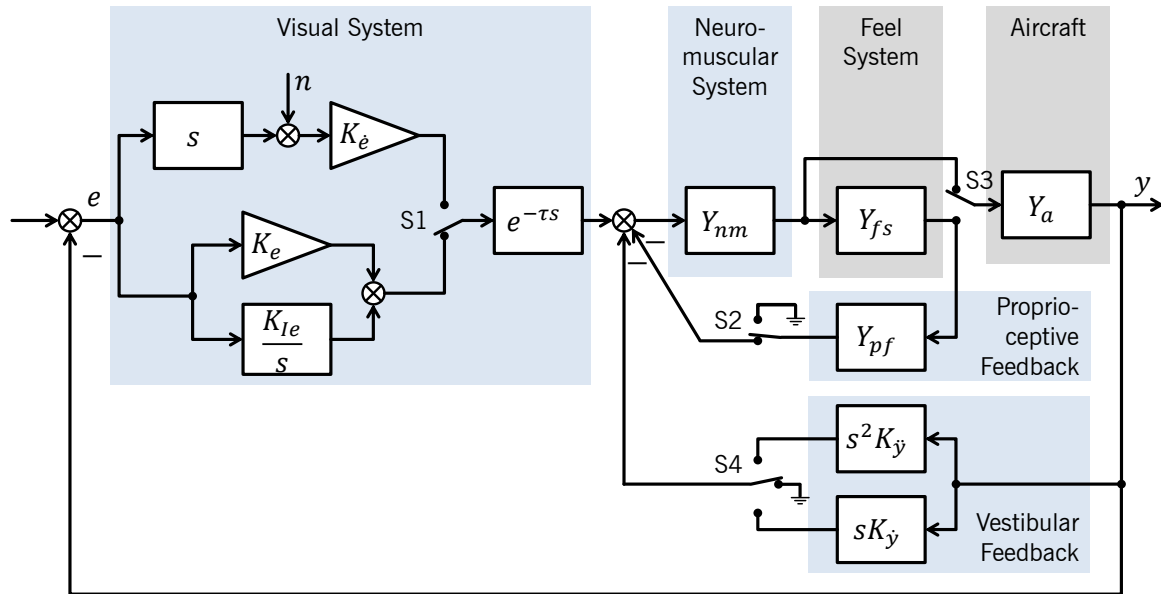


Figure 3.8 – Hess' revised structural model as in [94]

The model comprises several distinctive features. It explicitly contains the feel system (cf. section 2.2.2) and thereby acknowledges the importance of proprioceptive feedback from the inceptor. With the associated switch S3 in the up-position, the control system is force-sensing, and with the switch in the down-position, the control system is displacement-sensing. The innermost control loop indeed relies on proprioceptive feedback. It is the fastest loop and its characteristics are determined by the feel system and the vehicle dynamics. The form of Y_{pf} is chosen such that the open loop from e to y , with S1 and S2 in the down position and $K_{Ie} = K_{\dot{y}} = K_{\ddot{y}} = 0$, follows the dictates of the Crossover Model. In other words, Y_{pf} needs to satisfy equation (3.6) for $\omega \approx \omega_c$ and K arbitrary [94]. Y_{pf} can therefore be interpreted as an internal model of the controlled vehicle dynamics.

$$\frac{Y_a(j\omega)}{Y_{pf}(j\omega)} \approx \frac{K}{j\omega} \quad (3.6)$$

Hess furthermore proposes a vestibular feedback loop that allows either rate or acceleration cues to be used. The visual system part of the model is similar to that of Figure 3.3. Both the error and the error rate can be sensed, but instead of introducing an additional delay in the error rate perception path, a noise is added here. The integrator in the visual system describes the ability to accomplish low-frequency trim compensation. Switches S1 and S2 operate in unison, with the down position being the nominal case. Along with this revised structural pilot model, Hess proposes associated criteria to predict handling qualities and PIO criticality of a given configuration. Those criteria, for which he assumes $K_{Ie} = K_{\dot{y}} = K_{\ddot{y}} = 0$, are not discussed here, because they are ineffective in

treating control systems with large time delays. In fact, the tuning process of the model parameters does not take into account time delays, even if they are substituted by a Padé approximation. Thus, with the time delay values considered in this thesis, the closed loop of Figure 3.8 is normally unstable.

3.2 Time Delays and Existing Models of Nonlinear Behavior

3.2.1 The Effects of Large Time Delays

A first analysis of the effect of large time delays can be done using the Crossover Model or, in other words, by assuming that the pilot-aircraft open loop satisfies equation (3.2) around the crossover frequency. If the airplane exhibits optimal K/s dynamics and the pilot acts as a simple gain, the maximum stable crossover frequency for a given time delay (pilot τ_p plus aircraft τ_a) is equal to the gain margin of the system given in equation (3.7).

$$Y_p \cdot Y_a = \frac{1}{s} e^{-(\tau_p + \tau_a)s} \quad (3.7)$$

For instance, the minimum aircraft time delay considered in this thesis (1 s) combined with a pilot time delay of 0.2 s, which is at the low end of the time delay estimations made in established pilot models [86, 92, 94], results in a maximum attainable crossover frequency of 1.31 rad/s. Figure 3.9 shows how the maximum crossover frequency evolves with increasing combined pilot-aircraft time delay.

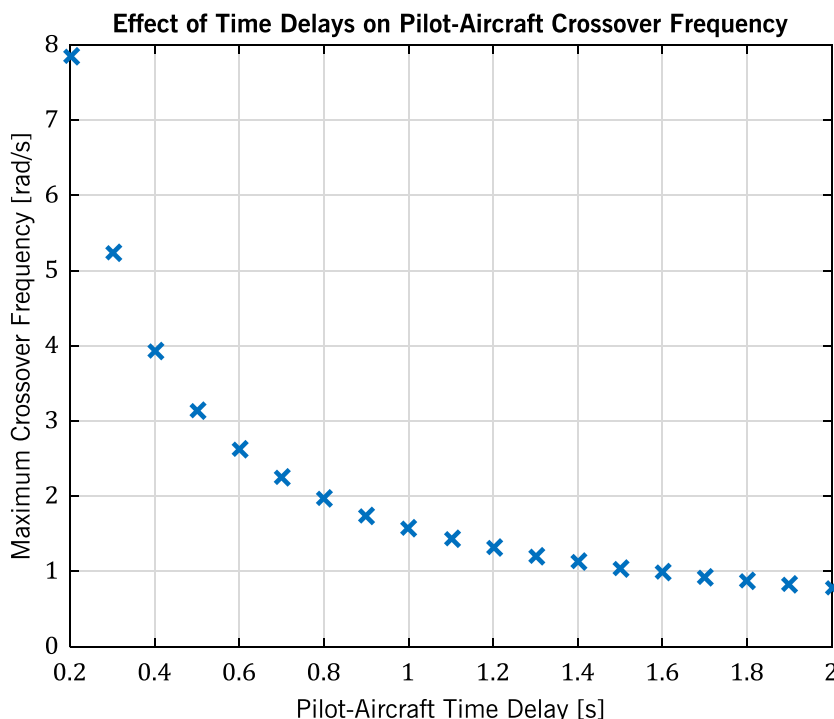


Figure 3.9 – Crossover Model evaluation for different time delays

As time delays increase, the maximum crossover frequency decreases. To counter this so-called crossover frequency regression, pilots could introduce lead, even though this is not what the Crossover Model postulates. Figure 3.10 shows the bode plot of a K/s aircraft

with 1 s time delay along with the open loop bode plots of this aircraft model combined with two different pilot models, each with a time delay of 0.2 s. A simple gain pilot achieves a maximum crossover frequency of 1.31 rad/s, as already determined above, whereas the exemplary lead-lag pilot described by equation (3.8) pushes the crossover frequency to 2.07 rad/s.

$$Y_p = 0.915 \frac{s + 1}{0.1 \cdot s + 1} e^{-0.2 \cdot s} \quad (3.8)$$

Note that only the open loop of simple gain pilot and aircraft follows the Crossover Model in that it can be approximated by an integrator in the crossover region. The slope of the magnitude curve is -20 dB per decade. When the pilot introduces lead, the magnitude curve is flattened, which introduces a new problem. Even a slight increase in pilot gain, which is quite probable due to the sluggish system response resulting from the generally low crossover frequency, causes a relatively dramatic increase of the crossover frequency. At the same time, the phase margin rapidly decreases, which results in a risk of PIOs.

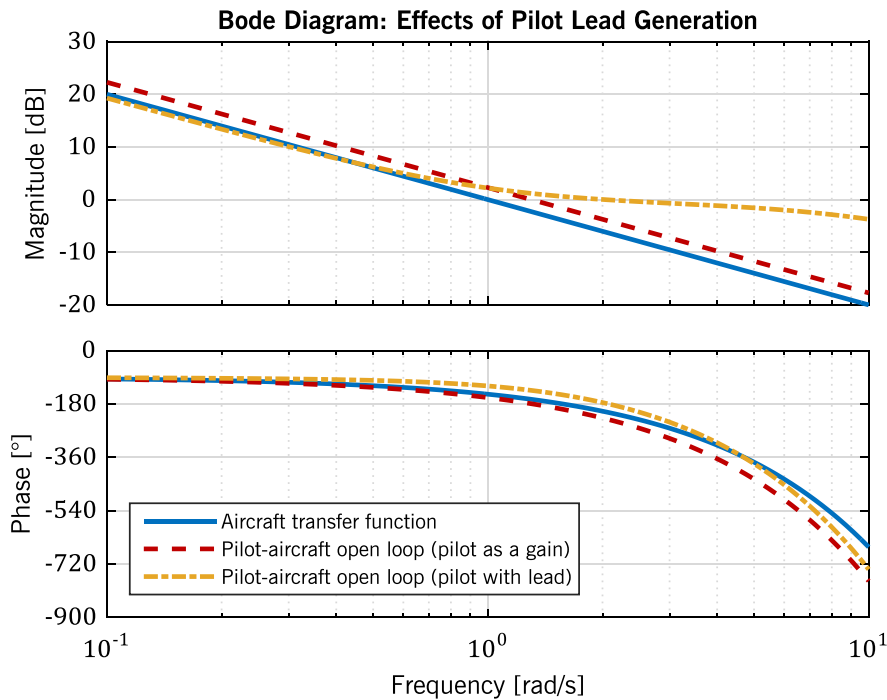


Figure 3.10 – Bode plot comparison of simple gain pilot and lead-lag pilot

These two effects – excessive pilot lead generation and regression of the pilot-aircraft open-loop crossover frequency – have been observed by Hess in his experiments on the effects of time delays in manual control [95]. The measured values of pilot-aircraft bandwidth were considerably smaller than those derived here from the Crossover Model (cf. Figure 3.9), but they show the same trend. Hess also found that a controlled element with K/s dynamics and time delay is compensated much like K/s^2 dynamics without time delay, resulting in a magnitude curve flattened in the crossover region. Since this is not what the Crossover Model predicts, it is evident that the Crossover Model is not valid for control systems with large time delays, even though it well predicts the crossover frequency

regression. It is interesting to note that the largest time delay Hess used in these experiments was 0.381 s. This value is far smaller than the delays sometimes found in RPA or BMI control, but it already makes some of the adverse effects of time delays apparent.

Most pilot models do not take into account pure time delays that are present in the controlled system. This means that the pilot model parameters determined for a certain aircraft do not vary when time delays are introduced. Such pilot models, like the Crossover Model and Hess' (revised) structural model, are therefore only valid for systems with negligible time delay. The delays considered here, however, are not at all negligible, which is why those pilot models and the handling qualities criteria derived from them are not suited for the present analysis. One exception is the Neal-Smith pilot model. Again considering a simple integrator with 1 s delay as controlled system, it is possible to achieve the desired Neal-Smith bandwidth ω_{-90} of 1.5 rad/s (cf. section 3.1.2) with the pilot transfer function of equation (3.9).

$$Y_p = 0.39 \frac{2s + 1}{0.15s + 1} e^{-0.3s} \quad (3.9)$$

It is no surprise that a considerable amount of lead is required. The pilot compensation as defined by equation (3.5) amounts to 54.9°. The peak gain of the closed loop is 10.5 dB. According to Figure 3.7, the system exhibits Level 3 handling qualities with a sluggish system response that is prone to PIO. Note that in this example, only the minimum Neal-Smith bandwidth has been achieved. Achieving higher bandwidths such as the 2.5 rad/s imposed for the landing task would require even more lead.

The high PIO risk caused by large time delays is also evidenced when applying Gibson's APR Criterion to an exemplary aircraft transfer function that may comprise one integrator, but no leads or lags. For such an aircraft, the phase lag can be written as in equation (3.10).

$$\varphi(\omega) = (k - \omega \cdot \tau_a) \cdot \frac{180^\circ}{\pi} \quad (3.10)$$

$$k = \begin{cases} 0 & \text{for proportional aircraft} \\ -\pi/2 & \text{for aircraft with integrator} \end{cases}$$

The APR is a function of the shape of the phase curve. Equation (3.11) shows that for the considered aircraft model, APR only depends on the time delay.

$$\begin{aligned} \text{APR} &= \frac{\varphi(\omega_{-180}) - \varphi(2\omega_{-180})}{\omega_{-180}} \cdot 2\pi \\ &= \frac{(k - \omega_{-180}\tau_a) - (k - 2\omega_{-180}\tau_a)}{\omega_{-180}} \cdot \frac{180^\circ}{\pi} \cdot 2\pi \\ &= \tau_a \cdot 360^\circ \end{aligned} \quad (3.11)$$

One second of time delay results in an APR of 360°/Hz. This value is off the chart given in Figure 2.9. From equations (3.11) and (2.26), the following equation (3.12) can be

derived for the time delay parameter τ_{BW} specified by the Bandwidth Criterion. Again, the values resulting from the time delays under consideration are far off the charts, both in terms of handling qualities levels (Figure 2.7) and PIO susceptibility (Figure 2.8).

$$\tau_{BW} = 0.5 \cdot \tau_a \tag{3.12}$$

The preceding analyses all assume a pure K/s airplane behavior, which constitutes an ideal best-case example. Real airplanes have additional dynamics, including additional lags that further deteriorate the situation. Based on the results above, an airplane or RPAS with at least 1 s time delay must be considered uncontrollable. This is probably the case if one would try to control such an RPAS the same way as a manned airplane, but human pilots being adaptive, they have strategies to cope with time delays.

3.2.2 Highly Nonlinear Pilot Behavior

The Bandwidth Criterion and Hess' structural models well describe quasi-linear pilot behavior. However, when the controlled element dynamics significantly differ from the first-order K/s optimum, human control behavior can be highly nonlinear. For instance, Young and Meiry [96] observed a pulse-like control behavior in control experiments with higher-order systems such as a double-integrator with lag. This behavior is characterized by rapid movements of the control inceptor to a certain deflection, where it is held for a variable amount of time, followed by another fast movement back to the neutral position. Figure 3.11 shows a time history plot of the control activity observed.

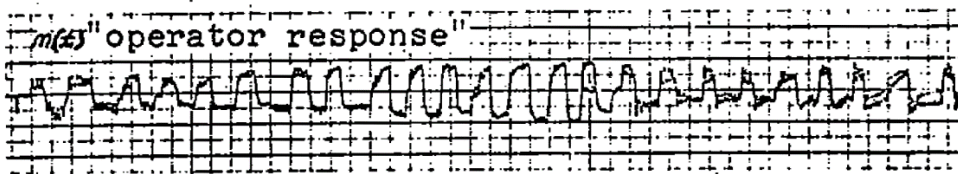


Figure 3.11 – Time history plot of pulse-like control activity from [96]

The authors attributed this pulse-like operator behavior to the mental computation required for the task. In the control of higher-order systems, where the output depends on a multiple integral of the control input, the operator has to mentally perform those integrations to estimate the future effects of a present control input. If control inputs are time- and value-continuous, this mental integration is a highly challenging task. Hess relies on his structural pilot model (cf. section 3.1.2) to demonstrate this effect [97]. Remember that in this model, the proprioceptive feedback loop is adapted to the controlled element dynamics. It can be derived from equation (3.6) that for zero-, first- and second-order controlled elements, the pilot differentiates, multiplies by a constant and integrates the force applied to the inceptor, respectively, so that the open loop follows the Crossover Model. Higher-order systems require multiple integrations. The considerable computational burden is caused by the fact that integration of muscle tension must be accomplished in higher levels of the nervous system [97]. By adopting a pulse-like behavior, the amplitude of the control input is more or less fixed. Instead of a full mental integration, operators only need to estimate the duration of their control inputs, which is a lot easier.

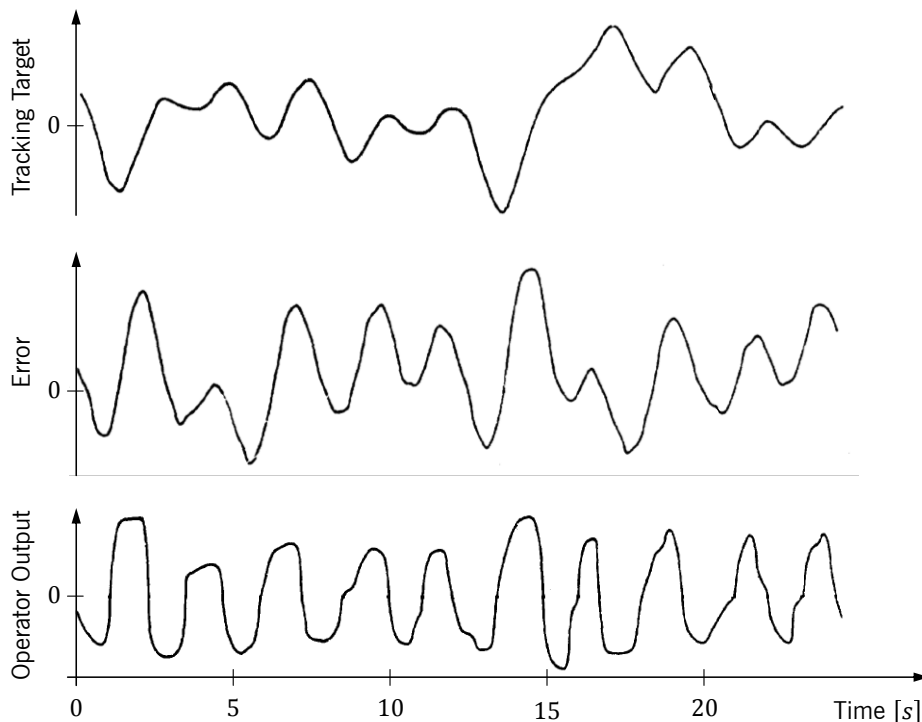


Figure 3.12 – Time history plot of pulse-like control activity, redrawn from [88]

Another observation and analysis of pulse-like pilot outputs was made by McRuer et al. [88], who attributed it to the low frequency lead generation required when controlling higher-order systems. They also showed that the pulse-like behavior in this case, shown in Figure 3.12, is characterized by a bimodal distribution of the control inputs, like the one shown in Figure 3.13.

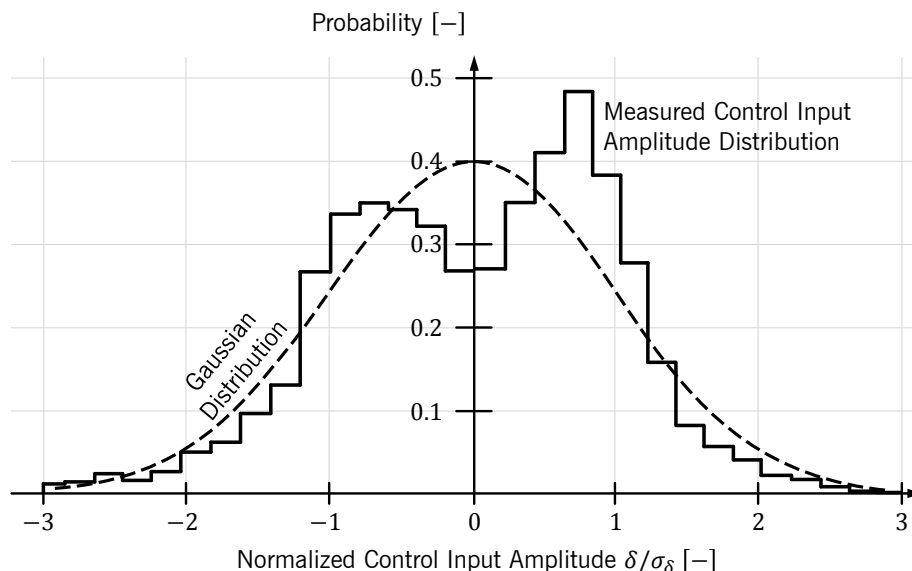


Figure 3.13 – Bimodal distribution evidencing pulse-like control, redrawn from [88]

It was already noted in section 3.2.1 that in Hess' experiments on large time delays [95], operators compensated a controlled element with K/s dynamics and time delay much like K/s^2 dynamics without time delay. This also meant that operators adopted the same pulse-like control behavior that had previously been associated with higher-order systems

control. In their experiments on hypersonic airplane control mentioned in section 1.2 [42, 43], the experimenters provoked control behavior with large lead as well. Remember that flight path lags attitude with 20 s or more in hypersonic flight. The piloting technique therefore was to immediately and positively react to changes in vertical speed and vertical acceleration and was appropriately named “aggressive stick technique” by the pilots involved in the experiments. Figure 3.14 shows a comparison of control activity between the conventional piloting technique and the aggressive stick technique. While the conventional technique produces gradual inputs with some high-frequency noise, the aggressive stick technique can indeed be distinguished by a shift of control activity towards higher frequencies.

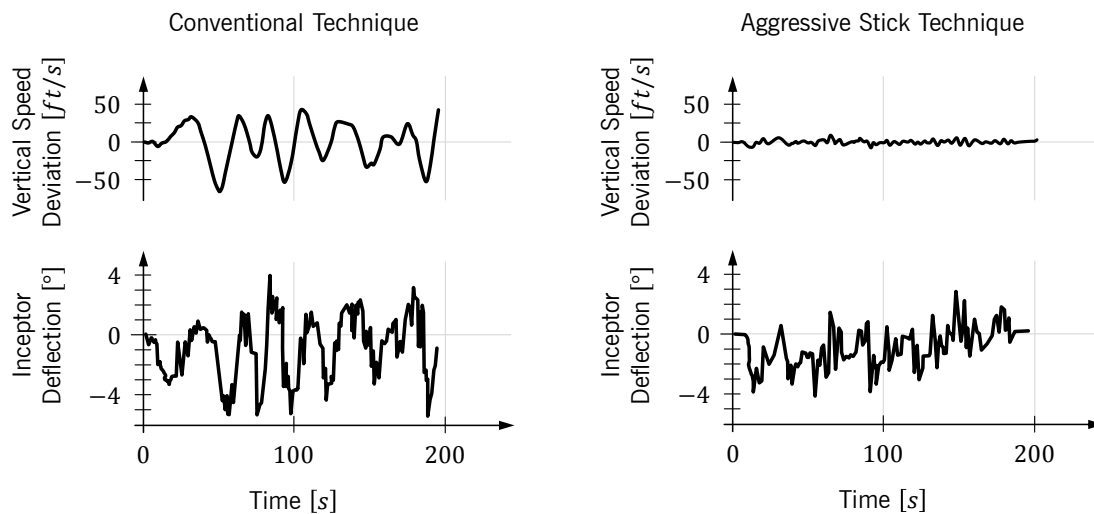


Figure 3.14 – Comparison between piloting techniques, redrawn from [43]

Control of a flexible system with up to 1 s time delay was investigated in [98]. Some of the subjects there adopted a pulse-like control behavior. The time history plot provided (cf. Figure 3.15) shows that the control pulses were made in quick succession, as if the control inputs observed by Young and Meiry and McRuer were broken down into multiple pulses. Here and in the above cases of higher-order systems or systems with large lags, the timespan between inputs is smaller than the time delay. This suggests that the pulse-like behavior had been induced primarily by the higher-order system characteristics.

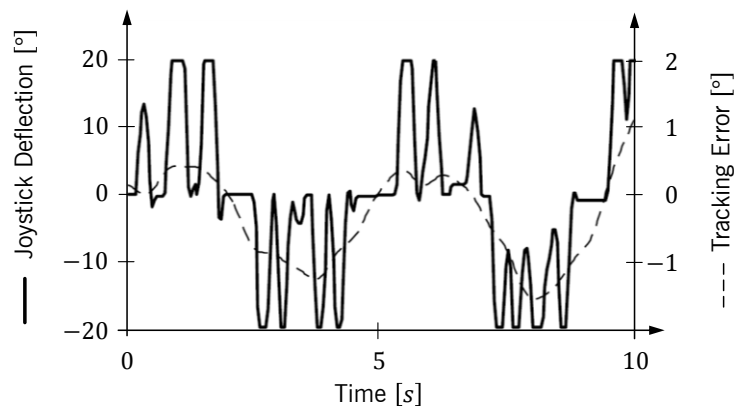


Figure 3.15 – Time history plot of pulse-like control activity, redrawn from [98]

A greater spacing between two consecutive, pulse-like control inputs, on the other hand, is an indication for a specific control strategy that humans naturally adopt when presented with large time delays. This control strategy is a hybrid open/closed-loop strategy, where operators make a brief command input, wait for the delayed system response, and repeat this process as required to accomplish the task given. Sheridan and Ferrell, who observed this strategy in remote manipulation experiments [23], described it and found the suitable name “move-and-wait strategy”. To visualize this strategy, think about how you adjust the temperature of a shower, where the temperature change lags the action on the faucet by a few seconds.

In most teleoperation tasks, the move-and-wait strategy needs to be applied cautiously to avoid collision with the environment. Thus, the time required to reach a target state is higher as compared to the continuous control strategy. In flight control, on the other hand, overshoots are often less critical, which is why errors can be reduced more aggressively or quickly. Likewise, when engineering the damping ratio of an airplane eigenmotion, some overshoot is usually allowed so that the motion can be sufficiently quick. In any case, though, the move-and-wait strategy requires the pilot to wait. And after he is done waiting, he may notice that some more control inputs are necessary, which, alas, could have been made earlier, during the wait phase. To compensate for the thereby increased time to reach the target, pilots often apply large, pulse-like control inputs during the move phase. In other words, they generate lead. Figure 3.16 illustrates the benefit of this lead generation. Here, a continuous and a pulse-like control input of same maximum amplitude and same area are made to a simple integrator. With the pulse-like control input, the new system state is reached considerably quicker, almost twice as fast in this case. Like the pulse-like control inputs during control of higher order systems, the pulse-like control inputs that can be observed when operators apply the move-and-wait strategy are a manifestation of low-frequency lead generation. The control input amplitude distribution, however, is different: the operators’ inactivity during the wait phase causes a large peak at zero amplitude.

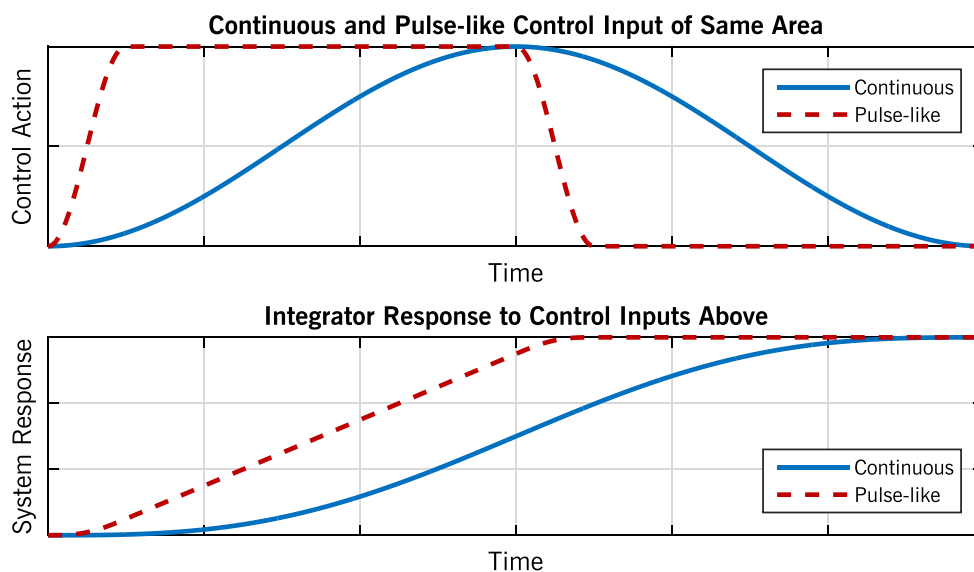


Figure 3.16 – Maneuver comparison between continuous and pulse-like control

For small maneuvers that are shorter than the system's time delay, the move-and-wait strategy needs to be purely open-loop, at least until the end of the wait phase. For larger maneuvers, the move-and-wait strategy really is a combination of closed-loop control with large pilot lead, as observed by Hess [95], alternating with open-loop wait phases that may contain occasional loop closures. The duration of each wait phase t_w may differ slightly from the time delay inherent to the controlled system. This fact is modeled by equation (3.13).

$$t_w = \tau + \Delta t \quad (3.13)$$

When undershooting or not noticeably overshooting the target, Δt is positive. It then represents the time required for the pilot to assess the new system state. When overshooting the target, however, Δt may be negative, as the overshoot can already be perceived before the system has settled at its new state. Indeed, the wait phase is closed-loop in this respect, at least to some extent. The problem when reducing the wait phase like this is that it is not clear just how large an opposite control input is needed to eliminate the overshoot. Thus, PIOs can easily develop, especially when the pilot is not familiar with the system.

As the previous paragraphs show, highly nonlinear pulse-like behavior is natural to human operators when faced with higher-order systems or large time delays. Interestingly, this behavior also bears some resemblance to BMI control. In both cases, control inputs are (approximately) value-discrete, with not more than three discrete levels: positive, neutral and negative. The introduction to BMIs given in section 3.4.1 makes this similarity clearer. Since the quasi-linear control-theoretic pilot models presented above do not describe pulse-like behavior, the question arises whether other models exist that can be applied in this case.

3.2.3 Models of Pulse-Like Control Behavior

Pulse-like control behavior is relevant to flight control with large time delays and to control of higher-order systems, as the previous section explains. Most efforts to model this kind of behavior were motivated by the latter problem. McRuer et al. [88] noted that the pulse-like operator behavior they associated with low frequency lead generation cannot be adequately described by existing linear pilot models. They therefore proposed two new models deemed appropriate for this nonlinear control behavior. The first model, the so-called differential displacement model, is derived from a slightly different pulse-like behavior observed, where pulses are constant in duration, but vary in amplitude. Constant pulse width is accomplished in the model through sampling. The pulse amplitudes A produced by the model are proportional to the differential displacement d of the sensed error e , i.e., the difference between current and preceding error sample. This relationship is shown in equation (3.14), where t_0 in square brackets denotes the current sample and t_s the sampling time.

$$\begin{aligned} A[t_0] &= K \cdot d[t_0] \\ &= K \cdot (e[t_0] - e[t_0 - t_s]) \end{aligned} \quad (3.14)$$

Note that the differential error displacement d divided by the constant sampling rate t_s would provide an estimation for error rate. The differential displacement model can therefore be considered a type of (visual) perception model. Like the measured control activity the model is derived from, the model outputs do not exhibit a bimodal distribution, but are instead of equal duration. A major shortcoming of the differential displacement model is that steady-state errors do not provoke any control activity.

The second model proposed in [88] is called velocity-sensing model. As opposed to the differential displacement model, it is time-continuous. The visual process of error velocity sensing, i.e., derivation of the error e , is accompanied in this model by a time delay τ_v , exactly like in Hess' model of visual perception presented in section 3.1.1 and Figure 3.3. According to the velocity-sensing model, pilot control activity δ is proportional to the sign of the perceived error rate and further delayed by the neuromuscular system (τ_{nm}). Equation (3.15) is a possible representation of the velocity-sensing model. Here, t in round brackets denotes continuous time.

$$\delta(t) = K \cdot \text{sgn}(e^{-\tau_v s} \cdot s \cdot e(t)) \cdot e^{-\tau_{nm} s} \tag{3.15}$$

Unlike the differential displacement model, the velocity-sensing model does produce a bimodal amplitude distribution of pilot control activity. However, it has the same major shortcoming of not explaining corrections of steady-state errors. It therefore also does not explain the pulse-like control behavior associated with the move-and-wait strategy.

Hess proposed an extension to his dual-loop structural pilot model [99], a predecessor of his structural model [86], to describe pulse-like control behavior [97]. The model structure is shown in Figure 3.17. Note the input n_e , the injected error remnant. It represents the difference between the linear model and the not-exactly-linear behavior of the human operator and is often modeled as a colored noise. The parameter d , on the other hand, represents disturbances. The only modification Hess applied to his original model is the nonlinear element Y_{pc} with the input c and the output c' .

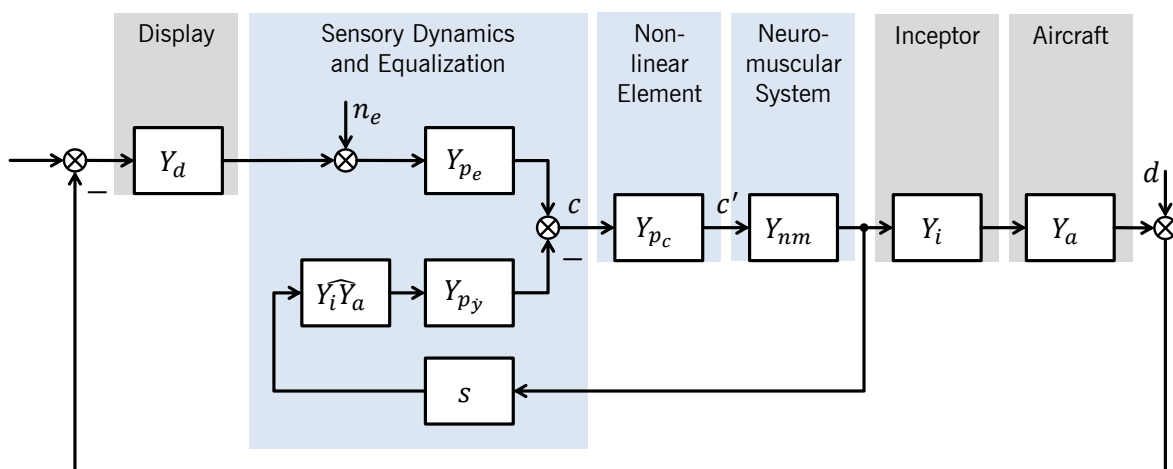


Figure 3.17 – Hess' pulsive control model as in [97]

Hess refrained from choosing relays or toggle nonlinearities as nonlinear element Y_{pu} , because he deemed the resulting control amplitude distributions, with nearly all control activity occurring at the relay limits, unrealistic. The characteristics of this nonlinear element as proposed by Hess are described by equation (3.16).

$$\begin{aligned} \dot{c}' &= 0 & \text{for } |\dot{c}| < k_1 \\ c' &= k_2 c & \text{for } |\dot{c}| \geq k_1 \end{aligned} \quad (3.16)$$

Hess shows that pulse-like control time histories similar to those obtained in human subject experiments can be produced by choosing appropriate values of k_1 and k_2 . However, this model, too, does not describe how pilots correct steady-state errors. Indeed, all models of pulse-like control presented above have been designed for the case of higher-order system control. This may be the reason why they all have some shortcomings when applied to the control of systems with large time delays. To address this issue, new pilot models are tailored to the problem of flight control with large time delays in the next section.

3.3 New Pilot Models Describing Control with Large Time Delays

As discussed above, the natural behavior of human operators when confronted with large time delays is to apply pulse-like control inputs and the move-and-wait strategy. The relevant pulse-like control behavior is characterized by (approximately) value-discrete control inputs that exhibit not more than three discrete levels (cf. section 3.2.2). It is therefore also similar to BMI control (cf. section 3.4). The three input levels shall be called “positive”, “neutral” and “negative”, but the reader can easily imagine that they could also stand for commands like “pitch up”, “maintain pitch attitude” and “pitch down”, respectively. This restriction of control inputs to three discrete amplitude levels constitutes a key characteristic of the following novel control-theoretic pilot models, where the three levels are represented by the numerical values +1, 0 and –1.

The restriction of control inputs to three discrete amplitude levels can be done by the pilot himself, but also by the flight control system. If this is the case, the control system shall be called “on-off control system”, whereas those control systems that enable value-continuous control inputs shall be called “continuous control systems”. McRuer et al. [88] noted that the control of on-off control systems cannot be described with quasi-linear pilot models and that nonlinear control theory like the phase plane method could be used instead. Indeed, this approach is taken in the following section.

3.3.1 Compensatory Tracking of a Stationary Target

In a first, exploratory step, a new pilot model for compensatory tracking of a stationary target is defined, in some parts based on the established models described in previous sections. Figure 3.18 shows the proposed pilot model in an initial, generic form. Note that neither the aircraft nor any feedback loops are shown here.

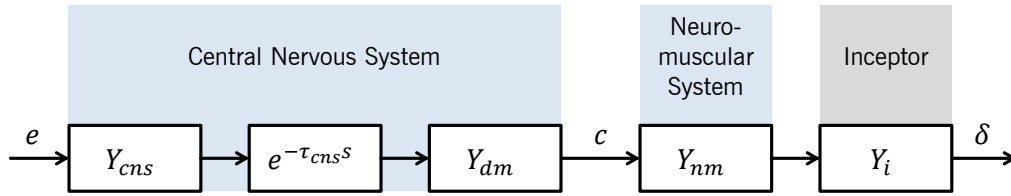


Figure 3.18 – Generic form of the proposed compensatory pilot model

The central nervous system (CNS), represented by some linear dynamics Y_{cns} , a time delay τ_{cns} and a nonlinear decision mapping function Y_{dm} , derives a control intention c from a perceived tracking error e . This control intention, which according to equation (3.17) can take three different values, is then translated into a limb movement by the neuromuscular system, with its linear dynamics Y_{nm} . Finally, a certain inceptor characteristic Y_i maps the limb force (or movement) to a control action δ on the aircraft. This inceptor characteristic is comparable to the feel system of Hess' structural model (cf. section 3.1.2).

$$c \in \{-1, 0, 1\} \quad (3.17)$$

In the case of a continuous control system, Y_i is another linear transfer function, whereas the inceptor of an on-off control system exhibits the same three-level output characteristics as Y_{dm} . Regardless of control system type, the steady-state control action δ equals the steady-state control intention c . The neuromuscular dynamics Y_{nm} in between merely introduce some lag. Hence, the generic model defined by Figure 3.18 can be simplified, as the following paragraph describes.

For Y_{nm} , either of the two neuromuscular transfer functions presented in section 3.1.1 could be employed. They are defined by equation (3.1) and the parameter values from Table 3.1. To further simplify the model, however, the approximation of the neuromuscular dynamics by a pure time delay, also presented in section 3.1.1, shall be used instead. This neuromuscular time delay τ_{nm} can be added to the CNS time delay. The resulting overall pilot time delay τ_p is defined by equation (3.18).

$$\tau_p = \tau_{cns} + \tau_{nm} \quad (3.18)$$

An additional simplification of the model can be achieved by neglecting the inceptor element. As stated above, this element simply reproduces the outputs of Y_{dm} . Assuming that Y_i introduces negligible lag, it is justifiable to only rely on Y_{dm} to generate the control action. The resulting simplified model is shown in Figure 3.19. Here, control intention c does not explicitly appear anymore. Note that this model can be applied to both manual and BMI control. In the case of BMI control, τ_{nm} must obviously be neglected and as a consequence, the pilot model's output is the control intention c . A BMI model such as the one presented in section 3.4.2 then needs to describe how the BMI translates this control intention into a control action δ .

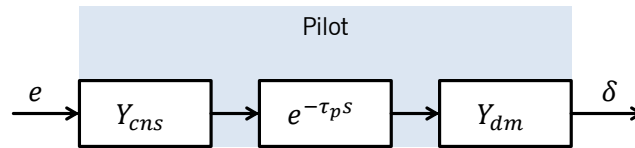


Figure 3.19 – Simplified generic form of the proposed compensatory pilot model

Next, the generic form of the decision mapping element Y_{dm} shall be replaced by a specific mapping function that adequately describes how pilots derive their control intention from the perceived error. This function is chosen to be a deadband connected in series with a sign function, shown in Figure 3.20. As long as the error, filtered by the CNS, lies within the deadband, the pilot has no control intention. Corrective control inputs are intended while the error is outside the deadband. The size of the deadband thus represents the pilot's desired steady-state precision. The deadband of the nonlinear decision mapping element can be defined in a normalized form, ranging from -1 to $+1$. The effective deadband size, i.e., the actual desired tracking precision, then is the inverse of the steady-state gain of Y_{cns} .

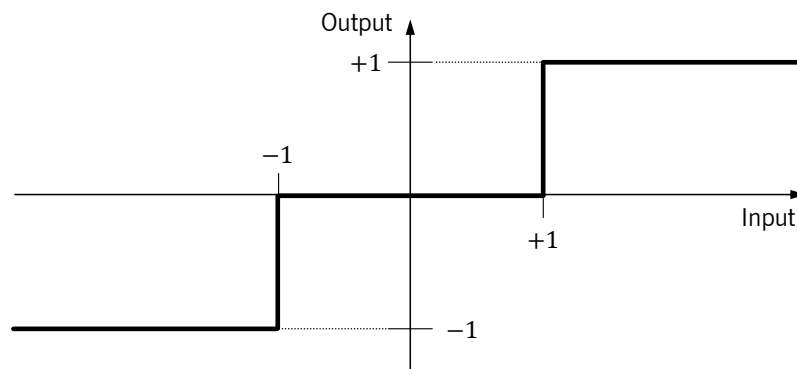


Figure 3.20 – Characteristics of the nonlinear decision mapping element

The pilot model of Figure 3.19 shall now be combined with a generic plant model, consisting of a time delay τ_a and the linear aircraft transfer function Y_a , to form a closed loop. The plant's single time delay τ_a groups all delays occurring between control action and sensory feedback, notably including all signal processing and transmission delays. Figure 3.21 shows the resulting closed loop along with system input u , system output y , error e and control action δ .

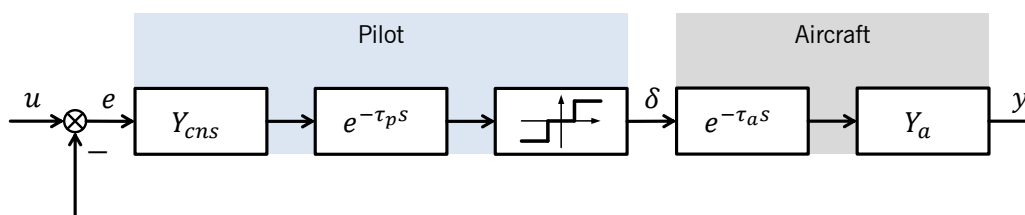


Figure 3.21 – Proposed compensatory control loop with pilot and aircraft

For an initial analysis, the CNS transfer function is assumed to consist of a single gain, as described by equation (3.19). The desired steady-state tracking precision is determined by this pilot gain only. The aircraft transfer function is chosen to be a pure integrator (equation (3.20)), which would be well controllable without the time delay.

$$Y_{cns} = K_p \quad (3.19)$$

$$Y_a = \frac{K_a}{s} \quad (3.20)$$

In a final step before actual analysis, the model is simplified by grouping both pilot and aircraft time delays in one total time delay τ_t (equation (3.21)), which may be positioned either before or after the decision mapping element.

$$\tau_t = \tau_p + \tau_a \quad (3.21)$$

This nonlinear control loop can now be analyzed using the phase plane method, which is considered one of the most powerful methods for studying the behavior of (first- or second-order) nonlinear systems [100]. By applying this method, the following paragraphs derive a novel, intuitive representation of pilot behavior. This representation not only describes the nonlinear, pulse-like behavior that occurs during control of systems with large time delays, but it is also well suited to analyze the implications of this behavior on flight control performance. Moreover, the sometimes rather abstract effects of parameters like pilot gain or pilot lead become clearly visible in the following phase plane diagrams.

First of all, some basic technical terms of the phase plane method need to be defined [100].

- A dynamic system is represented in phase space when it is described by its state and state derivative, e.g., position and velocity. For a first- or second-order system with one degree of freedom, the phase space is reduced to a phase plane.
- The variation of the system's state over time is described by trajectories in the phase plane.
- A family of trajectories that completely defines the transient system behavior is called phase portrait.
- The limit set of a trajectory is the state it reaches as time approaches $\pm\infty$
- If the dynamic system contains a relay-type nonlinearity such as the decision mapping element here, the phase portrait can be complemented by so-called switching lines. When a trajectory crosses a switching line, the relay-type element changes its state, i.e., the value of its output.

To analyze the nonlinear control loop under consideration, the evolution of the system output y is described in the phase plane. For this analysis of stationary target tracking, the system input can be assumed constant zero and the initial system output variable nonzero, as in equation (3.22).

$$\begin{cases} u(t) = 0 \quad \forall t \geq 0 \\ y(t = 0) = y_0 \\ \dot{y}(t = 0) = 0 \end{cases} \quad (3.22)$$

In the phase plane, the system output y is plotted along the abscissa, whereas its derivative, \dot{y} , is plotted along the ordinate. Figure 3.22 shows an exemplary trajectory. The phase portrait of the system consists of two horizontal lines $\dot{y} = K_a$ and $\dot{y} = -K_a$ and an infinite number of points along the abscissa. Within the effective deadband $[-1/K_p, 1/K_p]$, these points are stationary trajectory end points or starting points y_0 . Outside the effective deadband, they either constitute trajectory starting points y_0 or, in a special case that is discussed in one of the following paragraphs, waiting points. The example trajectory of Figure 3.22 is followed for all initial conditions $y_0 < -1/K_p$. Note that this phase plane of the system output y also illustrates the evolution of the error e , since a consequence of equation (3.22) is $e = -y$ and $\dot{e} = -\dot{y}$.

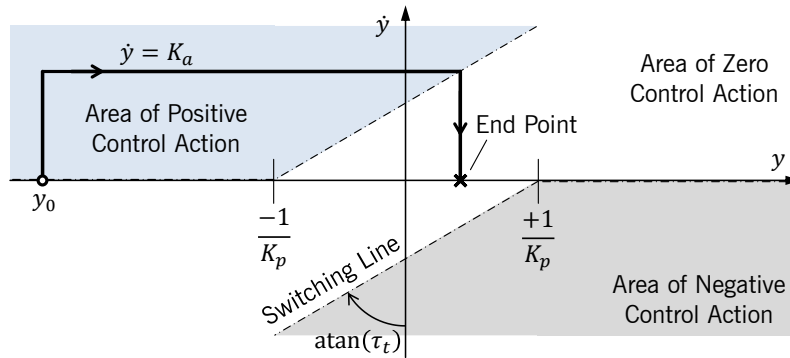


Figure 3.22 – Compensatory control loop: example trajectory in the phase plane

It can be seen that the switching lines divide the phase plane into three areas that correspond to the three possible values of control action δ . The initial state of the example trajectory causes the pilot to make a positive control input to reduce the error. Because of this control input, the error then diminishes at a constant rate. As soon as the pilot perceives that the error is within the deadband, he terminates his input. Due to the time delay, however, his perception lags the actual system state and thus, switching to zero control activity does not occur on the boundary of the deadband, but τ_t after the deadband has been entered. Hence, the trajectory progresses through the deadband for a distance $K_a \cdot \tau_t$ before terminating in a stationary point. In Figure 3.22, the effect of the time delay is graphically represented by the obliqueness of the switching lines. These lines lie at an angle of $\text{atan}(\tau_t)$ in relation to the ordinate.

In the example above, the slope of the switching lines is steep enough and the deadband is large enough for the system to reach a steady-state end point within the deadband. If the switching lines were shallower and/or the deadband smaller, it could happen that the trajectory progresses through the entire deadband before switching occurs. This is shown in Figure 3.23. Switching to zero control action occurs as the pilot perceives that the error has decreased below the deadband tolerance. Due to the time delay, however, the system

continues to move and ultimately moves beyond the opposite threshold of the deadband. As soon as the pilot perceives that, he applies an opposite control input. Next, the trajectory continues towards its starting point again until reaching another switching line, where the same events occur as before. This process may continue indefinitely in what is called a limit cycle.

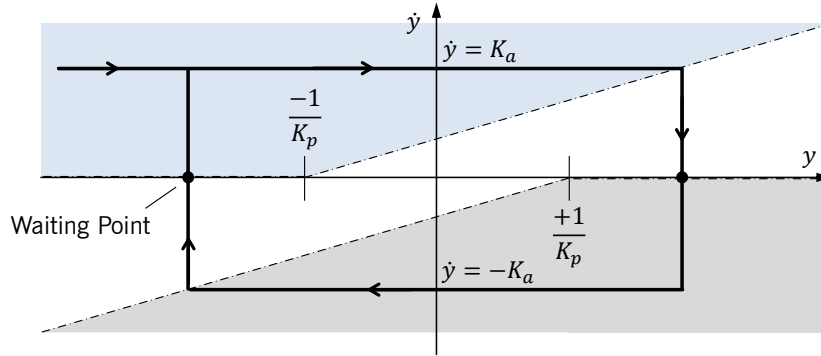


Figure 3.23 – Compensatory control loop: limit cycle in the phase plane

Limit cycles are oscillations of fixed frequency and amplitude that sometimes occur in nonlinear dynamic systems. Everyday examples of limit cycles include the beating of the human heart and the squealing of chalk on a blackboard [100]. In the phase plane, limit cycles are apparent as closed trajectories that constitute limit sets of other trajectories. The control loop under consideration exhibits a limit cycle if equation (3.23) is satisfied, which can be derived from the geometry of the phase portrait.

$$K_p > \frac{2}{K_a \tau_t} \quad (3.23)$$

As Figure 3.23 shows, the limit cycle is stable, since all initial conditions $y_0 \notin [-1/K_p, 1/K_p]$ produce trajectories that end up in the limit cycle as $t \rightarrow +\infty$. In each cycle there are two instants when no control input is made. These instants, during which y is constant, are evidenced by waiting points in Figure 3.23. The time spent at one waiting point t_w is the time required for the system to move through the deadband, since this is what the pilot perceives while not performing any control action ($\delta = 0$). The duration t_w is therefore defined by equation (3.24).

$$t_w = \frac{2}{K_p} \cdot \frac{1}{K_a} \quad (3.24)$$

The amplitude of the limit cycle, i.e., $y_{max} - y_{min}$, can be geometrically determined and is given by equation (3.25).

$$A_{LC} = 2K_a \tau_t - \frac{2}{K_p} \quad (3.25)$$

The limit cycle period is the sum of the time required to perform a system movement with the amplitude $2A_{LC}$ and of the time spent at the two waiting points $2t_w$. This information, combined with equations (3.24) and (3.25), results in equation (3.26).

$$T_{LC} = \frac{2A_{LC}}{K_a} + 2t_w = 4\tau_t - \frac{4}{K_p K_a} + \frac{4}{K_p K_a} = 4\tau_t \quad (3.26)$$

It is known that pilots also perceive the error rate and can thereby generate lead. This is effectively modeled in Hess' structural model [86, 94] (cf. section 3.1.2), the differential displacement model and the velocity-sensing model [88] (cf. section 3.2.3). Therefore, instead of the simple gain used above, consider the CNS transfer function of equation (3.27), which is a combination of gain and lead.

$$Y_{cns} = K_p(1 + T_p s) \quad (3.27)$$

By varying the lead time constant T_p , the pilot has a direct influence on the slope of the switching lines, as evidenced by Figure 3.24. Their angle with respect to the vertical axis is $\text{atan}(\tau_t - T_p)$.

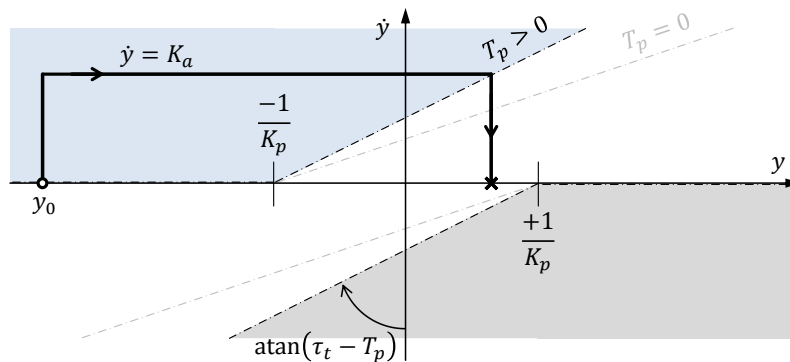


Figure 3.24 – Influence of pilot lead on phase plane switching lines

In this case with pilot lead, a limit cycle occurs if the inequality of equation (3.28) is satisfied.

$$K_p > \frac{2}{K_a(\tau_t - T_p)} \quad (3.28)$$

The amplitude of the resulting limit cycle then follows equation (3.29).

$$A_{LC} = 2K_a(\tau_t - T_p) - \frac{2}{K_p} \quad (3.29)$$

Finally, the limit cycle period, shown in equation (3.30), can be derived again from the limit cycle amplitude (equation (3.29)) and the duration of the wait phases (equation (3.24)).

$$T_{LC} = 4(\tau_t - T_p) \quad (3.30)$$

Note that equations (3.28) through (3.30) constitute a more general form of equations (3.23) through (3.26), which in turn represent the special case $T_p = 0$. The lead time constant can be interpreted as an internal model of the time delay τ_t , comparable to the idea of Y_{pf} as an internal model of the controlled vehicle dynamics Y_a in Hess' structural model (cf. section 3.1.2). It is naturally affected by estimation errors, which cause non-perfect pilot behavior. Moreover, even a perfectly estimated time delay in the form of a lead time constant would not eliminate the possibility of a limit cycle. An additional loop break is necessary for that, as the following sections show. Remember that the move-and-wait strategy really is a combination of closed-loop control with "excessive" lead as found by Hess [95] and occasional open-loop wait phases as described by Sheridan and Ferrell [23]. Note that the lead time constant is only excessive when compared to the theory of the Crossover Model. It may be not at all excessive when compared to the system's time delay.

The analyses above assume an ideal K/s controlled transfer function. Additional lags, which are usually present, have a detrimental effect which is evidenced in the phase plane by a distortion of the phase portrait. As an example, Figure 3.25 shows a qualitative phase plane plot of the same closed pilot-aircraft loop as above, but with the aircraft transfer function of equation (3.31). This transfer function is equivalent to the differential equation (3.32), from which the phase portrait equation (3.33) can be derived.

$$Y_a = \frac{K_a}{s(T_a s + 1)} \quad (3.31)$$

$$\dot{y} + T_a \ddot{y} = \delta K_a \quad (3.32)$$

$$\frac{d\dot{y}}{dy} = \frac{d\dot{y}}{dt} \frac{dt}{dy} = \frac{\ddot{y}}{\dot{y}} = \frac{1}{T_a} \left(\frac{\delta K_a}{\dot{y}} - 1 \right) = \begin{cases} \frac{1}{T_a} \left(\frac{\pm K_a}{\dot{y}} - 1 \right) & \text{for } \delta = \pm 1 \\ -\frac{1}{T_a} & \text{for } \delta = 0 \end{cases} \quad (3.33)$$

Upon initiation of a nonzero control input ($\delta \neq 0$), the system velocity $\dot{y} = K_a$ is not attained immediately, like in the cases without lag, but is approached asymptotically. Hence, the trajectories during any nonzero control input still intersect the abscissa at right angles, but are curved clockwise. Switching to zero control activity ($\delta = 0$) is again delayed by the time delay τ_t and when it occurs, the system still continues to move because of the lag. As a result, the waiting points degenerate into oblique lines with a constant slope of $-1/T_a$, which is evidenced by equation (3.33). (One may in fact see it the other way around: these oblique lines degenerate into waiting points when no lags are present.) If pilot gain, time delay and lag time constant are small enough, the oblique section of the trajectory ends on the abscissa and a desired end state is reached. However, the fact that the system continues to move after a control input is terminated, which is reflected by the obliqueness of the lines in the region of zero control action, makes an involuntary excursion

of the effective deadband more likely. Such an excursion is, again, only perceived after the time delay τ_t and then triggers an opposing control input. A limit cycle like the one shown in Figure 3.25 may develop. Of course, the pilot can correct for this adverse effect of system lags by further increasing his lead time constant T_p , but only at the cost of even higher mental workload.

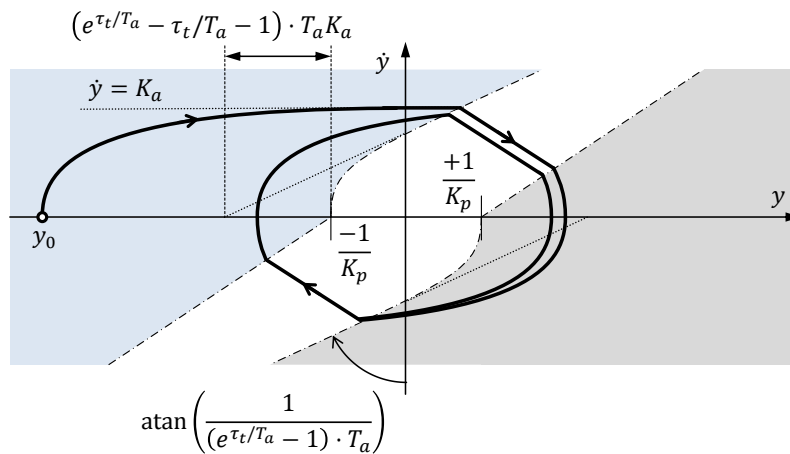


Figure 3.25 – Influence of aircraft lags on the phase portrait, derived from [100]

Lags and time delays within the controlled system indeed both have a delaying effect on the perceived system response. To successfully control systems with large time delays and/or large lags, operators must think ahead. An adequate control system design might support the pilot in controlling such difficult systems. The following section explores this possibility, based on the pilot model and the findings described above.

3.3.2 Implications on Flight Control System Design

Consider closed-loop control with large time delays as described by the model of the preceding section 3.3.1. If a limit cycle does not exist, the aircraft's state y always converges to a stationary value within the desired tolerance, represented by the effective deadband. This is a desirable behavior. The occurrence of a limit cycle, however, is not desirable. In fact, the limit cycle described above is a PIO and, as such, an unwanted handling qualities deficiency. It is potentially dangerous, especially in ground proximity or near the flight envelope boundaries. A limit cycle occurs when one or more of the parameters time delay τ_t , aircraft gain K_a and pilot gain K_p are too large. The first question is now, whether the occurrence of a limit cycle can be avoided or even prevented by control engineering.

Since the time delay τ_t is given and the pilot gain K_p varies, as noted above, with the desired precision, the aircraft gain K_a constitutes the only design parameter. However, trying to prevent limit cycle occurrence by choosing a small aircraft gain is impractical for two reasons. First, an excessively small aircraft gain results in insufficient control authority or maneuverability. Second, there is no practical upper limit for the pilot gain and the system may therefore exhibit limit cycles regardless of the aircraft gain value chosen. Hence, limit cycles cannot be prevented by control engineering. Flight control system design choices nonetheless influence the handling characteristics. It was noted at the

beginning of section 3.3 that the restriction of control inputs to three discrete amplitude levels can be done by the pilot himself, but also by the flight control system. The above pilot model can now be used to explore the differences between on-off control systems and continuous control systems.

The decision mapping element of Figure 3.20 can be applied to both control system types. For an on-off control system, possible input amplitudes are indeed fixed by design. Using a continuous control system, however, only the maximum input amplitude is fixed, which shall be characterized by $|\delta| = 1$. As a result, the two nonzero decision mapping levels may take other values within $[-1, +1]$, but it is assumed that their value does not change while control intention is nonzero. In other words, the pilot has an additional degree of freedom which shall be called input aggressiveness. Variations of this aggressiveness directly affect the open-loop gain (cf. section 3.1.2). When the controlled system exhibits excessive phase lags, high open-loop gains can destabilize the closed control loop. Even small disturbances can cause pilot corrections that are excessive in aggressiveness and thus trigger a PIO. The resulting limit cycle amplitude varies with pilot gain and aggressiveness, but is, according to equation (3.25), always smaller than $2K_a\tau_t$. Note that with a continuous control system, the PIO may start off at a small amplitude which then diverges and reaches a maximum when the pilot makes stop to stop control inputs. If, on the other hand, a PIO develops with an on-off control system, the amplitude is not divergent, but more or less fixed from the beginning. In this case, too, it is always smaller than $2K_a\tau_t$. Regardless of the control system type, the limit cycles' period only depends on the total time delay and therefore cannot be altered by control engineering. The time delay introduced by the pilot may vary, but only to a negligible degree. As a result, the limit cycles' period is primarily determined by the controlled system's time delay. For the time delay values under consideration, limit cycle periods are greater than about four seconds.

Since the magnitude of the aircraft's reaction to a given control input is governed by the gain K_a , this gain can also be referred to as the control sensitivity. When fixing the control sensitivity K_a of either control system type, maneuverability and PIO criticality have to be traded off against each other as described above. In both cases, higher values of K_a result in higher maneuverability and, at the same time, higher PIO criticality. As the control sensitivity of a continuous control system is reduced, it becomes more similar to an on-off control system, because pilots will, in an attempt to speed up the system response, start to displace the inceptor to its limit position, defined by $|\delta| = 1$, for every input they make. In terms of limit cycle amplitude, a continuous control system is then equivalent to an on-off control system, provided they employ the same control sensitivity K_a .

In terms of workload and performance, on the other hand, the on-off control system may have an advantage, since it increases the predictability of the aircraft response. It was noted previously that pilots apply pulse-like control inputs to reduce mental workload. With the control amplitudes fixed by design, pilots are relieved from manually generating pulse-like control inputs. Once they are familiar with the invariant control amplitudes, they only need to estimate control input duration to predict the airplane response. As a result, they can precisely fly maneuvers in an open-loop fashion. This form of pre-cognitive

tracking only requires the pilot to perceive his control input. It is especially valuable if feedback from the vehicle is delayed to an extent even greater than the duration of the desired maneuver. In this case, where the pilot can only rely on the open-loop part of the move-and-wait strategy, the ability to perform pre-cognitive control greatly reduces the time required to reach the target state. Since the move-and-wait strategy cannot be described with the compensatory tracking model presented in section 3.3.1, that model is extended in the following section to a dual-mode pursuit tracking model, which in turn constitutes a more complete description of pilot behavior during control tasks with large time delays.

3.3.3 A Dual-Mode Pursuit Tracking Model

As noted in the previous section, it is likely that pilots perform pre-cognitive tracking at least to some degree. Furthermore, compensatory tracking tasks are not directly representative for operational maneuvers [101]. Therefore, the model for compensatory tracking presented above, although well describing some basic characteristics, is insufficient. This section presents a dual-mode pursuit tracking model that combines the above closed-loop model with a model of the open-loop move-and-wait strategy to adequately describe the operator behavior during control tasks with large time delays.

The controlled system is assumed to comprise one and only one pure integrator, time delays and, possibly, lags. All time delays shall be grouped in one single parameter τ_a , whereas the remaining linear dynamics can be described by equation (3.34), where (...) stands for one or more lags of the form $(1 + Ts)$ or $(1 + 2\zeta s/\omega + s^2/\omega^2)$. Systems with more than one pure integrator are not considered here, because higher-order flying tasks such as altitude or ground path tracking are usually accomplished by closing multiple, cascaded control loops (cf. Figure 3.4), the innermost of which controls a single-integrator system.

$$Y_a = \frac{K_a}{s \cdot (...)} \quad (3.34)$$

When performing pursuit tracking, pilots rely on both the system output y and the system input u to derive appropriate control inputs (cf. Figure 3.5). In this present case, they use this information to decide whether to open or close the loop and whether to move or to wait. Since these three choices – closed-loop control, move phase and wait phase – can be seen as distinct operator states, the pilot can, to some extent, be described by a state machine, whose output is a control intention c . Figure 3.26 shows a diagram of the proposed state machine, whose development was guided by previously reported observations of human operator behavior and the author's own experience in flight control with large time delays. Care was taken to introduce as few states, transitions and parameters as possible. The result is a novel, highly general and intuitive description of operator behavior during control tasks with large time delays.

While the following paragraphs give a more vivid illustration of the state machine by describing the states and transitions in narrative form, Figure 3.26 provides a formalized definition of the state machine. Here, each box represents a state and each arrow a

transition. States are characterized by the actions that take place upon entry into the state, which are marked by the word “entry”, and the actions that occur while the state is active, which are marked by the word “during”. Initial states can be recognized by a transition originating from a black dot. A transition condition is noted next to each non-initial transition. Transitions are triggered as soon as the corresponding condition is satisfied. Rhombs indicate junctions of transitions. The conditions of transitions departing any state or junction are mutually exclusive, so that transition triggering is unambiguous. Beyond that, the conditions of those transitions departing a junction are collectively exhaustive, so that the transit character of junctions is ensured.

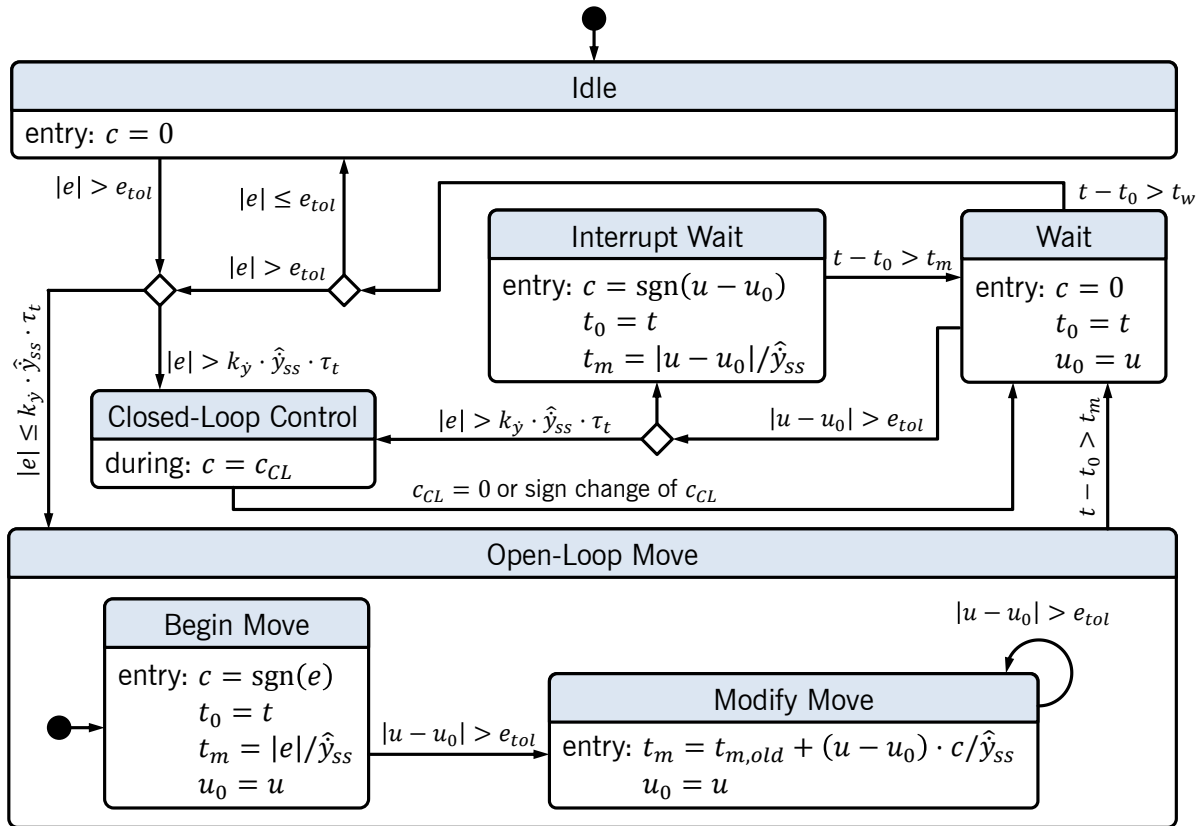


Figure 3.26 – State machine of the dual-mode pursuit tracking model

The initial operator state is “Idle”. When in this state, the pilot observes the error e , but does not have any control intention, i.e., $c = 0$. As soon as the error exceeds a certain tolerable value e_{tol} , the pilot decides whether to perform closed-loop control or to make an open-loop move. Suppose the error is so small that the control input needs to be shorter than the total time delay. This is the case if equation (3.35) is satisfied, where \dot{y}_{ss} is the steady-state system velocity during a positive control input.

$$|e| \leq \dot{y}_{ss} \tau_t \quad (3.35)$$

The operator then needs to rely on the open-loop move-and-wait strategy. Note that $\dot{y}_{ss} = K_a$ when an on-off control system, characterized by $\delta \in \{-1,0,1\}$, is employed and $0 \leq \dot{y}_{ss} \leq K_a$ in the case of a continuous control system with $\delta \in [-1,1]$. Like the control sensitivity K_a , the value \dot{y}_{ss} is a measure for the magnitude of the aircraft’s reaction to a

control input. However, \dot{y}_{ss} already takes into account the actual size of the control input and shall therefore be called effective reaction magnitude. Of course, pilots do not have perfect knowledge of the effective reaction magnitude \dot{y}_{ss} or the total time delay τ_t . Moreover, being aware of their imperfect knowledge and of possibly excessive overshoots in case closed-loop control is attempted by mistake, operators probably tend to make open-loop moves. Therefore, the condition for the state transition is formulated as in equation (3.36), where a factor $k_{\dot{y}} > 1$ is added to the product of estimated reaction magnitude \hat{y}_{ss} and τ_t . It is assumed here that $k_{\dot{y}} = 1.1$.

$$|e| \leq k_{\dot{y}} \hat{y}_{ss} \tau_t \quad (3.36)$$

The operator now enters the “Open-Loop Move” state, which in turn is composed of two states. The initial state “Begin Move” starts the maneuver by generating an appropriate control intention $c \in \{-1, 1\}$ to reduce the perceived error. Moreover, the duration of the move phase t_m is computed as in equation (3.37). Once this duration is over, the operator transitions to the “Wait” state.

$$t_m = \frac{|e|}{\hat{y}_{ss}} \quad (3.37)$$

It may happen, though, that the system input u shifts during the move phase. If such a shift is larger than the tolerance e_{tol} , the pilot transitions to the “Modify Move” state, where he re-computes t_m accordingly. If the target has shifted such that the error has been reduced, t_m is reduced as well to avoid overshooting the target. Similarly, if the target has shifted the other way, the move phase is prolonged.

Once transitioned to the “Wait” state, the operator terminates his control intention ($c = 0$) and waits for the system to settle. The duration of the wait phase is governed by equation (3.38). It is the sum of the total time delay τ_t and another delay Δt_w that models the time the operator needs to assess the outcome.

$$t_w = \tau_t + \Delta t_w \quad (3.38)$$

Total time delay is in turn defined by equation (3.39) as the sum of all pure time delays and equivalent time delays. The pure time delays are τ_{cns} within the CNS (cf. Figure 3.28) and τ_a within the controlled system, whereas the equivalent time delays are τ_{nm} for the neuromuscular system (cf. section 3.1.1) and τ_{lags} for any lags that may be present in the aircraft transfer function.

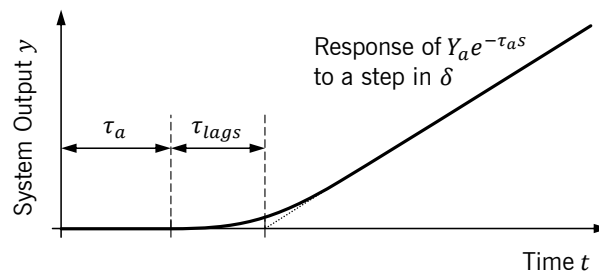


Figure 3.27 – Illustration of time delay values in the system’s step response

The parameter τ_{lags} can be geometrically determined from the step response plot of Y_a , as shown in Figure 3.27.

$$\tau_t = \tau_{cns} + \tau_{nm} + \tau_a + \tau_{lags} \quad (3.39)$$

Furthermore, it is assumed that Δt_w equals τ_{cns} (equation (3.40)). Thus, equation (3.38) can be rewritten as in equation (3.41). Note that neither the total time delay nor the wait phase duration need to be estimated by the pilot. The pilot simply waits for the system to settle, which always takes the time τ_t , and assesses the outcome within the duration Δt_w .

$$\Delta t_w = \tau_{cns} \quad (3.40)$$

$$t_w = 2\tau_{cns} + \tau_{nm} + \tau_a + \tau_{lags} \quad (3.41)$$

During the wait phase, the pilot observes the system input u . If a shift occurs in u that is larger than e_{tol} , he interrupts the wait phase. The change in u may have been so small that equation (3.36) is satisfied and a transition to the “Interrupt Wait” state occurs. Here, another brief open-loop movement is commanded to follow u . Then, the pilot transitions to the “Wait” state again. If, on the other hand, the wait phase is interrupted due to a large shift in u that causes equation (3.36) to be violated, the operator transitions to the “Closed-Loop Control” state. While in this state, the state machine feeds through a closed-loop control intention ($c = c_{CL}$), which is determined outside the state machine. The transition back to the “Wait” state occurs as soon as c_{CL} changes its sign or becomes zero. It is exactly this loop break that prevents the occurrence of limit cycles. If, at the end of the wait phase, the error is tolerably small, the operator becomes idle. If a larger residual error remains, he starts off again by deciding between closed-loop control and an open-loop move.

Now that the state machine as the core of the pursuit tracking model is defined, it needs to be embedded in a suitable control architecture. Most notably, the closed-loop control intention c_{CL} needs to be generated and the output of the state machine c needs to be translated into a control input to the aircraft. The resulting model, which comprises both pilot and aircraft, is shown in Figure 3.28. Note that some of the elements of the compensatory tracking model presented in section 3.3.1 can be found here again. The model of Figure 3.28 is only applicable to on-off control systems, but a variant describing control with continuous control systems is given later in this section.

First, the signal path from control intention c to control action δ is described. The control intention from the state machine c first passes the CNS’s time delay τ_{cns} , which is set to 0.2 s here. This value is slightly higher than those proposed elsewhere [86], to account for the increased mental load induced by switching between operator states. The delayed control intention is then translated to a limb force by the neuromuscular system. In this process, it is first multiplied by $1 + n_{nm}$, where n_{nm} is a zero-mean noise with a power spectral density (PSD) $S_{nn_{nm}}$ to be specified. This noise can be compared to the output-injected remnant of a quasi-linear model, such as the one in Hess’ initial version of the structural model [86]. Here, however, the noise is multiplicative, like, for instance,

in the model of visual perception proposed in [102]. Thus, the noise power in the motor system scales with the control intention, which is a concept that contributed to the prediction of arm movements described in [103]. For Y_{nm} , Hess' second-order transfer function [86] (cf. section 3.1.1) shall be used. Due to its unitary gain and given that $c \in [-1,1]$, its output can be considered a normalized limb force.

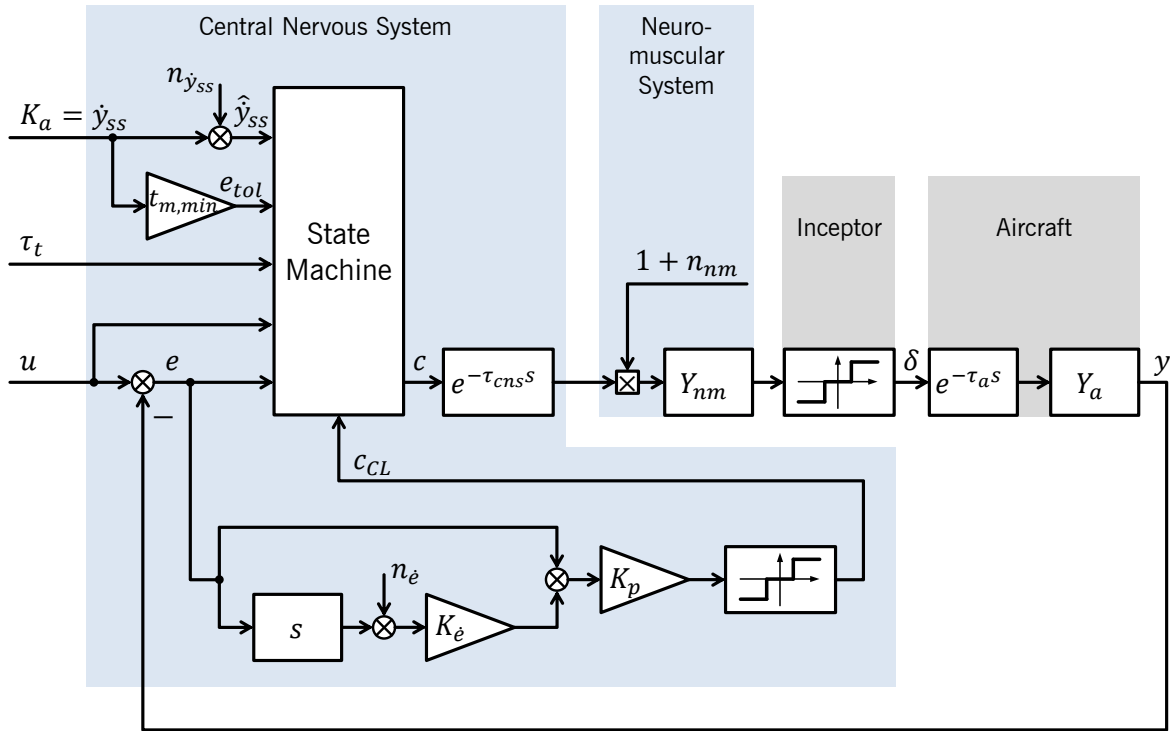


Figure 3.28 – Dual-mode pursuit tracking model, on-off control system

Figure 3.29 visualizes the effect of the multiplicative noise and the neuromuscular transfer function upon a control intention singlet. Both the noise n_{nm} and the low-pass effect of Y_{nm} can be recognized.

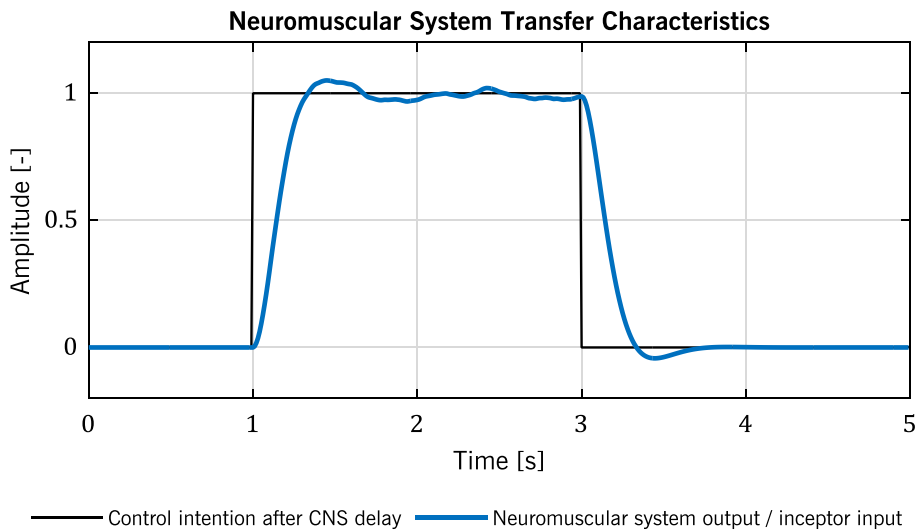


Figure 3.29 – Effects of the proposed pilot model's neuromuscular system

The equivalent delay of the neuromuscular system τ_{nm} , which appears in equations (3.39) and (3.41), shall be defined as the 50% rise time of Y_{nm} . In other words, this definition says that the step response of Y_{nm} reaches half of the step input's value after τ_{nm} . Using the definition of Y_{nm} chosen above, the value of τ_{nm} can be determined to be 0.14 s. This value is slightly higher than that given in section 3.1.1, which is due to the fact that it is derived only from Hess' neuromuscular transfer function, whereas the smaller value from section 3.1.1 approximates both Hess' and McRuer's transfer functions at the same time.

The inceptor finally translates the normalized limb force into a control action δ . The inceptor model here can be compared to the feel system in Hess' structural model (cf. section 3.1.2), with the difference that both force- and deflection-sensing control systems can be described by the same model structure due to the absence of a proprioceptive control loop. Given that an on-off control system is modeled here, the inceptor needs to exhibit the three-level output characteristic that is typical for this control system type. The inceptor mapping function is given by Figure 3.30. The threshold of switching between the "on" state and the "off" state is chosen to be halfway between neutral and limit inceptor input, i.e., halfway between 0 and ± 1 , so that switching always occurs at the same time after a change in control intention, regardless of the direction of change.

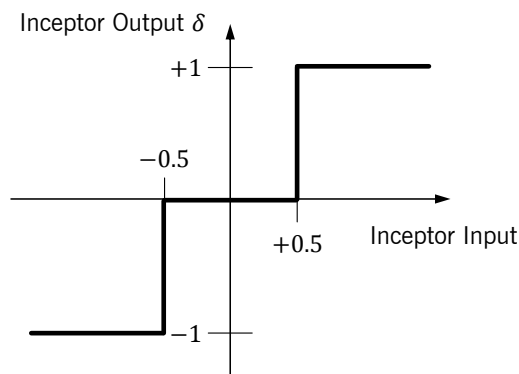


Figure 3.30 – Inceptor mapping function

Next, the signal path from error e to closed-loop control intention c_{CL} is described. Here, the compensatory tracking model of section 3.3.1 is employed. It is assumed that the pilot can derive the error rate and thereby generate lead, but that error derivation also introduces an additional zero-mean noise $n_{\dot{e}}$ with a PSD denoted $S_{nn_{\dot{e}}}$. This assumption is in line with established pilot models. The lead time constant $K_{\dot{e}}$ can be interpreted as an internal model of the time delay (cf. section 3.3.1). It is therefore assumed that $K_{\dot{e}}$ satisfies equation (3.42). The noise $n_{\dot{e}}$ represents estimation errors of both the error rate and the time delay. It ultimately causes the cancellation of the total time delay τ_t by the lead time constant $K_{\dot{e}}$ to be non-perfect.

$$K_{\dot{e}} = \tau_t \quad (3.42)$$

Like in section 3.3.1, the pilot gain K_p , which amplifies the sum of error and derived error, effectively represents the inverse of the desired accuracy. Therefore, it can be related to the parameter e_{tol} , as shown by equation (3.43).

$$K_p = \frac{1}{e_{tol}} \quad (3.43)$$

The subsequent decision mapping element has the same characteristic as the one employed in the compensatory tracking model of section 3.3.1. This characteristic is shown in Figure 3.20. The decision mapping element then feeds c_{CL} to the state machine.

Finally, the way some state machine inputs are generated requires further explanation. First, the task not always specifies the tolerated error e_{tol} . It is assumed that pilots then strive to attain the smallest e_{tol} that is practically achievable. Given that control inputs are of fixed magnitude, this value can in fact be related to the effective reaction magnitude \dot{y}_{ss} via the minimum move time $t_{m,min}$, as described by equation (3.44). This minimum move time is equivalent to the shortest control input that can be made with the inceptor and is assumed to be 0.15 s.

$$e_{tol} = \dot{y}_{ss} \cdot t_{m,min} \quad (3.44)$$

Second, an estimation of the effective reaction magnitude \hat{y}_{ss} is used in the state machine to compute the move phase duration. As Figure 3.28 shows, this estimation is obtained by adding a noise $n_{\dot{y}_{ss}}$ to the actual value of the effective reaction magnitude. This zero-mean noise with a PSD $S_{n_{\dot{y}_{ss}}}$ represents the fact that the pilot's internal model of the reaction magnitude is imperfect. Hence, it is comparable to the additive noise n_e on the derived error, which describes inaccuracies of the pilot's internal model of the total time delay. The total time delay τ_t used in the state machine, on the other hand, does not need to be disturbed by noise, because it is either multiplied by \hat{y}_{ss} and $k_{\dot{y}}$, which already account for the pilot's uncertainty, or it is introduced as a part of wait phase duration t_w , which is not estimated by the pilot and therefore not affected by estimation errors.

Regarding the overall structure of the proposed pilot model, which is motivated by previously reported observations of human operator behavior and the authors own experience, it can be noted that it does not contain proprioceptive or vestibular feedback loops. On the one hand, such feedbacks are not required to describe the operator behavior under consideration. On the other hand, their absence means that the model is applicable to both RPA and BMI control. To apply the above model, which in this form is suited only for manual control of on-off control systems, to BMI control, the neuromuscular system and the inceptor need to be replaced by a suitable BMI model, like the one presented in section 3.4.2 of this thesis.

A variant of the above model, which is detailed in the following paragraphs, describes manual control with a continuous control system. The structure of this variant is shown in Figure 3.31. There are only two modifications with respect to Figure 3.28: the gain K_{agg} is introduced to the CNS and a different inceptor characteristic is employed. The parameter K_{agg} describes the input aggressiveness, which is presented in section 3.3.2 as an additional degree of freedom available to the pilot. It is constrained as in equation (3.45).

$$0 \leq K_{agg} \leq 1 \quad (3.45)$$

When the pilot operates at maximum aggressiveness, i.e., $K_{agg} = 1$, he makes control inputs with the maximum possible magnitude. It is assumed that K_{agg} does not change during a control input, but that the pilot may change aggressiveness between control inputs. This assumption is justified by the observations of pulse-like behavior shown in section 3.2.2. Variations in aggressiveness effectively modify the steady-state system velocity \dot{y}_{ss} during a control input, as equation (3.46) shows. A change of K_{agg} thus not only affects the functioning of the state machine, but also leads to a change in e_{tol} , governed by equation (3.44). This is quite logical: small control amplitudes are employed during fine tracking, where the desired accuracy is highest.

$$\dot{y}_{ss} = K_{agg} \cdot K_a \quad (3.46)$$

The inceptor of the continuous control system is a feedthrough combined with a saturation that represents maximum and minimum inceptor deflections. The saturation ensures that $\delta \in [-1,1]$.

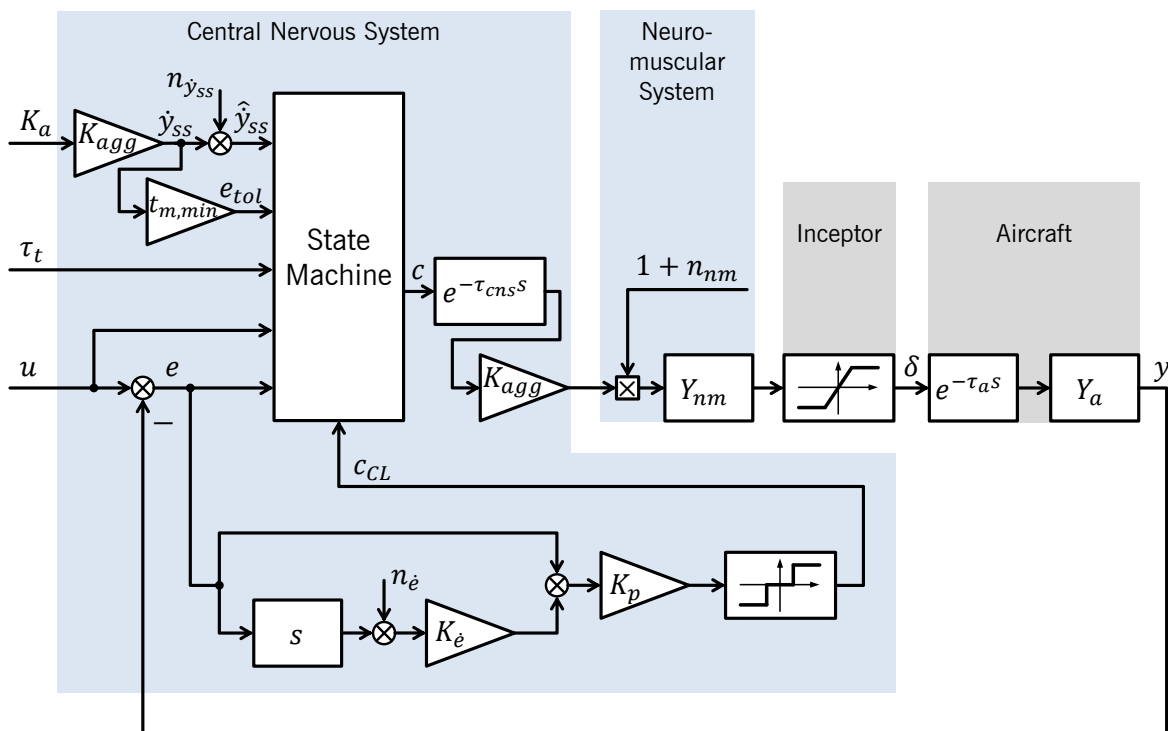


Figure 3.31 – Dual-mode pursuit tracking model, continuous control system

Apart from the changes in the model structure discussed above, only one of the parameters needs to be modified so that the model describes manual control with a continuous control system. Section 3.3.2 noted that an on-off control system, with its fixed control amplitudes, facilitates familiarization with these amplitudes. If, on the other hand, pulse-like control inputs are made with a continuous control system, it is more difficult to familiarize with the system's response, because the amplitude of two control inputs is

never exactly equal. An increased power of the noise $n_{\dot{y}_{ss}}$ shall reflect the reduced familiarity with the effective reaction magnitude when using a continuous control system.

To finalize the model description, the noise spectra need to be defined. First, consider the noise in the neuromuscular system. It passes the neuromuscular transfer function Y_{nm} with its physical low-pass characteristics before appearing as a disturbance in the force applied to the inceptor. Hence, n_{nm} can be considered a white noise with zero mean, like the motor noise in [103]. If also the same 1% coefficient of variation is chosen as in [103], one obtains the noise PSD defined by equation (3.47), which is constant across all frequencies. Note that Figure 3.29 and Figure 3.32 have been created using this noise spectrum.

$$S_{nn_{nm}} = 10^{-4} \quad (3.47)$$

The noises $n_{\dot{e}}$ and $n_{\dot{y}_{ss}}$ mainly describe errors in perception. Therefore, the model of visual perception affected by noise presented in [102] shall be used as a reference. There, a white noise is passed through a first-order low-pass filter with a time constant of 0.5 s. Likewise, measurements of human operator remnants also often exhibit first-order characteristics [86, 104]. Each of the noises $n_{\dot{e}}$ and $n_{\dot{y}_{ss}}$ is therefore assumed to resemble a first-order process with a time constant of 0.5 s. The power of the visual perception noise proposed in [102] scales with the perceived parameter. Similarly, the power of $n_{\dot{y}_{ss}}$ is hypothesized to scale with K_a . An additional scaling factor $k_{n_{\dot{y}}}$ is to be determined empirically. Equation (3.48) defines the resulting PSD of $n_{\dot{y}_{ss}}$.

$$S_{nn_{\dot{y}}}(\omega) = \frac{k_{n_{\dot{y}}} \cdot K_a}{0.5j\omega + 1} \quad (3.48)$$

The power of $n_{\dot{e}}$, on the other hand, is hypothesized to scale with $K_a \cdot \tau_a$. The additional factor τ_a is introduced because it is assumed that applying the correct amount of lead becomes more difficult as the time delay increases. The PSD of $n_{\dot{e}}$ is thus defined by equation (3.49). The additional scaling factor $k_{n_{\dot{e}}}$ has to be determined empirically.

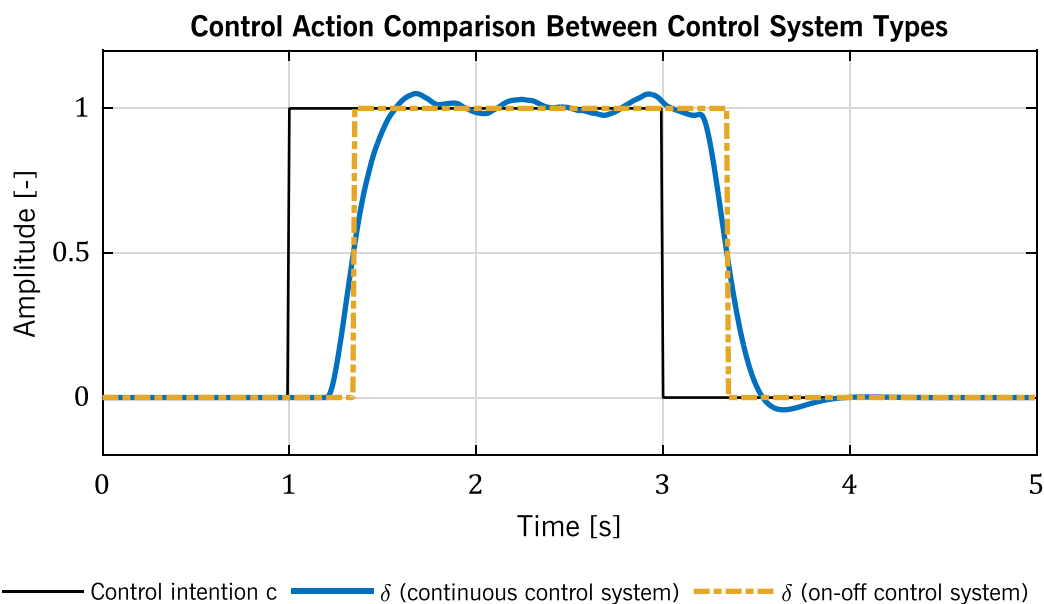
$$S_{nn_{\dot{e}}}(\omega) = \frac{k_{n_{\dot{e}}} \cdot K_a \cdot \tau_a}{0.5j\omega + 1} \quad (3.49)$$

The definition of the noise spectra finally concludes the model description. The structure and the parameters defined above together completely describe the proposed dual-mode pursuit tracking model. The model parameters can be categorized into dependent parameters such as e_{tol} , whose value can be derived from other quantities, and independent parameters like $k_{\dot{y}}$. Only the independent parameters, which are listed in Table 3.2, constitute degrees of freedom for fitting the model to experimental data. Based on previous research or good engineering judgement, four of these independent parameters, namely τ_{cns} , Y_{nm} , $t_{m,min}$ and $k_{\dot{y}}$, are fixed a priori. Therefore, the model is fitted to experimental data in section 6.5 by only varying the two noise parameters and, in case of a continuous control system, the input aggressiveness.

Table 3.2 – Independent parameters of the dual-loop pursuit tracking model

Symbol	Description	Value
τ_{cns}	CNS time delay	0.2 s
Y_{nm}	Neuromuscular transfer function	$\frac{100}{s^2 + 2 \cdot 0.707 \cdot 10 \cdot s + 100}$
$t_{m,min}$	Minimum duration of a control input	0.15 s
$k_{\dot{y}}$	Factor describing the preference for open-loop control	1.1
K_{agg}	Pilot aggressiveness (continuous control system only)	To be determined empirically
$k_{n_{\dot{e}}}$	Scale factor of the noise $n_{\dot{e}}$	
$k_{n_{\dot{y}}}$	Scale factor of the noise $n_{\dot{y}_{ss}}$	

Now that a version of the pilot model for each control system type is defined, the differences between on-off control systems and continuous control systems can be analyzed. First, the inceptor characteristic determines how the neuromuscular noise is propagated to the controlled system. The feedthrough inceptor characteristics of the continuous control system let the noise pass. With the on-off control system, on the other hand, the neuromuscular noise has almost no effect on the control input δ . This is illustrated by Figure 3.32.


Figure 3.32 – The effect of control system type on neuromuscular noise rejection

Here, the same control intention singlet is passed through the neuromuscular system and then either fed through by the continuous inceptor or mapped by the on-off inceptor. It can be seen that with the on-off control system, only the equivalent time delay of the neuromuscular system affects the signal, whereas the continuous control system also propagates the output-injected noise. Note that the saturation of control action δ at +1 is neglected here. This can be justified in case the two control systems have different gains

$K_{a,continuous} = k \cdot K_{a,on-off}$ with $k > 1$, which would enable both larger and smaller control inputs with the continuous control system as compared to the fixed on-off control magnitude. For the present analysis, this factor k can be moved from the aircraft to the inceptor, which then has a slope of k and saturation limits at $\pm k$. If, at the same time, $K_{agg} = 1/k$, the pilot produces a nominal $\delta = 1$ with either control system.

The second and probably more important difference between the control system types is the power of the noise $n_{y_{ss}}$. As discussed above, it is larger in case of a continuous control system, because the pilots' familiarity with the effective reaction magnitude is reduced. As a result, the duration of the move phases is more inaccurate, leading to larger over- or undershoots and an overall poorer tracking performance. With any control system, familiarity can be gained through training. This means that after extensive training, pilots may achieve a similar level of familiarity with the effective reaction magnitude using either control system type. Equivalently, the power of the noise $n_{y_{ss}}$ would then be similar between control system types and the difference in performance negligible.

Regardless of the type of control system employed, the aircraft transfer function Y_a should contain as few lags as possible. In the pilot model above, those lags are grouped in the equivalent time delay τ_{lags} and thereby cause the duration of the wait phase to increase. As a result, any given maneuver takes longer to accomplish. A lightly damped aircraft response as the other extreme is undesirable as well, because overshoots and oscillations make the system's steady state difficult to predict and pilots may thus apply unnecessary or incorrect control inputs before the system has settled. Alternatively, they can wait for the system to settle, which, again, prolongs the wait phase. Generally, the controlled system (without the time delay) should satisfy established handling qualities criteria or requirements to ensure an adequate response also in case large delays are present.

3.4 BMI Modeling

3.4.1 An Introduction to BMIs

A concise definition of BMIs, which are also often referred to as Brain-Computer Interfaces or BCIs, is given by Graimann et al. [52]: BMIs process electroencephalography (EEG) measurements of the brain's electrical activity in real time to detect brain patterns that reflect the user's intent. More concrete, a BMI is a type of neuroprosthesis that enables communication with the environment while bypassing the body's normal efferent pathways. This is illustrated by Figure 3.33. To operate a machine, humans usually move or apply forces with hands or feet. The muscle activity is commanded by the CNS through efferent nerves. When a BMI is used, these efferent nerves are bypassed. It has to be emphasized that the BMI communication pathway is unidirectional, whereas the efferent muscle activity is paired with the sense of proprioception. This means that even though BMI control bypasses the efferent pathways, the user has to rely on his senses and the afferent nerves to obtain feedback on his control activity.

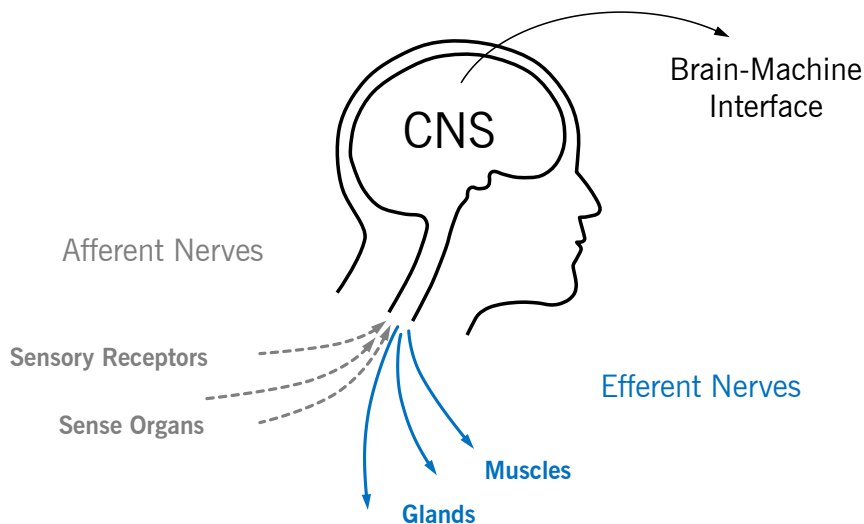


Figure 3.33 – Afferent and efferent pathways and the BMI pathway

EEG technology already existed in the 1920s and the first BMI was described in 1964 [52], but the computer performance required for adequate online EEG signal processing only became available or affordable some decades later. In recent years, BMI research has advanced with big steps and has led to successful control of prostheses [105, 106], cars [53], quadcopters [55] and simulated airplanes [57, 107].

The concept of brain control may still sound mystic to many, but the secret of BMIs really lies in very down-to-earth signal processing. As illustrated by Figure 3.34, it starts with the acquisition of EEG signals, which are subsequently amplified and preprocessed. The final steps of feature extraction and classification constitute the core of any BMI and result in an output signal that, ideally, reflects the user's intent.

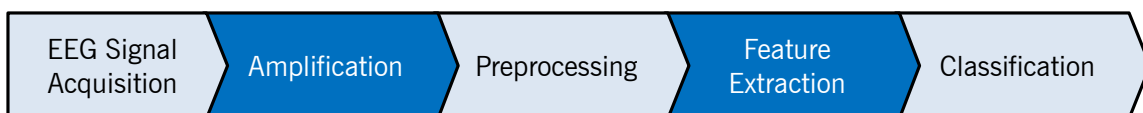


Figure 3.34 – Steps of BMI signal processing

Due to its noisy nature, the BMI output signal is usually filtered. Moreover, the output signal is normally presented to the user on a visual or other display to compensate for the unidirectional nature of the BMI pathway. It has to be stressed, however, that any filtering or feedback occurring after classification are not considered part of the BMI in the scope of this thesis. The BMI community usually considers all elements from EEG signal acquisition to user feedback part of the BMI. This definition is motivated by the fact that all these elements are required for the human operator to learn how to use the BMI. It is, however, not practical in the present case. The following paragraphs provide a more detailed description of the five BMI elements from Figure 3.34.

EEG signals can be acquired in different ways. The best signal quality is achieved with intracranial electrodes. However, this invasive method requires brain surgery, which is unacceptable for most potential users. Far more suited for a broad application of BMIs are

non-invasive EEG systems, which use electrode caps or nets placed on the user's scalp. The number of electrodes employed depends on the required spatial resolution and can range from a single one to over 256. Electrodes are either wet or dry. Wet electrodes are more common in research applications, because they generally offer a better signal quality [108]. Their application is, however, somewhat cumbersome. Beneath each electrode, the user's skin is prepared by light abrasion and an electrolyte gel is applied to reduce impedance [14]. This set-up process takes some time, depending on the number of electrodes used. After the cap is removed, the subject's head is still full of gel that needs to be washed out. Dry electrodes, on the other hand, are far easier to handle. Some consumer EEG systems look like headsets and comprise one or more dry electrodes [109, 110]. After the EEG signals have been captured by the electrodes, they are amplified. To achieve a high suppression of interference, pre-amplification can already be done at the electrode itself. Such electrodes are called active electrodes. The preprocessing stage is responsible for improving the signal-to-noise ratio (SNR). It usually employs low-pass or notch filters to suppress power supply noise and noise in frequency bands that do not contain EEG activity. Feature extraction and classification are the heart of every BMI. The signal processing done in these two stages is closely related to the approach the user has to take to issue commands. This is best illustrated by a description of two exemplary types of BMI.

The so-called Motor Imagery BMIs rely on the fact that when an individual imagines performing a movement of his body, the event-related desynchronization of the motor rhythm is similar to when the movement is actually performed [107, 111]. Feature extraction comprises localization of this event-related desynchronization on the scalp, which depends on the part of the body whose movement is imagined. Classification is done based on the outcome of this localization. For instance, if the user imagines a movement of his left/right hand or arm, relevant neuronal activity appears in distinct regions of the right/left [sic!] brain hemisphere. The feature extraction and classification algorithms detect this activity and thereby recognize the body part involved in the imagined movement. For this approach to work, the classifier needs to be trained for each user and each session. This machine learning process is based on a recording of EEG signals taken prior to each session, during which the user imagines the relevant movements.

In a different approach called Operant BMI, feature extraction consists in determining the power in different frequency bands. Classification then associates different power distributions with different user intentions. This approach is different to most other approaches in that it does not rely on machine learning, but on user training. Indeed, the user needs to learn how to generate the brain activity that the BMI can correctly classify. This is similar to learning how to play a musical instrument. An immediate feedback of control activity and a motivating task are key prerequisites for successful user training. At first, the BMI output appears to be random to the user, but through positive reinforcement, the user can ultimately find a strategy to influence the BMI output and thereby accomplish the given task.

It is common to all existing BMI approaches that the classification output matches the user's intention only with a certain probability, which is sometimes referred to as the

Single-Trial Reliability (STR). Typical STR values attainable with the BMI approaches existing today are $< 80\%$ (cf. section 5.5) and progress towards higher values is slow. It is important to note that the STR also depends on the human-machine adaptation, i.e., the quality of the machine learning result or the user's learning progress. This means that the same BMI algorithms usually yield different STRs for different users and different sessions. A strategy to increase reliability is to rely on several subsequent trials, i.e., BMI outputs, when estimating the user's intention [112, 113]. In other words, a low-pass filter can be applied. When designing such a low-pass filter, the potential increase in reliability has to be traded off against the amount of unwanted lags introduced to the control system.

3.4.2 A Simple BMI Model

It was noted earlier that analyses of the pilot-aircraft dynamic system often rely on pilot models. Existing pilot models make certain assumptions on the pilot's afferent and efferent pathways, which are not all valid in case of BMI control. The neuromuscular system, for instance, is not involved anymore. Instead, the BMI is introduced with its own dynamic characteristics. To illustrate some of those characteristics, to develop an understanding of their effects on control performance and to relate BMI control to the overarching topic of flight control with large time delays, a simple BMI model is set up in this section. A top-down modeling approach is taken, regarding the whole chain from user intention to BMI output as a whole instead of modeling each part of the chain – brain dynamics, EEG sensors and each BMI component – separately and assembling them bottom up. A restriction to one degree of freedom is justified given the single-axis nature of most pilot models and the current state of the art in BMIs. Like in section 3.3, it is assumed that the user intention can be either positive, noted P , neutral, noted Z for zero, or negative, noted N . These intentions can also be represented numerically as in equation (3.17).

BMI signal processing is digital. Thus, the output signal is necessarily time- and value-discrete. Value quantization can usually be neglected, considering that common coding precisions such as, for instance, single floating-point precision, are high enough and cover large ranges of values. BMI output sampling times t_s , however, can be as high as 0.25 s , which is why the time-discrete nature of the output has to be taken into account.

Like a real BMI, the BMI dynamic model has the user intention c , defined by equation (3.17), as input. The model output is the BMI control action $\delta_{BMI} \in \mathbb{R}$. Ideally, if the BMI would operate without uncertainty or latency, it would map inputs to outputs as described by equation (3.50).

$$\delta_{BMI} = c \tag{3.50}$$

However, the BMI classifies the user's intention only with a certain reliability. This characteristic can be modeled as a mapping from user intention to a random variable with a certain probability density function. As a first guess, the probability density function can be assumed to be a Gaussian distribution, defined by the two parameters mean μ and variance σ^2 . Equation (3.51) shows the resulting mapping from the three user intentions to three random variables Δ_P , Δ_Z and Δ_N .

$$\delta_{BMI} = \begin{cases} \Delta_P \sim \mathcal{N}(\mu_P, \sigma_P^2) & \text{for } c = 1 \\ \Delta_Z \sim \mathcal{N}(\mu_Z, \sigma_Z^2) & \text{for } c = 0 \\ \Delta_N \sim \mathcal{N}(\mu_N, \sigma_N^2) & \text{for } c = -1 \end{cases} \quad (3.51)$$

Furthermore, it is assumed that the BMI is not biased and that its output variance is independent from the user input. These assumptions are represented by the following set of equations (3.52).

$$\begin{aligned} \mu_Z &= 0 \\ \mu_N &= -\mu_P \\ \sigma_P^2 &= \sigma_Z^2 = \sigma_N^2 \end{aligned} \quad (3.52)$$

Experience has shown that the assumption of an unbiased BMI is not always valid (cf. chapter 5). It is, however, justifiable for the purposes of this model. Inserting the information from equation (3.52) into equation (3.51), the following equation (3.53) is obtained.

$$\delta_{BMI} = \begin{cases} \Delta_P \sim \mathcal{N}(\mu, \sigma^2) & \text{for } c = 1 \\ \Delta_Z \sim \mathcal{N}(0, \sigma^2) & \text{for } c = 0 \\ \Delta_N \sim \mathcal{N}(-\mu, \sigma^2) & \text{for } c = -1 \end{cases} \quad (3.53)$$

Remember that any filtering after classification is not considered part of the BMI. It is therefore assumed that feature extraction and classification in BMIs is done in a way that each sample is independent from all previous samples. As a result, the BMI output can be modeled as a zero-mean white noise n_{BMI} with shifting bias. The user intention is reflected by this bias. A true white noise exhibits infinite energy, which is not physically possible, but the noise considered here as BMI output is time-discrete and thus band-limited and of finite energy. Equation (3.54) defines the resulting BMI model, with t_0 in square brackets indicating the current sample. Note that the model includes a constant time delay τ_{sp} that represents the signal processing latency. This latency is difficult to quantify, but the sampling time t_s constitutes a good estimate for its minimum value.

$$\delta_{BMI}[t_0] = \mu \cdot \text{sgn}(c[t_0 - \tau_{sp}]) + n_{BMI}[t_0] \quad (3.54)$$

One might argue that the nature of the underlying brain processes could introduce some dependence between consecutive samples. One possible approach to address this issue is to low-pass filter the control intention c , which is the input to the proposed model. This would reflect at least the time required by the user to translate a changing control intention to a change in brain activity.

The idea to model a BMI as a communication channel with additive Gaussian noise has also been presented in [114] and [115]. Interestingly, the concept of this model bears some resemblance to existing quasi-linear pilot models, like Hess' models presented in earlier sections. The resemblance lies in the added noise. The noise injected into

quasi-linear pilot models represents the remnant, i.e., the nonlinear part of the human behavior. If the BMI model of equation (3.54) is combined with existing pilot models, it has to be inserted between pilot and aircraft. The form of the model is that of a delay, a sign function and a gain, followed by additive noise. This structure, shown in Figure 3.35, indeed resembles that of neuromuscular system, inceptor and output-injected remnant. As opposed to the noise n_{nm} of Figure 3.28 and Figure 3.31, which is still passed through the inceptor mapping function, the BMI noise affects the controlled system directly. More importantly, n_{BMI} has much more power than typical remnants. It is indeed the main hindrance to successful BMI control, as the following paragraphs demonstrate.

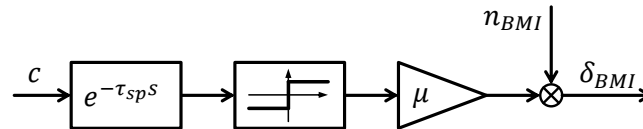


Figure 3.35 – Block diagram of the proposed BMI model

The BMI model given by equation (3.54) permits further analyses of some BMI characteristics. Without making any assumptions on the controlled system, the STR can be defined as the percentage of positive/negative BMI outputs during positive/negative user intention. Following this definition, the STR can be computed as in equation (3.55), where erf is the so-called error function.

$$\text{STR} = \frac{1}{2} \left(1 - \text{erf} \left(\frac{-\mu}{\sigma\sqrt{2}} \right) \right) \quad (3.55)$$

The definition above does not take into account neutral user intention. This would require an assumption on BMI signal mapping in the first place, which is considered a variable element of the controlled system. STR as defined by equation (3.55) is a suitable metric that characterizes the BMI alone. Another suitable metric is the SNR of the BMI output, which can be determined using the following equation (3.56).

$$\text{SNR} = \frac{\sigma_{\text{signal}}^2}{\sigma_{\text{noise}}^2} = \frac{\mu^2}{\sigma^2} \quad (3.56)$$

Both STR and SNR improve as the parameter μ increases and the variance σ^2 of the noise decreases. It is also evident that a nonzero μ is required for STRs greater than 50% (chance) and SNRs greater than 0. The relation between STR and SNR is in fact fixed for Gaussian distributions with arbitrary $\mu \geq 0$ and $\sigma > 0$. In this case, equation (3.56) can be inserted into equation (3.55) to obtain equation (3.57).

$$\text{STR} = \frac{1}{2} \left(1 - \text{erf} \left(-\sqrt{\frac{\text{SNR}}{2}} \right) \right) \quad (3.57)$$

Figure 3.36 illustrates the relation between STR and SNR for relevant STR values. Note the small SNR values.

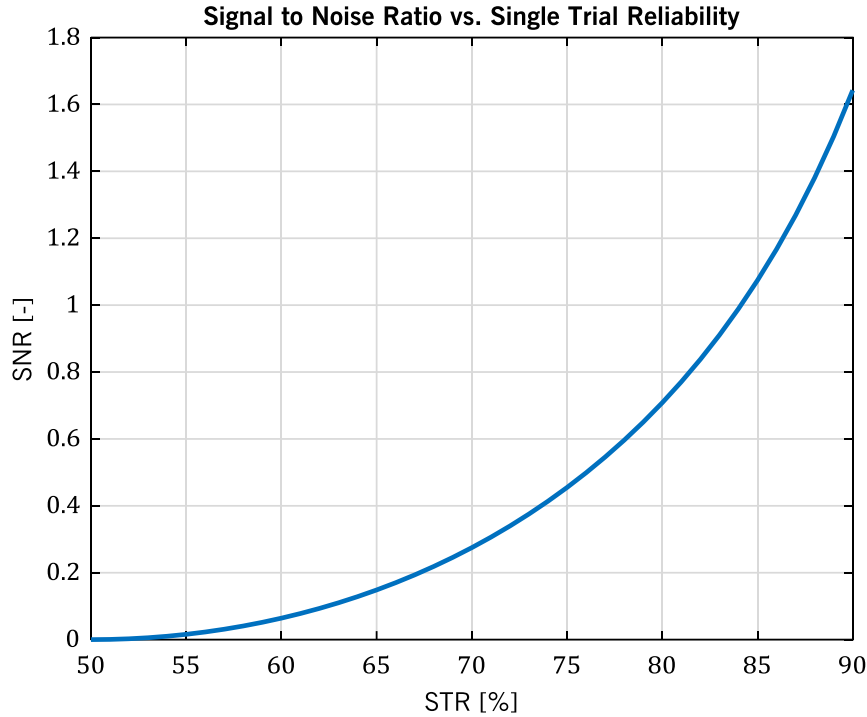


Figure 3.36 – Relation between SNR and STR

As described in section 3.4.1, the performance of any type of BMI control system depends on the quality of the mutual adaptation between human and BMI. In those cases where user training plays the leading part and machine learning is negligible, the proposed equation (3.57) models not only the BMI itself, but also to some extent the user's performance. STR and SNR thus become human performance metrics or measures of training success. In addition to metrics like Fitts' index of performance [116] or, more generally, the information transfer rate, which is usually measured in bits per second and often employed for BMI communication or target acquisition tasks, the SNR may be a valuable performance indicator for tracking tasks with asynchronous BMIs.

With STRs still well below 100% in current BMI systems and the resulting poor SNR, what can be done to improve reliability? If the user's intention can indeed be read from the mean value of the BMI output signal, a first attempt would be to employ a moving average filter. An n^{th} -order simple moving average (SMA) filter can be defined by the discrete transfer function given in equation (3.58), where z is the Z-transform variable.

$$H_n(z) = \frac{1}{n+1} \sum_{k=0}^n z^{-k} \quad (3.58)$$

Such a low-pass filter evidently produces phase lag. The phase lag introduced by an n^{th} -order simple moving average filter with sampling time t_s can be derived given that equation (3.59) holds for $|z| < 1$. The product $t_s \omega$ is the normalized frequency $\tilde{\omega}$.

$$z = e^{jt_s \omega} = e^{j\tilde{\omega}} \quad (3.59)$$

Using equation (3.59), equation (3.58) can be rewritten so that amplitude A and phase φ of the discrete transfer function explicitly appear (equation (3.60)).

$$\begin{aligned}
 H_n(j\tilde{\omega}) &= \frac{1}{n+1} \sum_{k=0}^n e^{-kj\tilde{\omega}} = \\
 &= \frac{1}{n+1} (1 + e^{-j\tilde{\omega}} + e^{-2j\tilde{\omega}} + \dots + e^{-nj\tilde{\omega}}) = \\
 &= \frac{e^{-\frac{n}{2}j\tilde{\omega}}}{n+1} (e^{-(0-\frac{n}{2})j\tilde{\omega}} + e^{-(1-\frac{n}{2})j\tilde{\omega}} + \dots + e^{-(\frac{n}{2}-1)j\tilde{\omega}} + e^{-(\frac{n}{2}-0)j\tilde{\omega}}) = \quad (3.60) \\
 &= \frac{e^{-\frac{n}{2}j\tilde{\omega}}}{n+1} \left(\underbrace{e^{\frac{n}{2}j\tilde{\omega}} + e^{-\frac{n}{2}j\tilde{\omega}}}_{=2 \cos(\frac{n}{2}\tilde{\omega})} + \underbrace{e^{(1-\frac{n}{2})j\tilde{\omega}} + e^{-(1-\frac{n}{2})j\tilde{\omega}}}_{=2 \cos((\frac{n}{2}-1)\tilde{\omega})} + \dots + \underbrace{+1}_{\text{if } n \text{ even}} \right) = \\
 &= A(\tilde{\omega}) \cdot e^{-\frac{n}{2}j\tilde{\omega}} \\
 &= A(\tilde{\omega}) \cdot e^{j \cdot \varphi(\tilde{\omega})}
 \end{aligned}$$

As a result, the phase lag of an n^{th} -order simple moving average filter with sampling time T_s can be written as in equation (3.61). Note that this equation only holds for frequencies below the smallest frequency where $A(\tilde{\omega})$ changes sign. The unit of φ_{SMA} is [rad] here.

$$\varphi_{SMA}(\omega) = -\frac{n \cdot t_s}{2} \omega \quad (3.61)$$

Remember that the phase lag introduced by a pure time delay τ , too, varies linearly with frequency. More exactly, it is defined by equation (3.62). Note that here, the unit of φ_τ is [rad] as well.

$$\varphi_\tau(\omega) = -\tau \cdot \omega \quad (3.62)$$

Both equations (3.61) and (3.62) can be combined to obtain the value of pure time delay that produces the same amount of phase lag as an n^{th} -order simple moving average filter with sampling time t_s . This, as it shall be called, filtering time delay τ_{filt} , which is given by equation (3.63), is helpful in relating the effects of BMI signal filtering to the effects of communication latencies in the case of RPA.

$$\tau_{filt} = \frac{n \cdot t_s}{2} \quad (3.63)$$

The total time delay apparent during BMI control is the sum of signal processing delay and filtering delay, as equation (3.64) indicates. Note that the breakdown of the total BMI delay into two separate delays is also apparent in the block diagram of Figure 1.2.

$$\tau_{BMI} = \tau_{sp} + \tau_{filt} \quad (3.64)$$

To get an idea about possible values of this BMI time delay, consider a BMI with a sampling time $t_s = 0.25 \text{ s}$. The noise introduced by the BMI is assumed white, i.e., its

components are equally distributed across the frequency spectrum from zero to the Nyquist frequency. To identify a stationary user intention with high reliability, a filter of fairly high order could be chosen. Suppose, however, that some target tracking is to be performed. The filter therefore needs to let some more frequencies pass. In the experiments described in chapter 5, a low-pass filter is employed which is comparable to an 8th order SMA filter. In this case, the filtering time delay resulting from equation (3.63) is 1.0 s. Adding this delay to the sampling time of 0.25 s, which is chosen here as an estimate for the signal processing time delay, a total τ_{BMI} of 1.25 s results. This result is in the range of time delay values considered in this thesis.

Consider that a BMI replaces the neuromuscular system, whose characteristics are described in section 3.1.1. This means that the time delay of about 0.13 s inherent to the neuromuscular system is not an issue anymore. However, the BMI reintroduces considerable lags. For a BMI to outperform the neuromuscular system in this regard, it would have to operate, for example, at 10 Hz and provide highly reliable outputs without filtering. Such a level of performance is still far from reality.

4 FLIGHT CONTROL SYSTEM DESIGN

A flight control system encompasses the entire chain from the inceptor (or BMI) through the flight control algorithms and the airplane dynamics to the feedback mechanisms or displays. From the pilot's point of view, this ensemble of augmented aircraft dynamics and human machine interfaces constitutes the controlled system. Establishing good handling qualities for this controlled system is one aim of flight control system design. In the scope of this thesis, the aircraft dynamics are considered given, thus leaving inceptor (or BMI), flight control algorithms and displays as the only elements that can be modified in the design process. The flight control system design process described in this chapter is guided by the information about aircraft and pilot as the two given elements, provided in previous chapters. Figure 4.1 illustrates the interrelations between the elements of the flight control system and the pilot.

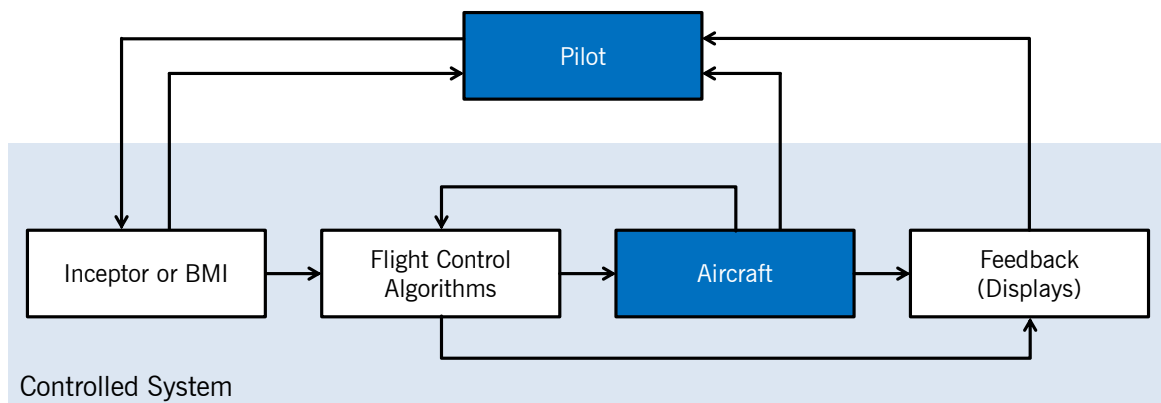


Figure 4.1 – Pilot and controlled system. Pilot and aircraft are considered given.

The pilot exerts control via the inceptors or the BMI, and in turn receives a feedback of his control activity (e.g., proprioceptive inceptor feedback). When onboard the aircraft, the pilot also perceives sensory cues from vehicle movement or engine noise. In any case, displays may provide additional feedback either of the aircraft state or of other parameters computed by the flight control algorithms. The flight control algorithms furthermore derive the control effector activities required to follow the inceptor or BMI inputs using aircraft measurements.

This chapter, which is in parts based on what the author has already presented in [73, 117, 118], first analyzes existing requirements and elicits some high-level design goals on the three elements to be laid out. Moreover, basic design choices are made based on these goals and the information presented in preceding chapters of this thesis. Handling implications of these choices are discussed as well. In a second step, the flight controller is laid out. The focus here is on the choice of command variables and on the protection mechanisms layout. The actual controller implementation and performance is only briefly described, since these control engineering aspects are not relevant to this thesis. Indeed, the controller is based on the dynamic model of the DA42 to obtain realistic simulations, but it is not meant to be applied in a real airplane. Third, a suitable inceptor dynamic design is elaborated and desirable BMI characteristics outlined. Finally, some considerations on sensory feedback are presented.

4.1 Design Goals, Basic Design Choices and Implications

Based on the information collected in the preceding chapters, high-level goals for the flight control system are now derived and basic design choices made. Goals are defined verbally and qualitatively only and shall not be confused with requirements. For actual implementation in a real airplane, those goals would need to be broken down to requirements on item level and these would need to be quantitative. This process is beyond the scope of this thesis.

For both example applications, the flight control system obviously cannot be purely mechanical or hydraulic. It needs some digital flight control algorithms that translate BMI output or remote control signal to control surface deflections. Hence, a maneuver demand system can readily be implemented instead of a direct mapping of pilot inputs to control surface deflections. Indeed, only a prudent choice of command variables may provide controllable handling qualities. Section 3.2.1 describes that time delays cause a crossover frequency regression of the open pilot-aircraft loop and section 3.4 explains why only low bandwidth control is possible with BMIs. Both facts result in the aim to choose command variables that vary on larger time scales. Thus, disturbances on small time scales are rejected by the flight controller, which itself does not have to deal with excessive time delays. The implementation of this design goal shall, however, not result in an excessively high degree of automation, as this would oppose the aim of this thesis to enable lower-level flight control, as defined in section 1.3.1. The choice of command variables shall also enable the pilot to conduct the mission described in section 2.1.2 with all its flight phases. Given that crosswinds during takeoff and landing are not considered, it can be assumed that the pilot does not need to make directional control inputs at all. This means that only a longitudinal and a lateral command variable need to be defined. In this case, coordinated flight needs to be ensured by the flight control algorithms. Airspeed control shall be performed via an autothrottle system that acquires and maintains the desired indicated airspeed (IAS). Another design goal is to facilitate pilot transition between the proposed flight control system and other manned or unmanned airplanes. Hence, the airplane's reactions to control inputs shall be of the same order as with the conventional behavior described in section 2.2.2. Furthermore, the control algorithms shall be designed to avoid

excessive lags between control input and command variable reaction, since these lags would prolong the wait phase (cf. section 3.3.3).

The BMI shall enable asynchronous control and thereby target tracking in two degrees of freedom. For each degree of freedom, it shall be possible to issue three control input levels: positive, neutral and negative. This performance is close to what has already been achieved with the current state of the art. However, it certainly seems that this three-level control capability constitutes a major restriction for flight control. Section 3.3.2, though, describes how the deliberate restriction of (manual) control inputs to few discrete levels may be beneficial in the case of flight control with large time delays. To recapitulate the previous analyses and findings, first recall that pilots adopt a pulse-like control behavior when facing large time delays (cf. section 3.2.2). The control inputs resulting from this behavior are actually similar to the three-level BMI inputs. Given that this pulse-like control behavior reduces mental workload and is adopted naturally, it may be helpful if the flight control system would support this strategy. When using, for example, an on-off control system with three discrete control input levels (positive, neutral and negative), the pilot is relieved from manually generating pulse-like control inputs with a continuous inceptor. Moreover, predictability is increased as the control input amplitude is indeed fixed (cf. sections 3.3.2). Pilots can quickly familiarize with the fixed aircraft reaction magnitude and can then fly certain maneuvers only by estimating the duration of their control inputs (cf. section 3.3.3). The highly predictable nature of the airplane's response gives pilots a pre-cognitive ability that is helpful for prolonged maneuvers and even more for maneuvers that are shorter than the time delay itself. In the latter case, pilots can only rely on the open-loop move-and-wait strategy. Relying on pre-cognitive tracking, chances are high that they only need to make one single move to reach a target. Furthermore, overshoots are generally less critical in flight control than in teleoperation tasks and control inputs can therefore be more aggressive (cf. section 3.2.2). By combining the move-and-wait strategy with more aggressive control inputs and pre-cognitive tracking, the time to reach a target state is greatly reduced.

Interestingly, the proposed on-off control system is similar to some control laws used for manual spacecraft control. This is probably due to the fact that manned spacecraft usually rely on reaction control systems with constant-thrust jets as control effectors. To generate forces and moments, one or more jets can be fired or, in other words, turned on and off again. Table 4.1 and the following paragraph show that manned spacecraft always offered a wide range of different control modes, including continuous control similar to airplane control, on-off control modes like the one chosen in this thesis and also pulse control, where both amplitude and duration of every control input are fixed. In the latter case, the human pilot can accomplish maneuvers by counting the pulses, which is even less mentally demanding than estimating control input duration. As section 3.2.2 points out, operators tend to use continuous controllers in an on-off manner when controlling higher order systems or systems with time delay. It is therefore not surprising that operators have been observed applying pulsed inputs, i.e., inputs of constant duration to on-off controllers, both in [96] and in the experiments described in chapter 6.

The Mercury spacecraft offered three control laws for attitude control [119]. The so-called “fly-by-wire mode” implemented on-off control of the low/high torque jets for small/large inceptor inputs. In the “manual proportional control mode” the jet vanes were opened to an extent proportional to the inceptor deflection. Finally, there was a “rate command mode” similar to that known from airplane flight control systems. The Gemini spacecraft, too, featured three different control laws for attitude control, including a “rate control mode” and a so-called “direct mode” similar to Mercury’s fly-by-wire mode [120]. The third mode, “pulse control”, delivered one thruster pulse for each inceptor deflection out of the deadband. Of those three modes, the direct mode was intended for standby or emergency control only. Translational control of the Gemini spacecraft was done using an on-off control system. The Apollo Lunar Module employed a rate control attitude hold system as major attitude control mode and a secondary, minimum impulse mode that was similar to Gemini’s pulse control mode [121]. To change the predicted location of touchdown, indicated by the landing point designator (LPD), astronauts could incrementally shift its downrange and lateral location in a pulse-control manner [122]. During final lunar descent, rate of descent too was controlled incrementally with discrete hand controller clicks. After the first landings had been accomplished, an advanced configuration of the so-called P66 control algorithm was implemented that allowed pilots to command incremental changes in horizontal velocity as well [122]. Pulse control was also employed by the National Aeronautics and Space Administration (NASA) on the Space Shuttle Orbiter and constitutes the baseline response type planned for their Orion and Altair spacecraft [123].

Table 4.1 – Example implementations of different control system types in spacecraft

Control System Type	Exemplary Spacecraft Control Modes
Continuous control	<ul style="list-style-type: none"> ▪ Mercury “manual proportional mode” ▪ Mercury “rate command mode” ▪ Gemini attitude control “rate command mode” ▪ Apollo Lunar Module “rate command attitude hold”
On-off control	<ul style="list-style-type: none"> ▪ Mercury “fly-by-wire mode” ▪ Gemini attitude control “direct mode” ▪ Gemini translational control
Pulse control	<ul style="list-style-type: none"> ▪ Gemini attitude control “pulse mode” ▪ Apollo Lunar Module attitude “minimum impulse mode” ▪ Apollo Lunar Module LPD and rate of descent control ▪ Apollo Lunar Module P66 advanced configuration ▪ Space Shuttle Orbiter ▪ Orion and Altair baseline

Some studies have investigated the effect of different control modes on manned spacecraft handling. The results of these studies are not directly transferrable to the present problem of large time delays, but they prove that implementing a non-continuous control mode is a valid approach in aerospace vehicle control. To determine required handling qualities for the Apollo Lunar Module, Cheatham and Hackler conducted piloted simulations of the lunar landing with different control system characteristics [124]. They concluded that

direct on-off thruster control exhibits inadequate handling qualities, rendering it acceptable only for emergency operations. They note, however, that they had obtained only extremely limited data and that their conclusion must not be transferred to other tasks than the lunar landing. The advanced P66 mode was never used in flight, but simulations indicated that precise landings could be achieved using this mode in conjunction with the LPD and a function to null horizontal velocity [125]. This landing strategy was in fact based on suggestions from Apollo 16 commander John Young. For NASA's future Orion and Altair spacecraft, the influence of different translational and rotational control modes on handling qualities during docking has been investigated in [123] and [126]. According to [123], the most promising configuration for translational control is pulse control with acceleration type vehicle dynamics. On-off control with acceleration type vehicle dynamics produced slightly higher workload, but still outperformed the highly automated control systems that provided either on-off or proportional control with integrator like dynamics. For rotational control [126], the main advantage of on-off rate control over pulse control of rate increments was found to be a lower physical workload. Research on satellite capture using a remotely piloted orbital vehicle found that pilots prefer on-off acceleration control over continuous acceleration control as time delays increase [45].

All in all, the investigations cited above show that on-off control has its limitations, notably when it comes to higher bandwidth tasks such as attitude control during the Apollo lunar landing. They also suggest that a pulse controller could enable even better performance. However, since a pulse control system does not exhibit the usual mapping of control input to aircraft reaction described in section 2.2.2, it is not in line with the aim to facilitate pilot transition between the proposed flight control system and other manned or unmanned airplanes and is therefore not considered. The proposed on-off control system can be seen as a favorable compromise between continuous and pulse control.

The following list sums up the high-level goals and design choices for the controller.

- An on-off control system with 2 degrees of freedom shall be implemented that gives the pilot control over the longitudinal and the lateral airplane motion.
- The controller shall ensure coordinated flight, i.e., $n_y = 0$
- An autothrottle system shall maintain the desired IAS
- Command variables shall be chosen that vary on a larger time scale.
- The mission described in section 2.1.2 shall be accomplishable.
- The airplane's reactions to control inputs shall be of the same order as with the conventional behavior described in section 2.2.2.
- The reaction of command variables shall not excessively lag the control inputs

Now that several design choices concerning the flight controller have been made, the design space of the inceptor needs to be narrowed down as well. For intuitive handling, the inceptor characteristics should reflect the controlled system's dynamic characteristics. In this present case, the on-off nature of the flight control system shall be apparent to the pilot through the inceptor. The inceptor shall also facilitate transition between different RPA and also manned aircraft. In the case of BMI control, the desired BMI performance stated in a previous paragraph, namely asynchronous control in two degrees of freedom, obviously replaces the inceptor design goals.

The third element of the flight control system, complementing controller and inceptor (or BMI), is pilot feedback. While some sensory feedback is inherently present, at least in the case of on-board manned flight control, some additional displays can be designed as required. For instance, a video feed from the RPA shall be available, covering at least the forward field of view. Apart from the usual cockpit instruments showing airspeed, altitude, etc., the display of additional parameters like the flight path vector may be helpful, depending on the choice of command variables and on whether or not those parameters can be easily perceived by the pilot. There is no doubt that predictor displays improve RPA handling, which is why such displays should be implemented for any operational system. Their positive effect is based on an apparent reduction of the time delay. In this thesis, however, time delays are assumed to be effectively present in the control loop (cf. section 1.3.1). Therefore, predictor display implementation is not further discussed.

In the scope of this thesis, the flight control system is only used in simulation experiments. Thus, the flight control system does not need to be certified. Moreover, the example applications either do not require (civil) certification or are not certifiable by today's standards. Nonetheless, a brief analysis of certification specifications is useful to derive further design goals. Remember that non-compliance with these specifications means that the required minimum level of safety is not met and that the concerned aircraft is unsafe to operate (cf. section 2.2.3). In Europe, EASA's CS-23 [60] apply to the reference aircraft. Within subpart B "Flight", relevant specification paragraphs have been identified. Table 4.2 lists them along with a brief description and possible implications for the two example applications.

Table 4.2 – Relevant paragraphs from EASA CS-23

Paragraph(s)	Description	Implications
CS 23.143 CS 23.145 CS 23.147 CS 23.149 CS 23.153 CS 23.161 CS 23.177	Specify maximum control forces	Void in the case of BMI control.
CS 23.155	Specifies limitations on stick force per g (maneuver stability)	Void in the case of BMI control. Effectiveness for RPA control with large time delays is questionable.
CS 23.171 CS 23.173 CS 23.175	Specify limitations on speed stability	Not satisfied if flight control system provides neutral speed stability.
CS 23.201 CS 23.203	Describe controllability during stall and stall recovery	The performance of both BMI control and RPA control with large time delays most likely is insufficient for stall recovery.

It can be seen that several paragraphs, notably all that are related to control forces or displacements, are void in the case of BMI control. These paragraphs mostly aim at establishing situational awareness through proprioceptive feedback or at preventing excessive pilot inputs. Limitations on maneuver stability may not be effective in preventing excessive structural loads also in the case of RPA control with large time delays. Even if a certain force is generated based on the current inceptor deflection and the latest aircraft state received, the resulting command will only become effective after a considerable timespan. By then, the aircraft state will have changed and pilot command may be in fact excessive. Another three paragraphs of CS-23 impose positive speed stability to establish appropriate speed awareness. Depending on the choice of command variables (cf. section 4.2.1), this requirement may be violated. In stalls and spins, certification specifications require docile handling qualities. However, a stall in even a very docile airplane possibly cannot be recovered with BMI control or RPA control with large time delays, because the necessary control inputs need to be well-coordinated and often quite rapid.

The result of the above analysis applies not only to the EASA CS, but to established regulations worldwide. For example, some of the corresponding FAA regulations have been identified in [18] as possibly inapplicable to RPA control. It is certainly no surprise that the two example applications are in dissonance with some existing requirements. On the other hand, even airliners flying today do not satisfy all the original certification specifications. For instance, Airbus fly-by-wire airplanes provide neutral speed stability in some major modes of the flight control system [127, 128]. Certifying authorities can permit non-compliance with the original specifications under the condition that so-called special conditions are satisfied. These special conditions can be seen as replacement paragraphs for the original certification specifications that ensure an equivalent level of safety. Similarly, the following paragraph presents ideas of how to provide an equivalent level of safety in the case of the two example applications.

The most striking problem is that control inputs cannot be limited by inceptor forces in the case of BMI control. Furthermore, situational awareness is diminished in both example applications because either vestibular or proprioceptive feedback is missing. The ability to return to a safe flight envelope after stall is also greatly reduced. The proprioceptive inceptor feedback felt in case of RPA control with large time delays is either decoupled from the actual aircraft state or delayed. Its contribution to handling and safety is therefore limited. An effective and proven way to mitigate these issues is to implement protection mechanisms and limitations within the control system. If the stick force per g cannot be implemented or designed to effectively prevent excessive structural loads, as it is the case for BMI control and possibly also for RPA control [18], the vertical load factor can be limited in the flight control algorithms. Similarly, a low-speed and a high-speed protection can be implemented to mitigate reduced speed awareness resulting from neutral speed stability. Attitude upsets and stalls that may be difficult or impossible to recover from can be prevented by control system limitations. Inadvertent wingtip strikes could be avoided by further limiting permitted attitudes in ground proximity. In a move that goes beyond the scope of this thesis, a terrain protection could be implemented that prevents controlled flight into terrain, thereby mitigating navigation issues rather than flight control issues. Although protection mechanisms and limitations can make an airplane's behavior

non-conventional and therefore rather counterintuitive, their effectiveness in keeping the airplane safely aloft is more important here.

4.2 Controller Design

4.2.1 Command Variables

A prudent choice of command variables is the first step towards good aircraft handling. The selection process is supported by experience with various configurations, like outlined for example in [71], by the theory of flight mechanics described in section 2.2 and by the analyses presented in chapter 3. The signal flow charts of Figure 2.3 and Figure 2.4 give a first idea on what parameters could be chosen as command variables in the longitudinal and the lateral motion, respectively. The body rates q and p are frequent choices and so are n_z and α in the longitudinal motion, but it is also common to choose a combination of multiple parameters as command variables. A prominent example is the C^* (pronounced “C star”) variable, which is defined by equation (4.1).

$$C^* = n_z + k_q \cdot q \quad (4.1)$$

Most maneuver demand systems, such as that of the Airbus A320 [59] and the Eurofighter Typhoon [59], are to some extent based on the C^* parameter [66]. The weighing factor k_q is normally chosen as 12.4 s [93], so that pitch rate and load factor equally contribute to the parameter at a velocity of 122 m/s . This value results from the constant speed approximation of the longitudinal motion (cf. Figure 2.3), which, for a steady-state pitch rate q_{ss} , predicts a steady-state $\dot{\gamma}_{ss}$ of the same magnitude and hence a corresponding load factor, as given by equation (4.2). At lower speeds, a C^* demand system is similar to a pitch rate demand system, whereas at higher speeds, it resembles a load factor demand system.

$$q_{ss} = \dot{\gamma}_{ss} = \frac{g}{V_0} \cdot n_{z,ss} \quad (4.2)$$

The reference flight mission described in section 2.1.2, which shall be accomplishable with the final choice of command variables, requires the pilot to control the airplane’s flight path in most flight phases. Only during takeoff and landing, when an incorrect attitude in ground proximity can lead to dangerous situations and accidents like tail strikes, wing strikes or nose wheel landings, attitude control is required. To account for the reduced pilot-vehicle bandwidth, command variables should be chosen that vary on a larger time scale. All in all, variables associated with the airplane’s translational dynamics, i.e., flight path variables (cf. Figure 2.3 and Figure 2.4), seem therefore suitable. Another design goal is to conserve the conventional order of airplane reactions to control inputs. An appropriate choice that satisfies these constraints would be a flight path demand system with $\dot{\gamma}$ and $\dot{\chi}$ as the command variables in the longitudinal and lateral motion.

Previous research on the choice of command variables for the longitudinal motion of a transport aircraft has shown that a $\dot{\gamma}$ control systems produces a very low workload level

when compared to pitch rate or C^* control [129]. The authors noted that control activity was lowest with the $\dot{\gamma}$ command system and that control inputs in fact were pulse-like with long stretches of inactivity between them. As a result, however, the concern grew that pilots could be less aware of the fact that the airplane was controlled manually. In the present case of flight control with large time delays, on the other hand, every additional decrease in workload is welcome. Moreover, pulse-like control is expected and even promoted by the on-off control system. The workload growth caused by the time delay and the reduced sensory feedback may again increase pilot activity and thereby awareness of being in (manual) control.

The choice of $\dot{\gamma}$ and $\ddot{\chi}$ as command variables results in an effective decoupling of horizontal and vertical airplane motion. This decoupling is comparable to the idea of a “software jig” for teleoperation with time delays [29] (cf. section 1.2) and is therefore considered beneficial in the present case. It also makes the airplane response more predictable, since a given lateral or longitudinal control input always results in the same amount of change in turn rate or flight path climb angle. Conventional airplanes, on the other hand, do not exhibit decoupled horizontal and vertical motions. Thus, pilots are used to applying longitudinal control inputs in a turn to compensate for the tilt of the lift vector (cf. section 2.2.2). Moreover, when they do apply longitudinal control inputs in a turn, these have no effect on the bank angle of the airplane. With the proposed flight path demand system, however, a turn does not require longitudinal control inputs. More than that, longitudinal control inputs in a turn cause the bank angle to change in an effort to maintain the turn rate. This behavior is very unconventional and may therefore confuse pilots. In the considered applications, however, this unconventional behavior is perceived only after some delay. Its adverse effects are therefore deemed less important than the beneficial effect of horizontal-vertical decoupling.

A flight path demand system may be well suited for most flight phases, but attitude-related command variables are likely better suited for takeoff and landing, when attitude control is needed. It is of course possible to implement dedicated modes for terminal and non-terminal flight phases. For optimum handling qualities, however, modes and mode transitions should be made unnoticeable for the pilot, so that the behavior of the airplane seems consistent (cf. section 2.2.2). Hence, a blending between command variables shall be implemented. A suitable attitude-related command variable in the vertical motion that corresponds to $\dot{\gamma}$ is pitch angle rate $\dot{\theta}$, which is equivalent to pitch rate q in wings level flight. In the horizontal motion, the flight control system could blend from $\ddot{\chi}$ to $\ddot{\Psi}$ or even $\dot{\Psi}$ to facilitate the de-crab maneuver that may be required in crosswind landings. Since the reference flight mission explicitly excludes crosswind landings, command variable blending in the horizontal motion is only implemented here for the sake of consistency. To actually fly takeoffs and landings, the flight control system would have to include even more modifications that are beyond the scope of this thesis. Summing up, the command variables of the lateral and the longitudinal axis C_{lat} and C_{lon} are defined by equation (4.3). The two blending functions f_{lat} and f_{lon} are responsible for a seamless transition between attitude control and flight path control.

$$\begin{aligned}
 C_{lat} &= f_{lat} \cdot \ddot{\chi} + (1 - f_{lat}) \cdot \ddot{\Psi} \\
 C_{lon} &= f_{lon} \cdot \dot{\gamma} + (1 - f_{lon}) \cdot \dot{\Theta}
 \end{aligned} \tag{4.3}$$

The two flight phases where attitude control is needed, namely takeoff and landing, are characterized by ground proximity, but also by low airspeed. Hence, it makes sense to provide attitude control at low airspeeds and flight path control at high airspeeds, with a regime of mixed attitude and flight path control in between. Lateral and longitudinal command variables are blended simultaneously, so that the airplane's behavior is coherent in all axes. Equation (4.4) defines the blending functions f_{lat} and f_{lon} , based on the indicated airspeed V_{IAS} and the upper and lower transition speeds $V_{T,U}$ and $V_{T,L}$.

$$f_{lat} = f_{lon} = \begin{cases} 1, & V_{IAS} > V_{T,U} \\ \frac{V_{IAS} - V_{T,L}}{V_{T,U} - V_{T,L}}, & V_{T,L} \leq V_{IAS} \leq V_{T,U} \\ 0, & V_{IAS} < V_{T,L} \end{cases} \tag{4.4}$$

The upper transition speed should be chosen slower than normal speeds during approach and initial climb. The lower transition speed should be at least a few knots slower than the upper transition speed, but not much slower than takeoff rotation speed or stall speed in landing configuration. Values of these characteristic speeds pertaining to the DA42, taken from [72], along with the resulting choice of transition speeds are given in Table 4.3. This design with flight path-related command variables at high speeds and attitude-related command variables at low speeds is similar to the C* control law. Here, however, the transition between the two regimes takes place in a narrow range of airspeeds. Moreover, the transition speed range is adapted to the reference aircraft and therefore slower than that of the C* parameter.

Table 4.3 – DA42 characteristic speeds from [72] and chosen transition speeds

Symbol	Description	Value [kt]
V_{REF}	Reference approach speed (IAS)	84
V_{climb}	Climb speed (IAS)	83 ... 90
V_R	Takeoff rotation speed (IAS)	76
V_{S1}	Stall speed in landing configuration (IAS)	69
$V_{T,U}$	Upper transition speed chosen (IAS)	80
$V_{T,L}$	Lower transition speed chosen (IAS)	75

4.2.2 Limitations, Protection Mechanisms and Supporting Functions

The analysis of existing certification specifications presented in section 4.1 indicates that limits and protection mechanisms need to be implemented in the flight controller to ensure adherence to a safe flight envelope. Moreover, the time delay values considered in this thesis can cause pronounced overshoots, possibly leading to upset flight states that are difficult to recover from. In addition to that, reduced sensory feedback means that the pilot

is deprived of some important cues on the state of the airplane and may therefore misjudge states or maneuvers and is also inclined to take more risks (cf. section 1.1).

A safe flight envelope is limited by a certain minimum and maximum load factor, a maximum airspeed and a maximum angle of attack. The latter is often translated to a minimum airspeed. This translation is motivated by the fact that most airplanes do not provide an angle of attack indication to the pilot. It has to be noted that it is only valid for straight and level flight and at a given vehicle mass. Load factor limitation can be achieved implicitly by limiting the longitudinal control sensitivity, i.e., the value of C_{lon} corresponding to the maximum possible control input amplitude. The longitudinal command variable C_{lon} is then further limited to protect against excursions in airspeed and angle of attack. In an approach similar to that presented in [130], speed protection is accomplished by dynamic limits on the kinematic flight path climb angle γ .

The point-mass equation (2.15) effectively relates the specific excess force, i.e., $(T - D)/mg$, to kinematic acceleration \dot{V}_K and flight path climb angle γ . Given that the specific excess force equals the longitudinal load factor in the kinematic frame $(n_x)_K$, equation (2.15) can be rewritten as in equation (4.5).

$$(n_x)_K = \frac{\dot{V}_K}{g} + \sin(\gamma) \quad (4.5)$$

To protect against speed excursions, one possible strategy is to limit \dot{V}_K as a linear function of the difference between limit IAS and current IAS (equation (4.6)).

$$\begin{aligned} \dot{V}_{K,max} &= k \cdot (V_{IAS,max} - V_{IAS}) \\ \dot{V}_{K,min} &= k \cdot (V_{IAS,min} - V_{IAS}) \end{aligned} \quad (4.6)$$

Equation (4.6) can then be combined with equation (4.5) to derive corresponding limits on γ , as equation (4.7) shows. For implementation in the flight controller, $(n_x)_K$ is replaced by its estimated value $(\hat{n}_x)_K$ (cf. section 2.1.1).

$$\begin{aligned} \gamma_{lim,U} &= \text{asin} \left((\hat{n}_x)_K - \frac{\dot{V}_{K,min}}{g} \right) \\ \gamma_{lim,L} &= \text{asin} \left((\hat{n}_x)_K - \frac{\dot{V}_{K,max}}{g} \right) \end{aligned} \quad (4.7)$$

Apart from an effective protection against speed and load factor excursions, a protection against extreme attitudes needs to be implemented, too. Hence, the pitch angle is limited to values $\Theta \in [-10^\circ, 20^\circ]$ and the bank angle Φ is not allowed to exceed $\pm 45^\circ$. Beyond a bank angle of $\pm 30^\circ$, spiral stability is introduced that brings the airplane back to $\pm 30^\circ$ of bank when there is no control input. To avoid wingtip strikes and extreme attitudes in ground proximity, the permissible bank angle range $\Phi_{max,att}$ is further narrowed at low heights, linearly from $\pm 45^\circ$ at 41 m above ground to $\pm 20^\circ$ at 15 m above ground and linearly again to 0° upon ground contact.

Dynamic bank angle limits are also used to prioritize vertical control over horizontal control. Assuming $\dot{\gamma} = 0$, equation (4.8) can be derived from the point-mass equation (2.17). The left side of equation (4.8) is the vertical load factor in the aerodynamic frame $(n_z)_A$. If wind is neglected, $(n_z)_A = (n_z)_K$, and if furthermore the angle of attack is assumed small, $(n_z)_K \approx (n_z)_B$. Any longitudinal pilot command produces an additional vertical load factor $\Delta n_{z,cmd}$ in the body-fixed frame, which explicitly appears in the flight controller structure (cf. appendix A). To avoid excessive structural loads, the sum of the vertical load factors in the body-fixed frame must be smaller than the limit load factor. In other words, equation (4.9) must be satisfied.

$$\frac{L}{mg} = \frac{\cos \gamma}{\cos \Phi} \quad (4.8)$$

$$\frac{\cos \gamma}{\cos \Phi} + \Delta n_{z,cmd} \leq n_{z,max} \quad (4.9)$$

Given that the climb angle and the additional vertical load factor are to be prioritized, a bank angle limit can be derived from equation (4.9). This limit is defined by equation (4.10). The overall bank angle limit is then defined by equation (4.11).

$$\Phi_{max,n_z} = \arccos\left(\frac{\cos \gamma}{n_{z,max} - \Delta n_{z,cmd}}\right) \quad (4.10)$$

$$\Phi_{lim} = \pm \min(\Phi_{max,att}, \Phi_{max,n_z}) \quad (4.11)$$

The bank angle limits are also translated to turn rate limits in the lateral controller. The relationship between bank angle and turn rate is taken from the equations of motion linearized around straight and level flight (cf. section 2.2.1). The resulting turn rate limitation is given by equation (4.12).

$$\dot{\chi}_{lim} = \pm \frac{g}{V_K} \tan(\min(\Phi_{max,att}, \Phi_{max,n_z})) \quad (4.12)$$

Limitations and protection mechanisms help to avoid departure from a safe flight envelope. Beyond that, supporting functions are implemented that help acquire and maintain common steady-state flight conditions. A so-called altitude hold mode becomes active when no longitudinal control input is made and vertical speed is small. Upon activation, an altitude setpoint value is generated such that the aircraft can approach it non-periodically with small command inputs, so that the mode transition is barely noticed by the pilot. The altitude is now held until the pilot makes a longitudinal control input. In this case, the altitude autopilot is immediately disconnected and the pilot can maneuver normally. Like the altitude hold mode in the vertical motion, there is a path straightener function in the horizontal motion. It engages when no lateral control input is made and the commanded turn rate is approximately zero, and then acquires and maintains zero turn rate, i.e., straight flight. From the pilot's point of view, this function behaves like a wings leveler. Similarly, if no lateral control input is made and the commanded turn rate

is close to the standard turn rate, the standard rate turn hold mode engages. As soon as the pilot makes a lateral control input, the path straightener or the standard turn rate hold mode are immediately disconnected and the pilot can maneuver normally. Apart from moderately helping the pilot accomplishing standard maneuvers, the altitude hold mode and the path straightener could also be used to bring the airplane back from any situation to straight and level flight. Section 4.3.1 explores this option.

4.2.3 Controller Implementation

With the desired controller characteristics and functionalities defined in the previous sections, the implementation of the control algorithms is discussed here. Controller implementation was done as a means to achieve a realistic simulation environment, but not for deployment in a real aircraft. The result should be seen as a prototype, produced in an informal design process that is only briefly described here. Block diagrams that illustrate the controller layout in detail are given in appendix A. It can be seen there, that only the measurements and estimations defined in section 2.1.1 were used. This controller layout was implemented in Simulink. Hence, interfacing controller and simulation model was straightforward. Gains were tuned by pole placement for one single operating point representative for the flight mission. This operating point was chosen to be straight and level flight at a true airspeed of 55 m/s , a density altitude of 1500 m , with a mass of 1626 kg and with the center of gravity at 2.42 m . Figure 4.2 relates this operating point to the reference airplane's operational limitations [72]. Note that density altitude represents air density and equivalent airspeed is a measure of dynamic pressure. Maximum altitude is not clearly defined for the aircraft. Maximum airspeed depicted here is the maximum structural cruising speed. By finding a relatively robust set of gains, it was possible to obtain a controller that provides stability and adequate performance in a sufficiently large range of speeds and altitudes around this design operating point.

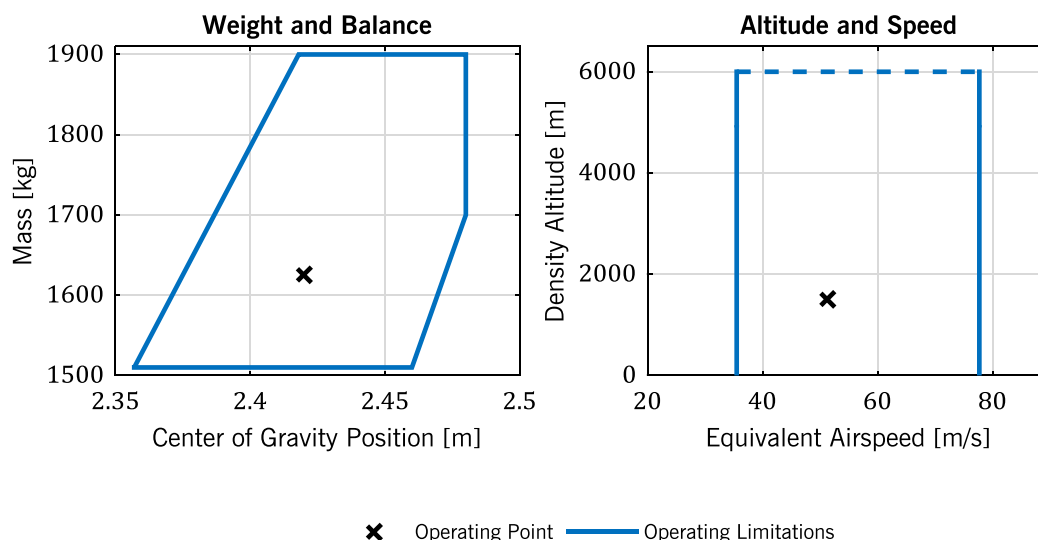


Figure 4.2 – Operating point for controller gains tuning

Prior to gain tuning, the nonlinear airplane model without actuators was linearized in the chosen operating point. In the longitudinal motion, the phugoid poles were removed from the linearized model to obtain the constant speed approximation. This was justified by the

later addition of the autothrottle. Each actuator was then modeled by the second-order linear transfer function of equation (2.7). Furthermore, a fourth-order Padé approximation of a 0.03 s time delay was added in each axis, representing lags and time delays of the digital flight control system. In the lateral-directional controller, a control allocation and a cross-feed were added based on the linear aircraft dynamics illustrated by Figure 2.4 to improve the decoupling of roll and yaw axis. The control allocation, shown in Figure A.9, aims at producing pure roll or yaw moments by deflecting ailerons and rudder in a coordinated manner. The cross-feeds of p to ζ and r to ξ effectively cancel L_r and N_p . The resulting longitudinal and lateral airplane models were then augmented for output-feedback pole placement. Poles were placed such that each control loop had a gain margin of at least 6 dB and a phase margin of at least 45°. At the same time, efforts were made to minimize the lag between control inputs and command variables, as one design goal dictated. The parameter τ_{lags} defined by Figure 3.27 (cf. section 3.3.3) can indeed be used as a handling qualities criterion when applied to the γ response to a step in δ_{lon} [71]. This so-called flight path delay is a time domain handling qualities criterion and as such can be applied to augmented and unaugmented aircraft alike. Limit values on flight path delay are derived from another well-established criterion: the Control Anticipation Parameter [67]. Those limit values were used as guidance here. For a subsequent analysis of the control algorithms, the linear model of airplane plus actuator was combined with a pure time delay instead of the Padé approximation. Then, all loops were closed with the previously determined gains. The reaction of the closed-loop system to step inputs was simulated to check whether the command variables evolved as desired and whether the actuators commands were within their position and rate limits.

It can be seen in appendix A that, for $V_{IAS} > V_{T,U}$, the lateral outer control loop in fact controls χ and the longitudinal outer control loop controls γ . Command filters shape the transfers $\delta_{lat} \rightarrow \chi_{cmd}$ and $\delta_{lon} \rightarrow \gamma_{cmd}$ in a way that, from the pilot's point of view, the command variables are $\ddot{\chi}$ and $\ddot{\gamma}$. The steady-state gain of these command filters, which corresponds to the control sensitivity, was set to $2^\circ/s$ in the vertical motion and $2^\circ/s^2$ in the horizontal motion. This choice was based on good engineering judgement and on the finding that a lower control authority is desirable for remote operations due to the pilot's reduced situational awareness [45]. To find out whether the control sensitivity values chosen are indeed suitable, the value of longitudinal control sensitivity was varied in the experiments described in chapter 6.

Section 3.3.1 discusses the effect of control sensitivity on the likeliness of PIOs when applying pulse-like control to transfer functions with one and only one pure integrator. For this specific flight control system, the same analysis can now be made for the transfers $\delta_{lon} \rightarrow \gamma$ and $\delta_{lat} \rightarrow \dot{\chi}$. It is furthermore assumed that the pilot does not introduce any lead. According to equation (3.23), a limit cycle is then unlikely to occur if the pilot's tolerance in target tracking is greater than $\pm K_a \tau_t / 2$. Moreover, the maximum limit cycle amplitude as predicted by equation (3.25) is $2K_a \tau_t$ and, according to equation (3.26), the limit cycle period is $4\tau_t$. That the thereby predicted values indeed closely match values measured in experiments is shown in section 6.4.1. Table 4.4 lists several relevant combinations of total time delay and control sensitivity and the resulting limit cycle characteristics of the longitudinal motion $\delta_{lon} \rightarrow \gamma$. For instance, with the control

sensitivity as chosen above and a total time delay of 2 s, a limit cycle is unlikely if the tolerance in γ is greater than 2° . If, with this configuration, a limit cycle of maximum amplitude occurs, γ varies by 8° . The same values, but with control sensitivity expressed in $[\circ/s^2]$ and target tolerance and maximum limit cycle amplitude expressed in $[\circ/s]$, apply to the lateral motion $\delta_{lat} \rightarrow \dot{\chi}$.

Table 4.4 – Possible limit cycle characteristics in γ

Total time delay	Control Sensitivity	Minimum Target Tolerance with Limit Cycle Unlikely	Maximum Limit Cycle Amplitude	Limit Cycle Period
τ_t	K_a	$\pm K_a \tau_t / 2$	$2K_a \tau_t$	$4\tau_t$
1 s	$2^\circ/s$	$\pm 1^\circ$	4°	4 s
2 s	$0.5^\circ/s$	$\pm 0.5^\circ$	2°	8 s
	$2^\circ/s$	$\pm 2^\circ$	8°	
	$3.5^\circ/s$	$\pm 3.5^\circ$	14°	
	$5^\circ/s$	$\pm 5^\circ$	20°	
3 s	$2^\circ/s$	$\pm 3^\circ$	12°	12 s

The values in Table 4.4 well illustrate why smaller control sensitivities are desirable in case of large time delays. For any sensitivity and time delay value shown, the target tolerance would need to be unpractically high to render the occurrence of limit cycle PIOs unlikely. Imagine an accuracy in γ of $\pm 2^\circ$ during a landing approach with a nominal glide slope $\gamma = -3^\circ$. Like in section 3.3.2, it can be seen here again that preventing PIOs by implementing small control sensitivities is not practical. Smaller sensitivities are nonetheless preferable, because maximum PIO amplitudes can be quite brutal otherwise. A PIO of 20° in γ , for instance, not only causes the trajectory to oscillate through a wide altitude band, but also brings the airplane close to its physical limitations. The same observations generally hold for control of the lateral motion, although the additional pure integrator in the controlled system $\delta_{lat} \rightarrow \chi$ makes control even more difficult.

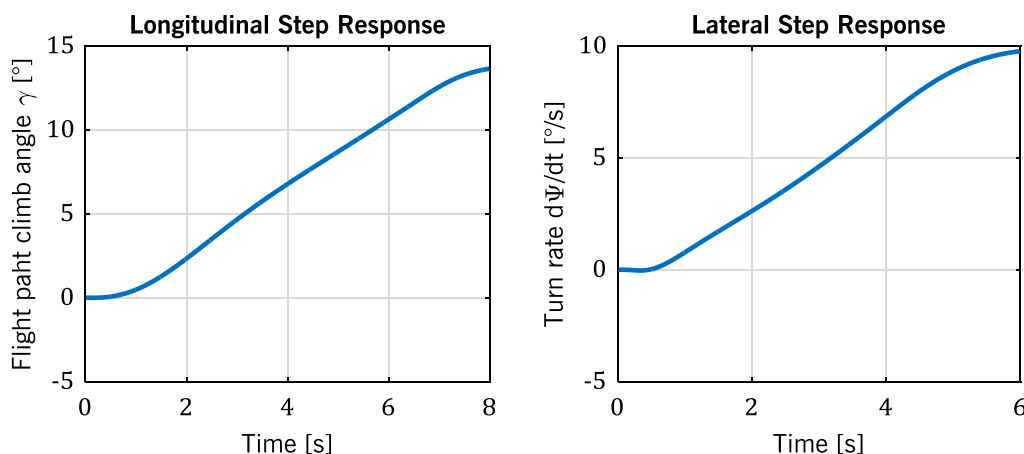


Figure 4.3 – Step responses of the nonlinear augmented airplane

For a final analysis of the augmented airplane, a simulation of the nonlinear airplane with all control loops closed is done. Figure 4.3 shows the evolution of γ and $\dot{\Psi}$ in response to a longitudinal and a lateral step input, respectively. Note that $\dot{\Psi}$ is equal to $\dot{\chi}$ here, because

the simulation did not involve wind. It can be seen that after an initial lag, γ and $\dot{\Psi}$ progress linearly, as expected given that step inputs have been applied to the command variables $\dot{\gamma}_{cmd}$ and $\dot{\dot{\chi}}_{cmd}$. Towards the end of each time history plot, the limitation or protection mechanisms engage that ultimately inhibit any further increase in flight path climb angle or turn rate. The initial lag in each response can be seen as an additional time delay τ_{lags} , which further complicates control (cf. section 3.3.3). Here, it amounts to roughly 0.8 s in the longitudinal motion and 0.5 s in the lateral motion. The more immediate attitude changes of the airplane, however, partly compensate these lags, because they help pilots to predict the flight path.

4.3 Human Control Input Interfaces

To fly the airplane augmented by the flight controller described above, the human pilot needs some interface to generate control inputs with. The conventional form of this interface is a manual control inceptor. Such a device shall be used here in the case of RPA control. In the case of BMI control, on the other hand, the BMI plays the role of this control input interface. This section describes adequate and desirable characteristics of the inceptor and the BMI.

4.3.1 Inceptor Characteristics

By assuming that RPA operators are specifically trained to fly a certain RPA and do not need to transition to other types or even to manned airplanes, one would obtain complete freedom for inceptor design. However, one design goal stated in section 4.1 is to facilitate exactly this transition between different RPA and also manned aircraft. Hence, one of the classical inceptor designs – yoke, center stick or sidestick – should be chosen. Such a choice also emphasizes the fact that an actual aircraft is being controlled, thus potentially reducing the risk of reckless flying. A sidestick is preferred over a center stick or a yoke because it leaves space in front of the pilot, which can be used for displays and kneeboards. Yoke and center stick may be better suited for mechanical control systems, where large displacements are required to actually deflect the control surfaces. A maneuver demand system like the one implemented here, on the other hand, can be easily controlled using a small stick-shaped inceptor with comparatively little travel [71].

Another design goal stated in section 4.1 says that the inceptor characteristics apparent to the pilot should match the controlled system's dynamic characteristics for intuitive handling. Here, this means that the value-discrete control inputs that the flight control system enables the pilot to make should be perceivable through the inceptor. One possible approach is to associate discrete inceptor deflections with the discrete control inputs. In this case, the pilot input to the inceptor is a certain force applied by hand and arm. The resulting deflection follows the force-deflection characteristic shown, in a general form, in Figure 4.4. When small control forces are applied, the inceptor practically does not move, but when a certain breakout force is exceeded, the inceptor snaps into its limit position. To bring the stick back to neutral, it is sufficient to ease off the force up to the point where the stick snaps to zero deflection. The inceptor output can then be associated with its deflection, as the dashed lines and the grey area in Figure 4.4 indicate. The individual

lines of the force-deflection curve are all oblique. On the one hand, the obliqueness accounts for elasticity in the inceptor. On the other hand, the force-deflection curve may need to be sufficiently smooth for practical implementation in an active sidestick to prevent limit cycles of the limb-inceptor system.

Inceptors for spacecraft offering similar control laws could not all exhibit such a force-deflection characteristic, because they were sometimes used for a variety of control laws, including such that enable value-continuous control. In some cases, however, inceptor characteristics were similar to those described here. For instance, the rate of descent switch used in the Apollo Lunar Module is described as “a three position toggle with a spring to return to detent” [122].

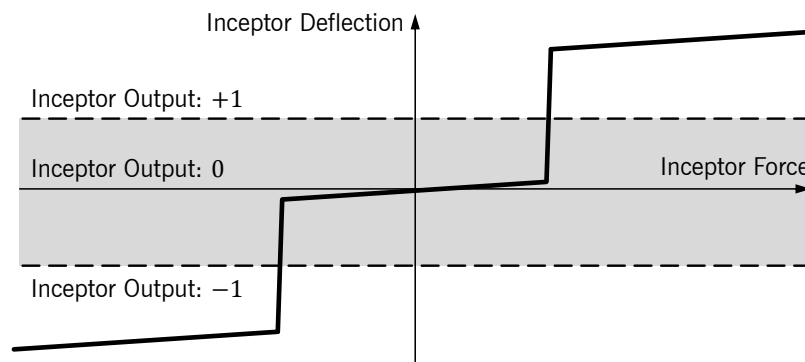


Figure 4.4 – Inceptor force-deflection characteristic

The idea of the proposed inceptor characteristic could be extended to multiple control input levels. For each additional level, another step can easily be added to the curve of Figure 4.4. Another possible extension of the proposed design would be to provide buttons that cause the airplane to return to straight and/or level flight. The functionality is already implemented in the form of path straightener and altitude autopilot. Although the main purpose of these buttons would be to provide a simple means to recover from unsafe flight conditions like PIOs, pilots would most certainly find them convenient in many other situations as well. They would therefore have an effect on piloting techniques.

A major issue with the proposed design of flight control system and inceptor is, that it does not provide the tactile and proprioceptive cues of conventional airplane flight, which are usually required by certification specifications (cf. section 4.1). Most notably, speed and maneuver stability are both neutral. This means that on the one hand, airspeed changes have no influences on stick deflections and forces. On the other hand, stick deflections and forces are always the same for a given $\dot{\gamma}$, although the resulting load factor changes with speed, as equation (4.2) indicates. There are certified control systems in operation today that provide neutral speed stability [127, 128], but they rely on protection mechanisms to ensure an equivalent level of safety. A more intuitive way could be to mimic stick fixed speed stability with a technical system, just like inceptor vibrations of an incipient stall are mimicked by a stick shaker. For instance, it is possible to reintroduce a proprioceptive feedback on airspeed by shifting the neutral position of the stick fore and aft for high and low airspeeds, respectively. Similarly, stick free maneuver stability, or the right amount of stick force per g, could be implemented by varying the breakout force with

airspeed. It must be stressed, however, that higher frequency adjustments of inceptor characteristics depending on the RPA state are impractical in the case of large time delays. The resulting changes in characteristics are very likely to be misleading, since they occur with a delay. More drastic even, any high-frequency force feedback loop would likely become unstable. This is in fact the very problem of remote haptic teleoperation (cf. section 1.2).

For the experiments described in chapter 6, the force-deflection characteristic of Figure 4.4 was implemented in an active sidestick manufactured by Wittenstein AG [131]. Guidance for the quantification of the breakout forces in this specific case was not available. The well-known pitch rate sensitivity criterion [132], for instance, had been developed for value-continuous pitch rate demand systems of fighter airplanes. The present case of RPA control employs an on-off flight path angle rate demand system and the occurring phase delays are far off the chart of the pitch rate sensitivity criterion. Breakout forces were therefore tuned based on the judgement of the author as a pilot. For lateral stick movements, a breakout force of 6.406 N was fixed whereas longitudinal stick deflections required a force greater than 8.341 N . The odd numbers are the result of various conversions within the active sidestick control software. The fact that lateral control forces in the sidestick are lower than longitudinal forces is supported by relevant aerospace and human factors standards [60, 133]. Accounting for the possibility that control forces slightly mismatched the airplane's reaction was one reason why control sensitivity was varied during the experiments described in chapter 6. Online changes of the stick's characteristics were not possible. Therefore, the neutral position shift and the breakout force variation discussed above were not implemented.

4.3.2 Brain-Machine Interface Characteristics

In the case of BMI control, the inceptor is obviously replaced by an EEG cap and the amplifiers and computers required for signal processing. To enable continuous tracking of a target parameter – be it attitude, flight path or any other parameter – the BMI needs to be asynchronous. For successful control, the STR needs to be well above 50%. A good SNR is obviously desirable. The experiments presented in chapter 5 were conducted either with an Operant BMI or with a Motor Imagery BMI, but other approaches may as well yield good results. From an operational point of view, however, the Operant BMI is superior to those types of BMIs that mainly rely on machine learning, as the following exemplary fictive scenarios illustrate.

Imagine an airplane whose left and right movements are controlled through a Motor Imagery BMI. Before each flight, the BMI algorithms need to be adapted to the pilot, which takes a couple of minutes. Then, during flight, the pilot needs to imagine movements of his left hand to turn left, or movements of his right hand to turn right. Now imagine the same airplane, employing an Operant BMI instead. The pilot has been trained to generate the required brain activity in a flight simulator. Thus, he associates this brain activity with airplane movements. No machine learning session is required prior to a flight. When flying, the pilot naturally generates the brain activity required to turn left or right, because BMI control of the airplane has been learned and automatized like a physical skill. In this second scenario, recurrent machine training sessions are made void at the expense of

initial pilot training time. More important, BMI control is comparable to a physical skill, whereas in the first scenario, it requires some cognitive effort.

Unfortunately, all BMI approaches still require considerable mental effort and there is still a long way to go before reality can only remotely approach these fictive scenarios. They nevertheless clearly illustrate the advantage of BMI approaches that rely on user training. While the inceptor characteristics of section 4.3.1 could be implemented more or less as desired, the actual BMI performance in the experiments described in chapter 5 fell short of the desired performance described here and in section 4.1. For instance, only one degree of freedom could be controlled. Section 5.1.2 elaborates on the actual BMI characteristics in the experiments.

4.4 Sensory Feedback

Section 3.1.1 already discussed the importance of vestibular and proprioceptive feedback for flight control. For both example applications – remote flight control with large time delays and BMI control – a strategy needs to be found that mitigates the disruption of one of these channels. Vestibular feedback can be partially restored by placing the ground control station on a motion platform [6]. This approach, which is also mentioned in section 1.2, is quite straightforward and actually similar to that of moving-base flight simulators, but it has the disadvantage of largely increasing ground control station complexity and cost. The complexity lies not only in the moving parts of the motion platform, but also in the algorithms that replicate the vestibular sensations of the RPA's linear and angular accelerations with the restricted translations and rotations of the motion platform. An alternative approach to restoring vestibular feedback would be to substitute it. In this case, the information normally conveyed through the vestibular channel would have to be presented in a different sensory channel. Both the visual and the aural channel are heavily used in flight, as the overview over the major sensory channels in section 3.1.1 describes. Presenting additional information in those channels further increases the likeliness of information being missed. The tactile channel, on the other hand, seems to offer a suitable alternative for information throughput. A similar argument can be made in the case of missing proprioceptive feedback. Reinstating proprioceptive feedback would undermine the original idea of hands-free flight. It is certainly possible to display information on BMI outputs visually, as is the case in many BMI research setups, including that described in chapter 5, but it is not desirable due to the same reason stated above. Again, tactile feedback could be a suitable replacement.

Although not widely used yet, tactile feedback in flight control tasks has already been subject to research. Several studies have investigated the use of vibro-tactile displays on the pilot's torso in helicopter flight control tasks [49, 50]. The focus was on landing performance in degraded visual environments such as brownout or whiteout (i.e., when sand or snow is stirred up and obscures outside visibility), or when wearing night vision goggles. In those situations it is difficult for the pilot to sense helicopter motion, which is why unwanted drift motions and position errors are more likely to occur. In a fixed-base simulator study [49] a 64-tactor display conveyed information either on the desired direction of motion only (towards the target position), or on both desired and current

direction of motion. It was found that the display improved hovering performance, i.e., the position error, for both flight with night vision goggles and flight in full-vision daylight conditions. Results also indicate that displaying both desired and current direction of motion clutters up the tactile display and thus claims more of the pilot's higher mental processing resources. In another study [50], 52 tactors on a test pilot's torso displayed altitude and groundspeed vector during inflight experiments of a helicopter landing maneuver. Again, the tactile display improved the pilot's performance. The maneuver was accomplished faster, more accurate and with less mental effort than without tactile support. Another helicopter flight test with tactile feedback, described by McGrath [48], was actually preceded by experiments with a fixed-wing airplane. In those experiments, a pilot flew various maneuvers, including aerobatic maneuvers, without any visual cues from instruments or the outside environment, but with the help of a vibro-tactile torso display. The display consisted of 20 tactors and presented information on the airplane attitude. All maneuvers were successfully accomplished, which shows that a tactile display can effectively communicate attitude information. McGrath concludes that a tactile display of attitude potentially allows pilots to concentrate on other visual tasks while maintaining spatial orientation, thereby increasing situational awareness and reducing workload. Moreover, pilot comments indicated that the tactile attitude display helped reducing common sensory illusions like vertigo or tumbling sensations. Further laboratory and inflight experiments on tactile attitude displays are described in [47], where subjects succeeded in capturing pitch and roll attitudes with an accuracy of about 5°, relying on tactile cues alone. Moreover, the authors propose tactile displays as an alternative to moving-base simulators with their inherent deficiencies described above. A technical report on tactile displays [51] mentions that their application to UAV operations could be beneficial. Among the four application areas identified is navigation and vehicle control information. The report furthermore acknowledges the possibility to reduce the demand on the RPA pilots' visual perception by providing tactile feedback and refers to a study that investigated tactile displays during the landing phase of a UAV. This study indicates that tactile feedback possibly reduces the amount of training required for novice pilots and that tactile cues may be useful for operational UAV pilots.

Summing up, the idea is to substitute the missing vestibular or proprioceptive feedback with a suitable tactile display. In the case of RPA control, where vestibular feedback is missing, a first guess would be to display the RPA attitude. Since the attitude can already be perceived visually, even on remote computer screens, it may be more interesting to display flight path variables. A study investigating the effect of various visual displays on workload and performance with a flight path demand system [134] supports the approach of displaying the flight path. The authors found that situational awareness was improved in this case. As mentioned earlier, instead of reinstating missing sensory feedback, it is possible to generally increase the pilot's situational awareness and thereby free up mental resources that can be used to cope with the reduced sensory feedback. This means that a tactile flight path display can also help in the case of BMI control, where proprioceptive feedback is missing. On the other hand, the missing proprioceptive (or vestibular) feedback is also compensated to some extent by the limitations and protection mechanisms of the flight controller. Thus, another purpose of a tactile display could be to increase awareness

with respect to these limitations and protection mechanisms. For instance, the known vibrations prior to stall (cf. section 3.1.1) could be replicated by vibro-tactile cues on the tactile display. A prototype tactile display feeding back γ and χ has been designed and implemented in project BRAINFLIGHT. It comprised 16 factors placed around the waist. Initial experiments with the display have been performed in the same flight simulator where BMI controlled flight was later tested (cf. section 5.1.2). Two pilots used the display and commented on it, indicating that a tactile flight path display could be useful. Unfortunately, there was no occasion for further investigations.

In addition to the tactile display and standard visual cues, visual predictor displays can be implemented to reduce the apparent time delay. Indeed, this should be done, as the plethora of positive experience with predictor displays indicates (cf. section 1.2). While the effect of predictors is experimentally analyzed in section 6.4.3, their detailed design is not within the scope of this thesis. One design issue, however, needs to be addressed here. In the case of RPA control with signal transmission latency, an undelayed control signal is available for prediction. In case of BMI control, on the other hand, the very control signal is already delayed. How can a prediction be done in this case? The key to a possible solution is that, according to section 3.4 and Figure 1.2, the delay in BMI control originates from two sources: signal processing and filtering. As a result, the raw, unfiltered BMI output can be used to make a prediction. An actual prediction, extrapolating future system outputs, is inadvisable because of the noisy nature of the signal. Instead, a simple display of this signal can already be used by the human operator for prediction. It can in fact be seen as a replacement of proprioceptive feedback. As such, it could also be interesting to show it on the tactile display instead of a visual display. Whether the tactile display of a highly noisy signal can adequately convey information without distracting the pilot, however, is questionable. Summing up, Figure 4.5 relates the proposed sensory feedback design to the problem stated in section 1.1 by complementing Figure 1.2 with the proposed feedback flows and channels.

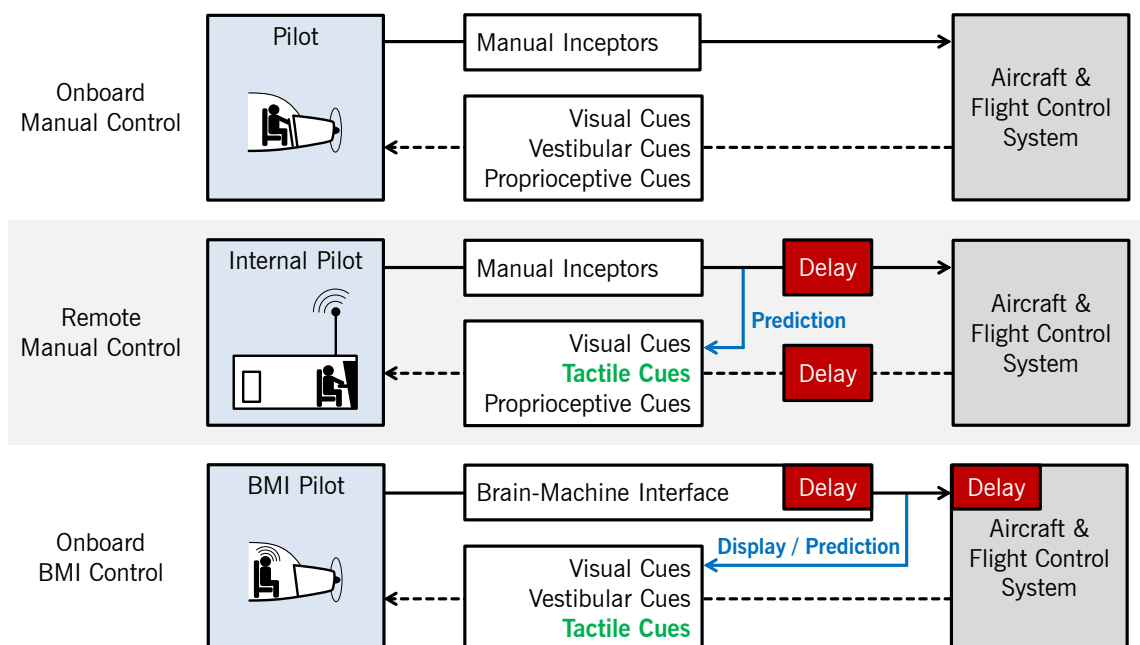


Figure 4.5 – Sensory feedback design proposed for the example applications

5 EXPERIMENTAL EVALUATION OF BMI CONTROLLED FLIGHT

So far, this thesis approached the topic of flight control with large time delays and reduced sensory feedback from a theoretical point of view. Beyond that, this and the following chapter describe experimental evaluations of some of the proposed concepts and theories. Involving the human user at an early stage of research and development is highly important to ultimately avoid a mismatched man-machine interplay. More than interviews and discussions with pilots, experimental evaluations using flight simulators played an important role in the research leading up to this thesis. Indeed, the various simulator experiments contributed immensely to the final picture of the problem and the possible solutions presented.

The first step was to combine the flight controller described in chapter 4 with a BMI to fine-tune the system so that control was possible. Moreover, the initial aim was to get a better understanding of how such a BMI (flight) control system could be improved. Fortunately, it was possible to conduct multiple experimental campaigns with a Motor Imagery BMI and an Operant BMI, which enabled an initial investigation on the performance of BMI controlled flight and the validation of the BMI model presented in section 3.4.2. The major challenge of the BMI experiments was that the control performance varied a lot between subjects and generally was a lot worse than in manual control. This had been expected and the experiments were planned accordingly. Nonetheless, the experiments on BMI controlled flight had a more explorative character, since parameters had to be tuned and some tasks or evaluation methods proved inapplicable. It also has to be stressed again that today's BMIs with their limited reliability were not seen as suitable flight control interfaces. Instead, the experiments aimed at applying methods from the aerospace domain to BMI control in general. The following sections describe the experiences reported in [107, 135, 136] in a consolidated and extended manner.

5.1 Experimental Setup

5.1.1 Participants

For the experimental campaign with the Motor Imagery BMI, seven male participants volunteered, six of whom had experience in piloting real airplanes. The seventh subject was merely familiar with the theory of flight and knew how to read the relevant aircraft instruments. Generally, all these seven participants, who are listed in Table 5.1, had different levels and types of flight experience. The reason for inviting participants with different backgrounds to the experiments was to obtain opinions from a broad spectrum of pilots. Moreover, it was hoped that they would achieve a similarly broad spectrum of BMI control performance. None of the participants had ever used any type of BMI before.

Table 5.1 – List of participants of the experiments with Motor Imagery BMI control

Subject No.	Age	Hours Flown	Status / Experience
M1	23	100	Student pilot (airline)
M2	30	4300	Airline pilot (Embraer E-Jet family [59])
M3	29	120	Private pilot
M4	52	270	Private pilot
M5	26	120	Student pilot (airline)
M6	32	1100	Former military pilot (PA-200 Tornado [137])
M7	27	none	none

For experiments with the Operant BMI, on the other hand, the group of possible participants was much more restricted. As described in section 3.4.1, the Operant BMI required some user training. With the BMI and the flight simulator usually not co-located, but a 3-hour flight apart, it was difficult to train subjects over several sessions and have the same subjects fly in the simulator. Therefore the researchers, who traveled between the two locations anyway, also played the role of experimental subjects. Subject O1 was a BMI researcher and private pilot who was initially naïve to the tasks defined and could therefore be treated like an uninvolved subject. Furthermore, the author had the opportunity to train with the Operant BMI a couple of times. For later experiments (cf. section 5.5), he flew in the simulator several times as subject O2. At this point, subject O1 was already far better trained. The data gathered in this experiment is only used for BMI model validation here. Not distinguishing between subjects and experimenters is obviously undesirable. What would usually be considered a major flaw, can be justified only by the explorative nature of the experiments, which therefore has to be stressed again at this point.

5.1.2 Flight Simulator and Brain-Machine Interface

The tests were performed in the DA42 simulator at TUM's Institute of Flight System Dynamics. This fixed-base simulator was built by the aircraft manufacturer with original aircraft components. The highly realistic cockpit environment is complemented by a three-channel External Visual System (EVS) that projects the simulated outside world on a 180° cylindrical screen. Together with the flight dynamics model, this simulator is

certifiable up to FTD level 5 as defined by the FAA [138]. For the experiments, the simulated flight dynamics were complemented by the flight controller described in chapter 4. A sketch of the simulator as it was set up for the experiments is shown in Figure 5.1. Details on the displays are given in section 5.1.3.

The BMIs ran on a different computer and transmitted their output signals via an Ethernet connection to the flight controller. The time delay introduced by this signal transmission was not quantified, since its contribution to the total time delay was deemed negligible compared to the delays inherent to BMI signal processing (and filtering). Both BMIs enabled binary control in only one degree of freedom. This means that users could actively try to either produce positive or negative BMI outputs. In the absence of a specific user intention, the BMIs would produce outputs with approximately zero mean and thereby provide the third, neutral control amplitude level.

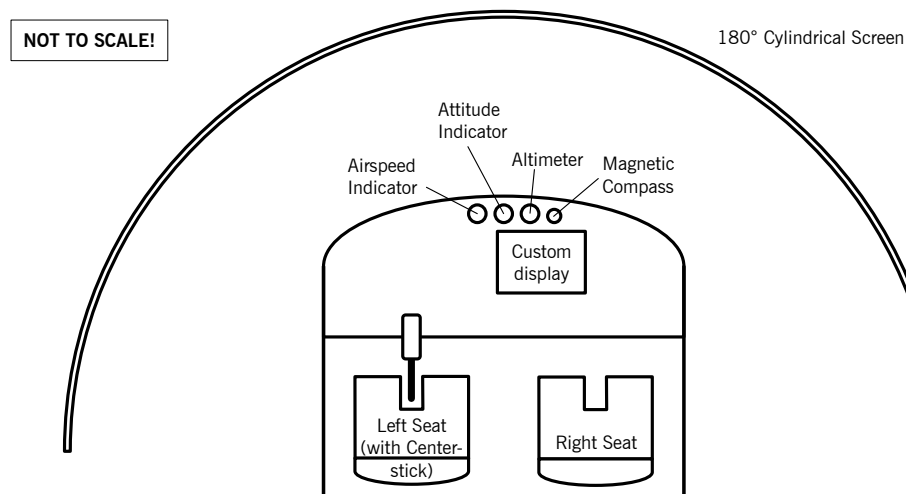


Figure 5.1 – Cockpit of the DA42 simulator as set up for the experiments

It was decided to apply the one degree of freedom to lateral control of the airplane, instead of longitudinal control. Thus, control was expected to be more intuitive with the Motor Imagery BMI, which usually relies on imagined movements of the left and right hand or arm. Furthermore, maneuvers were expected to be largely erroneous and while the simulated airplane was free to move horizontally, its vertical movements were restricted to the half-space above the simulated ground, which could have led to rather demotivating terminations of flight. Indeed, the Motor Imagery BMI distinguished imagined movements of the left hand or arm from that of the right hand or arm. On top of that, it also recognized imagined movements of the feet. Of these three types of movements, those two that had the best cross-validation estimate were selected for each session. Thus, some subjects in fact had to imagine movements of their feet and of one of their hands to steer the airplane.

Each BMI provided a single floating-point precision number as output. The output of the Motor Imagery BMI was truncated to $[-1,1]$, whereas the output of the Operant BMI was only bounded by the limits of data type encoding. Another difference was in the sampling time. The Motor Imagery BMI provided an output at 10 Hz, whereas the Operant BMI produced its output at 4 Hz. In both cases, the BMI output underwent some processing

on the receiving side, i.e., at the flight controller input. This is illustrated in Figure 5.2. Note that the control inputs ultimately act on a χ control loop (also cf. appendix A, Figure A.6). The command filter initially produced the $\ddot{\chi}$ command system described in section 4.2.1, but was then varied in the experiments. The Motor Imagery BMI output was merely mapped before entering the command filter, whereas the signal of the Operant BMI was also filtered before mapping. Mapping always constrained the BMI control action δ_{BMI} to $\delta'_{BMI} \in [-1,1]$. For the subjects, it was important to receive undelayed feedback from the BMI as the most direct way for them to recognize whether they produced correct outputs. Such an undelayed BMI feedback is also proposed in section 4.4 and Figure 4.5. In case of the Motor Imagery BMI, the mapped BMI output was presented to the pilot, because the mapping function did not introduce any delay. In case of the Operant BMI, on the other hand, visual feedback of the raw output was presented to avoid any lags or delays between BMI signal generation and BMI signal feedback caused by filtering.

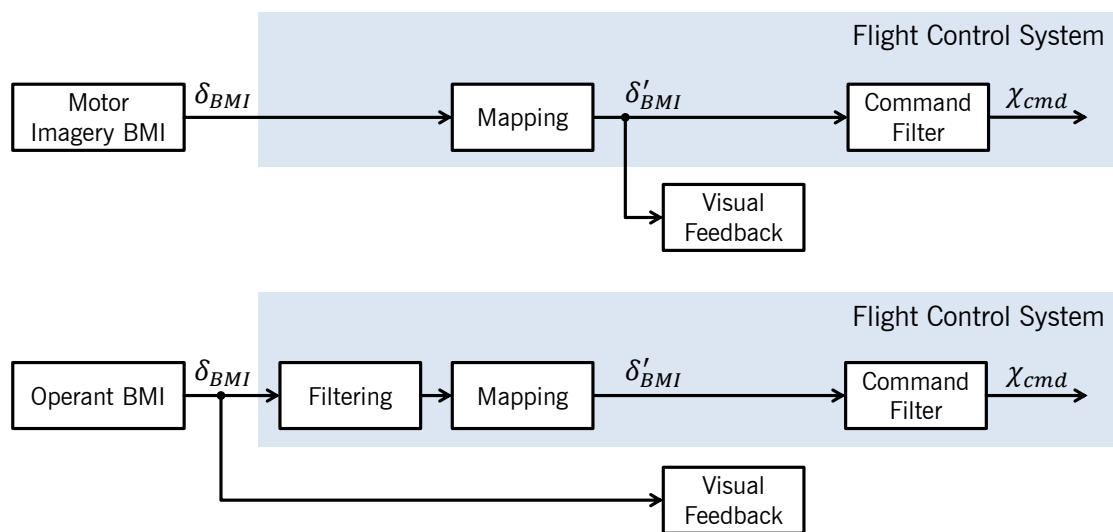


Figure 5.2 – Signal processing for Motor Imagery and Operant BMI

Both filter and mapping function were varied throughout the experiments to find an optimal configuration. For the initial experiments, which employed the Motor Imagery BMI, the filtering required to obtain information from the noisy BMI output was achieved only by the physical low-pass characteristics of the airplane. This somewhat brute method seemed most promising at the beginning, as it does not introduce any additional lags. According to section 3.4.2, the filtering time delay is thus $\tau_{filt} = 0$ and, as a result, the BMI time delay τ_{BMI} is reduced (equation (3.64)). By minimizing the time delay introduced by the BMI, the problem of large time delays is mitigated.

5.1.3 Displays

Only visual displays were employed in the experiments on BMI control. The two displays of the simulator's integrated flight instrument and avionics system were substituted by one single, custom display that had been specifically tailored for the experiments. Further visual cues were presented by the EVS and the four standby instruments (airspeed indicator, attitude indicator, altimeter and magnetic compass). A sketch of the display

setup is shown in Figure 5.1, whereas Figure 5.3 shows an actual photo of the DA42 simulator's cockpit as it appeared for the subjects.

The custom display, which can be seen in Figure 5.3 and more clearly in Figure 5.4, was similar in appearance to the original display of the airplane. The entire background was dedicated to an artificial horizon, whereas attitude indicator, airspeed indicator, altimeter and heading indicator were grouped in the standard T arrangement in the foreground. Vertical speed was displayed next to altitude and lateral acceleration was presented by a left- and right-moving bar below the bank angle indicator. The display was complemented by a flight path climb angle indicator in the form of a rear-view airplane symbol, an indication of the autothrottle target speed below the airspeed indication, a horizontal situation indicator (HSI) and, in the case an instrument landing approach was flown, a glide slope indicator next to the altitude reading. Current turn rate was shown by a magenta arc around the compass rose.



Figure 5.3 – Photo of the DA42 simulator cockpit setup with custom display

The central part of Figure 5.4 shows the display in its basic configuration. In this case, the airplane is in coordinated and level flight, pitched up by about 2.5° , banked 25° to the right, at an altitude of 5000 ft and an airspeed of 120 kt . It passes through heading 244° at positive, larger-than-standard turn rate. Around the central part of Figure 5.4, all BMI- and task-related elements can be seen. In the top left corner of the display, the visual feedback of the BMI output was given. The Motor Imagery BMI output (after command mapping, cf. Figure 5.2) was visualized by six balls. Left and right movements of the top ball indicated the current output, whereas the movement of each following ball was

delayed by 0.2 s with respect to the preceding one. Thus, the pilot could perceive a command history of 1 s. The Operant BMI output (before filtering, cf. Figure 5.2) was presented differently, because the subject's operant BMI training consisted in controlling the vertical movement of a ball with tail on a computer screen. With the tail visualizing previous outputs, the training display bore some resemblance to a flying ball. To facilitate transition between the Operant BMI training task and flight control in the simulator, the same symbology was used here. Up and down movements of the ball indicated the current Operant BMI output, whereas the ball's tail indicated previous outputs until 1.5 s into the past. Up/down movements of the ball were associated with left/right movements of the airplane. The two dashed and two solid white lines shown on the Operant BMI feedback indicated certain BMI output values that only had a meaning in the BMI training task. At later stages of the Operant BMI experiments, the BMI output feedback was moved to the lower left part of the display to facilitate concurrent observation of the HSI.

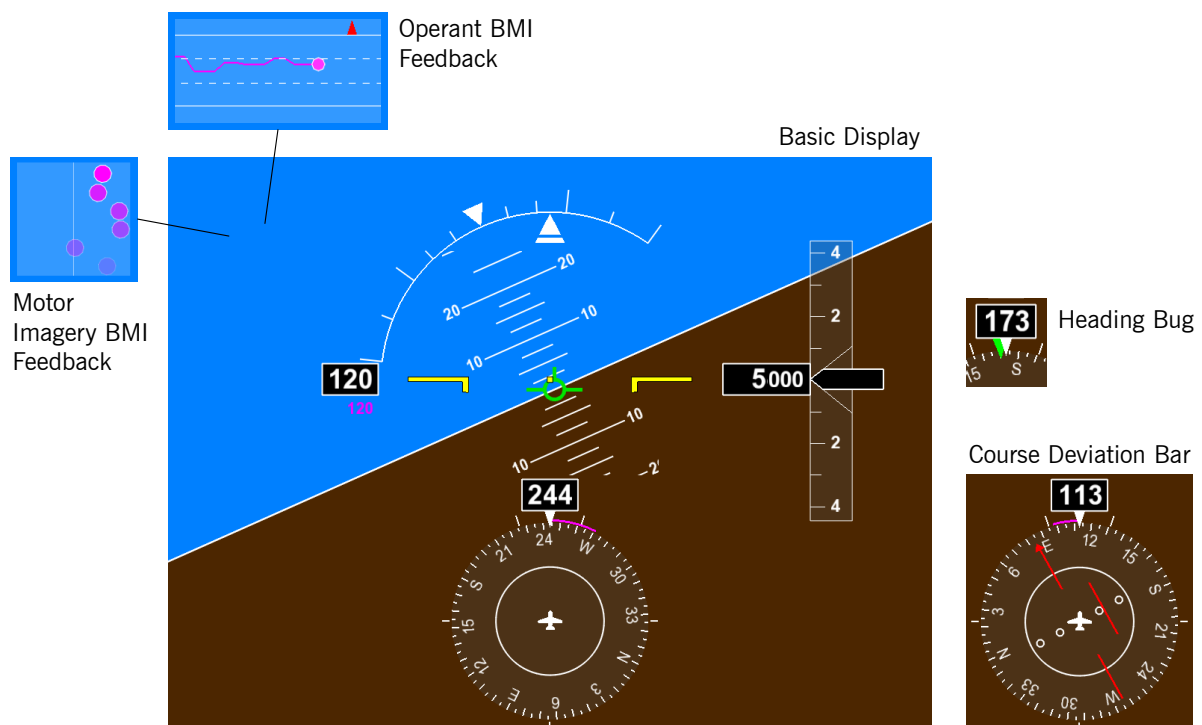


Figure 5.4 – Custom DA42 display: basic version, BMI- and task-related elements

The display furthermore showed several task-related elements that can also be seen in Figure 5.4. During tasks 0, 1 and 2, a heading bug was shown and during task 3, a course deviation bar within the HSI indicated the deviation from the (offset) localizer track. Both the heading bug and the course deviation bar changed color, depending on the tracking performance. When the tracking error was within the desired performance, the symbols were green, whereas yellow color indicated an error within adequate performance. The symbols were red otherwise, i.e., when tracking performance was less-than-adequate. Initially, this color code was designed to help subjects assessing their own performance for application of the CHR scale [70]. Although the idea to collect CHRs was abandoned, the colors of the target symbols still retained their purpose of motivating the subjects to achieve desired or at least adequate performance.

5.2 Tasks and Briefing

Task design was approached with the methods of handling evaluation established in the aerospace domain in mind. This novel approach to BMI testing was expected to yield a highly realistic experimental setting and thus results that are relevant for actual BMI application. Designing realistic tasks for the experiments on BMI controlled flight was a challenge due to the fact that control performance was uncertain and expected to be a lot poorer than with manual control. The first decision, already described in section 5.1.2, was to perform lateral control. Tasks of different levels of difficulty were then designed to address a wide range of possible performance levels. Efforts were made to design operationally meaningful tasks, since the participants were not trained test pilots and generally not familiar with pure tracking tasks. Furthermore, tasks generally progressed and terminated regardless of performance. Thus, subjects that performed poorly would not get stuck in a task.

Speed control was accomplished entirely by the autothrottle system. During tasks 0, 1 and 2, the vertical motion was controlled by the altitude hold mode already incorporated in the flight control system. For task 3, a simple autopilot was implemented that tracked the glideslope and also initiated a flare manoeuvre to give the pilots the cues they were used to in this flight phase.

Pilot briefings were given orally at the beginning of each session, guided by previously compiled notes. Subjects were introduced to EEG and BMIs and received instructions on how to use them in combination with the flight controller. The functionalities of the flight control system (altitude hold, path straightener, standard rate turn hold and bank angle protection) were explained, the tasks were outlined and all display elements were described.

5.2.1 Task 0 – Training

This preparatory task, which had been derived from Task 1, was intended to give subjects some time to familiarize with the BMI control system. A sequence of different target headings was indicated by the heading bug. As equation (5.1) indicates, the value of each new target heading Ψ_{tgt} was the sum of the current heading at the moment of the target change t_{ch} and the corresponding step from the predefined sequence given in Table 5.2. This method to compute target headings was chosen to avoid that changes in target heading reduced or even eliminated the tracking error, which was expected to be large at least in some cases.

$$\Psi_{tgt} = \Psi(t_{ch}) + \Delta\Psi_{tgt} \quad (5.1)$$

The sequence of steps comprised an equal number of left and right turns with increasing size. Each change in target heading was accompanied by an acoustic signal.

Table 5.2 – Sequence of heading target steps for task 0

Step No.	1	2	3	4	5	6	7	8	9	10
Step $\Delta\Psi_{tgt}$	20°	-20°	30°	-30°	45°	-45°	100°	-100°	160°	-160°

The time between targets t_{bt} was fixed as in equation (5.2). It allowed for target acquisition with standard turn rate ($3^\circ/s$) as well as for turn initiation, turn termination and about one minute of tracking. This choice resulted in a total task duration of about 15 minutes.

$$t_{bt} = \frac{\Delta\Psi_{tgt}}{3^\circ/s} + 63s \quad (5.2)$$

In fact, the task can be seen as being composed of two sub-tasks, namely heading acquisition and heading tracking. To acquire a target heading, pilots were advised to turn with standard rate of turn. For heading tracking, desired performance was defined as a heading error of less than 5° , which equals the heading tolerance defined in [139] for an instrument rating flight test. A heading error of less than 10° , which is required for private and commercial pilot license flight tests [139], was considered adequate tracking performance. This definition was mentioned during subject briefing and applied to the color code implemented for some of the task-related display elements. It would also have been required for an application of the CHR scale.

5.2.2 Task 1 – Turns

The motivation behind task 1 was to put the subjects into an operational setting and at the same time obtain a reproducible mission that enables an investigation of control performance. Hence, a sequence of target headings was given, like, for instance, during radar vectoring. Subsequent evaluation was facilitated by the well-defined sequence of targets. The only differences between task 0 and task 1 were the heading steps' direction and size. In task 1, the sequence of steps listed in Table 5.3 was presented. In this case, the sequence was random-appearing, but again comprised an equal number of left and right turns. The first two steps were given for initial familiarization, whereas steps three through ten were used for evaluation.

Table 5.3 – Sequence of heading target steps for task 1

	Familiari- zation		Turns for Evaluation							
Step No.	1	2	3	4	5	6	7	8	9	10
Step $\Delta\Psi_{tgt}$	40°	-20°	-45°	30°	-100°	160°	45°	100°	-30°	-160°

5.2.3 Task 2 – Heading Bug Tracking

Task 2 investigated tracking performance with a continuously moving target. Subjects were thereby confronted with a higher level of difficulty than in tasks 0 and 1. At the same time, this task was designed to explore the bandwidth of BMI control. Like in the previous tasks, the target was symbolized by the heading bug. Its movements were determined by a predefined, random-appearing forcing function. The design of the forcing function was guided by the recommendations in [84]. As shown by equation (5.3), it was composed of 10 sine waves of different frequencies and amplitudes.

$$\Psi_{tgt}(t) = \sum_{i=1}^{10} A_i \cdot \sin(\omega_i \cdot t) \quad (5.3)$$

Table 5.4 lists the parameters of the 10 component oscillations. Since the task duration was set to 300 s, the frequencies of the forcing function components had to be integer multiples of 1/300 Hz, so that an integer number of periods of each component would fit into the task duration and averaging errors would thereby be minimized. While respecting this constraint, component frequencies were chosen to be approximately logarithmically spaced. Component amplitudes and cut-off frequency were chosen based on the initial command filter configuration (see equation (5.4)) and good engineering judgement.

Table 5.4 – Task 2 forcing function components

Frequencies ω_i [Hz]	Frequencies ω_i [rad/s]	Amplitudes A_i [°]
1 / 300	0.0209	5
2 / 300	0.0419	5
3 / 300	0.0628	5
4 / 300	0.0838	5
7 / 300	0.147	5
12 / 300	0.251	5
21 / 300	0.440	0.5
34 / 300	0.712	0.5
57 / 300	1.19	0.5
95 / 300	1.99	0.5

A time history plot of the forcing function is shown in Figure 5.5. Note how all components fit into the task duration by integer multiples, evidenced by zero-crossings of the forcing function at 0 s, 150 s and 300 s. Finally, desired and adequate performance were defined like in tasks 0 and 1.

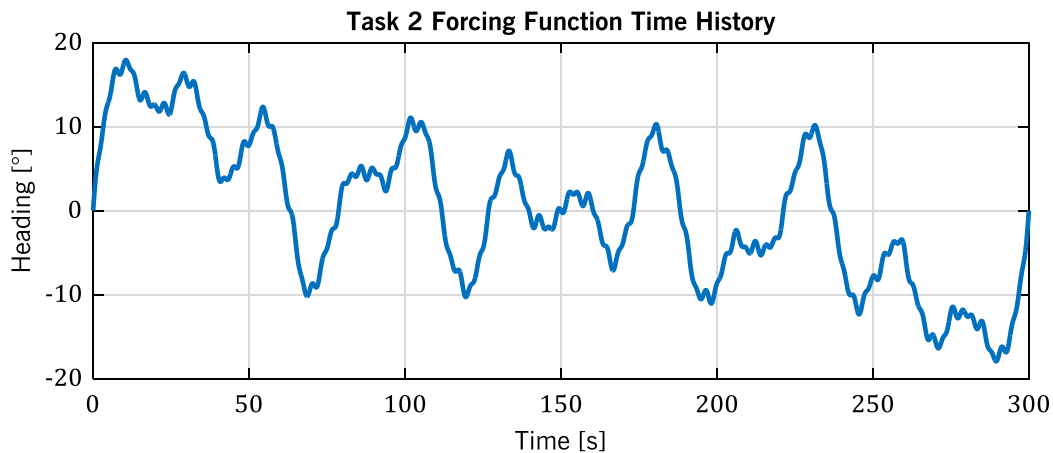


Figure 5.5 – Time history plot of the forcing function of Task 2

5.2.4 Task 3 – Approach

The third and final task was a landing approach with offset localizer. Its design was inspired by a task described in [93] and put the subjects into a very realistic, stressful and challenging scenario. As the sketch of the approach trajectory given in Figure 5.6 shows, the localizer track was offset from the runway centerline by 1 dot on the HSI (cf. Figure 5.4), which corresponds to half of the course deviation bar's Full-Scale Deflection (*FSD*) or approximately 1.3° . At the beginning of the task, the aircraft was positioned at a distance of 7 *NM* to the runway threshold and 1 *NM* to the left of the extended runway centerline. Its heading intersected the offset localizer track at an angle of 45° . Outside visibility was nil above 500 *ft* above ground and 10 *km* below. Throughout the approach, glide path and airspeed were automatically controlled to provide the familiar cues of a normal landing approach.

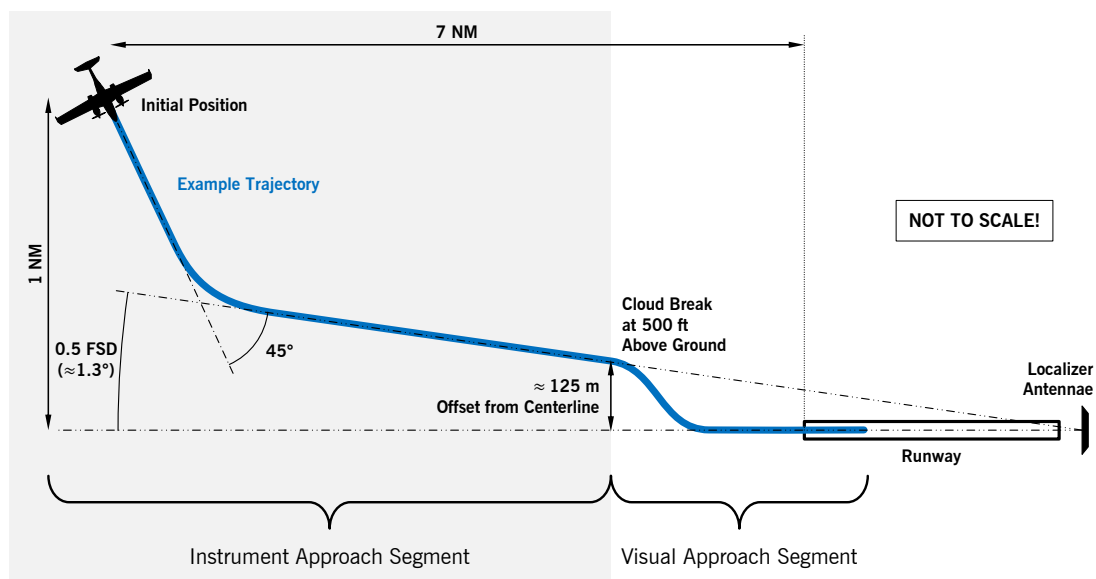


Figure 5.6 – Sketch of the approach flown in task 3

The first part of the task was to intercept the offset localizer and then track it down to simulated cloud break. As there were no outside visual references, it was not apparent to the pilot that the localizer was offset. However, since pilots generally flew this task more than one time, they were told that the localizer could be offset to the left, to the right, or not at all. Upon cloud break, the runway became visible. The pilots were instructed to then ignore their navigation instruments and to continue the approach only by outside visual references. Since the first part of the approach had been offset, the pilots were forced to conduct a sidestep manoeuvre. After that, they had to track the runway centerline, since they had been instructed to touch down as close to it as possible. The simulation ended a few meters above ground.

Again, desired and adequate performance had to be defined. Like in the requirements for a successful instrument rating flight test [139], adequate performance for localizer tracking was defined as the half-scale deflection (0.5 *FSD*) of the course deviation bar. Desired performance was chosen to be 0.25 *FSD*. A definition of desired and adequate centerline tracking performance would have been required only for an application of the CHR and is therefore not given here.

5.3 BMI Control System Tuning

Not only the task design, but also the initial testing phase was inspired by methods established in the aerospace domain. The first experimental sessions with each type of BMI were dedicated to control system tuning, where subjects played the role of evaluation pilots. Relying on the subjects' comments on handling and based on the flight control performance achieved, various parameters of the control system were adjusted after each run to obtain better performance and lower workload in the next run and, ultimately, a control system well adapted to the pilots. The following sections not only present the final control system configurations, but also report the tuning efforts, including all unsuccessful configurations. For better readability and comparability of the following figures, the colors red, blue and yellow are associated with particular subjects. The color grey is employed for all other subjects.

5.3.1 Motor Imagery BMI

The first experiments employed the Motor Imagery BMI and started off with subject M1 as single participant in three sessions that took place across two days and aimed at tuning the mapping function and the command filter. In these rather informal sessions, the subject began multiple runs of task 1 to assess each configuration. Later, he also performed tasks 2 and 3. Initially, the mapping function was chosen to simply feed through the BMI output. The command filter was a double-integrator that changed the turn rate by $1.5^\circ/s$ during each second the (mapped) BMI output was at its maximum level, i.e., $|\delta_{BMI}| = 1$. This command filter, named command filter A, is defined by equation (5.4).

$$Y_{cf,A} = \frac{1.5^\circ \cdot \pi/180^\circ}{s^2} = \frac{0.02618}{s^2} \quad (5.4)$$

During the first runs, the subject was able to initiate turns, but did not succeed in trying to terminate them. The left plot of Figure 5.7 is a good example for this problem: the lines of constant slope indicate that the aircraft flew at the turn rate limit for a prolonged time. Therefore, a small amount of spiral stability was introduced, which, according to the subject, improved the situation. To further facilitate straight flight, a deadzone was introduced as mapping function after a couple of runs. BMI outputs between -0.4 and $+0.4$ were mapped to zero, whereas all other values were fed through. Next, instead of merely relying on weak spiral stability, it was decided to use an altogether different approach. Controlling the double-integrator seemed too challenging, which is why one of the command filter's poles was changed from a pure integrator to a first-order lag. The resulting command filter B is given by equation (5.5). With this filter in use, steady-state turns required a constant, nonzero control input.

$$Y_{cf,B} = \frac{K_B}{(T_B s + 1)s} = \frac{0.1}{(3.820s + 1)s} \quad (5.5)$$

Performance seemed to be similarly inadequate with either command filter A and B (cf. Figure 5.7), but command filter B received more favorable comments from subject M1. It was therefore decided to let all other subjects test both command filters, together with the

same deadzone-type mapping function. At the same time, the idea to collect CHRs was abandoned. It was clear by now that the previously defined desired performance and even the adequate performance would be hard to achieve. Hence, only a small portion of the CHR scale was expected to be relevant, namely Level 3 handling qualities or a CHR of 10. Combined with the fact that the experimental subjects were not trained to use the CHR scale, the resulting CHRs would not have provided useful insights. Finally, task 0 was derived from task 1, so that subjects could familiarize with BMI control and each command filter before the actual experimental tasks 1, 2 and 3.

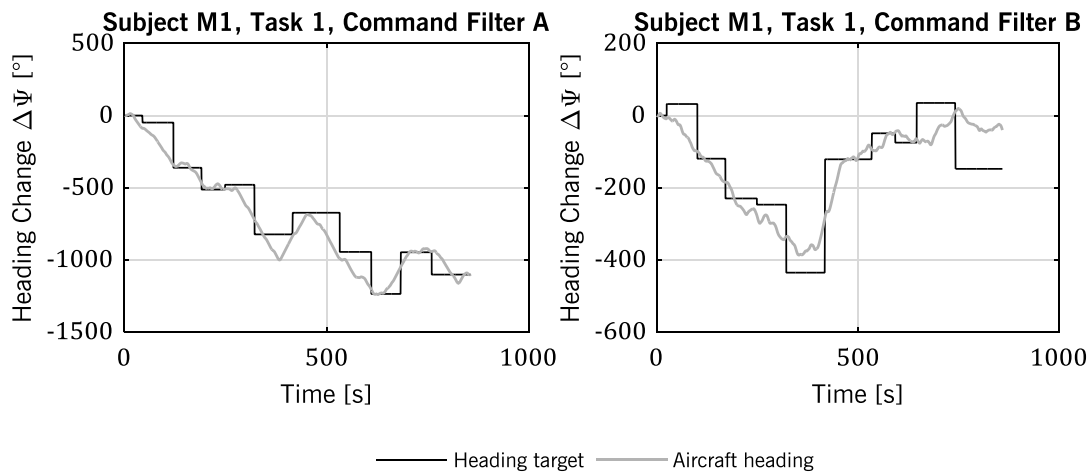


Figure 5.7 – Comparison of command filters: task 1, subject M1

The remainder of the experiments with the Motor Imagery BMI, namely the tests with subjects M2 through M7, followed a fixed procedure. After the initial briefing, the EEG cap was applied to the subject, who then took the left seat inside the cockpit. For the next 20 minutes, brain activity was recorded during imagined movements of the left hand, the right hand and the feet [135]. This data was then used to train the BMI algorithm. The pair of imagined movements that promised the best cross-validation was selected for the experiments. The subject then performed tasks 0 through 3 with one command filter and, after a pause, again with the other command filter. Half of the subjects M2 through M7 started with command filter A, the other half with command filter B. In total, an experimental session took about 4 hours. The outcome of this first experimental campaign is reported in section 5.4.2.

5.3.2 Operant BMI

All following experimental campaigns applied the Operant BMI. The first campaign, comprising five sessions in three consecutive days, again started with system tuning. Subject O1 performed tasks 0 and 1 in the first sessions and flew the other tasks only in the last two sessions. Initially, the control system configuration was based on the experience gained with the Motor Imagery BMI. Hence, the BMI output was not filtered, but fed directly to the mapping function. Moreover, command filter B was used initially, because it promised better results due to its single-integrator characteristics. Since the outputs of the Operant BMI were much smaller than those of the Motor Imagery BMI, the command filter gain was increased by a factor of 3 to $K_B = 0.3$. With the command filter

set to a promising configuration, the mapping function was the only element that was tuned initially. Its first configuration was a three-level mapping like the one shown in Figure 3.30, but with a deadzone within ± 0.23 . This value was chosen because it was the target threshold that had to be reached during BMI user training. While performing tasks 0 and 1, it was difficult for the subject to maintain turns, so the deadzone size was reduced to ± 0.18 and a linear mapping was implemented outside the deadzone, with the input to the command filter δ'_{BMI} still limited to $[-1, 1]$. Subject O1 still did not have control, also after varying the slope of the linear mapping segments. The left part of Figure 5.8 shows an exemplary time history. The subject reported that control felt sluggish.

Hence, command filter A was applied, with the gain tripled so that $K_A = 0.07854$. This configuration felt much better to the subject, although the sensitivity seemed excessive from the experimenters' point of view and the performance was still not comparable to what had been achieved with the Motor Imagery BMI. The value of K_A was therefore reduced to $2/3$ and $1/3$ of its initial value. Moreover, the path straightener was turned off, as it seemed to hinder the subject from initiating turns. Results were still not satisfying (cf. right part of Figure 5.8, where $K_A = 0.02618$), but the subject reported that it felt better. He also stated that he focused so much on the brain signal feedback that he had difficulties in observing the heading bug. The brain signal feedback was therefore moved to the lower part of the display, next to the HSI.

The fact that subject O1 relied a lot on the visual brain signal display shows, on the one hand, that the undelayed BMI feedback proposed in section 4.4 and Figure 4.5 indeed is a suitable aid. On the other hand, it is also a fine example for the challenges of missing proprioceptive inceptor feedback. To obtain the required information on their control inputs, subjects had to devote a considerable amount of attention to the visual display implemented. If the same information had been displayed in a different sensory channel, this problem may have been mitigated, but still not altogether solved. Ideally, both the inceptor deflections and the inceptor forces as the two major proprioceptive sensations would be substituted by a suitable display.

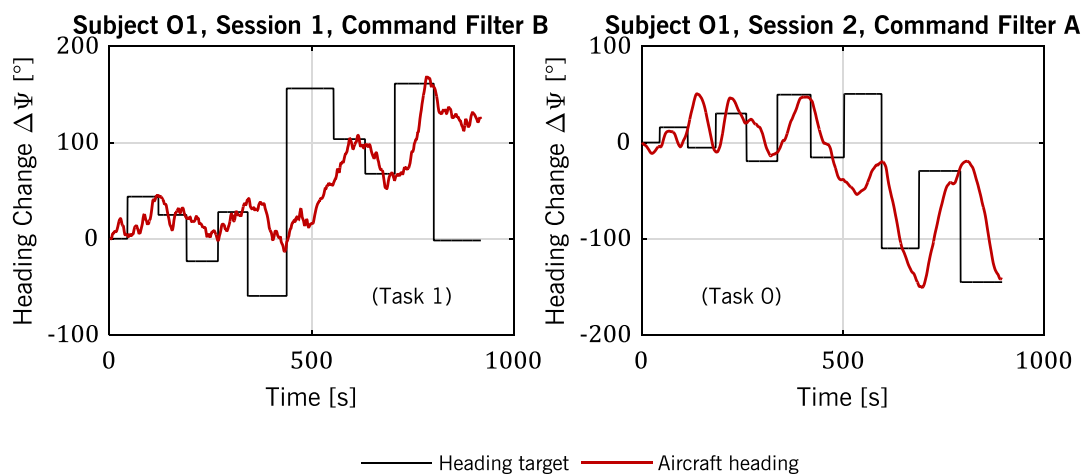


Figure 5.8 – Tasks 0 and 1, flown by subject O1 during system tuning

In an attempt to find a compromise between the sluggish response of command filter B and the overly sensitive response of command filter A, command filter B was employed again, but with a smaller time constant $T_B = 1.5$. The left part of Figure 5.9 shows the results of task 0 with this configuration. It can be seen that the subject was able to perform at least the right turns quite well. The right part of Figure 5.9 shows a recording that was made in a different session with the same configuration. During this run, the parameter K_B was slightly increased to 0.13 at 240 s and T_B was further lowered to 1.2 at 420 s. After this test run, the subject reported to feel in control. It can also be seen in the right part of Figure 5.9 that he consistently steered the aircraft towards the target heading.

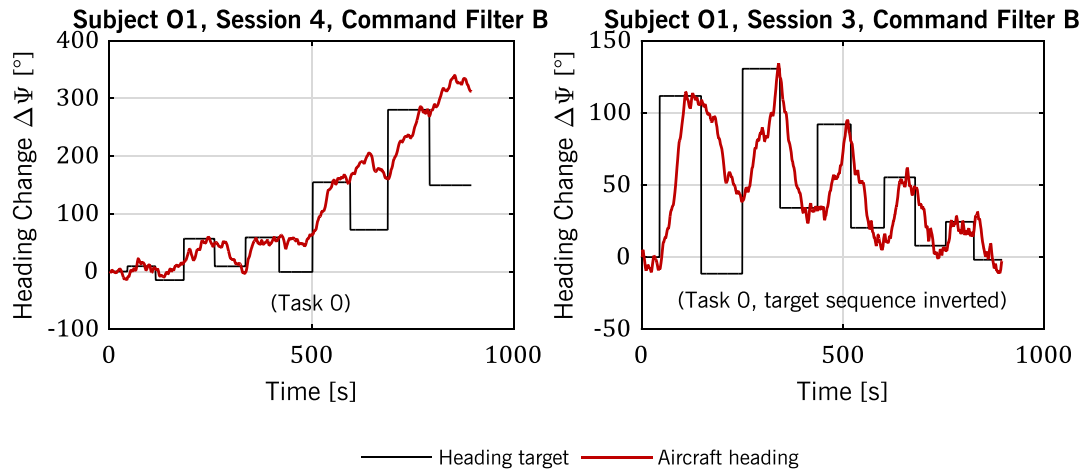


Figure 5.9 – Task 0 flown with a suitable configuration of command filter B

Finally, another attempt was made to reduce jitter while maintaining the responsiveness of the system. The BMI output was filtered by the low-pass filter described by equation (5.6). The deadzone of the subsequent mapping function was removed entirely. Instead, a cubic mapping function was used that assigned an output of ± 1 to an input of ± 0.15 . The output δ'_{BMI} , again, was restricted to $[-1,1]$.

$$Y_{filt} = \frac{1}{s + 1} \quad (5.6)$$

The resulting configuration of BMI output filtering, cubic mapping and command filter B with $K_B = 0.13$ and $T_B = 1.2$ shall be called configuration C. The subject reported in session 4 that it felt “perfect”. It has to be noted, however, that considerable lags were introduced together with the low-pass filter of equation (5.6). As section 3.4.2 discussed, these lags can also be seen as an equivalent filtering time delay τ_{filt} . To estimate the value of this parameter, Figure 5.10 shows the Bode diagram of Y_{filt} together with that of an 8th order SMA filter and that of a 1 s pure time delay. It can be seen that, for frequencies below the cutoff frequency (1 rad/s), the phase curves agree well. Thus, it can be concluded that a filtering time delay of approximately 1 s was introduced. Nonetheless, subject O1 made positive comments on configuration C. It was therefore decided that he would perform all tasks 0 through 3 with it. The performance in these experimental runs is analyzed in the following section 5.4.

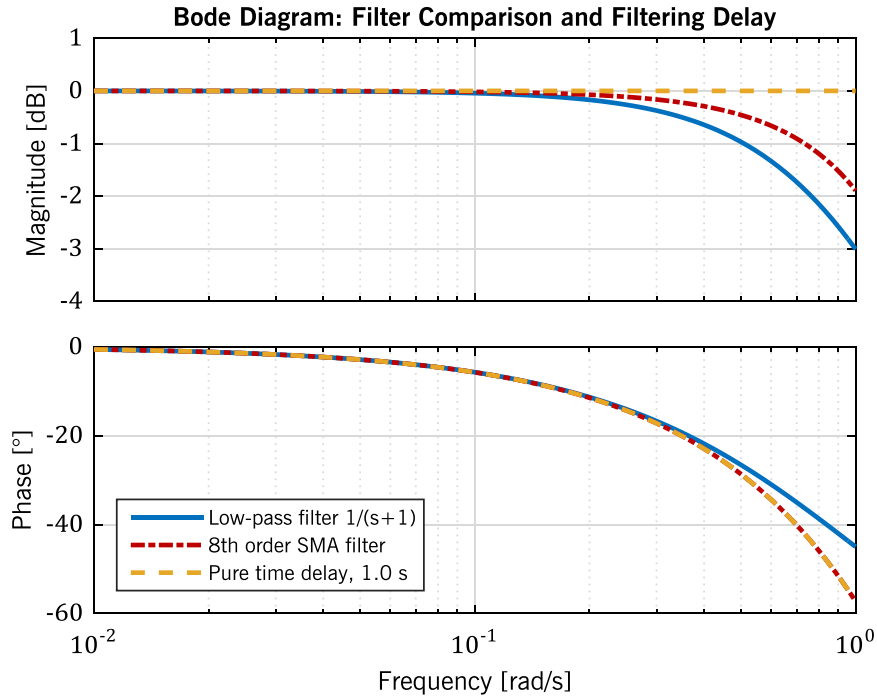


Figure 5.10 – Frequency-domain comparison of filters and a pure time delay

5.4 BMI Flight Control Performance

5.4.1 Performance Metrics and Baseline Performance

To objectively evaluate the subjects' performance in tasks 1 through 3, suitable, quantitative performance metrics have to be defined first. For task 1, the two sub-tasks heading acquisition and heading tracking are analyzed separately. To quantify heading acquisition performance, the Turn Rate Index (TRI) defined by equation (5.7) is used. It relates the average turn rate to the standard turn rate. Here, average turn rate is defined as the heading change necessary to achieve desired performance, divided by the time required for this maneuver Δt_{tgt} minus 2.5 s to account for reaction time and turn initialization. TRI values close to 1 indicate that turns have been flown approximately as instructed, namely at standard rate.

$$\text{TRI} = \frac{|\Delta\Psi_{tgt}| - 5^\circ}{\Delta t_{tgt} - 2.5s} \cdot \frac{1}{3^\circ/s} \quad (5.7)$$

Heading acquisition performance is also characterized by the overshoot produced upon capturing the target. In this case, overshoot is defined as the value of the heading error at the first moment that the turn rate becomes zero after the heading has crossed the threshold to the desired region around Ψ_{tgt} . Overshoot could therefore be negative, but not smaller than -5° . An overshoot within $[-5^\circ, 5^\circ]$ indicates that the turn has been stopped within the desired region.

Heading tracking is evaluated only across the tracking segment of each target. This segment begins at the moment the heading crosses the threshold to the desired region

around Ψ_{tgt} and ends as soon as the target changes again. Across each tracking segment, the Root Mean Square Error (RMSE) can be computed as in equation (5.8), with the error $e = \Psi - \Psi_{tgt}$ in this case and with N denoting the number of samples. A good tracking performance is indicated by low RMSE values.

$$\text{RMSE} = \sqrt{\frac{1}{N} \sum_{i=1}^N e_i^2} \quad (5.8)$$

The RMSE can be misleading in that large errors that persist for only a short time have little influence on the overall RMSE. Therefore, the maximum error during tracking is taken as an additional measure of performance. Note that due to the definition of the tracking segment, the maximum error cannot be smaller than the desired performance threshold, i.e., 5° in the case of task 1.

Low values of maximum error and RMSE can be produced either by a small and rather constant residual error or by continuing oscillations around the target. The second case is less desirable from the pilot's point of view, because it requires permanent control activity. Therefore, as proposed in [70], Error Variability (EVAR) is introduced as a parameter that indicates oscillations of the error. It is defined by equation (5.9).

$$\text{EVAR} = \frac{1}{N-1} \sum_{i=1}^{N-1} |e_{i+1} - e_i| \quad (5.9)$$

The performance in task 2 can be quantified by heading RMSE, EVAR and maximum error as well. In task 3, performance is analyzed separately for localizer-guided approach and the sidestep manoeuvre. For both localizer and centerline acquisition, overshoot is defined as for heading acquisition in tasks 0 and 1. The tracking segment, again, begins at the moment the error crosses the threshold to the desired region. The localizer tracking segment ends with the transition to visual approach at cloud break and the centerline tracking segment ends with the recording. Tracking RMSE, EVAR and maximum error are evaluated for both tracking segments. Due to the definition of the tracking segments, maximum localizer and centerline error cannot be smaller than 0.25 FSD and 8.23 m , respectively.

Apart from quantitative performance metrics, a baseline performance is required to which the experimental results with BMI control can be related to. To obtain this baseline, subject M7 was invited a second time, several months after his BMI control session, to perform the same tasks 0 through 3 using conventional, manual control. Subject M7 was chosen simply due to his availability. In this manual control session, longitudinal control was accomplished again by the combination of autothrottle, altitude hold mode and autopilot described above. In the horizontal motion, however, subject M7 manually controlled the unaugmented aircraft, because the unaugmented airplane in combination with the simulated control forces was known to have adequate handling qualities for manual control. The suitability of the BMI flight controller for on-board manual control, on the

other hand, was uncertain at that point. When flying the unaugmented airplane, lateral center stick inputs correspond to aileron deflections and pedal inputs deflect the rudder.

While a detailed evaluation of manual control performance is provided together with an evaluation of other configurations in section 5.4.2, the following figures already present the time history plots and approach trajectories for later reference. Figure 5.11 shows tasks 1 and 2 as flown manually by pilot M7. Remember that the first two steps in task 1 were dedicated to familiarization and only the last eight steps were evaluated.

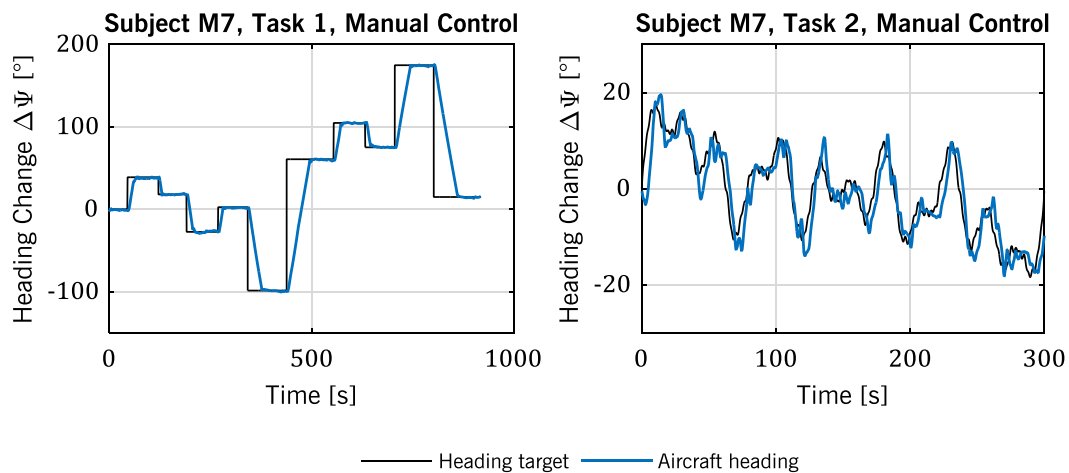


Figure 5.11 – Time history plots of tasks 1 and 2, manual control

Figure 5.12 illustrates manual control performance during task 3. The localizer tracking error over time, shown on the left plot, is quickly reduced during acquisition and then held at a low level throughout the rest of the instrument approach. The sidestep maneuver, visible in the right plot showing the airplane’s horizontal trajectory, contains some overshoot and subsequent oscillation. Nonetheless, the centerline tracking error was small and ultimately, i.e., above the runway, stationary.

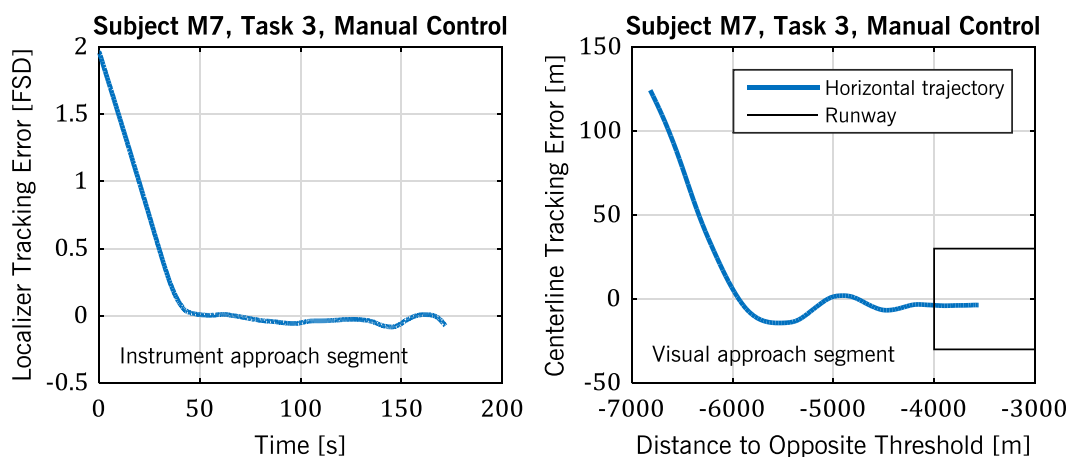


Figure 5.12 – Evolution of tracking errors during task 3, manual control

5.4.2 Comparison of Different Configurations

During BMI control system tuning, several possibly suitable configurations of command filtering and mapping were identified. Moreover, the experimental campaigns comprised

multiple subjects who attempted BMI control. The performance of these various combinations of subjects and control system configurations, including manual control, are compared with each other in this section. It can already be said that those control system configurations deemed suitable for control with a Motor Imagery BMI, namely configurations A and B, proved unsuccessful for Operant BMI control, at least for subject O1 (cf. section 5.3.2). Whether the Operant BMI control configuration C enables successful control with a Motor Imagery BMI could not be tested.

The experiments with the Motor Imagery BMI revealed large differences in performance between subject pilots. Subjects M4 and M6 did not have control. Subject M4 flew in circles, whereas subject M6 performed undirected manoeuvres. As a result, both sessions were terminated after only a couple of training runs. Subjects M2 and M5 generally did not perform well. However, they sometimes managed to acquire and track a heading target during task 0 or 1. Figure 5.13 shows example plots of subject M2. It can be seen that he was rather successful in task 0 with configuration B, whereas he mostly turned left during task 1 with command filter A. He then completely lost control during task 3, when he seemed to be stressed and quickly got frustrated. Indeed, task 3 aimed at generating more stress to investigate performance under realistic, operational conditions. Although it is not possible to pinpoint the cause for subject M2 losing control, it is safe to say that BMI control performance varied within a relatively short time frame. This is obviously undesirable.

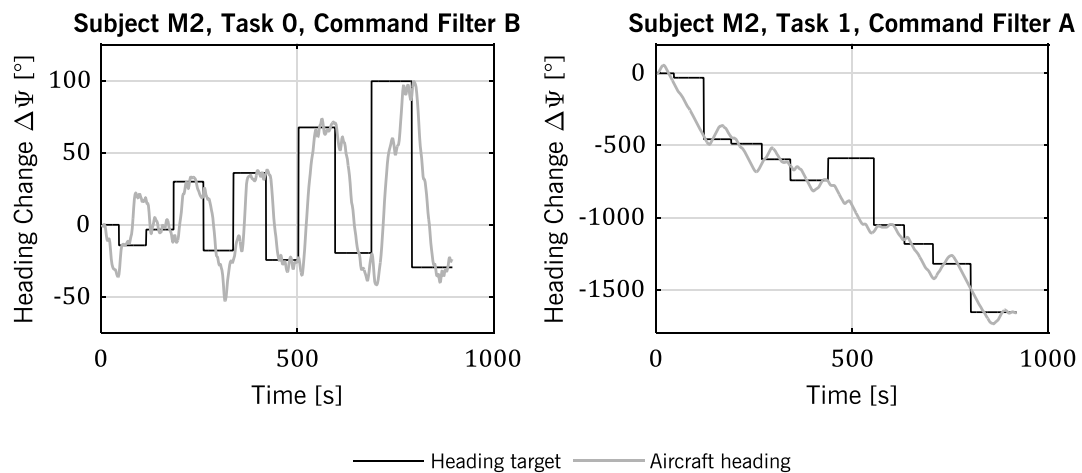


Figure 5.13 – Exemplary time history plots of subject M2

Subjects M3 and M7 performed noticeably better than all others. This is already apparent from the time history plots of subject M3 in task 1, shown in Figure 5.14. It can be seen here that every target was reached. While heading control was highly oscillatory with command filter A, command filter B enabled tracking with less jitter. The cause for the oscillations lies in the nature of this subject's BMI outputs, as section 5.5 illustrates. Unfortunately, the duration of task 1 with command filter A was shorter than normal due to an erroneous task setting. All targets were presented, but the tracking phases were shorter. As a result, the comparability of these tracking phases with those of other runs is reduced.

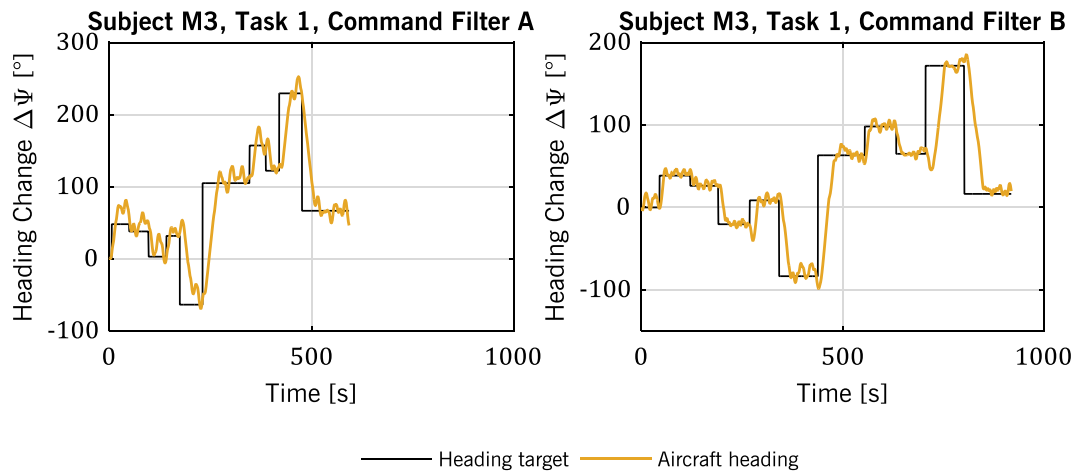


Figure 5.14 – Time history plots of subject M3 in task 1

Next, Figure 5.15 shows how subject M7 performed in task 1 with each configuration A and B. It can be seen quite clearly that, in general, the system outputs were less oscillatory than those of subject M3. With command filter A, subject M7 reached every target, but using command filter B, one target was just not reached. It can be noted that heading control was comparatively sluggish with command filter B.

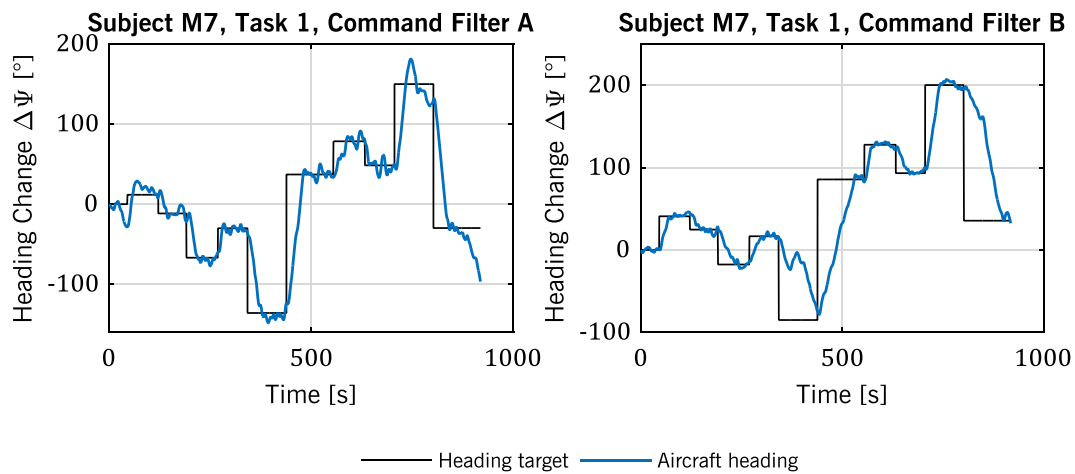


Figure 5.15 – Time history plots of subject M7 in task 1

Task 2 was indeed more challenging for the subjects. Figure 5.16 shows that even subjects M3 and M7, who generally outperformed all others, had difficulties following the moving target. As opposed to other subjects, they managed to stay close to the target, but only subject M7 with command filter B was able to actually track the target.

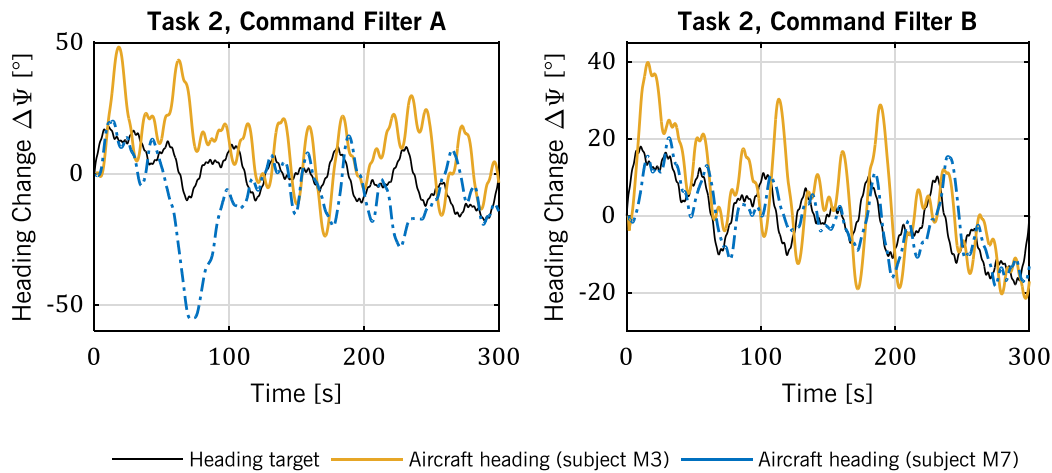


Figure 5.16 – Time history plots of subjects M3 and M7 in task 2

Task 3, being again more challenging, was rarely flown with acceptable performance and even more rarely accomplished in its entirety. One notable exception was the second try of subject M3, who in this case used configuration B. As Figure 5.17 shows, he successfully tracked the offset localizer and subsequently managed to fly the sidestep maneuver. The trajectory is quite oscillatory, but it generally complies with the adequate performance thresholds and finally ends over the runway, close to the runway centerline.

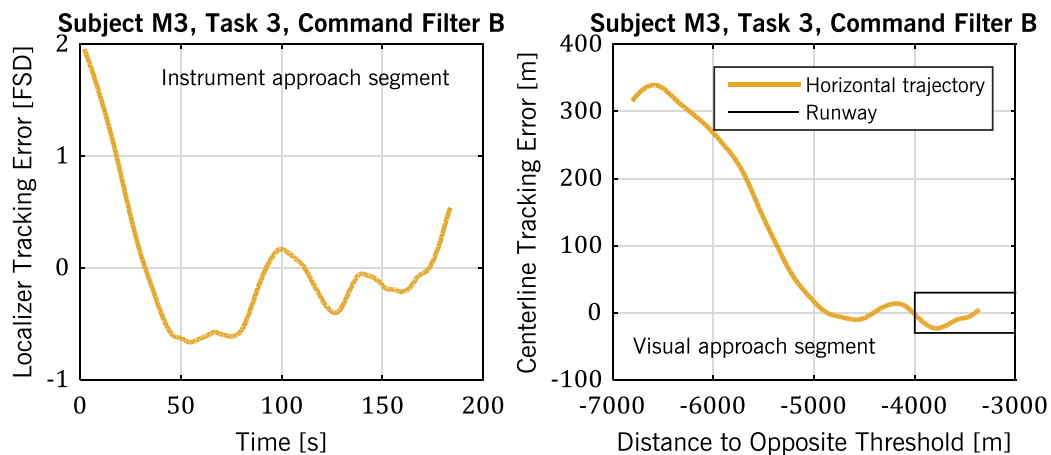


Figure 5.17 – Evolution of tracking errors during task 3, subject M3, configuration B

Due to his generally outstanding performance, subject M3 was invited for a second, more informal experimental session on the following day. In this second session, similar BMI outputs and similar performance could be observed. Apart from a few training runs, tasks 1 and 2 were performed a second time with command filter B. Moreover, several additional attempts to steer the airplane onto the runway in task 3 were made. Subject M7, who also performed comparatively well, was also keen to achieve a landing on the runway, which is why his single experimental session with BMI control was prolonged by another three tries at task 3. Figure 5.18 shows all trajectories of subject M3 and M7 during task 3 using BMI control. Note that most trajectories strayed off course sooner or later, although many headed for the runway for quite some time. It can be seen again here that heading

control with configuration B was sluggish for subject M7. With configuration A, on the other hand, subject M7, too, reached the runway once, even though he had grossly departed the target approach track before.

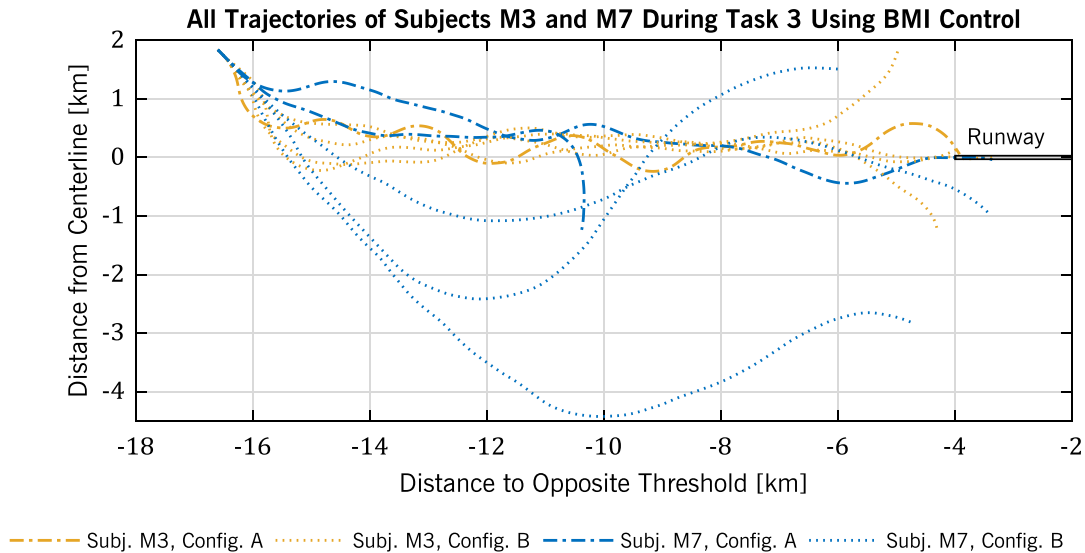


Figure 5.18 – Horizontal trajectories during task 3, subjects M3 and M7

After this qualitative description of performance with the Motor Imagery BMI, the same overview is now given over the Operant BMI experiments. As described in section 5.3.2, it took until the 4th session of subject O1 to find a suitable configuration for control with the Operant BMI, namely configuration C. The subject then started off again with task 0 and proceeded with tasks 1, 2 and 3. Like subject M3 and M7, subject O1 then flew task 3 several more times during a 5th session in an attempt to successfully steer the airplane to the runway. Task 2 was also flown a second time in the 5th session.

First, Figure 5.19 illustrates tracking performance in tasks 0 and 1. Again, short-term variations in BMI control performance can be noted. While some targets were tracked quite accurately, others were not even reached. In earlier sessions it was noted that using configuration C, turns were generally flown slower than standard rate. Instead of increasing an aircraft gain and thereby compromising controllability, the time between targets was increased to re-establish an adequate duration of tracking segments. This was done by scaling the denominator of the right side of equation (5.2), which stands for the expected turn rate, down from $3^\circ/s$ (standard rate) to $1.5^\circ/s$. This explains the longer duration of tasks 0 and 1 in Figure 5.19 when compared to the same tasks performed in the context of the Motor Imagery BMI experiments.

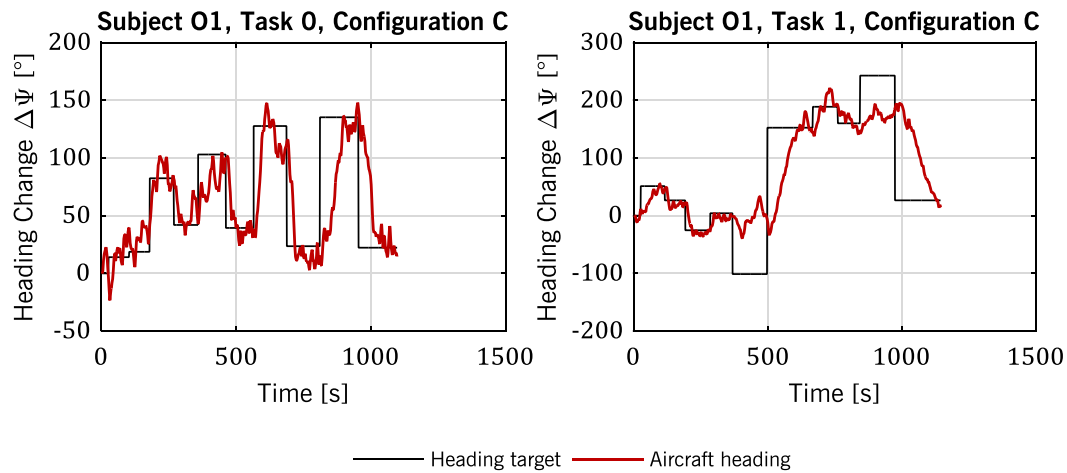


Figure 5.19 – Time history plots of subject O1 in tasks 0 and 1

Next, Figure 5.20 shows how subject O1 tracked the target heading in his two attempts at task 2. Like subjects M3 and M7, he managed to maintain the approximate direction of the target. Moreover, each run exhibits phases where the target is tracked quite accurately. These phases may indicate a temporary improvement in controllability, but they may as well be due to chance.

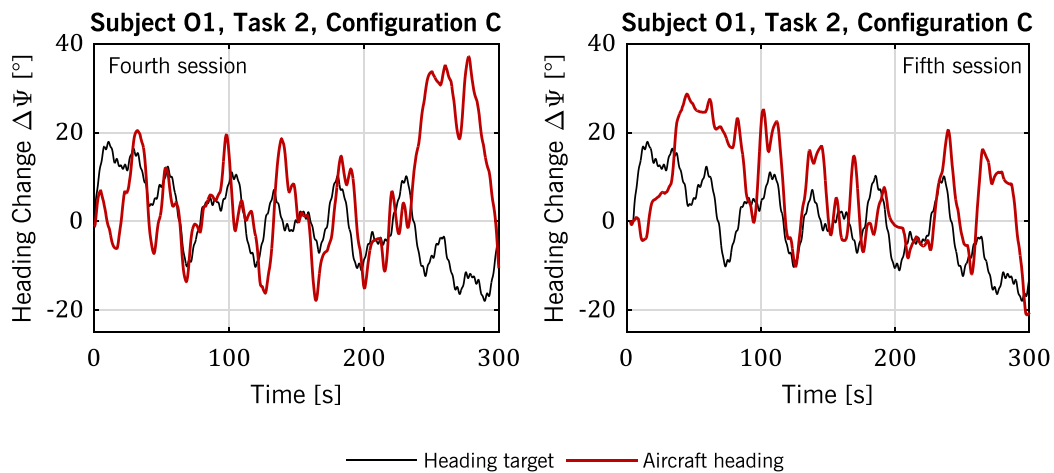


Figure 5.20 – Time history plot of subject O1 in task 2

Subject O1's four attempts at task 3 are shown in Figure 5.21. Localizer tracking was generally unsuccessful and all trajectories ended up grossly misaligned with the runway centerline. Interestingly, however, subject O1 achieved the closest approach to the runway in a flight that first deviated by almost 10 km from the extended runway centerline.

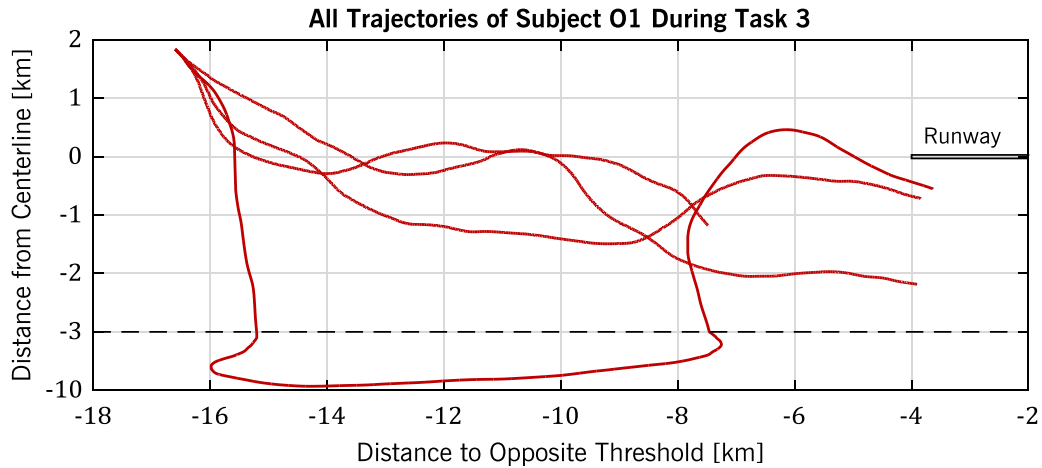


Figure 5.21 – Horizontal trajectories during task 3, subject O1

Now that the qualitative overview of performance with both the Motor Imagery and the Operant BMI is concluded, the different configurations are quantitatively compared in the following paragraphs, using the performance metrics defined in section 5.4.1. First, performance in task 1 is analyzed, which can be described by TRI, overshoot, RMSE, EVAR and maximum error. Figure 5.22 compares the first parameter, TRI, between subjects and configurations. Remember that TRI values close to 1 indicate that turns have been flown approximately as instructed, namely at standard rate. The value of n shown above each box in Figure 5.22 indicates how many of the eight target steps were reached. The boxes below visualize the distribution of TRI across these n steps. Each box indicates the 1st, 2nd and 3rd quartile of the data, whereas the mean value is designated by a cross symbol. In all box plots shown in this thesis, data points outside 1.5 times the interquartile range are marked by a circle as outliers. Whiskers extend to the most extreme data value that is not an outlier.

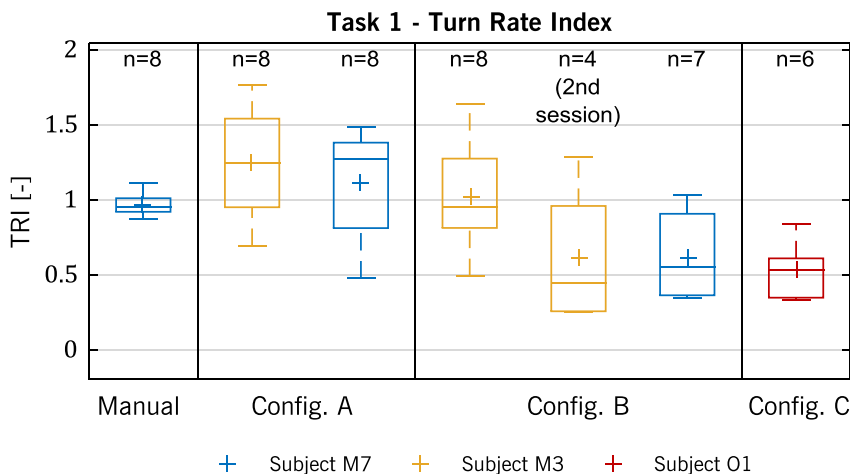


Figure 5.22 – Task 1 TRI comparison of different configurations

It is evident from Figure 5.22 that subject M7 with manual control turned at standard rate with the highest accuracy and consistency. Using BMI control, each subject produced a comparatively wide range of TRI values, which indicates a much less consistent

performance or, in other words, a lack of controllability. Subject M3 tended to turn faster than subject M7, which can be explained by the fact that subject M3 produced BMI outputs of limit amplitude ($\delta_{BMI} = \pm 1$) more often than subject M7 (cf. section 5.5). Similarly, both of these subjects turned faster with configuration A than with configuration B, which in turn is due to the characteristics of the flight control system configurations. With command filter B, a maximum turn rate of 0.1 rad/s could be achieved if BMI outputs were always correct. For $STR < 1$, the effective maximum turn rate was smaller. Using command filter A, on the other hand, subjects could initiate and maintain a turn with a greater turn rate despite their noisy control signals, especially during long turns. Little by little, they would increase the turn rate until reaching the bank angle limit. Thus, the strategy of initiating and maintaining a turn by constantly communicating a positive/negative intention indeed could have been the same for both configurations. In this case, the bank angle limitation would have been utilized as a support for turning flight. Note that to stop a turn, the two configurations A and B called for different strategies. Using configuration B, it was enough to communicate neutral intention, whereas with configuration A, subjects had to actively decrease the turn rate by communicating opposite intention. Looking at Figure 5.22, it is also interesting to note how TRI values differed between the two sessions of subject M3. This again shows that performance can vary from session to session, at least when using a Motor Imagery BMI. Subject O1 with configuration C achieved comparatively consistent TRI values, but generally turned at a slow average rate.

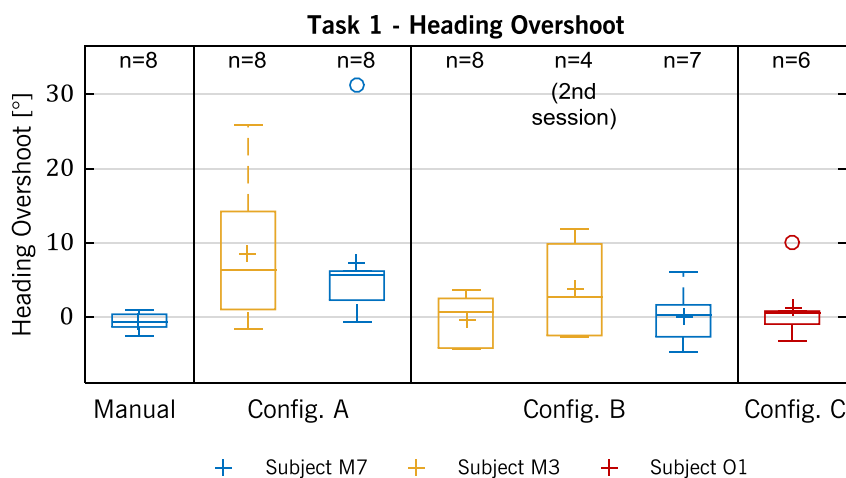


Figure 5.23 – Task 1 overshoot comparison of different configurations

The second parameter that describes target acquisition performance is heading overshoot. The distribution of overshoots is shown in Figure 5.23. Again, manual control enabled the best and most consistent performance, but subject O1 with configuration C achieved similarly accurate acquisition maneuvers. This is in good agreement with the observation that turns were slow for this subject and configuration. It seems that it was more difficult to initiate and maintain a turn for subject O1 with configuration C than to fly straight. In other words, there was a tendency for the mapped BMI control action δ'_{BMI} to be 0 in this case. The overshoot values of subject M7 varied a little more than those of subject O1, but the largest variance of overshoot values was produced by subject M3. The largest

absolute heading overshoots occurred when subjects M3 and M7 used configuration A. This is probably due to the fact that with this configuration, an established turn rate had to be actively reduced. To account for the noisy BMI outputs, pilots had to start this reduction some time before reaching target. If a subject did not introduce a sufficient amount of lead, a large overshoot occurred.

After the analysis of target acquisition, a look is taken at target tracking performance during task 1. It has to be noted again at this point that not all tracking segments had the same duration. As mentioned above, subject M3 with configuration A experienced shorter tracking segments. Moreover, subject M7 with configuration B achieved rather low TRI values, which in turn shortened his tracking phases. Similarly low TRI values were observed for subject O1, but in his case, the task duration was adapted.

As first performance metric of target tracking, heading RMSE is shown in Figure 5.24. Like in the preceding analyses, manual control excels in accuracy and consistency. Slightly larger and more variable RMSE values were produced with configuration B. The second session of subject M3 is an exception here, as it produced the largest average RMSE value. Note that at the same time, only four out of eight targets were reached. This again well illustrates possible variations in performance. RMSE values achieved with configurations A and C are similar and, apart from subject M3's second session, highest.

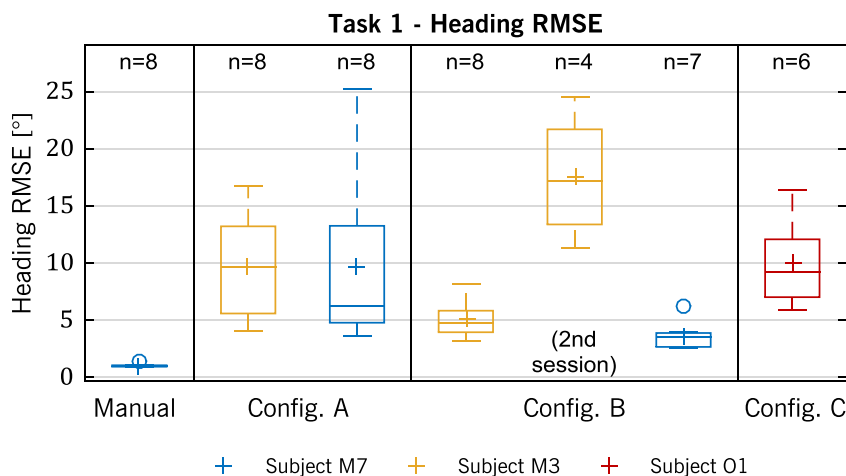


Figure 5.24 – Task 1 RMSE comparison of different configurations

Next, Figure 5.25 shows the distributions of maximum heading error. Here, basically the same observations can be made as for heading RMSE. Additionally, it can be noted that the maximum errors produced by subject M7 with configuration B were consistently small and always within the adequate performance boundaries ($\pm 10^\circ$).

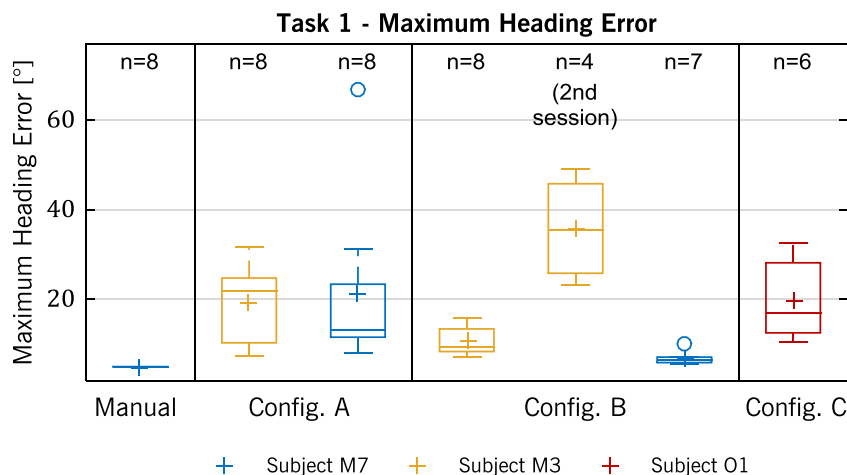


Figure 5.25 – Task 1 maximum error comparison of different configurations

To conclude the analysis of target tracking during task 1, Figure 5.26 shows the distributions of heading EVAR. It is no surprise that manual control enabled the lowest and most consistent EVAR values. Like the TRI values, EVAR values tended to be higher for subject M3 than for subject M7, which is again due to the nature of the BMI outputs produced (cf. section 5.5). Likewise, both of these subjects produced higher EVAR values with configuration A than with configuration B. The second run of subject M3 again stands out here, with larger EVAR values than with the same configuration in the first session. Subject O1 with configuration C achieved average EVAR values.

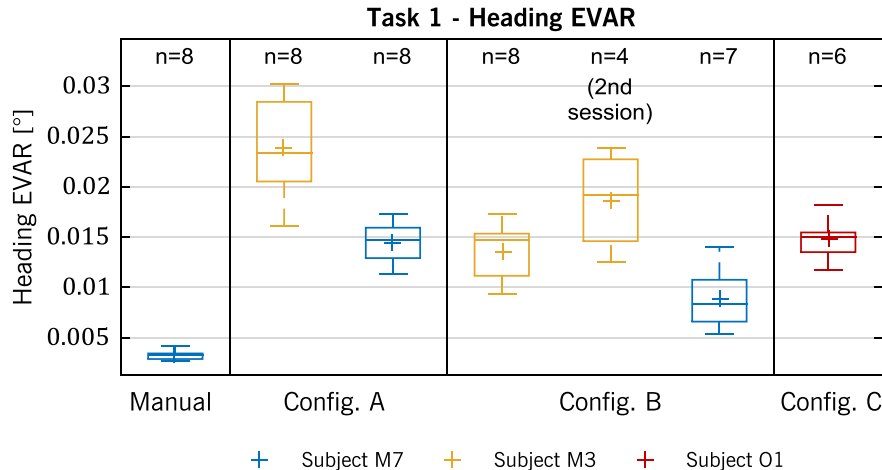


Figure 5.26 – Task 1 EVAR comparison of different configurations

After the detailed comparison of performance in task 1, task 2 is evaluated next. As mentioned in section 5.2.3, it was planned to compute the pilot-aircraft bandwidth based on the recordings of task 2. However, it became evident during post-processing of the data that the transfer from tracking error to aircraft heading was dominated by the nonlinearity of the BMI. The measure of coherence [70], which should be approximately 1 for results to be valid, was generally smaller than 1. Hence, values of pilot-aircraft bandwidth are not reported here. Instead, Figure 5.27 shows the RMSE achieved in each case during task 2. Here, very similar observations like for the RMSE in task 1 can be made. Again, subject

M7 with configuration B delivered the best performance after manual control. The poor performance of subject M3 in his second session stands out, but otherwise configuration B enabled better performance than configurations A and C.

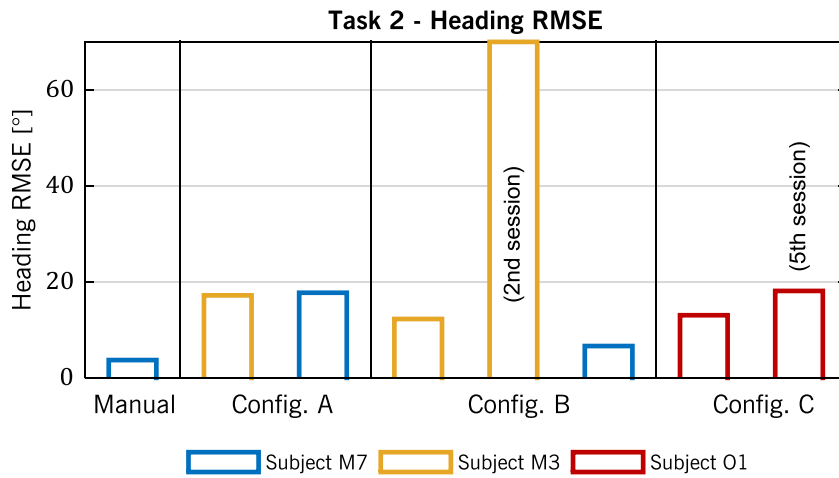


Figure 5.27 – Task 2 RMSE comparison of different configurations

The maximum heading errors of the task 2 runs under consideration, shown in Figure 5.28, well agree with the corresponding RMSE values shown in Figure 5.27. This means that subjects who produced larger average errors also produced larger maximum errors.

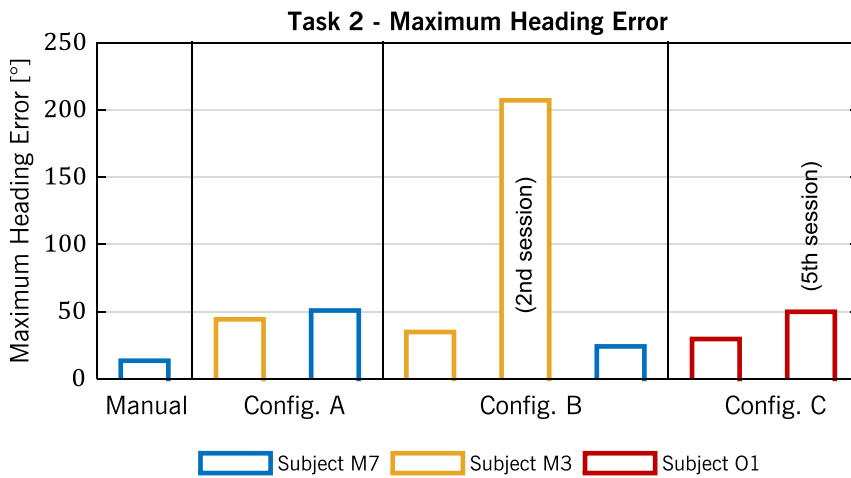


Figure 5.28 – Task 2 maximum error comparison of different configurations

The comparison of heading EVAR, shown in Figure 5.29, concludes the analysis of task 2. Due to the nature of BMI outputs, EVAR values tended to be higher for subject M3 than for subject M7. This was already observed in task 1. The greater EVAR values produced with configuration A as compared to configuration B in task 2 also well agree with the findings from task 1. Subject O1 with configuration C again achieved average EVAR values. It is quite striking in task 2, however, that the EVAR achieved with manual control is not noticeably smaller than all other EVARs, but instead similar to the EVAR subject M7 achieved with configuration B.

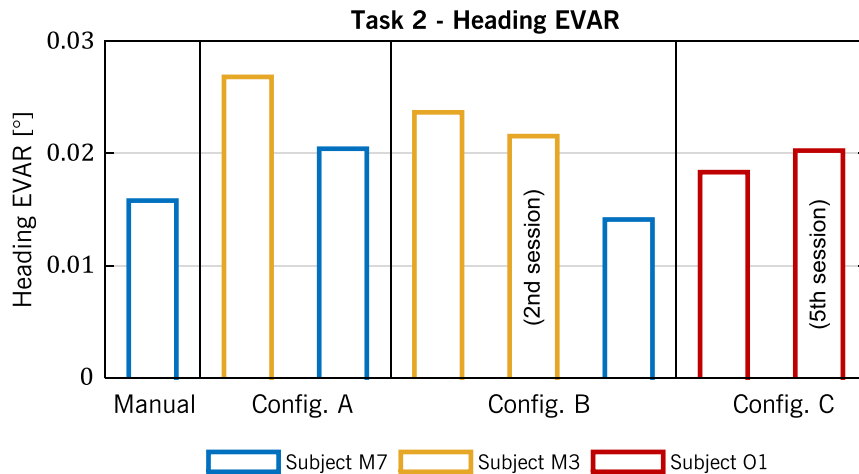


Figure 5.29 – Task 2 EVAR comparison of different configurations

Finally, for task 3, a meaningful quantitative comparison cannot be made, because the subjects' performance was generally poor.

All in all, it can be concluded that some subjects were able to perform closed-loop control of the horizontal airplane motion in a realistic environment, using a BMI and the flight control system described in chapter 4 (or variations thereof). The performance of manual control, however, was not matched by far and some subjects did not have control at all. The main reason for this expected shortcoming is that controllability requires sufficiently reliable BMI outputs in the first place. The experiments have shown that significant improvements of the algorithms that identify the user's intention from the measured electromagnetic brain signals are a prerequisite for BMI controlled flight in particular or for any closed-loop control application of BMIs in general. Another major problem encountered was that BMI control performance strongly varied not only between subjects, but also between sessions, runs and sometimes even within a run. Biases, which occurred from time to time, also hindered or even prevented control. All these issues will have to be mitigated. Controllability and handling, however, not only depend on the BMI characteristics, but are also influenced by the plant dynamics. This is evident from the tuning efforts and the comparison between control system configurations.

The comparison between configurations A and B showed that the control of a single pure integrator is easier and allows more precise tracking than control of a double pure integrator. This finding is supported by objective as well as subjective measures. For configuration B, subject comments were more favorable and overshoot, RMSE, EVAR and maximum error all tended to be lower. This is not surprising in the light of previous research. Remember, for instance, that the optimum transfer function predicted by the Crossover Model is a simple integrator and that higher-order controlled system dynamics cause pulse-like operator behavior (cf. chapter 3). In any case, the filtering and mapping algorithms must be adapted to each subject and BMI, possibly even to each session. Here, agility can be traded off against stability. A control system configuration that enables fast changes of the controlled parameter makes it difficult to keep this same parameter constant. Regardless of the control system configuration used, protections are necessary to prevent dangerous system outputs. In the experiments, the protections within the flight

control system effectively prevented upset attitudes and flight envelope excursions, but it is suspected that in some cases the bank angle limitation was misused as a supportive feature in turning flight.

Another aspect to be noted is that those subjects who had control reported that they had to constantly anticipate the airplane movements to successfully track target headings or ground tracks. This corresponds to the extensive lead generation expected in this case of large time delays. Interestingly, however, only subject O1 faced any filtering time delay originating from the flight control system. According to section 3.4.2 and equation (3.64), all other subjects would thus have experienced a comparatively minuscule time delay $\tau_{BMI} = \tau_{sp} \approx t_s = 0.1 \text{ s}$. The observations on the BMI output spectrum made in the following section 5.5, however, provide an explanation for the subjects' comments on lead generation. Subjects furthermore stated that they had to concentrate a lot on generating the required brain activity. Prior to an actual application of closed-loop BMI control in the context of a more complex task environment such as that of an airplane pilot or merely that of a car driver, this problem will have to be overcome. In addition to the high concentration required to generate the brain activity, subjects also felt that they allocated a lot of attention on the visual BMI feedback. Thus, not much more information could be perceived visually. However, even if the BMI output were to be conveyed in a different sensory channel, the amount of attention devoted to this feedback would not be available for other displays. Finally, those subjects who used the Motor Imagery BMI and who imagined hand or arm movements to turn in one direction and feet movements to turn in another direction noted that this mapping of imagined body movements and airplane reactions is not intuitive and thus adds mental workload. This underscores that those types of BMIs that rely on user training are better suited for an operational application, as section 4.3.2 already noted.

In conclusion, it can be said that even though control was possible for some subjects, it came at the cost of extreme mental workload. This workload has to be reduced and, at the same time, BMI output reliability has to be improved on the way towards operational application of BMIs in closed-loop control tasks. In any case, plant dynamics need to be adapted to the BMI. In this process, the experiences reported in this thesis can be used as a point of reference. An effective means to substitute the undelayed cues of proprioceptive feedback still has to be found, since a simple visual display proved unsatisfactory.

5.5 Experimental BMI Model Validation

To be able to validate the BMI model proposed in section 3.4.2, additional experiments were conducted with the operant BMI and subjects O1 and O2. Task and system dynamics had to be chosen in a way that the user intention during the task would be implicitly given. Therefore, task 1 was selected and the transfer function from the filtered and mapped BMI input to airplane heading Ψ was simply modeled by equation (5.10). If, in this case, the error in Ψ lies within a tolerance deadband, defined by the task, the user's intention can be assumed neutral. If the signed error is greater/smaller than the upper/lower deadband

limit, user intention implicitly is negative/positive. Thereby, the probable user intention at every time step can be determined during post-processing.

$$Y_{\Psi\delta'_{BMI}} = \frac{0.1}{(1.5s + 1)s} \quad (5.10)$$

Subject O1 performed 12 runs in 2 sessions, whereas subject O2 performed 9 runs in 2 sessions. BMI filtering and mapping was altered between the runs, but it never changed the integrator-with-lags dynamics of the open loop given by equation (5.10). With the user intention thus identifiable at every time step, BMI outputs were grouped into those that occurred during positive, neutral and negative intention. To validate the assumptions behind the BMI model of section 3.4.2, the BMI outputs of all runs of each single subject were analyzed as a whole, as the following paragraphs describe. It has to be noted that the results may therefore be slightly distorted, because subjects advanced their training with each run.

The first assumption of the BMI model, namely that the BMI output is a random variable drawn from a Gaussian distribution, can be tested using Lilliefors' test of normality [140]. When applied across all runs of each subject, but for each intention separately, this test shows that BMI outputs indeed are normally distributed. This result is supported by the fact that skewness is always close to 0 and kurtosis is approximately 3 in all cases. Figure 5.30 well illustrates the similarity between the Operant BMI output amplitude distributions obtained from one run of subject O1 and Gaussian distributions with equal μ and σ^2 .

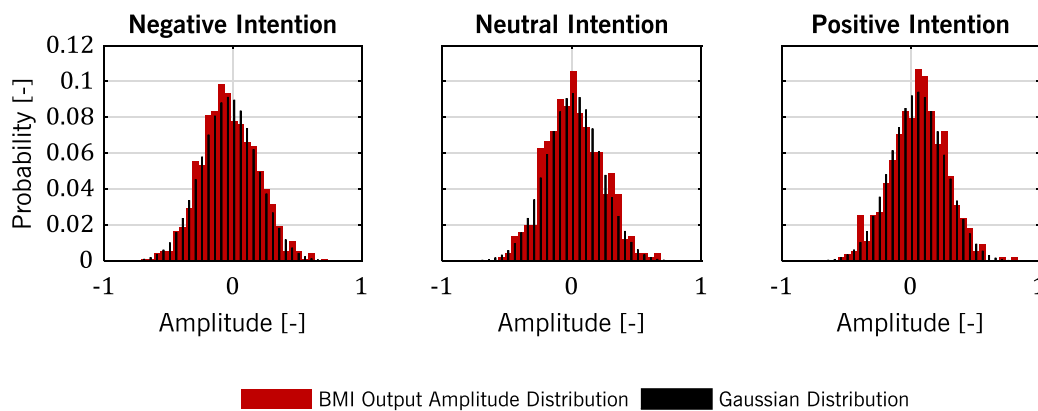


Figure 5.30 – Exemplary Operant BMI output amplitude distributions

The second assumption that the BMI model is based on states that $\sigma_p^2 = \sigma_z^2 = \sigma_N^2$. This assumption, which by the appearance of the distributions in Figure 5.30 seems to hold, can be broken down into $\sigma_p^2 = \sigma_N^2$, $\sigma_p^2 = \sigma_z^2$ and $\sigma_z^2 = \sigma_N^2$. Subsequent two-tailed, dependent t-tests for each subject across all runs indicate, after Bonferroni correction, that the alternative hypotheses ($\sigma_p^2 \neq \sigma_N^2$, $\sigma_p^2 \neq \sigma_z^2$ and $\sigma_z^2 \neq \sigma_N^2$) cannot be confirmed. Corresponding t-values, which are given in Table 5.5, are quite small, especially for subject O1. Hence, the assumption $\sigma_p^2 = \sigma_z^2 = \sigma_N^2$ is likely valid, even though the null hypotheses $\sigma_p^2 = \sigma_N^2$, $\sigma_p^2 = \sigma_z^2$ and $\sigma_z^2 = \sigma_N^2$ were not accepted, but only not rejected. The third assumption behind the BMI model is that the mean value for neutral intention $\mu_z = 0$. For

each subject, a two-tailed, dependent t-test across all runs shows that the alternative hypothesis $\mu_Z \neq 0$ cannot be confirmed. Considering the small t-values ($t(1) = 0.08649$ for subject O1 and $t(1) = 0.6864$ for subject O2), the assumption $\mu_Z = 0$ can be considered valid. The fourth and final assumption of the BMI model, $\mu_P = -\mu_N$, can be tested with a two-tailed, dependent t-test for each subject across all runs as well. The resulting t-values ($t(1) = 0.5725$ for subject O1 and $t(1) = 0.5198$ for subject O2) show that the alternative hypothesis $\mu_P \neq -\mu_N$ cannot be confirmed and that the assumption $\mu_P = -\mu_N$ is likely valid. However, the right plot of Figure 5.13 and the STR variations illustrated by Figure 5.31 indicate that a bias can indeed occur in individual runs. Generally, the data of well-trained subject O1 seem to better support the assumptions behind the BMI model than the data of novice subject O2.

Table 5.5 – Some quantitative statistical results for BMI model validation

Alternative Hypothesis	$t(1)$	
	Subject O1	Subject O2
$\sigma_P^2 \neq \sigma_N^2$	0.3191	1.158
$\sigma_P^2 \neq \sigma_O^2$	0.03499	0.9544
$\sigma_O^2 \neq \sigma_N^2$	0.7983	0.8292

Apart from testing the BMI model assumptions, the task design also allows to measure the STR. Like in section 3.4.2, this is done without making any assumption on BMI output mapping. Hence, positive/negative STR can be obtained by computing the percentage of BMI output samples that had a positive/negative sign during positive/negative intention. Figure 5.31 shows the resulting positive and negative STRs along with the overall STR, i.e., the arithmetic mean of positive and negative STR, for each run of subject O1. It can be seen that the overall STR varied slightly across runs. Variations in STR during positive and negative intention were even more pronounced. Large differences between positive and negative STR indicate a strong bias towards one direction. Ideally, BMI outputs have little bias, such as those of runs 6 through 9, and at the same time a large overall STR, which makes runs 6 through 8 preferable over run 9.

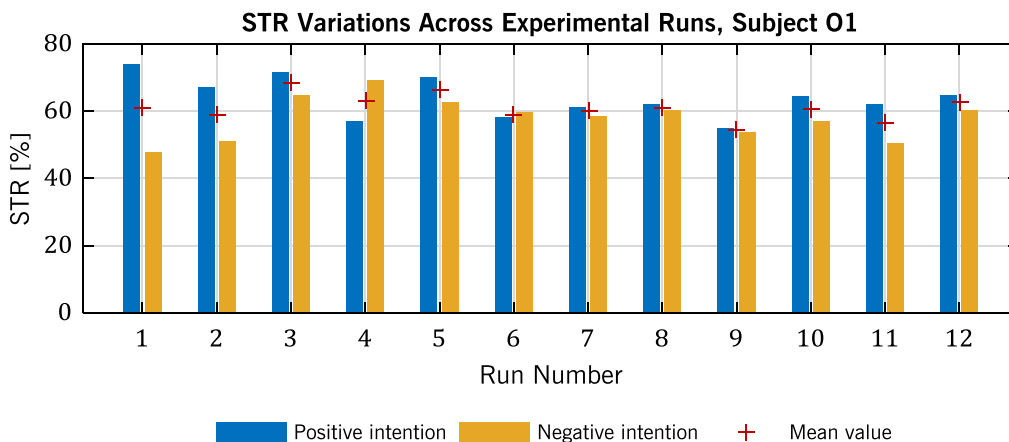


Figure 5.31 – Variations in measured STR for subject O1

Apart from the STR, the values of the parameters μ_P , μ_N , σ_P^2 , σ_Z^2 and σ_N^2 can be determined empirically from the grouped BMI outputs. The BMI model parameters μ and σ^2 can then be fitted to the experimental data using equations (5.11) and (5.12).

$$\mu = \frac{\mu_P + |\mu_N|}{2} \tag{5.11}$$

$$\sigma^2 = \frac{\sigma_P^2 + \sigma_Z^2 + \sigma_N^2}{3} \tag{5.12}$$

To obtain more insight into the quality of the model, the measured overall STR, averaged across all runs of a subject, can be compared to the STR of the BMI model fitted to those same measurements. Table 5.6 lists both the measured STRs and the model STRs, as well as the SNRs determined from the model parameters μ and σ^2 . Measured STRs and model STRs agree very well. Note their very low values, which are also reflected by small SNRs and an apparent similarity of all three distributions in Figure 5.30. It can be seen that subject O1 achieves better STR and SNR values than subject O2, which is in good accordance with the fact that he had a lot more training. It has to be noted that in several runs of subject O2, STR was below 50%, which means that control was effectively inverted in those cases. On average, it seems that subject O2 indeed had no control at all. Note that the model STR and SNR values in Table 5.6 do not satisfy equation (3.57), because they are mean values across all runs of each subject. A slight distortion occurs because the averaging operation is linear, whereas equation (3.57) is nonlinear.

Table 5.6 – Comparison of measured STR, model STR and model SNR

BMI Type	Subject	Mean Measured STR	Mean Model STR	Mean Model SNR
Operant	O1	60.92%	60.52%	0.1004
	O2	52.17%	52.88%	0.05911
Motor Imagery	M3	73.55%	74.39%	0.4906
	M6	47.73%	48.42%	not applicable
	M7	72.94%	72.12%	0.3466

In a second step, the proposed BMI model is applied to the Motor Imagery BMI. From the experiments made, those runs of task 0 or 1 with command filter B allow to determine the probable user intention, using the same method as discussed above. The subsequent determination of μ_P , μ_Z , μ_N , σ_P^2 , σ_Z^2 and σ_N^2 , however, has to be done differently in some cases. Remember that the Motor Imagery BMI produced outputs within $[-1,1]$. This would pose no problem if the majority of any amplitude distribution fits into this range. Otherwise, the distribution is truncated and, as a consequence, the variance changes. Indeed, all Motor Imagery BMI subjects produced truncated BMI output amplitude distributions. Figure 5.32 shows an example of subject M3, which constitutes an extreme case. (Note the logarithmic ordinate scale!) The method to fit Gaussian distributions to the measured distributions is therefore as follows. If the probability for the amplitude -1 and that for the amplitude $+1$ are both smaller than 0.1, mean and variance are determined as above for

the Operant BMI. The Gaussian distribution is then truncated to $[-1,1]$, like the data it is derived from. If the measured probability for the amplitude -1 or that for the amplitude $+1$ is higher than 0.1 , mean and variance are chosen such that the probabilities of the output amplitudes -1 and $+1$ are reproduced once the Gaussian amplitude distribution is truncated.

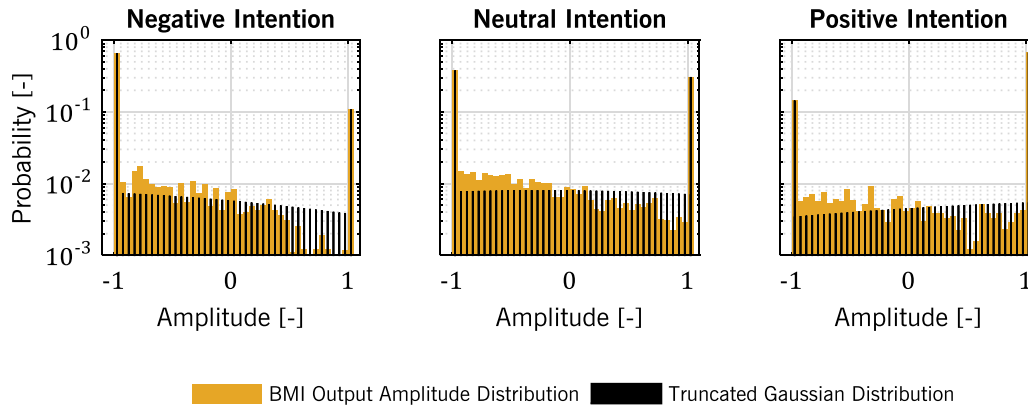


Figure 5.32 – Exemplary output amplitude distributions of subject M3

Subject M3 always produced outputs like the ones shown in Figure 5.32, although with slightly less truncation in his second session. This type of quasi-binary output was in fact the cause for the oscillatory nature of his flights, reported in section 5.4.2. The Gaussian distributions in Figure 5.32 were fitted to the extreme values of the measured distributions, which is why they perfectly agree. In between the extremes, measured and Gaussian distribution seem to disagree. However, due to the fact that the probabilities in this range are negligibly small when compared to the probabilities at -1 and $+1$ amplitude, this disagreement is irrelevant. The fact that subject M3 had control is already qualitatively apparent in Figure 5.32: for negative/positive intention, the probability for an output of -1 is much higher/lower than for an output of $+1$. For neutral intention, these two probabilities are similar.

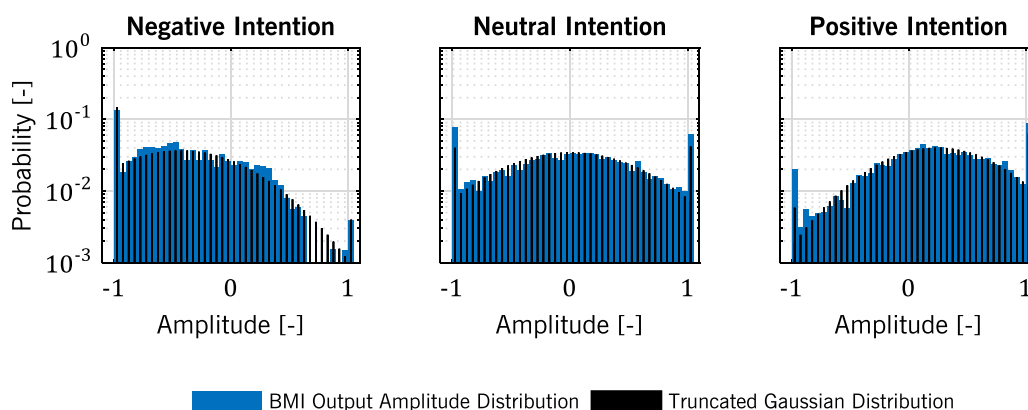


Figure 5.33 – Exemplary output amplitude distributions of subject M7

The BMI output amplitude distributions of subject M7 were not as heavily truncated. Examples are shown in Figure 5.33. Here, only the Gaussian distribution for negative user

intention was fitted to the probabilities at -1 and $+1$ amplitude, whereas the two other truncated Gaussian distributions have the same mean and variance as the respective measured distribution. For all three intentions, the truncated Gaussian distributions agree well with the measured distributions. Like above, it can be seen qualitatively from Figure 5.33 that subject M7 had control.

As mentioned above, not all subjects in the Motor Imagery BMI experiments had control. The BMI output amplitude distributions of subject M6, who did not have control, are shown in Figure 5.34. Here again, all three Gaussian distributions were fitted to the respective extreme values. The fact that all three distributions look alike already implies that control was impossible.

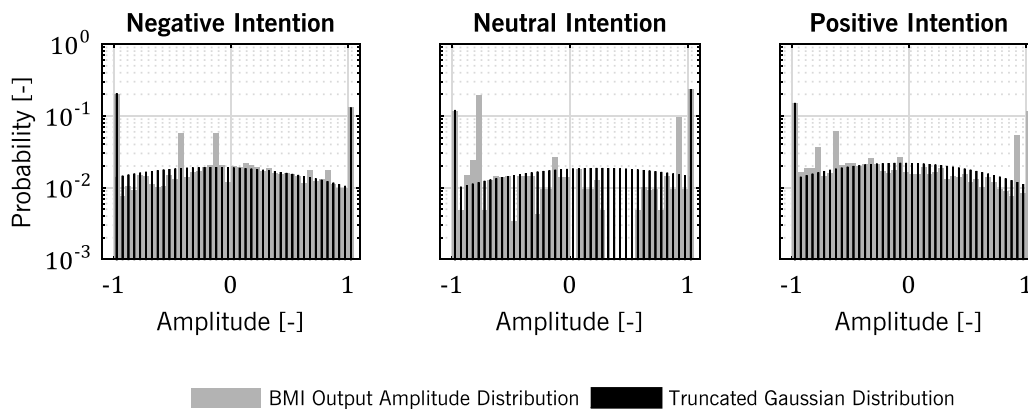


Figure 5.34 – Exemplary output amplitude distributions of subject M6

Having fitted Gaussian distributions to each intention of each subject, equations (5.11) and (5.12) can again be used to obtain the BMI model parameters for each subject and each run. The resulting mean model STRs and SNRs across all runs of each subject are reported in Table 5.6, along with the measured STRs. Like for the Operant BMI, measurements and model do well agree. Note that subjects M3 and M7 achieved much better STR and SNR values than subject O1, which well agrees with the findings of section 5.4.2. Since the STR of subject M6 is below 50%, a SNR cannot be computed. The STR values of subjects M6 and O2 are all similarly close to 50%, indicating that they did not have control.

It is interesting to note that in case of subject M3, machine learning produced a cross-validation estimate of 95% [135], whereas the actual STR during the experiment was only 73.55%. This important insight puts cross-validation estimates generally into perspective. There are various possible explanations for this discrepancy, including a variation of the subject’s strategy and a change in the subject’s general state. For instance, the data for machine learning was obtained while the subject was still relaxed, whereas the actual experiment put him into a more stressful situation.

When comparing the SNR and STR values in this section with the quantitative analysis of subject performance in the previous section 5.4.2, it can be seen that higher SNR or STR values correspond to an overall better performance, which perfectly makes sense. Nonetheless, a subject and BMI that achieve a high STR/SNR do not perform similarly

well with any type of controlled system. The controlled system's dynamics, too, influence task performance, as can be seen in section 5.4.

The last test of the BMI model concerns the PSD of BMI outputs. Figure 5.35 shows the PSDs estimated from BMI outputs of subjects M3, M7 and M6 on the left and of subject O1 on the right. It can be seen that the spectra are not constant across all frequencies up to the Nyquist frequency, but that higher frequencies are attenuated, especially in the case of the Motor Imagery BMI. This means that the assumption that each BMI output sample is independent from all previous samples is incorrect. This is a deficiency of the simple BMI model presented in section 3.4.2. A correction of this deficiency could possibly be achieved by introducing a suitable low-pass filter into the model. The location of the poles of this low-pass filter then constitute additional degrees of freedom that can be used to fit the BMI model to experimental data. Note that this observation explains the fact that some subjects of the Motor Imagery BMI experiments stated that they had to anticipate the airplane movements a lot, even though the BMI output was not processed by a dedicated filter in the flight control system and thus, no additional lags were introduced.

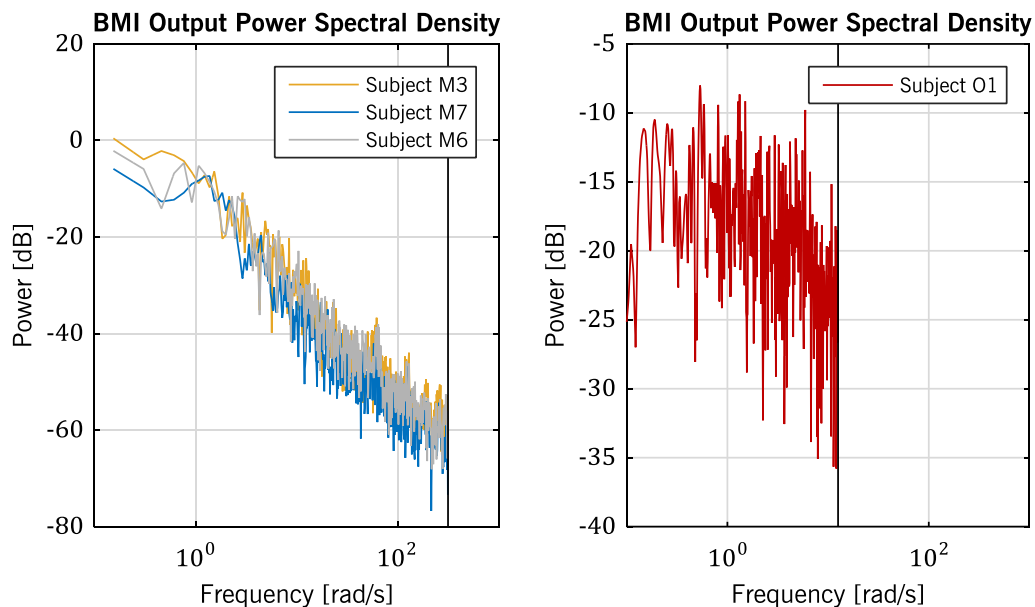


Figure 5.35 – Estimated PSDs of BMI outputs

Summing up, it can be said that the concept of the BMI model presented in section 3.4.2, which was tested against experiments with two different types of BMIs, is generally valid. Changes in user intention indeed cause shifts of the mean BMI output, but do not significantly affect the variance of the signal. A BMI output can therefore be seen as a noise with shifting mean. It is valid to assume that this noise is Gaussian. However, the noise is not exactly white, because some high frequency attenuation is present. This means that two consecutive BMI output samples are not independent. The metrics associated with the BMI model, namely STR and SNR, were found to be a suitable quantification of the control performance of a subject-BMI combination. Problems with the application of the model arise when STR is below chance (50%), which is the case for subjects who do not (yet) have control.

6 EXPERIMENTAL EVALUATION OF MANUAL REMOTE FLIGHT CONTROL

The experiments on BMI controlled flight were of highly explorative nature and faced several challenges beyond the problem of flight control with large time delays and reduced sensory feedback. It was therefore imperative to conduct another test campaign that would thoroughly evaluate the proposed flight control system in the scope of manual remote flight control. Some preliminary experiments aimed at comparing on-off control to continuous control [118], but they had several shortcomings. First, only two subjects were invited, which did not allow for a really meaningful interpretation of the results. Second and even more important, the inceptor characteristics were not as described in section 4.3.1, because the experiments were set up in the DA42 flight simulator, where only the force gradient of the control stick could be varied. Since these preliminary experiments pale in comparison to the later, larger-scale test campaign, they are not discussed here at all.

As opposed to the experiments on BMI control, which were used to tune the system and explore some of its characteristics, one important aim of the test campaign on manual remote flight control was to confirm or disprove certain hypotheses. These hypotheses stem from previous parts of this thesis and are detailed in the following section. Beyond that, the experiments investigated the role of control sensitivities in control with large time delays, evaluated some of the flight control system features and generally compared workload and performance under various circumstances. They also explored the approach of naïve subjects to the problem and collected data for pilot model validation.

6.1 Hypotheses

In section 4.1, it is hypothesized that restricting manual control inputs to few discrete amplitude levels, i.e., implementing an on-off control system instead of a continuous control system, is beneficial in the case of flight control with large time delays. What does beneficial mean in this case? First, remember that fixing the control input amplitude renders the airplane response more predictable and thereby makes pre-cognitive control easier (cf. section 3.3.2). This directly corresponds to a handling improvement, because

less mental effort is required to predict the airplane's response to control inputs. Hence, the first hypothesis can be formulated as follows:

Hypothesis 1:

“Workload is less with an on-off control system as compared to a continuous control system.”

Second, implementing an on-off control system is hypothetically beneficial because it helps pilots apply the pulse-like control strategy they naturally adopt when confronted with large time delays. This also means that they can find this strategy sooner than with a continuous control system. The second hypothesis therefore reads:

Hypothesis 2:

“Pilots naïve to flight control with large time delays find an appropriate control strategy quicker with an on-off control system than with a continuous control system.”

The previous hypotheses claim that an on-off control system has advantages in workload and training time, but what about performance? The restriction in maneuverability that is inevitably introduced with an on-off control system is actually rather minuscule. As soon as at least one integrator is between the on-off control input and the system output under consideration, the only restriction is that a certain speed of movement is prescribed. Although this restriction evidently influences the maximum agility and also the size of the smallest possible movement, it does not prevent the operator from reaching any desired system output. Moreover, the improved predictability given by an on-off control system reduces the time required to familiarize with the system's dynamics and thereby accelerates the transition from compensatory or pursuit tracking to pre-cognitive tracking, which enables precise control with little workload. This combination of slightly reduced maneuverability and greatly improved handling leads to the conclusion that an on-off control system can be expected to enable at least the same, if not better performance than a continuous control system. This expectation is formulated as follows by the third hypothesis:

Hypothesis 3:

“Performance with an on-off control system is comparable or better than performance with a continuous control system.”

Although the design of predictor algorithms and displays is not within the scope of this thesis, their effect on human-machine interaction is investigated here. The large number of previous studies on predictor displays (cf. section 1.2) already proved that they can

reduce workload and improve performance. The fourth and fifth hypotheses are therefore no surprise:

Hypothesis 4:
“Predictor displays reduce workload.”

Hypothesis 5:
“Predictor displays improve performance.”

Apart from these already well-proven statements, another effect of predictor displays were suspected. Predictor displays usually add one or more symbols on an already existing visual display. The advantages of predictor displays therefore come at the price of increased clutter in the visual channel. Moreover, since a predictor symbol is crucial for flight control, it necessarily constitutes one of the primary display elements from the pilot’s point of view. Hence, the sixth and final hypothesis can be stated as follows:

Hypothesis 6:
“Visual predictor displays bind a significant amount of visual attention.”

Other, already existing visual cues would need to compete with the predictors and would therefore receive less attention, should this last hypothesis be confirmed. Apart from the five formal hypotheses, the following Figure 6.1 illustrates the qualitative expectations concerning workload and performance for the four possible combinations of control system and predictor. It thereby visualizes some of the above hypotheses. Moreover, it shows that the beneficial effects of the on-off control system were expected to be less pronounced when a predictor display is provided.

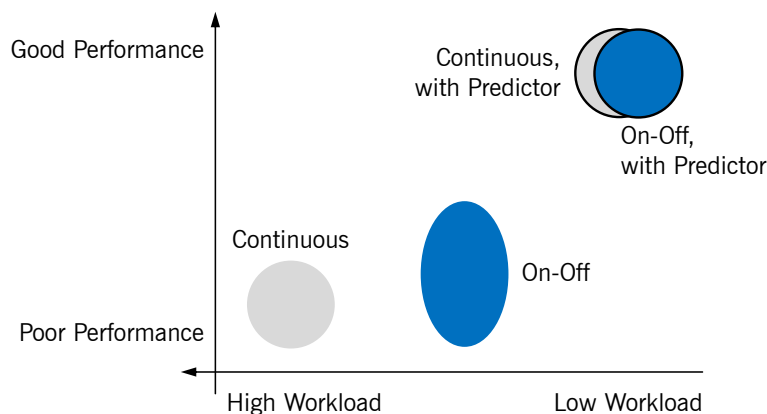


Figure 6.1 – Expected workload and performance for different configurations

6.2 Experimental Setup

6.2.1 Participants

A total of 18 unpaid volunteers participated in the experiments. All of them were male pilots, but they had very different backgrounds and experience. The detailed information on the subjects given in Table 6.1 reveals that large spectra were covered in terms of age, hours flown and type of flying experience. (Table 6.1 also lists the sequence of experimental runs. An explanation of this sequence follows in section 6.3.) Student pilots, glider pilots and private pilots participated as well as commercial pilots, an airline transport pilot, a former military pilot and an RPAS pilot. Among the airplanes flown by those pilots are gliders, light single- and multi-engine piston airplanes, light turbine airplanes, the Cessna Citation [59], the Bombardier Challenger [59], the Airbus A320 [59], the Boeing 737 [59], the PA-200 Tornado [137], a French version of the Hunter UAV [141], the SIDM UAV [11] and the Tracker UAV [142]. Note that hours flown in simulators are not included, mainly because this parameter is difficult to quantify, since even aviation enthusiasts usually do not log their flights in a desktop computer simulation. However, some subjects indicated that they had considerable simulator experience. This experience may have helped them in the experiments, especially if it covered aircraft augmented by digital flight control laws. Of the 18 subjects, 15 had never performed (flight) control with large time delays as defined in this thesis and were naïve to the move-and-wait strategy. The RPAS pilot obviously had some experience with time delays. Two other subjects had already participated in the preliminary experiments [118] and therefore not only knew about possible piloting strategies, but also about on-off control.

Figure 6.2 provides more insight into the distribution of age and experience across all subjects. Remember that in all box plots shown, data points outside 1.5 times the interquartile range are marked by a circle as outliers. Whiskers extend to the most extreme data value that is not an outlier. The mean value is designated by a cross symbol.

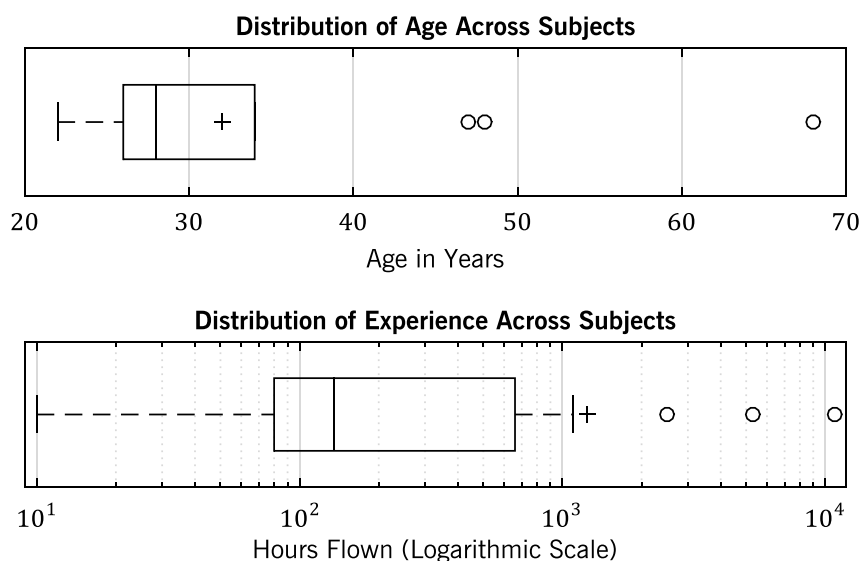


Figure 6.2 – Distribution of age and experience across all subjects

Table 6.1 – List of subjects and sequence of experimental runs

Subject	Age	Hours Flown	Status / Experience	Sequence of Experimental Runs															
				Ac	Ao	B4c	B2o	B1c	B3c	B1o	B3o	B2c	B4o	Cc	Co	Dc	Do		
1	26	105	Student pilot (airline)	Ac	Ao	B4c	B2o	B1c	B3c	B1o	B3o	B2c	B4o	Cc	Co	Dc	Do		
2	25	260	Airline pilot (Airbus A320)	Ao	Ac	B4o	B2c	B1o	B3o	B1c	B3c	B2o	B4c	Co	Cc	Do	Dc		
3	31	150	Former private pilot			B2c	B4o	B1c	B3o	B2o	B3c	B4c	B1o	Cc	Co	Dc	Do		
4	28	80	Private pilot			B2o	B4c	B1o	B3c	B2c	B3o	B4o	B1c	Co	Cc	Do	Dc		
5	34	1100	Former military pilot (PA-200 Tornado)	Ac	Ao	B1c	B3c	B2o	B4c	B3o	B4o	B2c	B1o	Cc	Co	Dc	Do		
6	22	80	Private pilot	Ao	Ac	B1o	B3o	B2c	B4o	B3c	B4c	B2o	B1c	Co	Cc	Do	Dc		
7	26	11	Student pilot (private)	Ac	Ao	B2c	B4o	B3o	B1c	B2o	B3c	B4c	B1o	Cc	Co	Dc	Do		
8	26	70	Private pilot	Ao	Ac	B2o	B4c	B3c	B1o	B2c	B3o	B4o	B1c	Co	Cc	Do	Dc		
9	68	5300	Commercial pilot (piston and turbine)	Ac	Ao	B2c	B4o	B1o	B3c	B4c	B2o	B1c	B3o	Cc	Co	Dc	Do		
10	28	660	Glider pilot	Ao	Ac	B2o	B4c	B1c	B3o	B4o	B2c	B1o	B3c	Co	Cc	Do	Dc		
11	25	120	Student pilot (airline)	Ac	Ao	B1c	B3o	B4c	B3c	B1o	B2c	B4o	B2o	Cc	Co	Dc	Do		
12	25	98	Student pilot (airline)	Ao	Ac	B1o	B3c	B4o	B3o	B1c	B2o	B4c	B2c	Co	Cc	Do	Dc		
13	28	2500	Commercial pilot (B. Challenger)	Ac	Ao	B3c	B1o	B2o	B4c	B3o	B1c	B2c	B4o	Cc	Co	Dc	Do		
14	26	400	Student pilot (airline)	Ao	Ac	B3o	B1c	B2c	B4o	B3c	B1o	B2o	B4c	Co	Cc	Do	Dc		
15	47	10860	Former airline pilot (Boeing 737)	Ac	Ao	B3c	B2o	B4c	B1c	B4o	B2c	B3o	B1o	Cc	Co	Dc	Do		
16	30	120	Private pilot	Ao	Ac	B3o	B2c	B4o	B1o	B4c	B2o	B3c	B1c	Co	Cc	Do	Dc		
17	48	400	RPAS pilot (F. Hunter, SIDM, Tracker)	Ac	Ao	B3c	B1o	B4c	B2c	B4o	B2o	B1c	B3o	Cc	Co	Dc	Do		
18	34	10	Student pilot (glider)	Ao	Ac	B3o	B1c	B4o	B2o	B4c	B2c	B1o	B3c	Co	Cc	Do	Dc		

It can be seen that although most subjects were rather young and had little experience in real airplanes, most of the relevant spectrum of ages and hours flown was covered. Hence, ratings and opinions could be gathered from many types of pilots. However, since some pilot types were represented by a single person only, it is not advisable to compare the ratings or the performance of those different types of pilots. Instead, the whole sample of pilots was analyzed as a whole. From a statistical point of view, the sample size of 18 is small. When compared to the number of pilots in other handling qualities studies, however, it is relatively high. For instance, Hodgkinson mentions a minimum of three evaluation pilots and an optimum of seven [79]. Evaluation pilots in that case are test pilots who are trained for control system evaluation. Those pilots would use the long established CHR scale in the evaluation process. Due to their training and their experience, they would produce rather consistent ratings. Instead of relying on test pilots, the experiments described here had to make do with a sample of professional and leisure pilots who were neither trained to evaluate control systems, nor to apply the CHR scale. This was addressed by inviting a larger number of subjects and also by other decisions on experiment design, as the following sections show.

6.2.2 Flight Simulator and Inceptor

The experiments on manual remote flight control required a simulation model of the Diamond DA42 plus flight controller and an inceptor with the characteristics described in section 4.3.1. A cockpit was not required, so the experiments could have taken place on a regular desktop computer. However, the desired inceptor characteristics were achieved with an active sidestick mounted in the cockpit of the so-called Research Flight Simulator at TUM's Institute of Flight System Dynamics, and since any simulation model can be used in this simulator, the decision was made to conduct the experiments there.

Since most of the simulator elements have been custom-built by institute staff and students, it is highly customizable. Its cockpit resembles that of a large transport airplane with two seats side by side and sidesticks on the outboard side of each seat. Four large screens inside the cockpit show customizable displays and a 180° EVS had been implemented. To imitate the restricted field of view common to RPAS, two of the three projectors of the EVS were turned off. The remaining projection showed the forward view from the aircraft with a field of view of approximately 50° by 50°. To implement a head-up-display (HUD), an additional projector was installed between the cockpit and the cylindrical projection screen. Due to the small distance between the screen and this projector, it produced a rather small landscape format projection of approximately 10° by 18°, as seen by the pilot. The projector itself could not be seen from the pilot's station. Figure 6.3 shows a sketch of the simulator setup.

The sidestick characteristics for on-off control are described in section 4.3.1 of this thesis. For continuous control, the default force gradients of 2 N/° laterally and 3.336 N/° longitudinally were used. With a limit deflection of 10.5° in both axes, the resulting maximum control forces were 21 N in the lateral axis and 35.03 N in the longitudinal axis. Throughout the experiments, control sensitivity of the continuous control system was 2.5 times as high as the control sensitivity of the on-off control system. Thus, the continuous control system gave pilots the possibility to produce both smaller and larger aircraft

reactions as compared to the fixed amplitude of the on-off control system. With both the control sensitivity and the control forces higher for the continuous control system than for the on-off control system, the same force applied to either control system resulted in a similar airplane reaction.

In preliminary tests with this setup for continuous control, it was found that inaccuracies in the force applied by hand to the inceptor together with the time delay led to large disturbances in the airplane's reactions. For instance, if during a lateral control input the stick was inadvertently also slightly pushed or pulled, a longitudinal reaction would follow. The pilot would recognize his involuntary control input only after the large time delay and by then, the disturbance would have grown considerably. To prevent this type of disturbance, the deadzone in both axes was successively increased until the effect did not occur anymore. The detrimental effect of deadzones on handling qualities is known [143], but it was deemed much less critical in the case of systems with large time delays and the pulse-like control behavior associated with it.

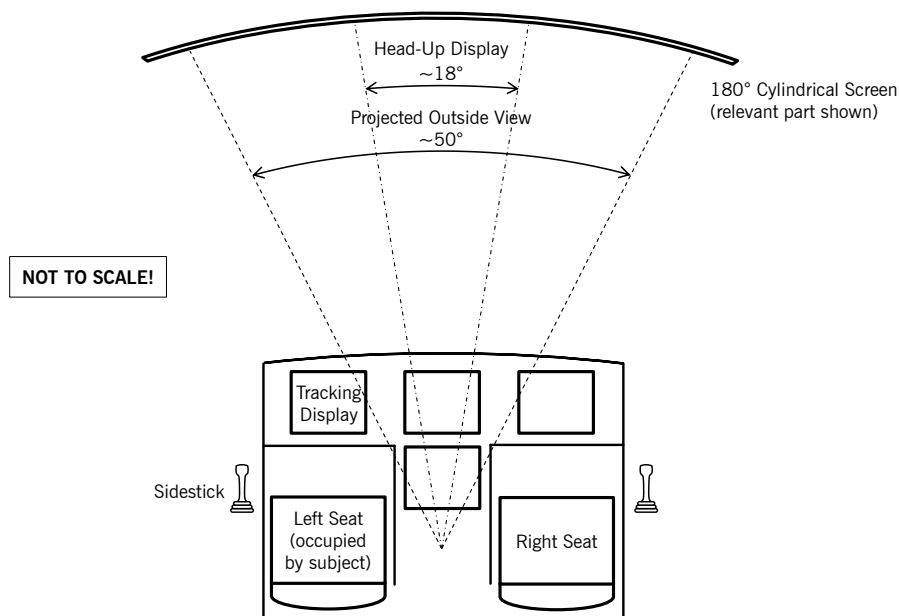


Figure 6.3 – Cockpit of the Research Flight Simulator as set up for the experiments

6.2.3 Displays

Only visual displays were used in the experiments on manual remote flight control. EVS and HUD were active only during tasks B, C and D. During those tasks, all screens inside the cockpit were turned off or covered. During task A, a single screen in front of the pilot showed a tracking display, which is depicted in Figure 6.4. For better readability on printed paper, black and white colors have been inverted in this figure. The cross in the background was provided for orientation. The green ball represented the tracking target, which had to be acquired with the airplane symbol. A tracking score was indicated by the height of the large, vertical bars on each side of the display. The contour of their maximum size is shown in white (black in Figure 6.4). Tracking performance was indicated by the color of the airplane symbol and the two bars. Red color indicated a large tracking error, i.e., offset between airplane symbol and target ball. Yellow color indicated a small but still excessive error and green color indicated a negligibly small error.

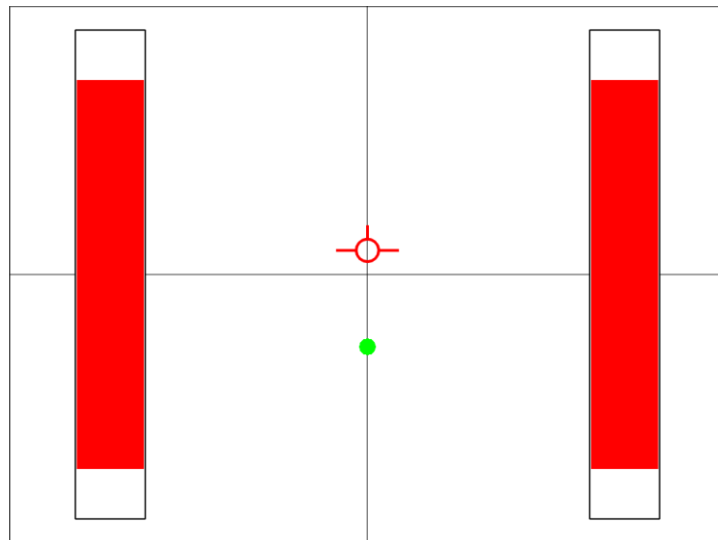


Figure 6.4 – Tracking display (black and white colors inverted)

During tasks B, C and D, a HUD was shown whose appearance differed between the tasks, although some elements remained the same. Figure 6.5 shows the configuration for task B. For the sake of readability on printed paper, the background is white and all HUD elements are drawn in black here, whereas in the actual HUD all symbols were lime-green, with high contrast against the simulated outside view.

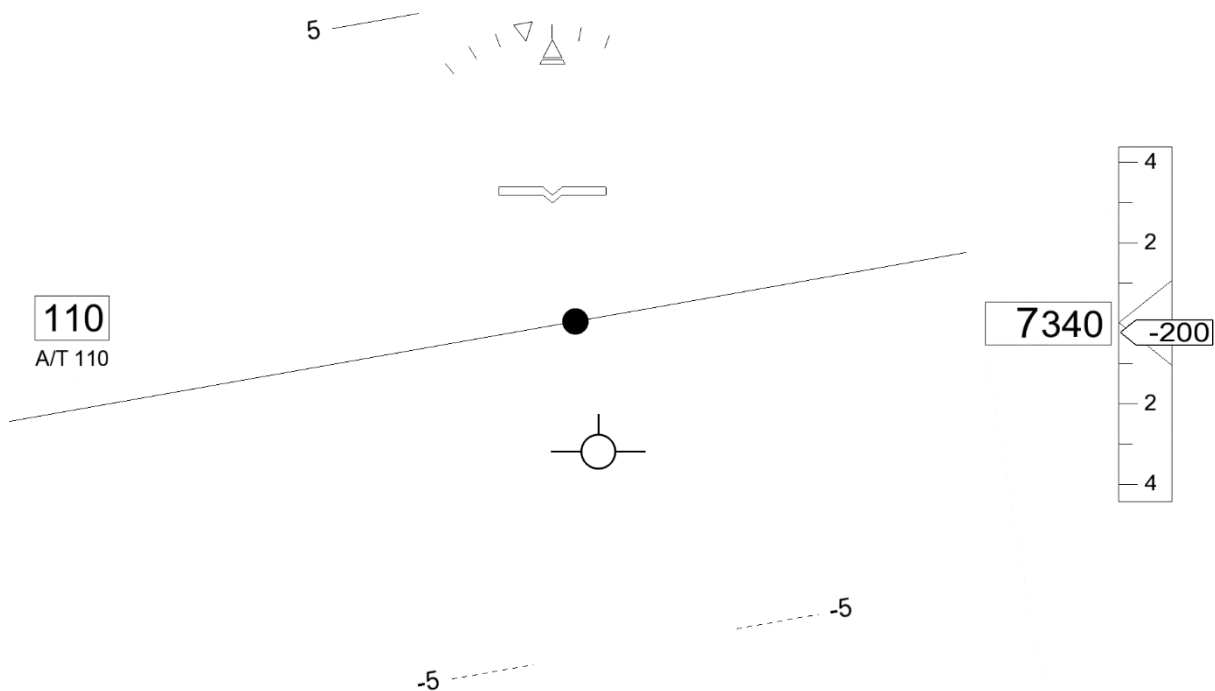


Figure 6.5 – HUD with tracking target (no background shown)

Both the target ball and the airplane symbol from the tracking display (Figure 6.4) can be found again on the HUD. Here, they represent target/current flight path climb angle. Some other elements are similar to the display of the experiments on BMI control (Figure 5.4). In the background, a horizon line and a pitch/climb angle scale with marks at each 5° can be seen. The horizontal bar with a bend represents the airplane's nose and indicates the

pitch angle. The curved scale on top shows 5° , 10° and 15° bank angle. The bar below the bank angle indicator indicates lateral acceleration. Altitude and vertical speed are shown on the right and airspeed and autothrottle target speed are shown on the left. If the HUD appeared as in Figure 6.5, the airplane was in a coordinated 5° banked right turn with a pitch angle of 2° , descending at -2° and -200 ft/min through an altitude of 7340 ft above mean sea level. The autothrottle held 110 kt indicated airspeed and the target flight path climb angle was 0° .

Figure 6.6 shows the HUD as it appeared in tasks C and D. A first thing to notice is that the target ball is not shown. A compass rose is introduced instead, with a heading indication inside. An arc along the compass rose's circumference indicates the current turn rate. Two large radial marks intersect this arc at the standard turn rate. The triangle inside the compass rose indicates the target heading, whereas the current heading can be read beneath the outside triangle on top of the compass rose. The target altitude is shown in a bracket next to the altitude indication. The bracket moves so that it aligned with the top/bottom end of the vertical speed strip when the airplane is below/above the target altitude by 500 ft or more. When current altitude equals target altitude, the bracket embraces the altitude indication box and the target altitude reading disappears behind.

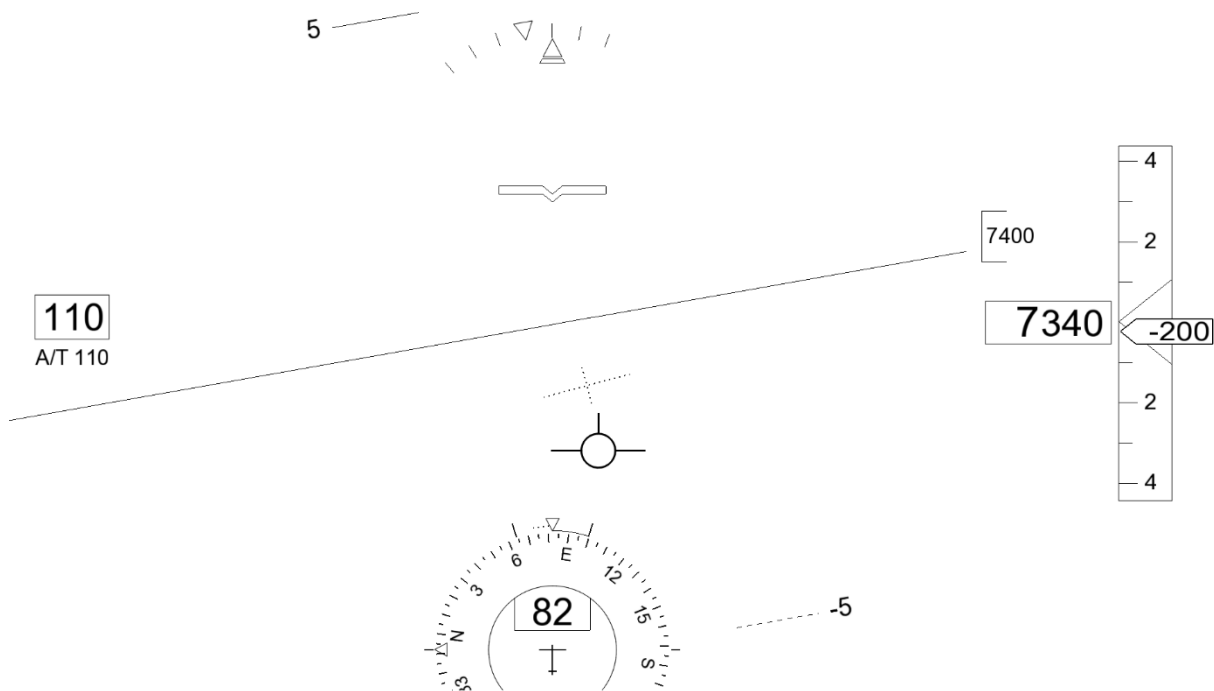


Figure 6.6 – HUD with compass rose, target altitude, target heading and predictors

The two dotted symbols were only shown during task D. They are predictors of flight path climb angle, bank angle and turn rate. The dotted cross can be understood as predicted position and tilt of the airplane symbol. It thereby indicates future flight path climb angle and future bank angle. The dotted arc around the compass rose corresponds to the predicted turn rate. The HUD as shown in Figure 6.6 indicates a target altitude of 7400 ft and a target heading of 352° . Current heading is 82° and current turn rate is $3^\circ/\text{s}$ (standard turn rate) to the right. Predicted flight path climb angle is -1° , predicted bank angle is -2.5° (i.e., to the left) and predicted turn rate is $-1.5^\circ/\text{s}$ (i.e., to the left).

To give an impression of the visual environment during the experiments, Figure 6.7 shows a photo taken from the position where subjects sat in the Research Flight Simulator. In this photo, the EVS is active and the HUD is in the configuration of task C. Note that the HUD was well readable, even though in the photo its size may seem small and its content blurry. At the lower left end of the photo, the upper half of the display used during task A can be seen.



Figure 6.7 – Photo illustrating the visual cues during task C

6.2.4 Data Collection

During the experiments, all relevant states of the simulation model were logged, along with inceptor deflections and all task-related variables, such as target altitudes. Subjects were given an experiment handbook (cf. appendix B) that contained instructions, questionnaires and rating scales. This handbook was given out in four parts (pages 1-7, 8-17, 18-21 and 22-26) to ensure that subjects

- would not browse the entire handbook at an early stage of the session and thereby obtain information from later sections that would facilitate or otherwise influence their performance in earlier tasks of the experiment,
- had a clear understanding of the current task and not get confused by future tasks,
- filled out the correct rating scales and questionnaires.

The questionnaires and rating scales aimed at capturing subjective pilot opinions. A few open questions had to be answered in the form of written free text. Other questionnaires had the formalized form of binary checkboxes or of discrete scales. In addition to that, the task load index (TLX) developed by NASA [144] was used as a metric for subjective pilot workload. Like in the experiments on BMI controlled flight described in chapter 5, the commonly used CHR scale was considered unsuitable. First, flight control with large time delays would always produce inadequate handling qualities as defined on the CHR scale. Hence, only a small range of CHRs could effectively be used, thus reducing possible differences between the examined configurations and hindering quantitative comparison. Second, the subjects were pilots but not test pilots and therefore only familiar with a very limited number of airplanes and normally completely unfamiliar with the CHR scale and its application. As a result, CHR ratings could be invalid [70]. The TLX, on the other hand, can be applied in a variety of situations by unprepared subjects. The TLX manual advises, however, to let subjects practice using the rating scale with a few tasks [145].

The English version of the experiment handbook, which also contained the original, English version of the TLX, was given to the only French subject (no. 17), who also fluently spoke English. All other subjects were German and were provided with a German version of the handbook that also contained a translation of the TLX, which was based on that given in [146]. Unfortunately, thorough literature research did not confirm the statements found in some sources, saying that this translation has been validated. (The TLX itself, of course, is validated.) The questionnaires and rating scales were filled out immediately after completion of a run, usually inside the cockpit and sometimes, for example between tasks, on a desk next to it. Finally, oral comments of the subjects and any exceptionalities were documented in an experiment log.

6.3 Tasks and Briefing

The primary aim of task design was to enable an investigation that helps to ultimately confirm or disprove the hypotheses from section 6.1. Moreover, several other aspects, such as the influence of control sensitivity, were chosen to be investigated, so corresponding tasks or task elements had to be added. All in all, four tasks were set up for this purpose, which covered different situations from laboratory-type tracking to operational flight maneuvers. In all these tasks, a constant time delay $\tau_d = 2\text{ s}$ was introduced between the simulation model and the visualization on the displays and the EVS to simulate the overall time delay inherent to the controlled system.

To gain insights into the initial learning phase, subjects had to be naïve with respect to possible piloting strategies in the first task. With the subjects initially naïve, a very poor performance was expected at the beginning of the experiment. Therefore, it was decided to start off with a simple integrator as controlled system, which is known to be easily controllable, at least without delay. The display, too, was kept simple (cf. section 6.2.3 and Figure 6.4). After task A, all subjects were briefed about the move-and-wait strategy, even if they had naturally applied it themselves until then. Next, task B confronted the subjects with the longitudinal dynamics of the augmented airplane, which can be described as integrator-like with lags. They had to perform flight path tracking with

different control sensitivities. EVS and HUD provided an already more complex visual feedback. A break after task B allowed subjects to take a brief rest. Then, task C put them into an operational setting with target altitudes, headings and tracks, thereby introducing two-axis control and increasing the order of the controlled system in each axis to a double-integrator and, in the case of ground track following, even a triple-integrator. Finally, task D repeated task C, but subjects were provided with predictor symbols on the HUD. None of the previous tasks featured these predictor symbols as not to reduce the apparent time delay. Moreover, the effect of the predictor symbols can thus be investigated by comparing tasks C and D.

The sequence of experimental runs for each subject can be seen in Table 6.1, where each run is represented either by two letters or by two letters and a number. The first letter of each run indicates the task. The last letter is either “c” for continuous control or “o” for on-off control. Since task B was flown with different control sensitivities, an additional number indicates the sensitivity level in this case. Tasks A, C and D were each flown once with every type of control system. Counterbalancing between subjects was therefore straightforward: half of them started with the continuous control system whereas the other half started with the on-off control system. Task B had to be flown once with each of the eight possible combinations of control sensitivity level and control system type. Runs were counterbalanced between subjects such that the order was random, under the conditions that the same control sensitivity level would not appear twice in a row and that the control system type would change after each one or two runs. Moreover, the last run of task A and the first run of task B as well as the last run of task B and the first run of task C were chosen to differ in control system type. In total, a session took between 2 and 2.5 hours, depending on how long subjects took to fill out the questionnaires and on how long they chose the break to be. Beverages and snacks were available throughout the session.

6.3.1 Task A – Generic Tracking

The aim of this first task was to confront subjects with the unfamiliar situation of flight control with large time delays to be able to investigate how they would react to this initial exposure. In fact, this situation is quite similar to that of a UAV operator who usually only observes the highly autonomous system and who, due to an unforeseen event, has to suddenly take over manual control. In this situation, the operator is not well accustomed to flight control with large time delays and likely experiences high stress. Implementing a realistic, operational task, however, would necessarily be more complex from the subjects' point of view and would nonetheless not generate nearly as much stress as the actual real-life operation. Instead, a generic task was implemented and gamified to incite the subjects and generate stress. Prior to performing their first run, subjects received no instructions on suitable piloting strategies, but were only introduced to the task and instructed about a constant time delay in the order of seconds (cf. appendix B). As Table 6.1 shows, half of the subjects started with continuous control, whereas the other half began with using the on-off control system.

The task was to align airplane symbol and target ball shown on the tracking display (cf. Figure 6.4). Only this display was shown, while EVS and HUD were turned off during this task. The transfer function between sidestick inputs and the airplane symbol was a simple

integrator. Such a system would be easily controllable without time delay. Control sensitivity K_a was chosen so that a constant input with the on-off control system would move the airplane symbol from one end of the screen to the other end in 6.667 s. As mentioned in section 6.2.2, control sensitivity was 2.5 times as high with the continuous control system. Thus, with a maximum control input amplitude applied to the continuous control system, the same maneuver would take 2.667 s. When describing control sensitivity in units of half-screen size (*HSS*) per second, it would be $K_a = 0.3 \text{ HSS/s}$ for on-off control and $K_a = 0.75 \text{ HSS/s}$ for continuous control. To prepare the subjects for the following tasks, they were told that the airplane symbol behaved like the flight path of a real airplane at high speeds: with the display appearing as in Figure 6.4, they had to push the sidestick forward to make the airplane symbol move downwards on the screen.

Table 6.2 – List of task A tracking target steps

Step No.	Δu [<i>HSS</i>]	Step No.	Δu [<i>HSS</i>]	Step No.	Δu [<i>HSS</i>]	Step No.	Δu [<i>HSS</i>]
1	+0.8	6	+1.0	11	+0.3	16	-0.9
2	-0.7	7	-1.6	12	-0.5	17	-0.1
3	-1.0	8	+0.7	13	+0.9	18	+0.3
4	+1.6	9	+0.6	14	-0.4	19	+0.4
5	-0.8	10	-0.6	15	+0.5	20	+0.1
Step sizes constrained, cf. equation (6.2)				Step sizes not constrained			

During the run, the target ball jumped to different positions on the vertical axis and waited there until the airplane symbol followed before jumping anew. When the tracking error was negligibly small, as defined by equation (6.1) and as indicated to the subjects by the green color of airplane symbol and score bars, no further correction was required and after 5 s, the target ball jumped to the next position. The limit tolerance above which, according to equation (3.23), a limit cycle is unlikely, is 0.3 *HSS* in the case of on-off control and 0.75 *HSS* in the case of continuous control and full inceptor deflections. This means that PIOs can be expected unless the pilots introduce significant lead or make very cautious movements, i.e., short inputs with the on-off control system or small-amplitude inputs ($|\delta| < 0.067$ so that $\dot{y}_{ss} < 0.05 \text{ HSS}$) with the continuous control system.

$$e \leq e_{tol} = 0.05 \text{ HSS} \quad (6.1)$$

The target always followed the same, random-appearing sequence of steps given in Table 6.2. The size and number of upward (positive) and downward (negative) steps was the same. At the beginning of the task, the steps were large enough to allow the subjects to make and hold a control input until the airplane's delayed reaction could be perceived without risking to overshoot the target. In other words, they could initially perform closed-loop control. Equation (6.2) quantifies this step size constraint, where Δu is the target step amplitude, K_a the control sensitivity and τ_a the 2 s delay.

$$|\Delta u| \geq \tau_a \cdot K_a \quad (6.2)$$

Steps presented later in the task were not constrained. Indeed, small steps were introduced on purpose to force the subjects to terminate some of their control inputs before they could even perceive any reaction. While large steps (as defined by equation (6.2)) can be accomplished by estimating the future system state based on the current system behavior, the small steps force subjects to perform a very pure form of the move-and-wait strategy, where the estimation of the future system output can only be based on previous experience.

Subjects were told that they were given an initial score that would decrease as long as the error was excessive (yellow or red color). The score, which was represented by the height of the two bars, was depleted after 20 s of excessive error and topped up again at the beginning of each new target. The sole aim of this score was to generate stress.

Since the target waited for the pilot to follow, the duration of the task varied depending on the pilot's performance. The time to complete the task was therefore identified as a suitable measure of performance. The theoretical minimum completion time was 161.5 s for continuous control and 186.2 s for on-off control. The difference is due to the fact that full sidestick deflections with continuous control produced larger reactions than the fixed-amplitude outputs of the on-off control system. The theoretical minimum completion time is achieved when at each moment a new target is given, a full deflection control input is made immediately and for the exact duration that reduces the error not completely, but only just to the acceptable value e_{tol} .

6.3.2 Task B – Flight Path Tracking

Task B was designed to obtain insights into the effects of control sensitivity and to find out whether the initial choices of control sensitivity (cf. section 4.2.3) and of control forces (cf. section 4.3.1), fell in a suitable region. In this task, subjects controlled the DA42 simulation model, augmented with the flight controller proposed in chapter 4 of this thesis. Lateral command inputs were ignored, so that the airplane maintained straight flight while the subjects controlled the flight path climb angle γ only. Since the command variable of the longitudinal motion is $\dot{\gamma}$, the airplane symbol on the HUD behaved very similar to that on the tracking display of the previous task A. Instead of a simple integrator, however, the subjects had to control an integrator with some additional dynamics (mainly lags), which can be considered more challenging due to $\tau_{lags} > 0$. The tracking display was turned off, while HUD and EVS were shown instead.

Like task A, task B was a tracking task. This time, however, the target flight path, represented by the target ball, followed a predefined forcing function. In an approach similar to that presented in [70], the random-appearing Θ tracking sequence defined in [67] was low-pass filtered following equation (2.14) to obtain a suitable γ forcing function. The value for the low-pass filter time constant T_{θ_2} was derived from a linear model of the bare DA42 at the operating point that was also used for gains tuning of the controller (cf. section 4.2.3). Furthermore, the original Θ forcing function was extended by an initial singlet for familiarization and a plateau at the end. After preliminary tests had shown that the resulting forcing function was too fast to be followed with 2 s simulated delay, it was stretched to double the time span. Figure 6.8 shows original, extended and final forcing

function. It can be seen that the final forcing function also comprised shorter steps that provoked subjects not to wait for the system to settle after their control input, but to directly ensue with another input.

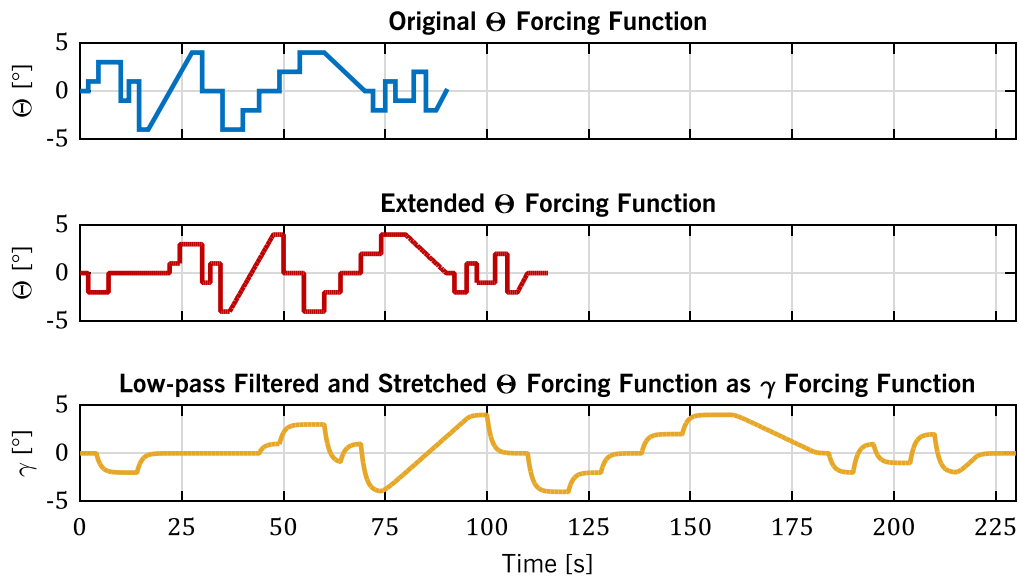


Figure 6.8 – Construction of the γ forcing function

Shortly after the initial singlet, manual control was inhibited and γ was automatically nulled. Upon the beginning of the actual tracking sequence that was used for evaluation, manual control was enabled again. (More exactly, control was inhibited between 24 s and 40 s into the task, so that subjects had 10 s to track each step of the initial singlet.) This way, the initial conditions for evaluation were identical for each subject and in each run. To prevent subjects from using landmarks in the simulated outside view to memorize the forcing function, the aircraft, which always departed from the same initial position, was set on a random heading for each run.

As discussed in section 4.2.3, the baseline sensitivity was chosen to be $2^\circ/s$, based on good engineering judgement. Here, this baseline value of the longitudinal control sensitivity applies to the on-off control system, whereas the sensitivity of the continuous control system is again 2.5 times as high (cf. section 6.2.2). In task B, four different, equally spaced levels of sensitivity were tested, which are listed in Table 6.3.

Table 6.3 – Control sensitivity levels in task B

Sensitivity Level	S1	S2	S3	S4
Longitudinal K_a with On-Off Control	$0.5^\circ/s$	$2^\circ/s$	$3.5^\circ/s$	$5^\circ/s$
Longitudinal K_a with Continuous Control	$1.25^\circ/s$	$5^\circ/s$	$8.75^\circ/s$	$12.5^\circ/s$

Sensitivity levels S1 and S4 constitute extremes that were included to produce a wide range of ratings and thereby facilitate subsequent analysis, as recommended in [79]. The altitude hold mode was permanently deactivated during task B, so that it could not interfere with target tracking. Limitations and protections, however, were armed to prevent

demotivating crashes and the associated reduction of data available for evaluation. They would only become active during extreme excursions from the target flight path.

6.3.3 Task C – Approach

After two laboratory-type tracking tasks, task C first placed subjects into an operational setting, namely a daylight approach to a large airport. This task again raised the level of difficulty, including higher-order tracking tasks in two axes. It also aimed at producing elevated pilot gains, requiring a swing-over maneuver during final approach in ground proximity. Simulated weather was fair, with no clouds, a visibility of 20 NM, no wind and light turbulences. These turbulences were simulated with a von Kármán spectrum as specified in [67]. The approach pattern is illustrated by Figure 6.9.

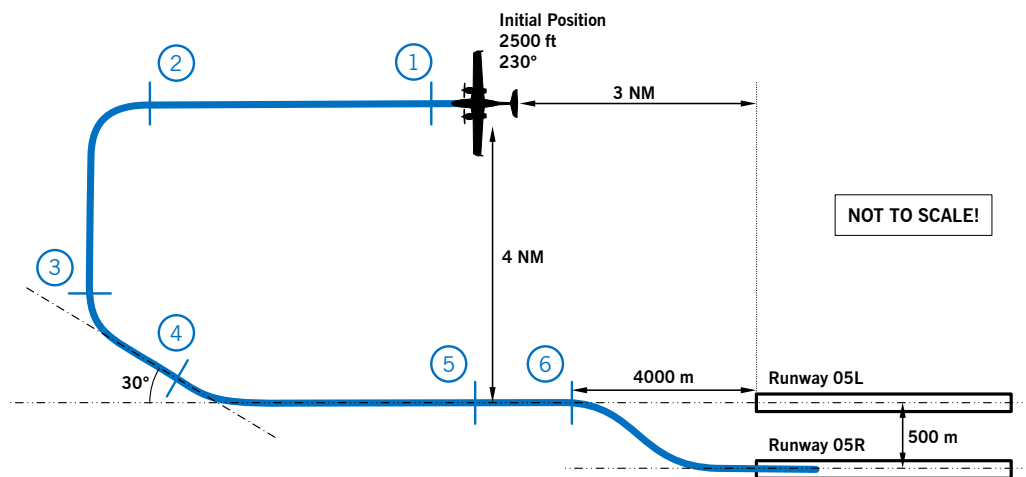


Figure 6.9 – Sketch of the approach flown in tasks C and D

At each of the positions 1 through 6, prerecorded announcements were played that specified new target parameters or maneuvers and thereby guided the pilots through the approach. Table 6.4 gives a definition of each position and lists the corresponding announcements. It can be seen that the maneuvers increased in difficulty throughout the task, so that for subjects with normal performance it would be easy in the beginning and slightly beyond their capabilities at the end. The first maneuver was a pure altitude change, followed by a pure heading change as second maneuver. In the first run of task C, this was the first time that each subject made lateral control inputs. At that moment, they had to transfer their experience from the longitudinal axis to the lateral axis. After that, a combined altitude and heading change was commanded. Next, the target heading was replaced by a target ground track, making horizontal tracking more difficult. The end of the approach was characterized by combined horizontal-vertical tracking and a swing-over maneuver that aimed at provoking high pilot gains.

Target altitude and heading were not only announced, but also shown on the HUD. Prior to their first approach, subjects were instructed to always maintain altitude between position 4 and 5 and to perform lateral guidance visually. At position 5, the heading target disappeared from the HUD and the ball, known from task B as target, fell through the display a couple of times before disappearing again. This meant to complement the announcement with a visual cue on the HUD, just like at all previous positions. Similarly,

the ball appeared again at position 6, flashing several times inside the airplane symbol before disappearing again. The simulation was stopped several meters above ground, if a considerable length of the runway had been overflowed or if a subject was not properly in control and therefore deviated extremely from the prescribed trajectory. Subjects were instructed to start a flare on short final, which should result in level flight slightly above the runway. It has to be stressed here that the aim of the task was not to demonstrate landing performance. Swing-over and short final approach were only means to provoke increases in pilot gains. Similarly, the simulated light turbulence was rather a stressor than an actual source for error, since the onboard flight control system countered most of the disturbances. In the case of glide slope, localizer and centerline tracking, however, the turbulence did cause minor errors that had to be corrected by the subject pilots.

Table 6.4 – List of positions and announcements during tasks C and D

Position	Definition	Announcement
1	15 s after beginning	Descend one thousand five hundred feet!
2	Less than 24° deviation from runway 05L localizer	Turn left heading one four zero!
3	Less than 9.9° deviation from runway 05L localizer	Turn left heading zero eight zero! Descend one thousand two hundred feet!
4	Less than 1.5° deviation from runway 05L localizer	Turn left, runway heading zero five three! Cleared visual approach runway zero five left!
5	Zero-crossing of runway 05L glide slope error	Start descent!
6	Less than 4000 m distance from runway 05L threshold	Swing over runway zero five right! Cleared to land runway zero five right!

In task C as well as in task D, the baseline control sensitivity defined in section 4.2.3 was used in both axes. Again, these baseline values of control sensitivity apply to the on-off control system, whereas the sensitivities of the continuous control system are 2.5 times as high (cf. section 6.2.2).

6.3.4 Task D – Approach with Predictors

The final task D was not an individual task in the strict sense, but a variation of task C. Subjects had to fly the same landing approach under the same conditions. The only difference was that two predictor symbols were introduced to the HUD (cf. section 6.2.3). These symbols indicated predicted values of γ , θ and $\dot{\chi}$. Instead of implementing a prediction algorithm for this task, the reference values of the corresponding flight controller loops were fed to the display. This perfect prediction was only possible because the time delay had been introduced artificially between simulation and visualization. Real predictors, on the other hand, necessarily exhibit some imperfections like transient movements caused by model updates. The configuration examined in task D must therefore be considered an ideal case, which is nevertheless suitable for investigating the general effect of predictors. This investigation can be done by comparing data from tasks

C and D. Given that task C always preceded task D, any difference between the two is partly due to learning. At this final stage of the experimental session, the effect of learning was expected to be minor as compared to the effect of the predictors. The deliberate decision to let pilots fly with predictors only during the final two runs was made because it was expected that after subjects had once experienced the highly beneficial effects of predictors, they would be biased against all other configurations in their opinion and possibly also in their performance.

6.4 Experiment Evaluation

For the following evaluations, the recorded simulation data was processed using MATLAB. The results from this data processing as well as all the questionnaire entries were entered into Microsoft Excel [147] sheets, where statistical analysis was performed. Statistical computations were verified and complemented using SPSS [148] or MATLAB. Table 6.5 lists all factors and factor levels defined for the statistical analysis of each task. With the exception of factor Group, which is a between-subject factor, all factors are within-subject factors. When an analysis of variance (ANOVA) was performed, data was positively checked for normality (Lilliefors-test [140]) and homoscedasticity (test according to O'Brien [149]), unless stated otherwise. As most factors have only two levels, sphericity is automatically satisfied. In task B, two estimates of sphericity were obtained: $\hat{\epsilon}_{GG}$ according to Greenhouse and Geisser [150] and $\hat{\epsilon}_{HF}$ according to Huynh and Feldt [151]. If $\hat{\epsilon}_{GG} < 0.75$, degrees of freedom were corrected by multiplication with $\hat{\epsilon}_{GG}$, whereas if $0.75 \leq \hat{\epsilon}_{GG} < 1$, the degrees of freedom were multiplied with $\hat{\epsilon}_{HF}$. All t-tests presented are one-sided, because the hypotheses from section 6.1 all specify a direction. In all box plots shown, data points outside 1.5 times the interquartile range are marked by a circle as outliers. Whiskers extend to the most extreme data value that is not an outlier and the mean value is designated by a cross symbol.

Table 6.5 – Factors and factor levels for statistical analysis

Task	Factor 1	Factor 1 Levels	Factor 2	Factor 2 Levels
A	Control System	<ul style="list-style-type: none"> ▪ Continuous ▪ On-off 	Group	<ul style="list-style-type: none"> ▪ First run: Ac ▪ First run: Ao
B	Control System	<ul style="list-style-type: none"> ▪ Continuous ▪ On-off 	Sensitivity	<ul style="list-style-type: none"> ▪ S1 ▪ S2 ▪ S3 ▪ S4
C and D	Control System	<ul style="list-style-type: none"> ▪ Continuous ▪ On-off 	Predictors	<ul style="list-style-type: none"> ▪ With predictors ▪ Without predictors

6.4.1 Initial Exposure and Learning

In task A, most subjects were confronted with the problem of flight control with large time delays for the first time. Thus, an analysis of the data gathered with this task should provide some insights into the pilots' behavior during initial exposure and the initial learning phase. Since subjects 3 and 4 already took part in preliminary simulator experiments on pulse-like control [118], they were excluded from task A here. Subject 17 was familiar with RPAS operations through large time delays, but it was uncertain whether he had already consciously employed pulse-like control inputs or the move-and-wait strategy. He therefore began with task A like all other subjects, who confirmed that they had no experience in flight control with large time delays. For the following analyses, the 16 subjects who completed task A need to be categorized into two groups of 8 subjects: those who started with the continuous control system and those who started with the on-off control system. This categorization ensures that the effects of the initially steep learning curve do not amplify or weaken any effects that the different control system types may have. This section first analyzes some global workload and performance metrics, then takes a detailed look at the subjects' behavior throughout task A and finally presents the pilots' subjective opinion and self-assessments.

The primary source of information about pilot workload is the TLX rating, which quantifies the pilots' subjective impression of workload. It would be useful, however, to back up this information by an objective measure. A suitable parameter for this purpose is control energy as defined by equation (6.3), where δ_i is a sample of the pilot's control input, t_s the sampling time and N the number of samples in a recording. Since two different control system types with different control sensitivities K_a are to be evaluated, it is necessary to include K_a into the equation as well. Moreover, the absolute value of δ appears here instead of its square as not to overly penalize large-amplitude inputs and thereby possibly the pulse-like control strategy.

$$E_{ctl} = K_a \cdot t_s \cdot \sum_{i=1}^N |\delta_i| \quad (6.3)$$

Every maneuver and every task require a certain minimum control energy, which can be created either by brief and large, or by prolonged and small control inputs. If pilots generate more control energy, they simply work more than they need to. This can happen when a tracking target is initially overshoot, when oscillations around the target occur or when large-amplitude maneuvers are chosen to complete the higher-order tracking tasks in parts C and D. In any case, a higher control energy indicates that pilots are physically, and therefore very likely also mentally more involved in the control task. In the case of on-off control, control energy is equivalent to control activity, since $|\delta| = 1$ whenever an input is made and 0 otherwise.

Box plots of TLX ratings and control energy are shown in Figure 6.10. Initially, the TLX ratings of the first two runs, i.e., of task A, were only meant to familiarize subjects with the rating scale. After data analysis, however, they were found to be worth mentioning,

even though the subjects' little experience with the TLX scale and also the learning process may have slightly distorted the results.

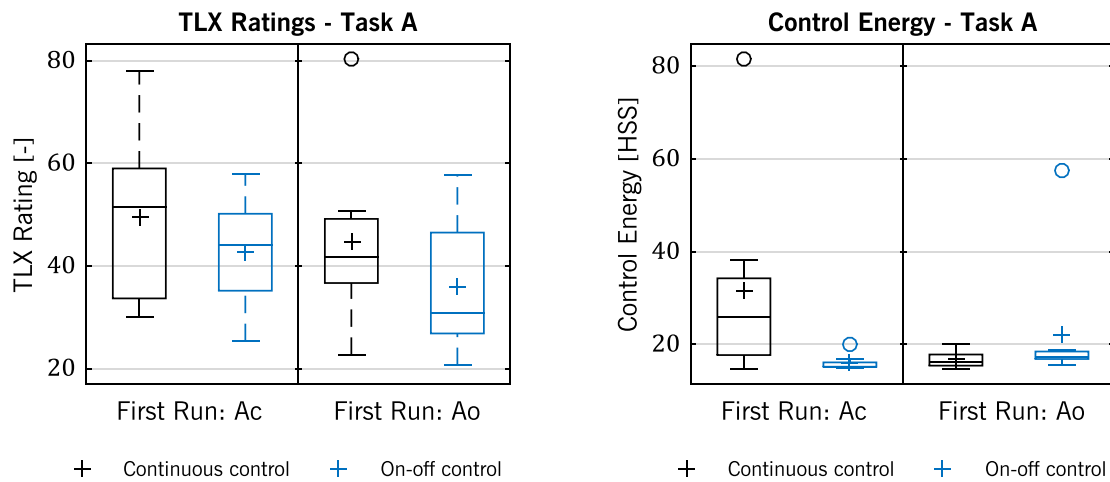


Figure 6.10 – Box plots of TLX ratings and control energy in task A

A mixed ANOVA was computed across the data of task A. Numerical results are given in Table 6.6. It can be seen that mean TLX ratings for the on-off control system are significantly lower than for the continuous control system. Rating differences between the two groups of subjects and the interaction Control System \times Group are not significant. Regarding control energy, it has to be noted that the data failed the Lilliefors-test for normality. Here, neither the differences between subject groups, nor those between control system types are significant. The interaction Control System \times Group, on the other hand, is significant. Figure 6.10 clearly indicates that those subjects who started the experiment with continuous control produced much less control energy in the second run, i.e., with on-off control, whereas the other subject group already started at a low level of control energy that did not decrease much in their second run. This is already a first indication for a steeper learning curve with on-off control, as compared to continuous control.

Table 6.6 – Quantitative statistical results for TLX ratings and control energy, task A

Factor	TLX Rating		Control Energy	
Control system	$F(1,14) = 6.427$	$p < 0.05$	$F(1,14) = 1.177$	$p = 0.2962$
Group	$F(1,14) = 0.7859$	$p = 0.3903$	$F(1,14) = 0.8207$	$p = 0.3803$
Control system \times Group	$F(1,14) = 0.1176$	$p = 0.7367$	$F(1,14) = 5.266$	$p < 0.05$

As mentioned in section 6.3.1, the subjects' performance in task A can be quantified by the time they required to complete the task. This time shall be called completion time. Since the theoretical minimum completion time differed between the control system types, completion time was also normalized, i.e., divided by the respective theoretical minimum. Box plots of both completion time and normalized completion time can be seen in Figure 6.11.

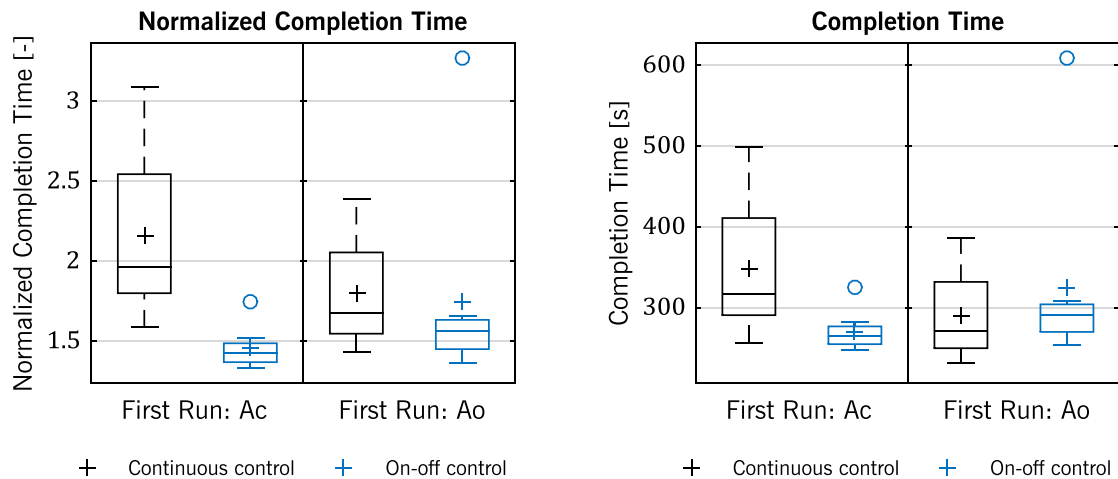


Figure 6.11 – Box plots of normalized completion time and completion time (task A)

In both cases, a mixed ANOVA was performed, even though the data was not normally distributed. Results are listed in Table 6.7. The difference in normalized completion time between continuous control and on-off control is highly significant. Moreover, there is a significant interaction between group and control system, whereas the difference between groups is not significant. Subsequent t-tests for each subject group individually showed that the improvement in normalized completion time of 0.8, i.e., 80 percentage points, within the group that started with continuous control is highly significant. Again, like the differences in control energy discussed above, this is a strong indicator in favor of the hypothesis that pilots learn quicker how to tackle the problem of time delays when using an on-off control system.

The analysis of normalized completion time shows that the on-off control system enables better performance in terms of target acquisition than the continuous control system and that it probably shortens the learning phase. However, this type of control system faces skepticism from pilots (cf. section 6.4.5), because it seems to restrict the airplane's maneuverability and to thereby decrease the maximum possible performance. Indeed, the maximum rate of movement of the airplane symbol (i.e., the control sensitivity) was lower and the minimum theoretical completion time was greater for the on-off control system. To find out what influence this restriction had, data from the (non-normalized) completion time are analyzed and compared to the results above. Interestingly, there is neither a significant difference between the control system types, nor between the groups. The interaction between group and control system, however, is significant. T-tests for each subject group individually indicate that only the reduction in completion time within the group that started with continuous control is significant. While mean normalized completion time has been reduced by 36% in this case, completion time dropped by only 22%. This means that the restriction in maneuverability introduced by the on-off control system is noticeable, but outweighed by the positive effects on workload and learning – at least in this initial phase.

Table 6.7 – Quantitative statistical results for (normalized) completion time in task A

Factor	Normalized Completion Time		Completion Time	
Control System	$F(1,14) = 9.271$	$p < 0.01$	$F(1,14) = 1.038$	$p = 0.3256$
Group	$F(1,14) = 0.03954$	$p = 0.8452$	$F(1,14) = 0.006425$	$p = 0.9372$
Control System × Group	$F(1,14) = 6.680$	$p < 0.05$	$F(1,14) = 6.549$	$p < 0.05$
Control System, First Run: Ac	$t(7) = 4.221$	$p < 0.01$	$t(7) = 2.974$	$p < 0.05$
Control System, First Run: Ao	$t(7) = 0.3089$	$p = 0.3832$	$t(7) = -0.9642$	$p = 0.8165$

In all three objective parameters – control energy, completion time and normalized completion time – it can be seen that the variance of the data points appears to be smaller for on-off control than for continuous control (cf. Figure 6.10 and Figure 6.11). Likewise, regarding each control system type individually, variance appears to be smaller when it is used in the second run. This indicates that the subjects' behavior and performance was generally more consistent with on-off control than with continuous control and that it got more consistent as they learned. The most consistent performance across subjects is observed in the case of on-off control as the second run.

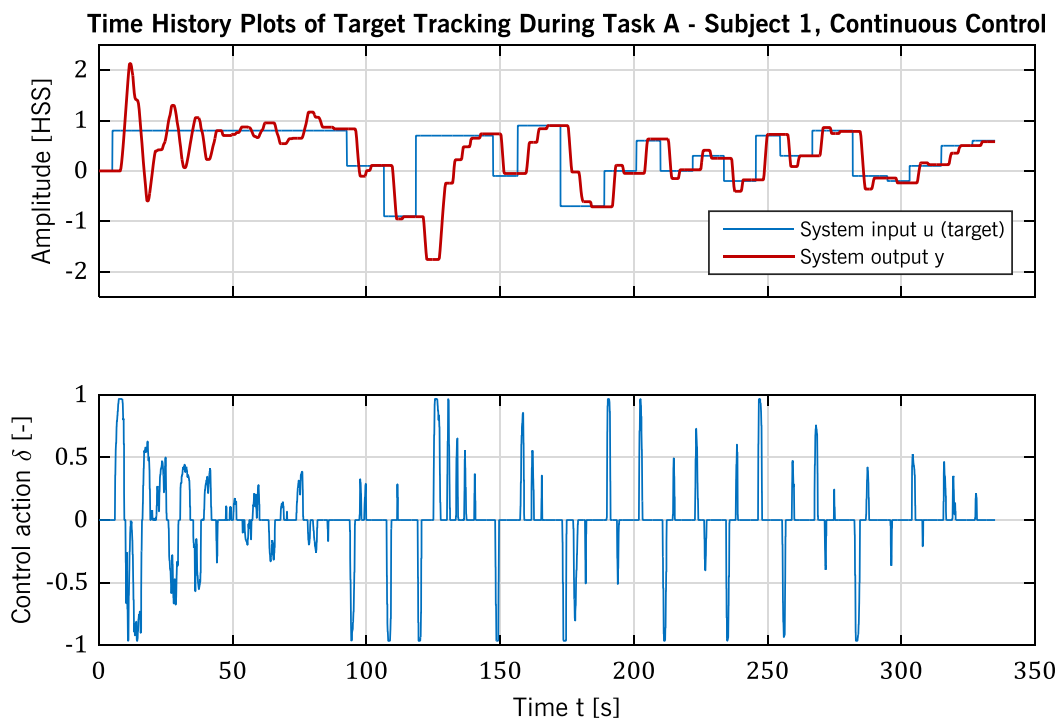


Figure 6.12 – Time history plots of run Ac, subject 1

After this global analysis of task A, which already revealed some interesting results, a more detailed look is now taken at the subjects' behavior throughout the task. Take for instance the time history plots of the first run of subject 1 (Ac, cf. Table 6.1), given in Figure 6.12. Using the continuous control system, the subject started off with a pronounced PIO, which

is evident from the 180° phase shift between sidestick input and system output. This was expected (cf. section 6.3.1). The period of the PIO amounts to approximately 10 s, which is slightly higher than the 8 s predicted by the compensatory pilot model without lead (cf. equation (3.26)). This difference is due to the fact that the amplitude of each single control input was not constant, but varied more or less drastically. The amplitude of the first PIO cycle is about 2.7 and thus slightly below the maximum of 3.0 predicted by equation (3.25). These observations indicate that subject 1 started off with a high pilot gain, high input aggressiveness and almost no lead. After about 50 s, however, he managed to stop the PIO. He then continued for a few seconds struggling to reach the target, but once he got this first one, he managed to reach the rest comparatively quickly and without much overshoots or oscillations.

The difference in performance between the first target and all other targets is due to a change in control strategy. This change is evidenced qualitatively by the appearance of control inputs in Figure 6.12, which start to become pulse-like at around $t = 95$ s. A quantitative measure for this change in strategy is the time between control inputs (TBI), which is depicted in Figure 6.13 for the same run.

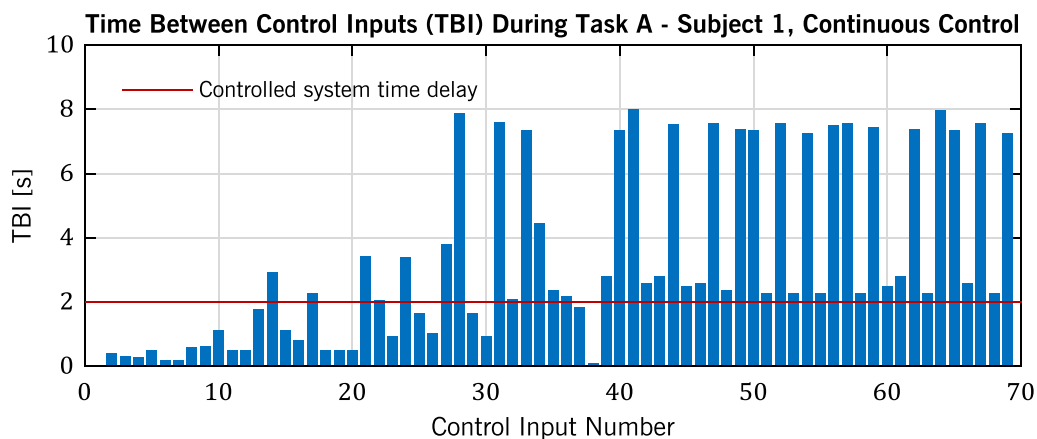


Figure 6.13 – TBI in run Ac, subject 1

The TBI is very low in the beginning of the run, indicating that the subject is moving the control stick almost continuously, without stopping at neutral for long. Then, the TBI gradually becomes longer until, after the 38th input, it is consistently greater than 2 s. In other words, the subject has adopted the move-and-wait strategy, with all wait phases at least as long as the time delay, which was 2 s in this experiment. Accompanying the move-and-wait strategy is an increase in control amplitudes. As described in section 3.2.2, these pulse-like inputs can be seen as an attempt to compensate for the increased time to reach the target caused by the wait phases.

The first run of subject 1 described above is characteristic for the initial behavior of most subjects. It occurred with both control system types, as the following example of subject 6 shows. Figure 6.14 shows time history plots of his first run, which he performed using the on-off control system. Again, the run starts with a PIO, whose period of approximately 12 s is larger than the predicted 8 s (cf. equation (3.26)) because control inputs were intermittent in the beginning. The initial PIO amplitude of about 1.1 is slightly below the maximum of 1.2 predicted by equation (3.25). Like subject 1, subject 6 seems to have

applied a high pilot gain and almost no lead in the beginning. After 2.5 cycles, however, the PIO is stopped and after a few more control inputs, a consistent and effective behavior is adopted.

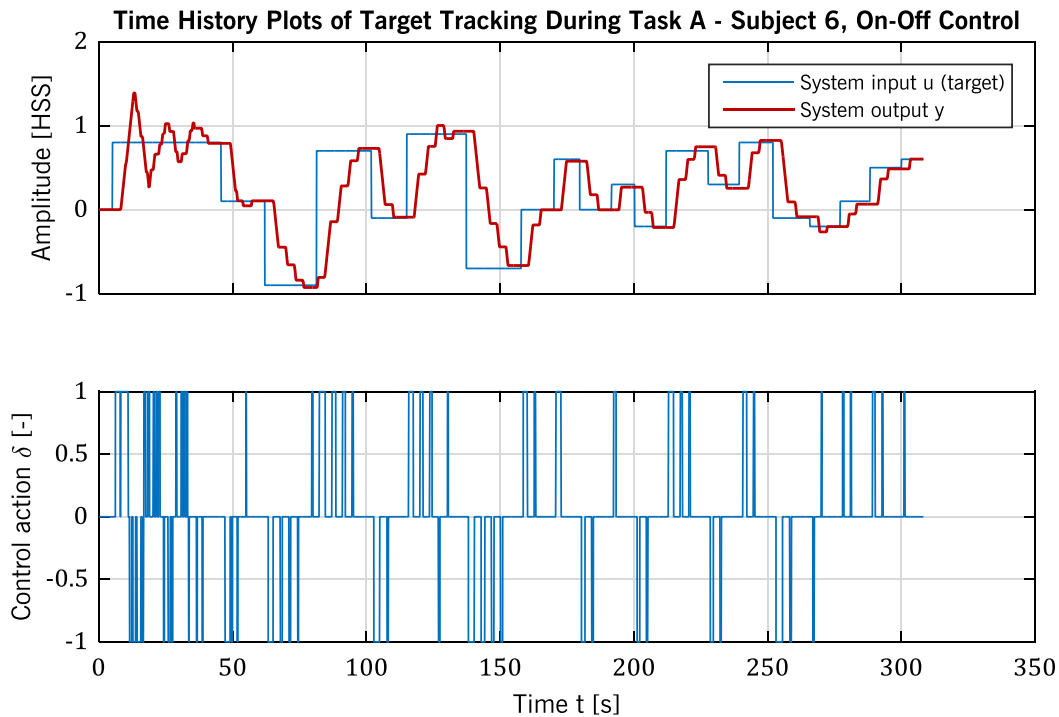


Figure 6.14 – Time history plots of run A₀, subject 6

Like in the case of the continuous control system, the strategy change is evidenced quantitatively by an increase in TBI (cf. Figure 6.15).

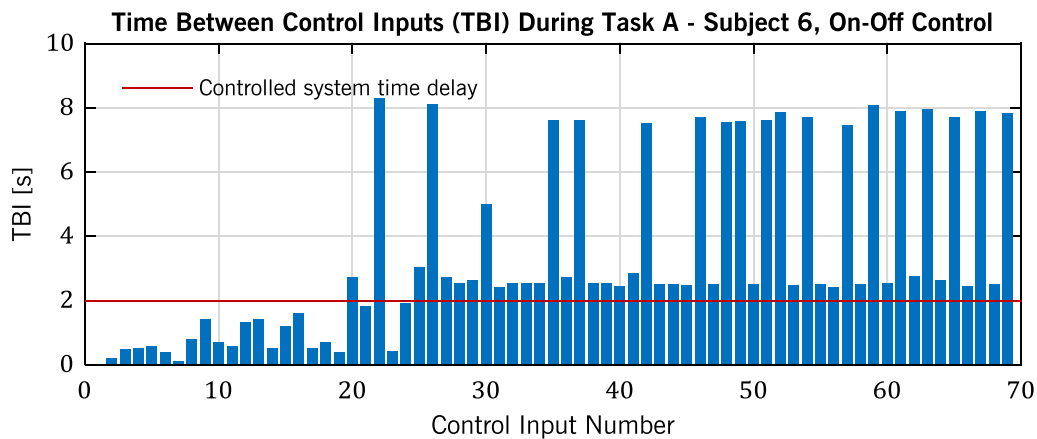


Figure 6.15 – TBI in run A₀, subject 6

Only few subjects started their first run with a suitable control strategy. Subject 7, for instance, began with cautious inputs to the continuous control system and with a high TBI, thereby successfully avoiding PIOs. After two targets, his inputs became pulse-like – again probably to accelerate the system response. Subject 18, who started with the on-off control system, also naturally employed the move-and-wait strategy right from the beginning. The third and final subject to start with a suitable control strategy was subject 17, who was familiar with RPAS control through time delay. It can be concluded that he

knew about the move-and-wait strategy. Since his first run was with the continuous control system, the effect of his prior knowledge about a suitable control strategy may attenuate the expected positive effect of the on-off control system. It is therefore possible to include subject 17 in the analysis without introducing a bias towards the hypotheses of section 6.1.

Some other subjects managed to adopt the move-and-wait strategy right after the first or second input. In the second run, almost all subjects used this strategy from the start. Another type of strategy change is noteworthy at this point. Some subjects deliberately made pulsed inputs of short duration and with equally short TBI at some time during task A. Subject 5, for example, briefly produced this kind of inputs, which can be seen in Figure 6.16 at around $t = 150$ s.

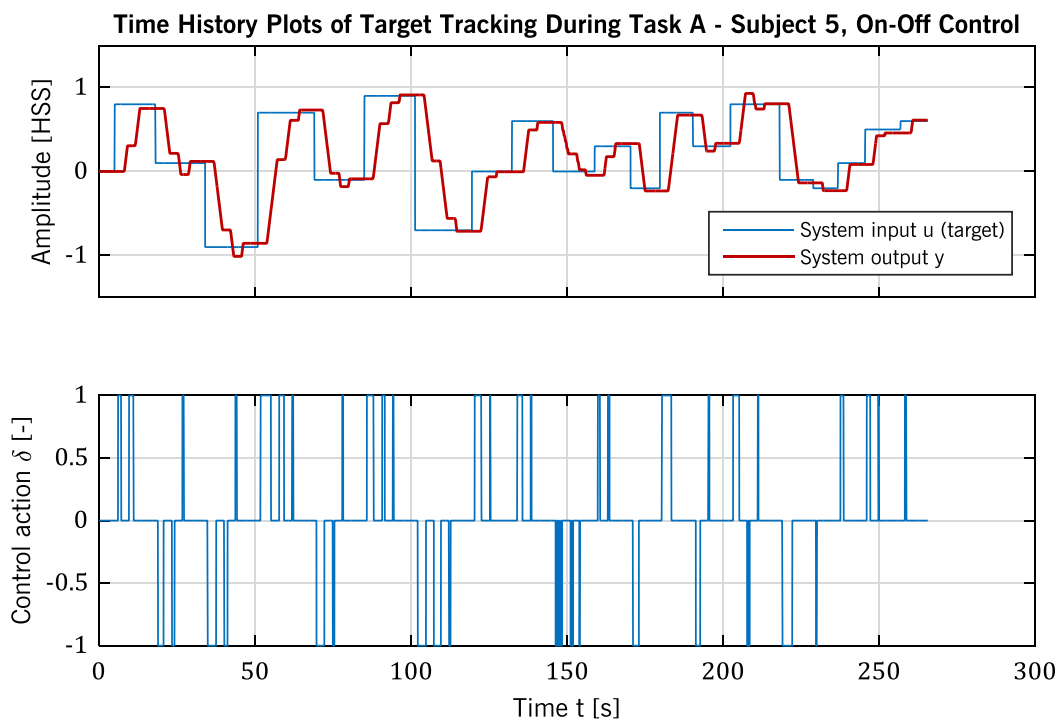


Figure 6.16 – Time history plots of run A_o, subject 5

Pulsed inputs have the advantage that the system reaction can be estimated by counting the pulses, which is still easier than estimating the duration of an input (cf. section 4.1). However, such inputs again increase the time required to reach a target, which is evidenced by the shallower slope of system output y following these inputs. Given that subject 5 returned to applying pulse-like inputs of variable duration, it seems that for him, this disadvantage of pulsed inputs outweighed the associated reduction of mental load. His strategy change can also be seen in the TBI plot of Figure 6.17, where the pulsed inputs can be recognized by the very small TBI value of multiple inputs in a row.

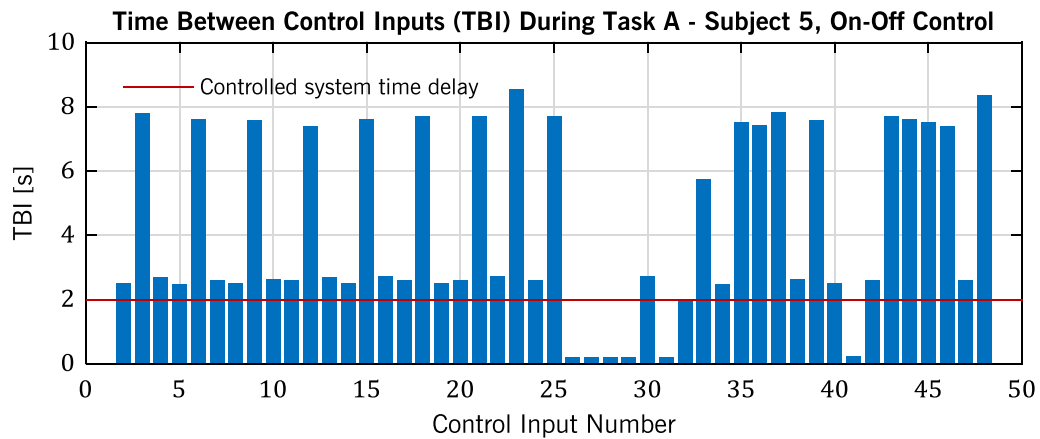


Figure 6.17 – TBI in run Ao, subject 5

All in all, pulsed control inputs were rarely employed and subjects always returned to pulse-like control. To test hypothesis 2, a quantitative criterion must be found that allows to find the time of the strategy change towards the move-and-wait strategy, associated with either pulse-like or pulsed control. A suitable assumption is that the move-and-wait strategy can be considered adopted when, for the first time in a run, 3 out of 4 consecutive TBIs are larger than 2 s. Note that this method does not work for subject 9, who started run Ao with pulsed inputs and thereby produced small TBI values at the beginning. In this case, the time until strategy change was manually corrected to 0. Figure 6.18 shows the resulting box plots of the time until strategy change.

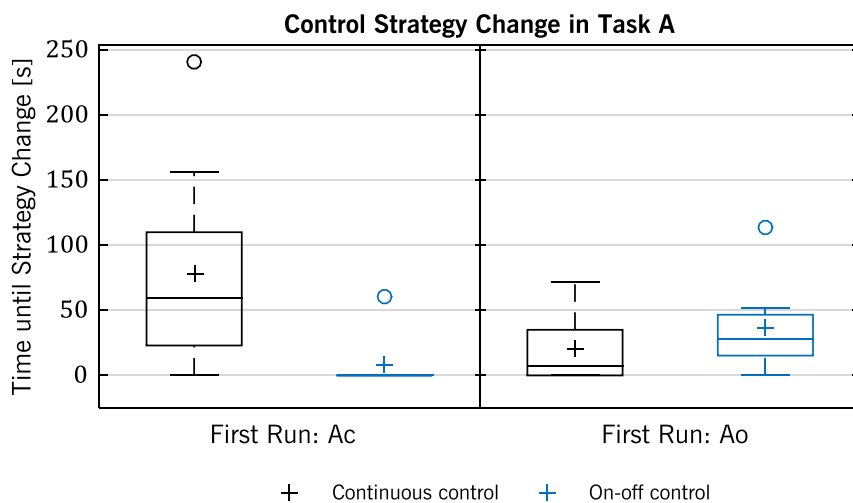


Figure 6.18 – Box plots of time until strategy change in task A

A mixed ANOVA was computed across the time until strategy change in task A. The data was not normally distributed, thus compromising the validity of the results shown in Table 6.8. The difference in mean time until strategy change between control system types is not significant, but there tends to be a noticeable difference between groups. The interaction Control System \times Group is strong. Together with Figure 6.18, this again indicates that an on-off control system expedites the subjects' learning process.

Table 6.8 – Quantitative statistical results for time until strategy change in task A

Factor	$F(1,14)$	p
Control System	0.5786	0.4595
Group	3.749	< 0.1
Control System × Group	10.05	< 0.01

The objective measures and the TLX ratings presented in the preceding part of this section can be complemented by pilot opinions to obtain a better insight into subjective aspects. Apart from the TLX scales, the experiment handbook therefore contained additional questions that were answered on scales or in the form of free text (cf. appendix B). After each run of task A, three questions addressed the familiarization with the time delay, the learning of a strategy to cope with it and the role of the control system in this strategy. Figure 6.19 shows the answers of all 16 subjects of task A to the first question. They indicate how the subjects themselves estimated the time they had needed to find a suitable control strategy. Interestingly, there are no clear distinctions between control system types or subject groups. In the group that started with the continuous control system, however, subjects tended to think that they found a strategy quicker with the on-off control system. Pilots generally estimated that they found a suitable strategy quite early in the run, probably because they had to find the strategy already to reach the first target and it still took them quite some time to reach all the other targets afterwards.

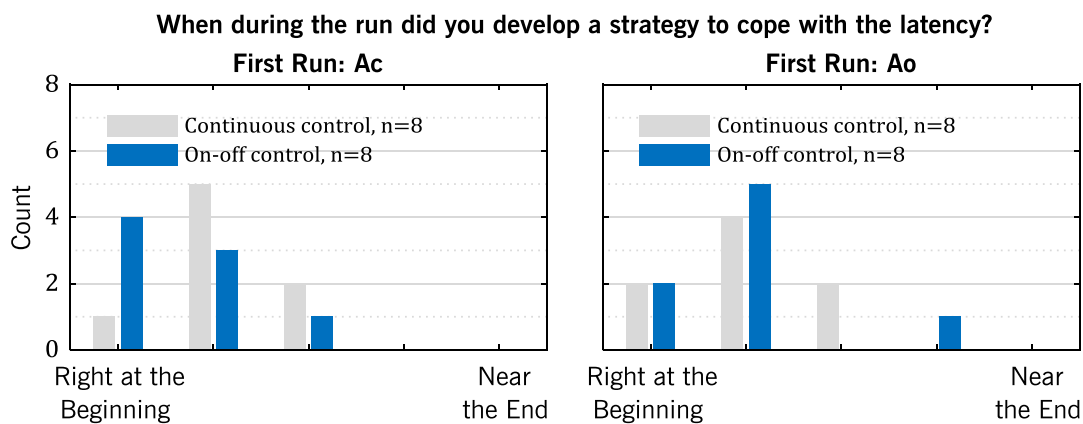


Figure 6.19 – Self-assessments on piloting strategy

It had already been expected that the answers to the first question might be somewhat unclear due to the many possible interpretations, which are partly induced by the decision not to brief the subjects on possible control strategies before or during task A. Therefore, another question tried to approach the same aspect from a different angle. Figure 6.20 shows how subjects estimated the time they had required to get accustomed to the amount of latency in the controlled system. Here, the result looks more like the data from the objective measures shown above. There seems to be no difference between control systems in the group of subjects who started with on-off control. Those subjects who started with continuous control, however, noted that they initially had trouble familiarizing

with the controlled system’s delay. This observation supports the objective findings presented above and thereby hypothesis 2.

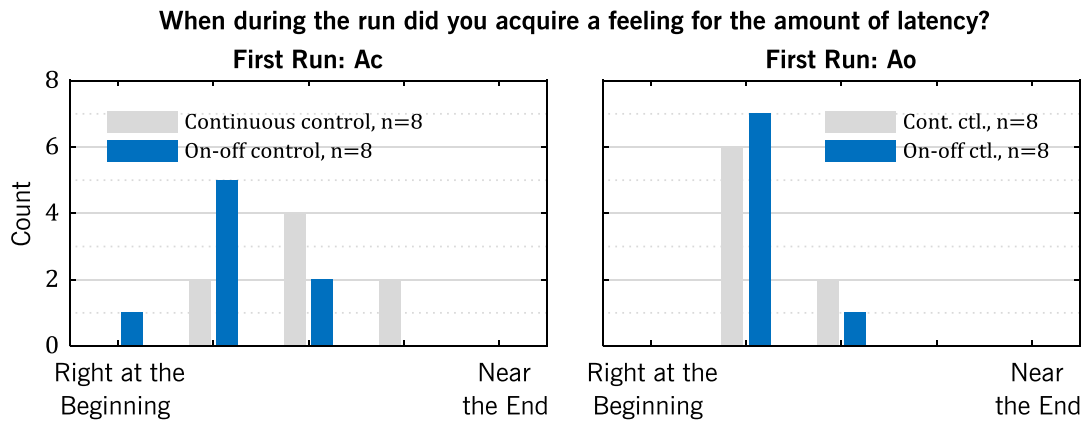


Figure 6.20 – Self-assessments on latency estimation

A third question directly asked the subjects whether they thought that the control system supported or hindered their control strategy. The results, shown in Figure 6.21, are unclear. This may again be due to various interpretations of the word “strategy”.

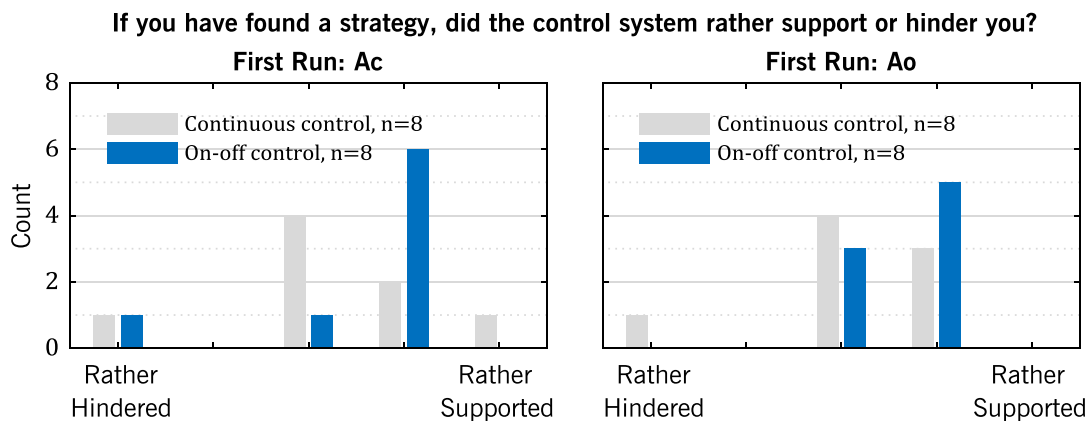


Figure 6.21 – Pilot ratings on control system support

All in all, taking into account the objective measures, the TLX ratings and the self-assessments, there is strong evidence that pilots naïve to flight control with large time delays find an appropriate control strategy quicker with an on-off control system than with a continuous control system. Hypothesis 2 can thus be confirmed. While the objective measures provide quite strong indications, the subjects’ own self-assessments on this matter is not as clear, but tends to support this finding.

6.4.2 Tracking and the Influence of Control Sensitivity

In this section, the analysis of task B reveals the tracking performance achievable with a time delay of 2 s. Moreover, differences between control system types and control sensitivity levels are exposed, thus providing insights into the suitability of on-off control and into the influence of control sensitivity on workload and performance. Ultimately, the choice of control sensitivity level S2 as baseline can thereby be evaluated. Task B was different from task A in that all subjects had some experience controlling a system with

large time delays and therefore knew about possible piloting strategies, most notably the move-and-wait strategy. This was also ensured by the debriefing of task A (cf. appendix B). Furthermore, counterbalancing of experimental runs (cf. section 6.3) mitigated the effects of learning. Thus, no distinction is made between groups of subjects in the following analyses.

First, Figure 6.22 shows the box plots of TLX ratings in task B. The boxes show how the subjects evaluated the workload experienced with each configuration.

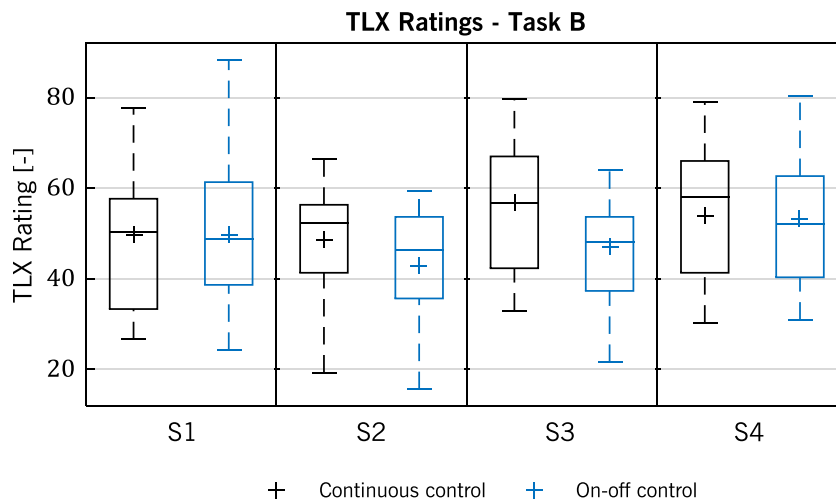


Figure 6.22 – Box plots of TLX ratings in task B

The results of a two-way repeated-measures ANOVA across this data, which are summarized in Table 6.9, indicate that TLX ratings were significantly smaller when subjects used the on-off control system. Looking at Figure 6.22, it can be seen that this is especially the case for sensitivity levels S2 and S3. The ANOVA furthermore indicates that there are significant differences in TLX ratings between sensitivity levels, whereas the interaction Control System \times Sensitivity is not significant. An evaluation of the contrasts of factor Sensitivity shows that TLX ratings of sensitivity level S2 were significantly lower than those of sensitivity levels S3 and S4. All in all, these results indicate that subjects experience less workload when using the on-off control system as compared to the continuous control system and that the sensitivity level S2 is preferable over all other levels in terms of workload.

Table 6.9 – Quantitative statistical results for TLX ratings in task B

Factor	F	p
Control System	$F(1,17) = 5.396$	< 0.05
Sensitivity	$F(2.100,35.70) = 5.116$	< 0.05
Control System \times Sensitivity	$F(2.649,45.03) = 2.002$	0.1338

Like in task A, the TLX ratings obtained can be complemented by the measure of control energy. Figure 6.23 shows the box plots of control energy in task B. Remember that,

according to equation (6.3), control sensitivity K_a is a factor in the computation of control energy. While K_a increased by a factor of 10 between sensitivity levels S1 and S4, the increase in control energy was less pronounced. This shows that subjects adapted their behavior to the control sensitivity, accelerating slow system responses and moderating fast system responses.

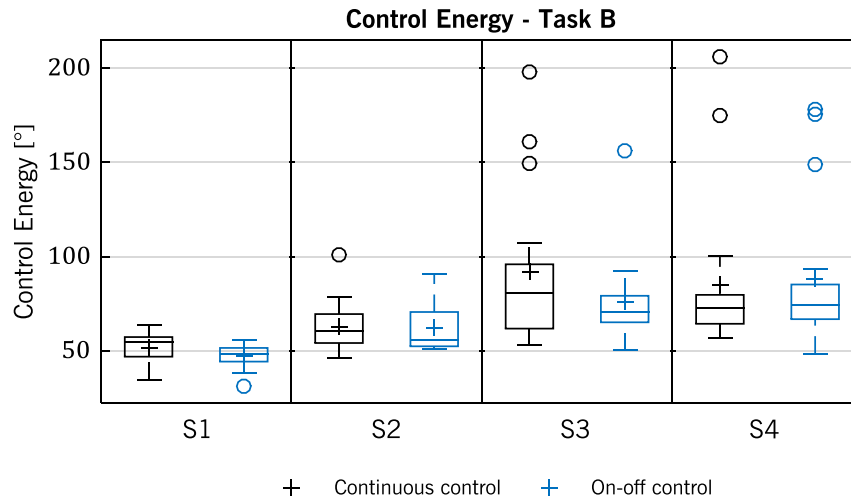


Figure 6.23 – Box plots of control energy in task B

Although the data failed the Lilliefors-test for normality and O’Brien’s test for homoscedasticity, a two-way repeated-measures ANOVA was conducted to obtain quantitative indications. Its results, listed in Table 6.10, show that the difference in control energy between control system types is not significant. Moreover, there is no significant interaction Control System \times Sensitivity. The differences between sensitivity levels, however, are highly significant. More exactly, all contrasts with the exception of S3 vs. S4 are highly significant. The measurements of control energy agree with the TLX ratings in that sensitivity levels S3 and S4 are less preferable. However, while control energy is smallest with sensitivity level S1, TLX ratings are smallest with level S2. This may be due to the fact that the slow system response with level S1 effectively prevented larger control energies and thereby also required considerable pilot compensation which had a negative effect on perceived workload.

Table 6.10 – Quantitative statistical results for control energy in task B

Factor	F	p
Control System	$F(1,17) = 1.326$	0.2654
Sensitivity	$F(2.001,34.02) = 16.49$	< 0.01
Control System \times Sensitivity	$F(1.675,28.48) = 1.201$	0.3134

After the analysis of TLX ratings and control energy as measures of workload, tracking performance is analyzed in the following paragraphs. Box plots of the first evaluation parameter, tracking RMSE, are shown in Figure 6.24.

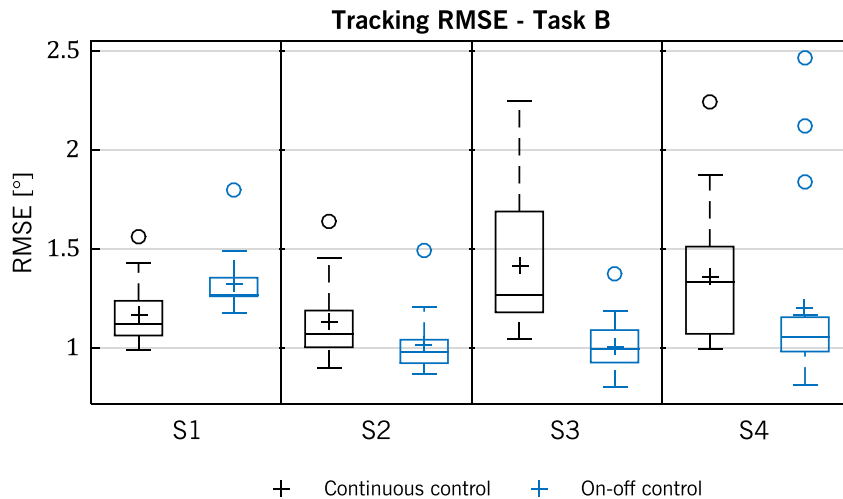


Figure 6.24 – Box plots of tracking RMSE in task B

The RMSE data, too, proved to be non-normal and heteroscedastic, but a two-way repeated-measures ANOVA was computed nonetheless. The results, listed in Table 6.11, indicate that the difference between control systems as well as differences between sensitivity levels and the interaction Control System \times Sensitivity are all significant. Generally, subjects produced smaller RMSE values with the on-off control system as compared to the continuous control system. In the case of sensitivity level S1, however, performance with the on-off control system was poorer than with the continuous control system. The reason for this observation may be that the slow system response, which greatly restricted the tracking bandwidth, could be accelerated more easily with the continuous control system and its higher value of K_a by increasing input aggressiveness and thereby the effective reaction magnitude (cf. sections 6.2.2 and 3.3.3). An analysis of the contrasts between sensitivity levels shows that RMSE values were significantly lower with level S2 than with each other level. This indicates that S2 is the most preferable sensitivity level not only in terms of workload, but also in terms of performance.

Table 6.11 – Quantitative statistical results for RMSE in task B

Factor	F	p
Control System	$F(1,17) = 11.53$	< 0.01
Sensitivity	$F(2.126,36.14) = 4.416$	< 0.05
Control System \times Sensitivity	$F(2.149,36.53) = 10.98$	< 0.01

It is also interesting to compare the RMSE values observed here with values attainable without time delays in the controlled system. This can be done by taking a look at the experiments reported in [70], which were conducted in the DA42 simulator of TUM's Institute of Flight System Dynamics and which employed the same airplane simulation model combined with a rate-command/attitude-hold flight controller. As mentioned in section 6.3.2, the construction of the forcing function of task B followed the approach presented in [70]. The only difference is that here, in the case of large time delays, the

forcing function was finally stretched by a factor of 2. The RMSE values in both experiments are similar, although both larger and smaller values were produced here, where subjects controlled the airplane with a 2 s time delay. The fact that performance is similar if, in the case of 2 s time delay, the task is slowed down by a factor of 2 indicates that the pilot-vehicle bandwidth is effectively halved. At the same time, it can be noted that the decision to stretch the forcing function by a factor of 2 established a suitable level of task difficulty.

Finally, as the second tracking performance metric, EVAR is shown in Figure 6.25. The appearance of these box plots is strikingly similar to those of control energy, shown in Figure 6.23. This is not surprising, because in the present case of a non-oscillating target, a higher amount of control energy is indicative for oscillations around the target, i.e., oscillations of the error, as mentioned in section 6.4.1.

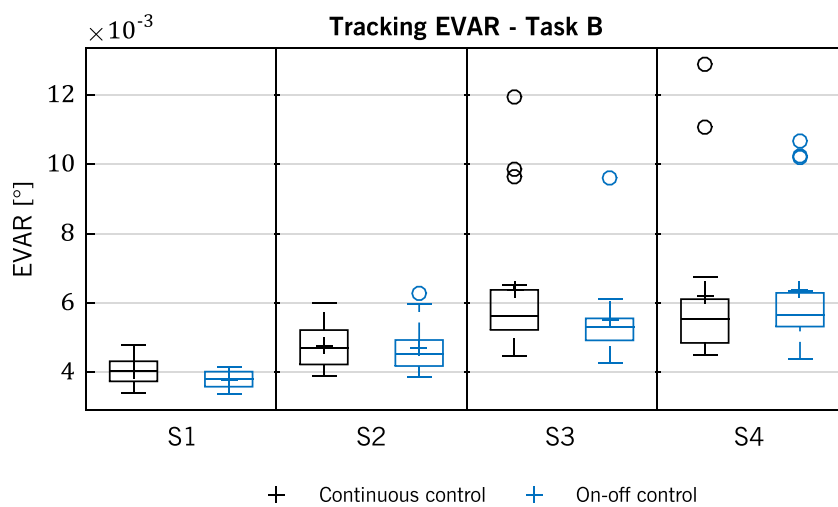


Figure 6.25 – Box plots of tracking EVAR in task B

The EVAR data, too, fails the Lilliefors-test for normality and O'Brien's test for homoscedasticity. The two-way repeated-measures ANOVA conducted over the EVAR data produces similar results as the ANOVA of the control energy data reported above. As shown in Table 6.12, only the differences between control sensitivity levels are highly significant. More exactly, all contrasts with the exception of S3 vs. S4 are highly significant. Thus, the same conclusions can be drawn as above: sensitivity levels S3 and S4 are less preferable and sensitivity level S1 effectively prevented oscillations.

Table 6.12 – Quantitative statistical results for EVAR in task B

Factor	<i>F</i>	<i>p</i>
Control System	$F(1,17) = 1.440$	0.2465
Sensitivity	$F(1.766,30.02) = 22.36$	< 0.01
Control System × Sensitivity	$F(2.079,35.34) = 1.457$	0.2466

All in all, it can be said that an extremely low control sensitivity, such as level S1, prevents oscillations, but at the same time compromises tracking performance due to the restricted maneuverability. The resulting pilot compensation adversely affects workload. Extremely high control sensitivities, on the other hand, such as that of level S4, promote oscillations around the tracking target and thereby also deteriorate tracking performance. To moderate the system response and to prevent oscillations, pilots again have to apply considerable compensation, which leads to an increase in workload. These findings are in line with the thoughts on trading maneuverability against PIO criticality formulated in section 3.3.2. According to the results from task B, the baseline control sensitivity level S2 seems to be well chosen. It enabled the best tracking performance and, at the same time, produced the lowest workload. Tracking accuracy with 2 s time delay is generally less consistent than without time delay. RMSE values similar to those achieved without time delay can be achieved with 2 s time delay if the same task performed at half the pace.

6.4.3 Operational Context and Predictors

Evaluation of the data gathered with tasks C and D sheds light on how the flight control configurations under scrutiny influence workload and performance in an operational context. Furthermore, by examining the differences between tasks C and D, the effect of predictors can be studied. Since task C always preceded task D, learning effects may have diluted or strengthened any effects that the predictors might have had. Considering that these were the final tasks of the session, it is assumed that the learning curve was rather flat and that most of the effects are due to the presence or absence of predictors. Hence, the second factor for statistical analysis is Predictors instead of Task (cf. Table 6.5), which would be more precise but less easy to read. Nonetheless, the possible falsification caused by learning shall be kept in mind when reading the following paragraphs.

The first aspect to be analyzed is workload. Figure 6.26 shows the box plots of TLX ratings for all four configurations under scrutiny, which are an indication of how pilots perceived workload.

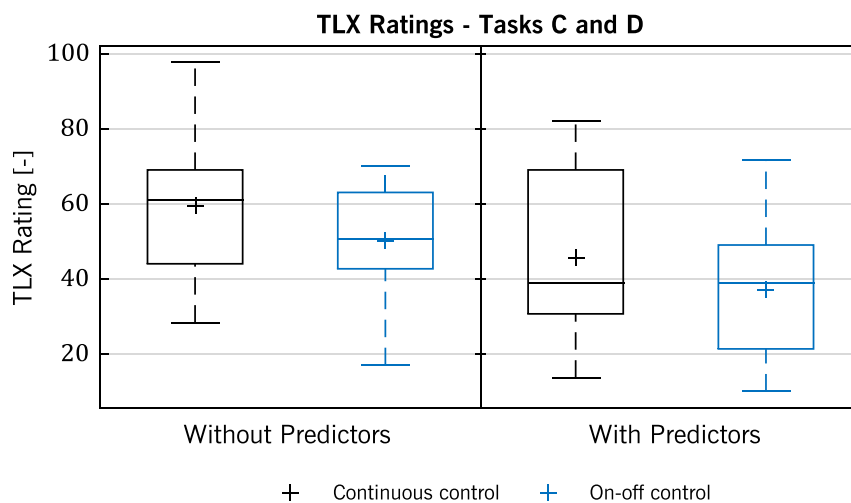


Figure 6.26 – Box plots of TLX ratings in tasks C and D

A two-way repeated-measures ANOVA across this data indicates that there is a trend for mean TLX ratings to be lower for on-off control than for continuous control. In other words,

many subjects perceived a lower level of workload when using on-off type control. This observation holds for both configurations with predictors and without predictors. Mean TLX difference between continuous control and on-off control is 9.1 without predictors and thus slightly greater than with predictors, where it is 8.2. It has to be noted, however, that there were four subjects who consistently reported higher TLX values for on-off control as compared to continuous control. This indicates that at least for some pilots, continuous control may be preferable in terms of workload. When comparing the configurations with and without predictors, i.e., tasks C and D, Figure 6.26 and the ANOVA results show that TLX ratings are significantly lower when predictors are present. Table 6.13 summarizes the quantitative results of the ANOVA.

Table 6.13 – Quantitative statistical results for TLX ratings in tasks C and D

Factor	$F(1,17)$	p
Control System	3.648	< 0.1
Predictors	29.63	< 0.01
Control System × Predictors	0.05790	0.8127

To back up these subjective ratings on workload, control energy is analyzed once again. Figure 6.27 illustrates the control energy of both longitudinal and lateral sidestick movements. Since both the Lilliefors-test for normality and O'Brien's test for homoscedasticity failed, an ANOVA was not performed here. It can be seen quite clearly, however, that lateral control activity is much lower with the on-off control system than with the continuous control system. The presence of predictors seems to have a similar, although slightly weaker effect. Longitudinal control energy, on the other hand, seems to be similar between control system types, but is also noticeably reduced with predictors. These observations taken together are in good agreement with the TLX ratings. Pilots may have noticed the positive effects of the on-off control system in the lateral axis, but they may not have seen a similar improvement in the longitudinal axis. Predictors, on the other hand, had a noticeable beneficial effect in both axes.

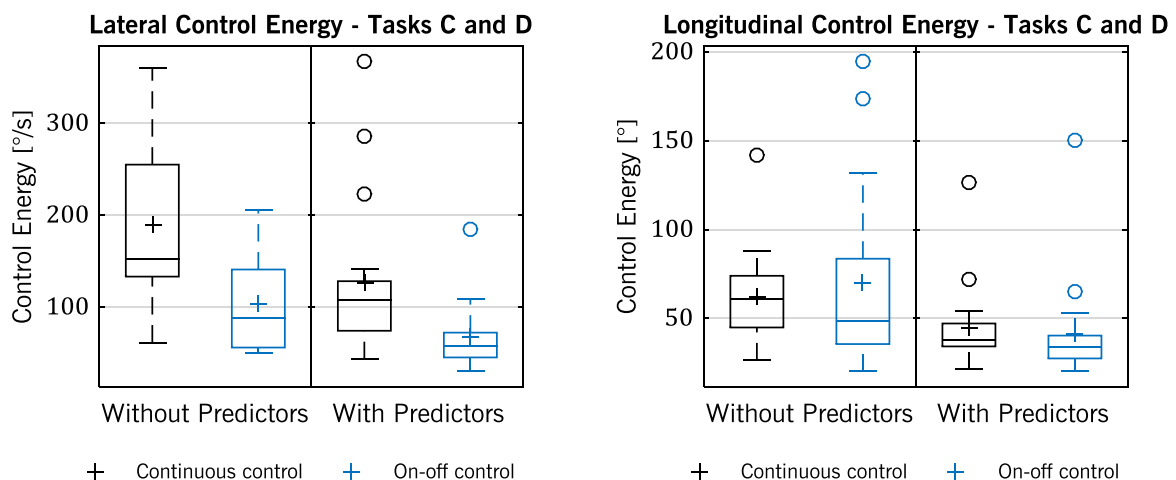


Figure 6.27 – Box plots of control energy in tasks C and D

To analyze the subjects' performance during tasks C and D, appropriate evaluation segments need to be defined first. Table 6.14 sums up these segments, which are described in detail in the remainder of this paragraph. Between positions 1 and 3, the pilots' task was to descend to and maintain 1500 *ft*. No instruction was given on how quick to descend, so the beginning of evaluation segment I is defined as the first moment when the airplane descends below 1600 *ft*. This segment ends at position 3. Likewise, evaluation segment II with a heading target of 140° starts when the airplane first passes 150° and ends at position 3. Two additional segments can be defined in the same way for the altitude and heading targets between positions 3 and 4. Between positions 4 and 6, subjects had to align the airplane with the runway. At these distances to the runway, an angular deviation is far easier to perceive and also more relevant than a linear deviation. Hence, angular localizer deviation is evaluated instead of linear centerline error in segment V. Between positions 6 and the end of the recording, a segment VI can be defined where glideslope tracking is analyzed. As soon as the runway 05R centerline tracking error decreases below 250 *m*, the last evaluation segment begins. Here, linear centerline error is evaluated. The last segment ends with the recording.

Table 6.14 – Definition of evaluation segments for tasks C and D

Segment No.	Parameter / Target	Segment Start	Segment End
I	Altitude: 1500 <i>ft</i>	After position 1, error < 100 <i>ft</i>	Position 3
II	Heading: 140°	After position 2, error < 10°	Position 3
III	Altitude: 1200 <i>ft</i>	After position 3, error < 100 <i>ft</i>	Position 4
IV	Heading: 080°	After position 3, error < 10°	Position 4
V	Runway 05L Localizer	Position 4	Position 6
VI	Runway 05R Glide Slope	Position 6	End of recording
VII	Runway 05R Centerline	After position 6, error < 250 <i>m</i>	End of recording

Considering that the task description said that altitude had to be maintained between positions 4 and 5, it should be possible to evaluate altitude tracking along this segment. However, many subjects intentionally started their descent right after position 4, ignoring the instructions to maintain altitude. Admittedly, the task design or the instructions are to blame for this problem. Because of the two following other problems, segments V, VI and VII are analyzed across 17 subjects instead of all 18 participants. First, position 4 was indicated much too late for subject 9 in run Dc due to a technical problem, which adversely affected his localizer tracking performance. Moreover, the same subject entered a severe and sustained lateral PIO in run Cc, so that the run was terminated before position 6. The rest of the task simply seemed not accomplishable for the subject. For these two reasons, subject 9 is not taken into account for evaluation segments V, VI and VII.

The first parameter under scrutiny in the analysis of task performance is altitude. RMSE and EVAR were computed for both segments I and II combined, as in equations (6.4) and

(6.5). This combined evaluation is in fact equivalent to an averaging operation that weighs RMSEs and EVARs of each segment by its length.

$$\begin{aligned}
 \text{RMSE}_{1,2} &= \sqrt{\frac{1}{N_1 + N_2} \left(\sum_{i=1}^{N_1} e_i^2 + \sum_{i=1}^{N_2} e_j^2 \right)} \\
 &= \sqrt{\frac{N_1}{N_1 + N_2} \text{RMSE}_1^2 + \frac{N_2}{N_1 + N_2} \text{RMSE}_2^2}
 \end{aligned}
 \tag{6.4}$$

$$\begin{aligned}
 \text{EVAR}_{1,2} &= \frac{1}{(N_1 - 1) + (N_2 - 1)} \left(\sum_{i=1}^{N_1-1} |e_{i+1} - e_i| + \sum_{i=1}^{N_2-1} |e_{i+1} - e_i| \right) \\
 &= \frac{(N_1 - 1)}{(N_1 - 1) + (N_2 - 1)} \text{EVAR}_1^2 + \frac{(N_2 - 1)}{(N_1 - 1) + (N_2 - 1)} \text{EVAR}_2^2
 \end{aligned}
 \tag{6.5}$$

It has to be noted at this point that both RMSE and EVAR are to some extent influenced by the simulated turbulence. This means that their absolute value is not a good indication for flight control performance. However, since all subjects and all runs were affected by the same amount of turbulence, differences between configurations may be interpreted. Box plots of altitude RMSE and EVAR are depicted in Figure 6.28.

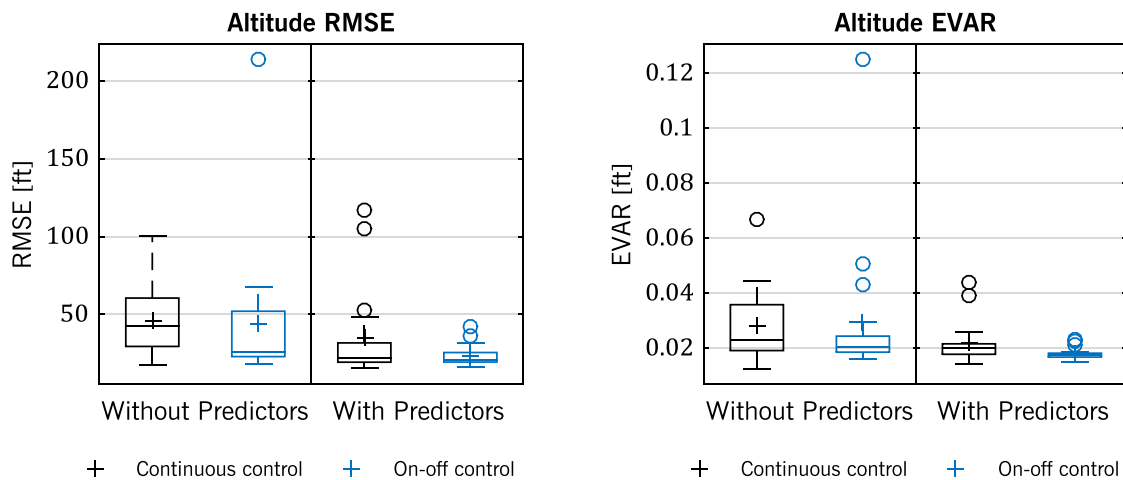


Figure 6.28 – Box plots of performance in altitude tracking

A two-way repeated-measures ANOVA was computed for both altitude RMSE and EVAR, even though the Lilliefors-test for normality failed. The ANOVA’s quantitative results are summarized in Table 6.15. Differences between continuous control and on-off control are neither significant in altitude RMSE, nor in altitude EVAR. A t-test for the configurations with predictors, however, indicates that subjects achieved significantly smaller RMSEs and EVARs with on-off control than with continuous control in this case. (This result has to be put into perspective, though, because the interaction Control System × Predictors is not significant in either RMSE or EVAR.) Concerning predictors as the second factor of the

ANOVA, results indicate that both mean altitude RMSE and EVAR are significantly lower with predictors as compared to the configurations without predictors. Given that the data is not normally distributed and the sample size is small, some skepticism of these results is advisable. It is, however, quite striking that the data points in the case of on-off control with predictors are closer together than those of any other configuration. This indicates a rather consistent performance between subjects in this particular case.

Table 6.15 – Quantitative statistical results for altitude tracking

Factor	Altitude RMSE		Altitude EVAR	
Control System	$F(1,17) = 1.137$	$p = 0.3012$	$F(1,17) = 0.1453$	$p = 0.7078$
Predictors	$F(1,17) = 6.668$	$p < 0.05$	$F(1,17) = 6.299$	$p < 0.05$
Control System × Predictors	$F(1,17) = 0.5887$	$p = 0.4535$	$F(1,17) = 0.6796$	$p = 0.4211$
Control System, With Predictors	$t(17) = 1.862$	$p < 0.05$	$t(17) = 1.989$	$p < 0.05$

The same observation concerning the consistency of data points can also be made in Figure 6.29, which shows box plots of heading tracking RMSE and EVAR. Again, two evaluation segments were combined for evaluation using equations (6.4) and (6.5), namely segments II and IV.

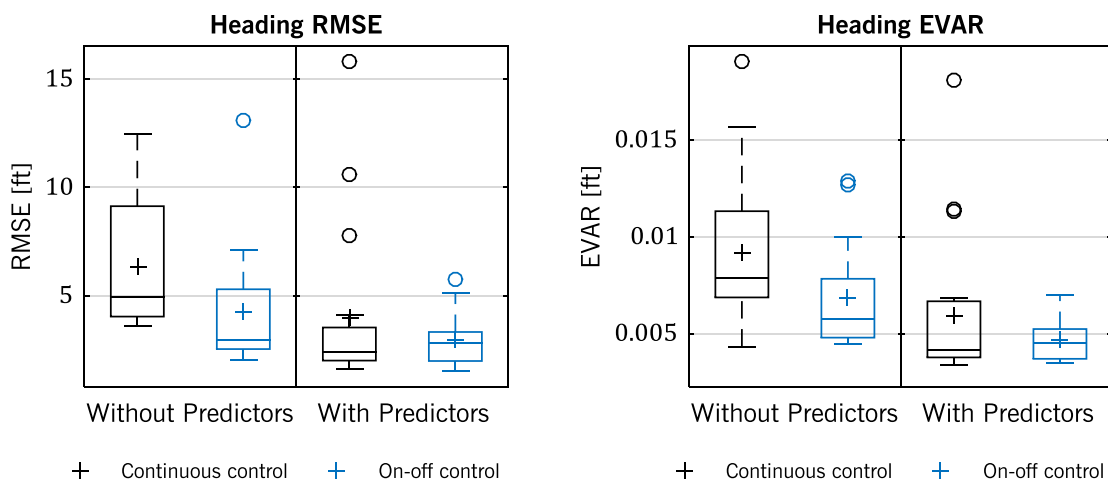


Figure 6.29 – Box plots of performance in heading tracking

Here, the data fails the Lilliefors-test for normality, too. Moreover, homoscedasticity is weak ($p = 0.07482$) for heading EVAR. Nonetheless, a two-way repeated-measures ANOVA was computed for both heading RMSE and EVAR. Results (cf. Table 6.16) show that mean heading RMSE is significantly lower with on-off control as compared to continuous control. This improvement in mean performance caused by the on-off control system is not only greater without predictors (2.165° difference as compared to 1.008°), but, as t-tests for configurations with and without predictors individually indicate, also more pronounced. Furthermore, heading EVAR tends to be lower with on-off control as compared to continuous control. When comparing configurations with and without

predictors, it can be seen that both mean heading RMSE and EVAR are significantly lower when predictors are present. It has to be stressed again, though, that not all requirements for the ANOVA are met.

Table 6.16 – Quantitative statistical results for heading tracking

Factor	Heading RMSE		Heading EVAR	
	$F(1,17) = 5.459$	$p < 0.05$	$F(1,17) = 3.582$	$p < 0.1$
Predictors	$F(1,17) = 9.157$	$p < 0.01$	$F(1,17) = 52.98$	$p < 0.01$
Control System × Predictors	$F(1,17) = 5.617$	$p < 0.05$	$F(1,17) = 2.957$	$p = 0.1037$
Control System, Without Predictors	$t(17) = 3.131$	$p < 0.01$		
Control System, With Predictors	$t(17) = 1.344$	$p < 0.1$		

Over the next evaluation segment V, tracking of the runway 05L localizer can be examined. Box plots of the subjects' tracking performance are shown in Figure 6.30.

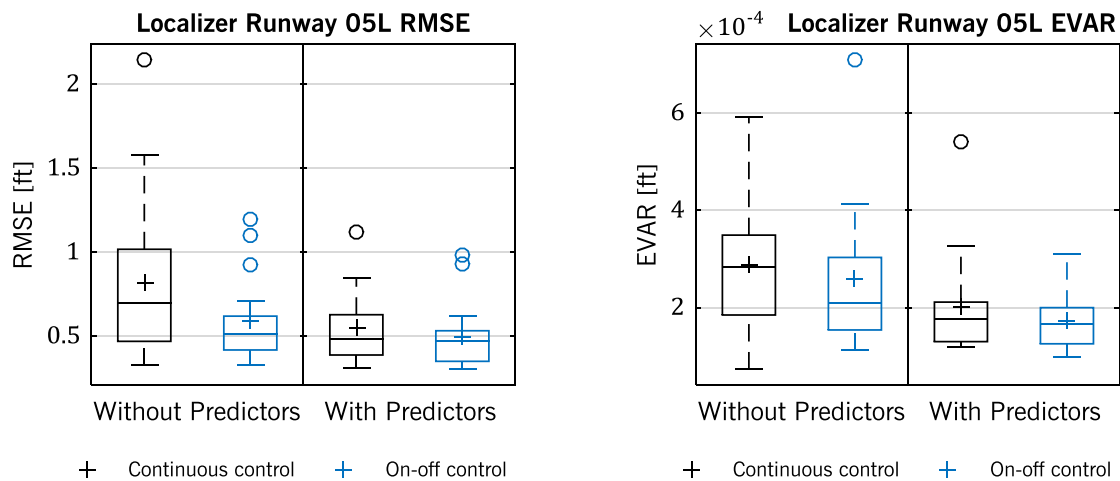


Figure 6.30 – Box plots of performance in localizer tracking

For both localizer RMSE and EVAR, a two-way repeated-measures ANOVA was computed. Quantitative results are shown in Table 6.17. Here, the Lilliefors-test for normality failed and homoscedasticity is low ($p = 0.08932$) for localizer RMSE, which again compromises the validity of the ANOVA results. Mean localizer RMSE tends to be lower with on-off control as compared to continuous control. T-tests for configurations with and without predictors individually show that this apparent performance improvement is more pronounced when predictors are not present. Differences between control systems in localizer EVAR are not significant. The effect of predictors, on the other hand, is again clearly discernible. Their presence significantly reduces both mean localizer RMSE and EVAR.

Table 6.17 – Quantitative statistical results for localizer tracking

Factor	Runway 05L Localizer RMSE		Runway 05L Localizer EVAR	
	<i>F</i> or <i>t</i>	<i>p</i>	<i>F</i> or <i>t</i>	<i>p</i>
Control System	$F(1,16) = 3.251$	< 0.1	$F(1,16) = 1.992$	0.1773
Predictors	$F(1,16) = 11.28$	< 0.01	$F(1,16) = 32.48$	< 0.01
Control System × Predictors	$F(1,16) = 1.536$	0.2331	$F(1,16) = 0.003892$	0.9510
Control System, Without Predictors	$t(16) = 1.682$	< 0.1		
Control System, With Predictors	$t(16) = 0.6644$	0.2580		

In the horizontal plane, localizer tracking during segment V is followed by centerline tracking during segment VII. Figure 6.31 depicts box plots of the pilots' centerline RMSE and EVAR.

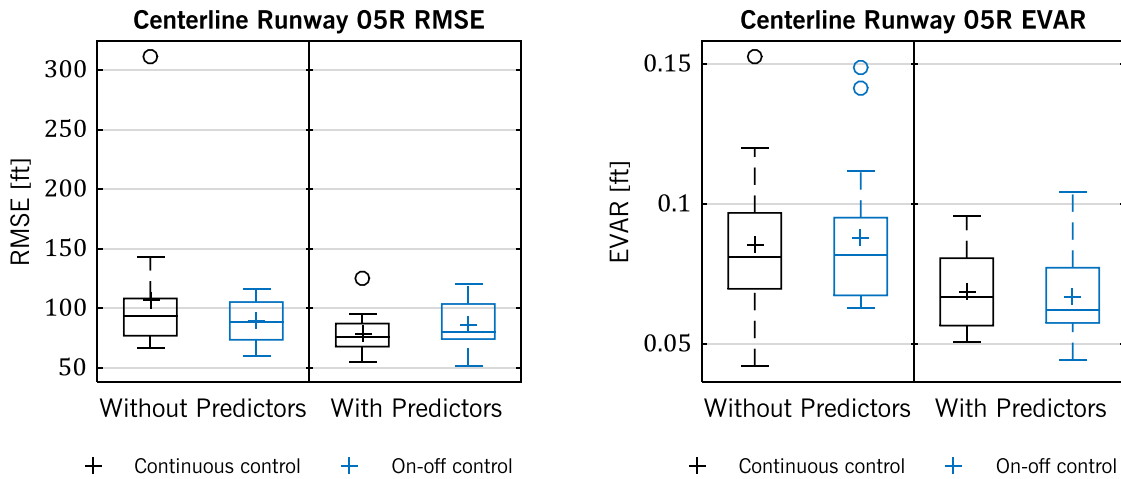


Figure 6.31 – Box plots of performance in centerline tracking, runway 05R

A two-way repeated-measures ANOVA was computed for both centerline RMSE and EVAR, even though the Lilliefors-test failed for centerline RMSE and the centerline EVAR data cannot be considered homoscedastic. The results listed in Table 6.18 indicate that both metrics do not significantly differ between on-off control and continuous control. The predictors, on the other hand, do seem to have an effect. Mean centerline RMSE tends to be lower when predictors are present. Mean centerline EVAR even is significantly lower with predictors as compared to configurations without predictors.

Table 6.18 – Quantitative statistical results for centerline tracking

Factor	Runway 05R Centerline RMSE		Runway 05R Centerline EVAR	
	<i>F</i> (1,16)	<i>p</i>	<i>F</i> (1,16)	<i>p</i>
Control System	0.4787	0.4989	0.0005899	0.9809
Predictors	3.238	< 0.1	10.25	< 0.01
Control System × Predictors	3.652	< 0.1	0.5396	0.4732

Figure 6.32 illustrates all subjects' horizontal trajectories during final approach. Remember that the swing-over command was given at a distance of 4000 m from the threshold. Instead of showing all individual trajectories, the plots only show five characteristic lines. The minimum/maximum lines constitute the outer limits, within which all trajectories lie. Half of the trajectories lies between the 25%/75% quantile lines and a quarter lies each above and below. Finally, the 50% quantile line separates all trajectories in two halves. A first glance at the plots already reveals that excursions from an ideal maneuver are much greater in the cases without predictors. Generally, performance is more consistent between subjects with predictors. This qualitative observation is in accordance with the quantitative results above. The plots in Figure 6.32 also show that the lateral deviation from runway centerline is, in all configurations, still considerably high at the end of some trajectories. In other words, many subjects missed the 45 m-wide runway.

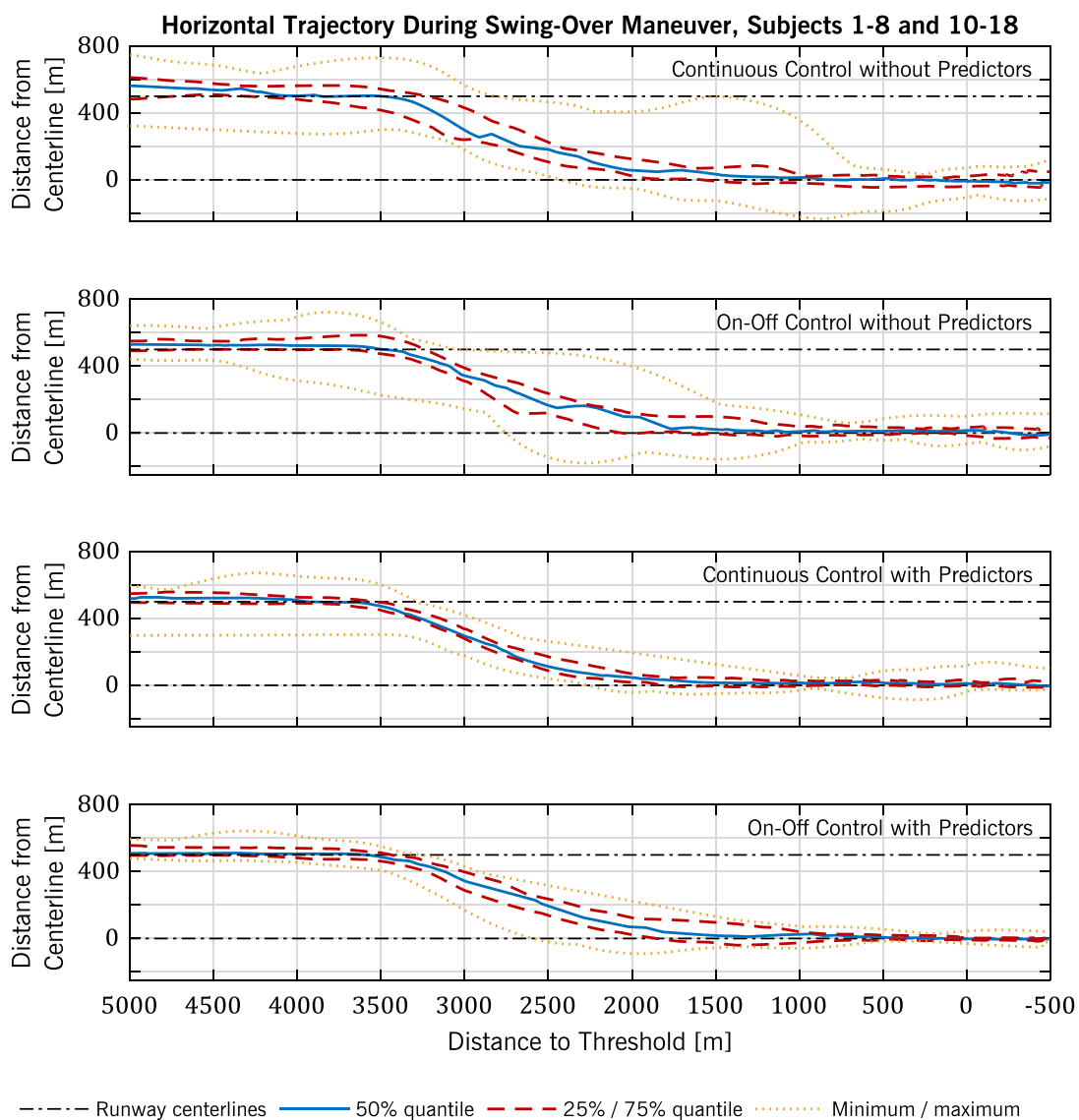


Figure 6.32 – Centerline tracking errors during the swing-over maneuver

Finally, glide slope tracking during segment VI is analyzed. Box plots of glide slope RMSE and EVAR across all subject are depicted in Figure 6.33.

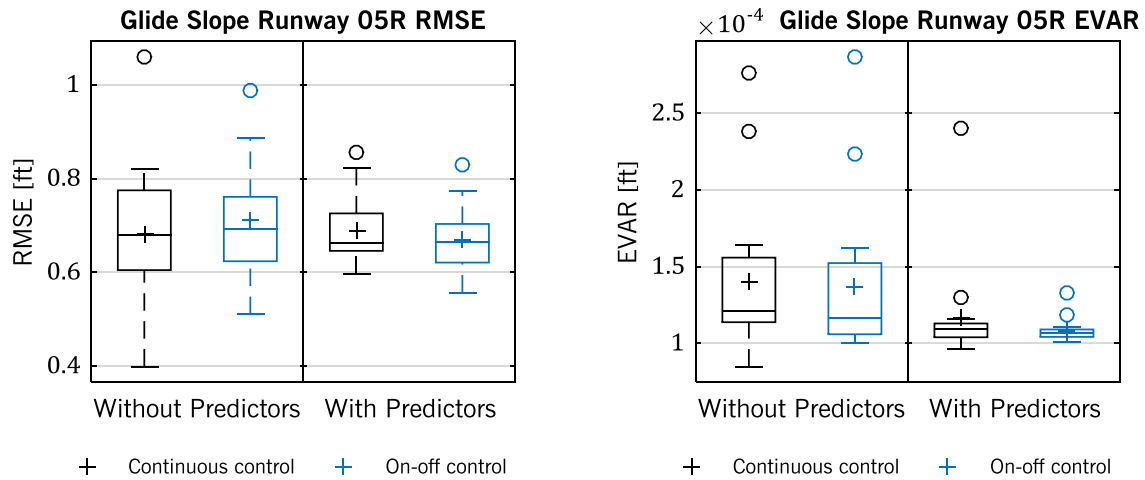


Figure 6.33 – Box plots of performance in glide slope tracking, runway 05R

The data of glide slope RMSE and EVAR fails the Lilliefors-test. Moreover, homoscedasticity is weak ($p = 0.09168$) for glide slope EVAR and cannot be assumed for the RMSE. Therefore, the results of the two-way repeated-measures ANOVA, which are listed in Table 6.19, have only limited validity. The visual appearance of Figure 6.33 and the ANOVA results indicate that there is no significant difference between continuous control and on-off control in both glide slope RMSE and glide slope EVAR. Similarly, predictors do not seem to have an effect on glide slope RMSE. Glide slope EVAR, on the other hand, is significantly lower when predictors are present. The data points in Figure 6.33 also appear to be more consistent in those cases with predictors.

Table 6.19 – Quantitative statistical results for glide slope tracking

Factor	Rwy. 05R Glide Slope RMSE		Rwy. 05R Glide Slope EVAR	
	$F(1,16)$	p	$F(1,16)$	p
Control system	0.05629	0.8155	1.328	0.2661
Predictors	0.8171	0.3795	10.08	< 0.01

Figure 6.34 illustrates the vertical trajectories of all subjects. Note that the abscissa here indicates the distance to the aiming point, i.e., the point where the glide slope intersects the ground, not the distance to the threshold. The first feature to notice is that excursions from the nominal glide slope are, by far, largest in the case of continuous control without predictors. The trajectories in Figure 6.34 seem more consistent when predictors are present, which well corresponds to the consistency of data points in Figure 6.33. In all four configurations, however, many trajectories end up high above the runway or come in very low on final approach. Together with the observation that subjects often missed the runway laterally (cf. Figure 6.32), a rather disappointing picture concerning the actual landing performance emerges. Indeed, only very few runs ended a few meters above the

runway and in an attitude suitable for landing. This fact shows how very difficult it is to perform high-bandwidth tasks with 2 s time delay.

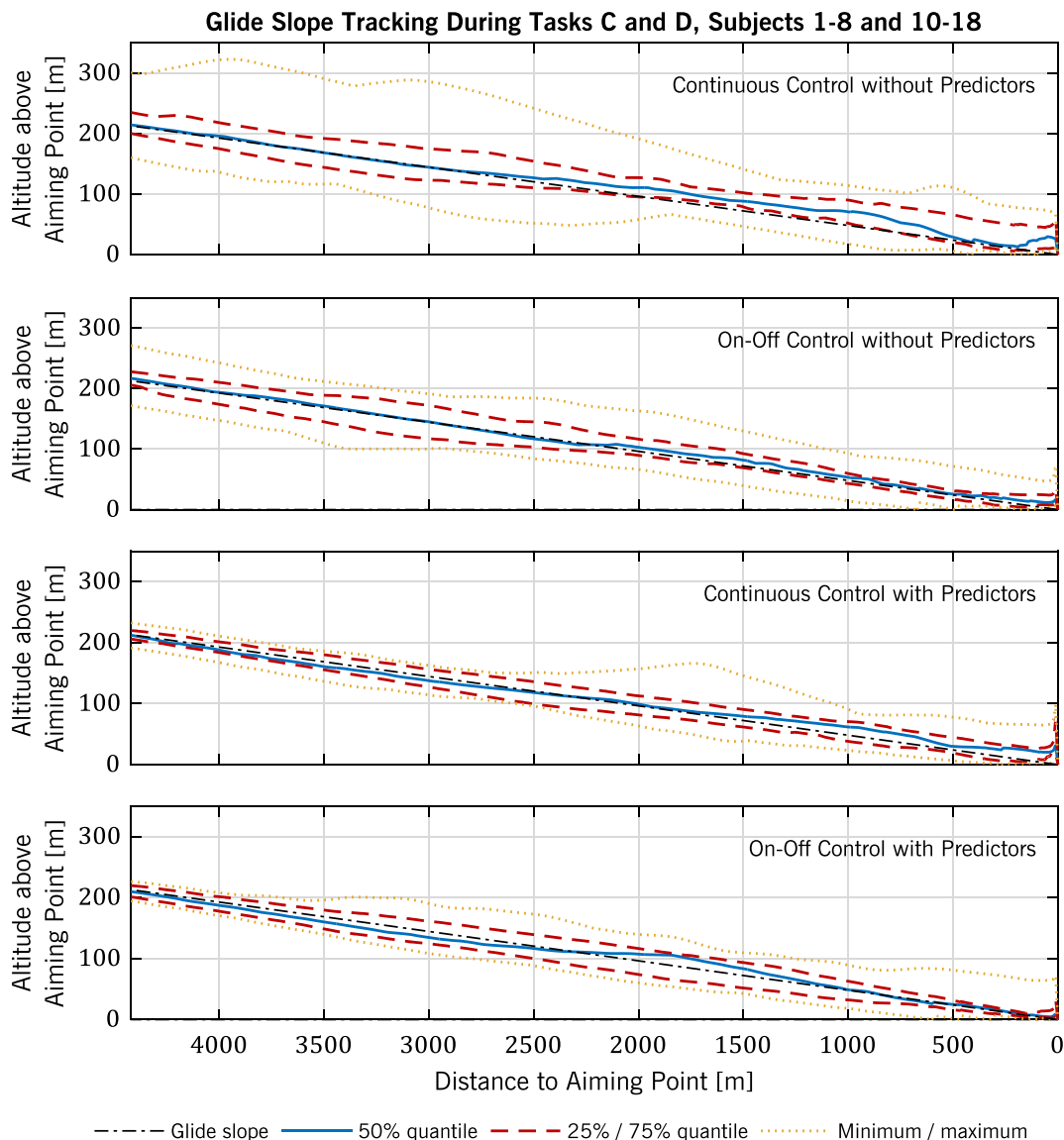


Figure 6.34 – Glide slope tracking errors during final approach (with swing-over)

All in all, concluding the evaluation results of flight control in an operational context with and without predictors gathered up to this point, it can be said that subjects performed at least as well with the on-off control system as with the continuous control system. In some cases, performance was even better when using on-off control. Thus, hypothesis 3 can be accepted: performance with an on-off control system is comparable or better than performance with a continuous control system. Regarding pilot workload in tasks C and D, the effect of control system type is not very clear. It seems, though, that on-off control positively affects the metrics of perceived and measured workload. Also looking at the observations from the preceding sections 6.4.1 and 6.4.2, it can be concluded that hypothesis 1 can be accepted: workload is less with an on-off control system as compared to a continuous control system. Another thought on the influence of control system type on workload mentioned in section 3.3.3 and also backed up by pilot opinion (cf. section

6.4.5) is, that the beneficial effect of an on-off control system becomes weaker as pilots become more familiar with flight control with large time delays. The predictors' positive effect on workload and performance, on the other hand, is quite pronounced. This finding is backed up by pilot ratings of the predictors, produced after each run of task D on a five-point scale between "very annoying" and "very helpful". Figure 6.35 shows all the subjects' ratings of the predictors. The subjects generally agreed that the predictors are quite helpful, regardless of the control system employed. Based on these ratings and the objective measures above, hypotheses 4 and 5 can be accepted, even though the predictors' positive effect on workload and performance may have been strengthened by learning. Predictor displays reduce workload and improve performance. This corresponds to what previous studies have found.

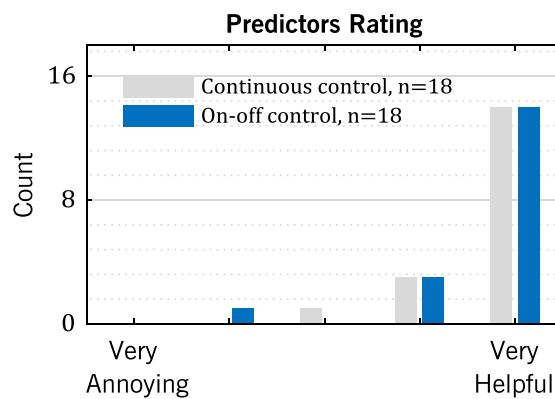


Figure 6.35 – Mean pilot ratings for predictors

Interestingly, however, subject 15 reported that the reason for the severe PIOs encountered during and after the swing-over maneuver was due to his focused attention on the predictors. Indeed, the (visual) attention required to use a predictor possibly is a shortcoming of this approach to tackle time delays. To get more insight into this matter, subjects were asked to estimate how much attention they had devoted to the HUD. Figure 6.36 shows the resulting ratings.

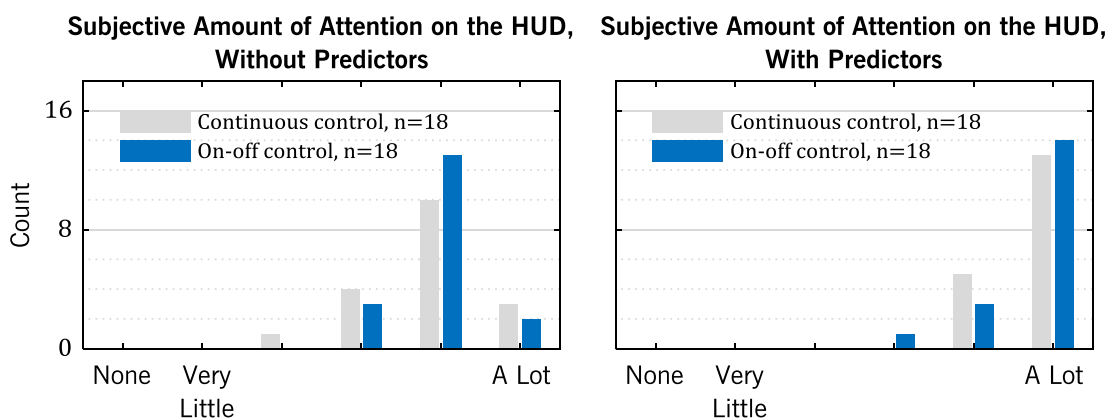


Figure 6.36 – Mean subjective amount of attention on the HUD

Across these ratings, a two-way repeated-measures ANOVA was conducted, whose quantitative results are listed in Table 6.20. While there is no significant difference

between continuous and on-off control, subjects felt that they allocated significantly more attention to the HUD when predictors were presented. The findings of the ANOVA may be compromised by the fact that ratings were not normally distributed, which is a consequence of the discrete-scale questionnaire design (cf. appendix B). Therefore, a sign test was additionally performed. Of the 36 differences in rated attention on the HUD between task C and D, 24 were positive (more attention on the HUD in task D), 10 were neutral and 1 was negative (less attention on the HUD in task D), yielding a significant effect between the two tasks in the sign test and backing up the findings from the ANOVA.

Table 6.20 – Quantitative statistical results for amount of attention on the HUD

Factor	$F(1,17)$	p
Control system	0.2742	0.3927
Predictors	23.61	< 0.01

It can be noted that the subjective attention on the HUD is high in both cases. This is partly due to the fact that it is possible to, as one subject put it, see through the HUD and thereby almost permanently look at it. Moreover, there were no other displays or visual tasks to work with. All in all, hypothesis 6 may be accepted based on this data, although more experimental research is necessary to obtain deeper insights into this matter.

6.4.4 Conclusion on Hypotheses

Most of the statistical analyses presented in the previous sections are related to the hypotheses formulated in section 6.1. Hence, the preceding sections also interpret the outcome of these analyses in the context of the top-level hypotheses and indicate whether each hypothesis can be accepted or whether it must be rejected. Considering that the hypotheses were the main driver behind the experiments presented, this section recapitulates their outcome in a compact and concise manner. It can therefore be understood as the concluding counterpart to section 6.1. Table 6.21 lists all hypotheses and their respective outcome. Based on the experiments made, all six a priori hypotheses can be accepted.

Table 6.21 – Summary of hypotheses outcome

N°	Hypothesis	Outcome
1	Workload is less with an on-off control system as compared to a continuous control system.	Accepted
2	Pilots naïve to flight control with large time delays find an appropriate control strategy quicker with an on-off control system than with a continuous control system.	Accepted
3	Performance with an on-off control system is comparable or better than performance with a continuous control system.	Accepted
4	Predictor displays reduce workload.	Accepted
5	Predictor displays improve performance.	Accepted
6	Visual predictor displays bind a significant amount of visual attention.	Accepted

Apart from the six hypotheses, section 6.1 also formulates the qualitative expectations concerning workload and performance for the four possible combinations of control system type and predictor displays. The following Figure 6.37 qualitatively relates the four configurations of tasks C and D in terms of workload and performance and thereby represents the actual experimental results, as opposed to the prior expectations. It has to be stressed, however, that this simplified, qualitative sketch should be understood as a graphic summary and must not be interpreted like the quantitative plots of other sections.

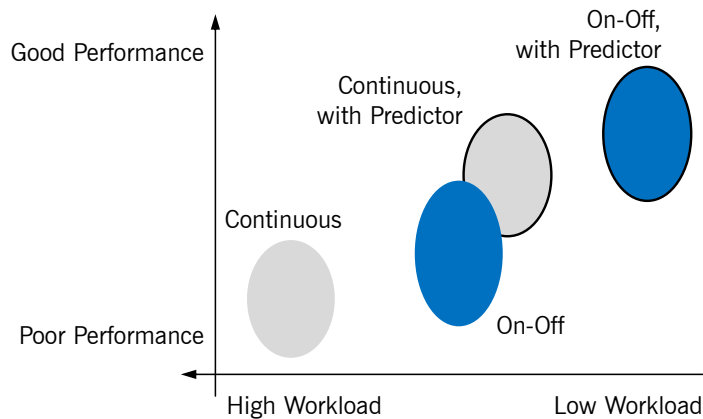


Figure 6.37 – Qualitative differences in actual workload and performance

The sketch shows that, departing from continuous control without predictors as the baseline, gains in workload and performance can be achieved with predictor displays and with an on-off control system alike, although these gains are higher with predictors. This fact corresponds to what had been expected. Quite unexpectedly, though, there is a considerable difference between the continuous control system with predictors and the on-off control system with predictors. This means that the beneficial effects of the both elements can be combined. At the same time, the difference between the continuous control system with predictors and the on-off control system without predictors is smaller than expected.

6.4.5 Pilot Opinion

Apart from the various objective measures of performance and the formalized quantification of workload in the form of the TLX, the pilots' subjective opinion is an important element to consider. Therefore, the experiment handbook contained additional questions that were answered on scales or in the form of free text. The self-assessments related to learning are analyzed above in section 6.4.1 and questions concerning the predictors and attention on the HUD are presented in section 6.4.3, whereas this section covers all the following other questions. In tasks C and D, pilots were asked to rate the various control system functions. Moreover, the pilots' preference between continuous control and on-off control was recorded at three instances. On the final page of the experiment handbook, they had the possibility to elaborate on the two control system types and any other aspect of the control system or the experiments.

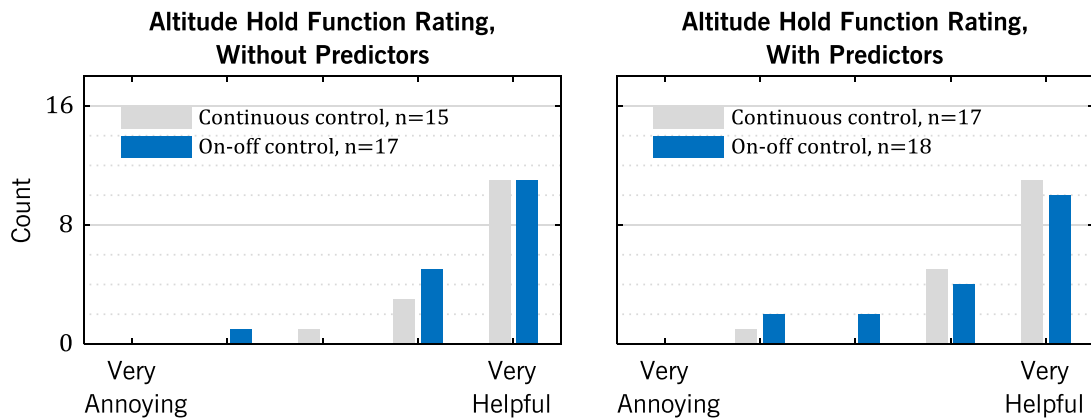


Figure 6.38 – Pilot ratings of the altitude hold function

First, ratings of the four flight controller functions (Altitude Hold, Path Straightener, Standard Rate Turn Hold and Protections) are analyzed. Those ratings were produced after each run of tasks C and D on a five-point scale between “very annoying” and “very helpful”. They also had the option to check “function was not observed or was not active”. Figure 6.38, Figure 6.39, Figure 6.40 and Figure 6.41 show the resulting ratings, taking into account only valid answers on the five-point scale. The number of valid answers is indicated next to each group of ratings by the value of n .

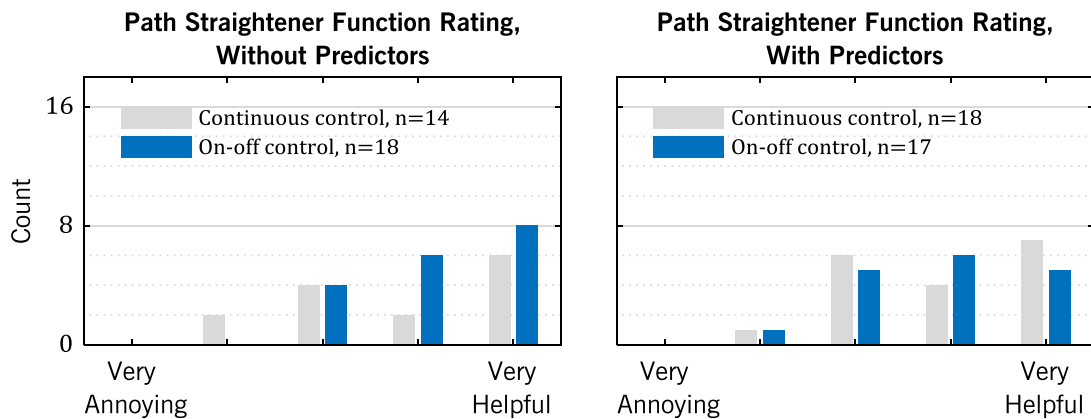


Figure 6.39 – Pilot ratings of the path straightener function

The three functions Altitude Hold, Path Straightener and Standard Rate Turn Hold were active in all runs of all subjects for at least a couple of seconds. Thus, the value of n in these cases is equal to the number of subjects who correctly recognized that the functions had been active (“correct hits”). The other $18 - n$ subjects did not notice the functions (“misses”). It can be seen that the three functions Altitude Hold, Path Straightener and Standard Rate Turn Hold were generally rated rather helpful, without notable differences between control systems or tasks. The number of misses is noteworthy only in case of the Standard Rate Turn Hold function, which may be due to the fact that a constant altitude and a wings level attitude are easier to recognize than a constant, standard turn rate. Valid ratings of the protections were scarce and do not permit any conclusions. On the one hand, the protections’ activity was missed in a total of 17 runs. On the other hand, five ratings

were given after runs where none of the protections was active (“false alarms”) and therefore have to be considered invalid.

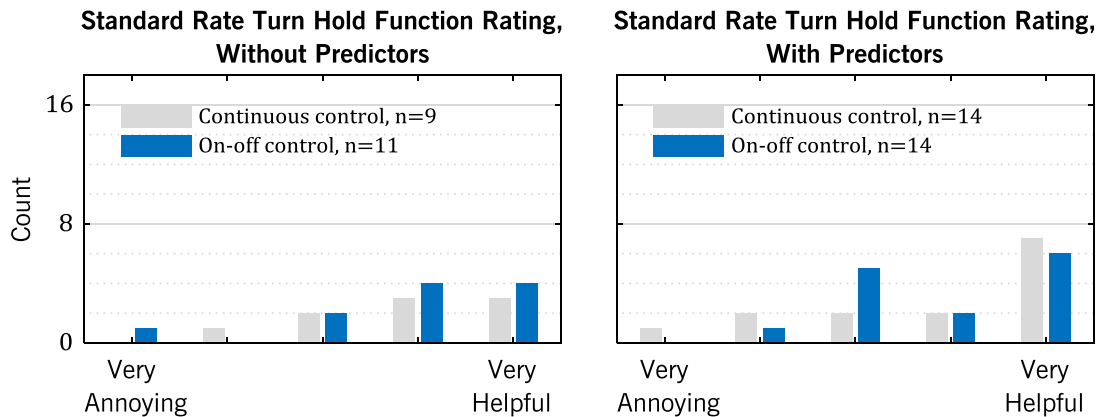


Figure 6.40 – Pilot ratings of the standard rate turn hold function

The fact that the protections often acted without the subjects noticing it, which is indicated by the large number of misses, can be good and bad. On the one hand, it shows that the protections do not suddenly take over control, thus possibly confusing pilots, but blend in rather seamlessly with the airplane’s behavior. On the other hand, the subject’s lack of awareness with respect to protections is in fact a lack of situational awareness that can lead to inadequate decisions and control inputs that may further deteriorate the situation. The fact that false alarms occurred in the rating of protection mechanisms shows that some pilots already felt restricted by the flight control system without protections. This may be due to delayed aircraft reactions not being associated with control inputs.

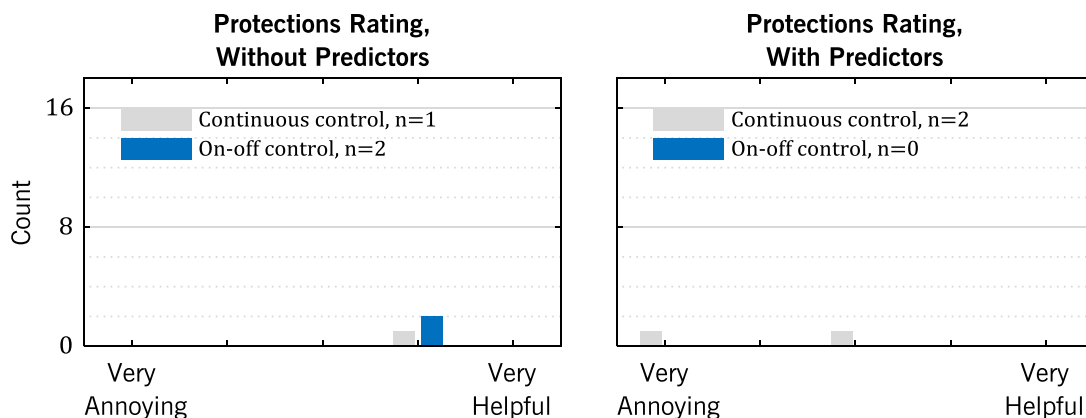


Figure 6.41 – Pilot ratings of the protections

Subjective opinions were not only gathered about the predictors, but also about the control system types. At three times during an experimental session, subjects were asked to state which control system type they preferred. After task C and after task D, they had to decide whether they liked the configuration of the task’s first run or that of the second run better. (Note that some of the subjects started off with continuous control, whereas others began with on-off control, as indicated in Table 6.1.) At the end of the session, they were asked about their overall preference between continuous control and on-off control. Figure 6.42 shows the results.

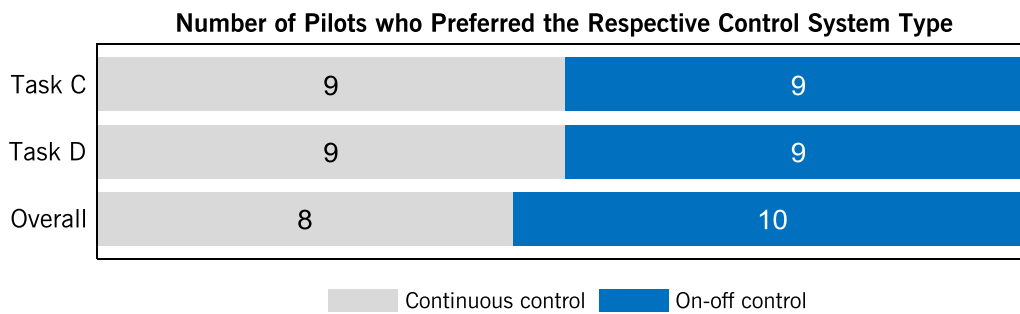


Figure 6.42 – Pilot preference for either control system type

Surprisingly, there seems to be no clear preference. In the operational scenario of tasks C and D, the same number of subjects voted for on-off control as for continuous control. Interestingly however, the presence of predictors did not seem to change the pilots' opinion in this regard. Overall preference is slightly in favor of on-off control, but still very balanced. Some subjects indicated in verbal comments or written notes that their preference would change under certain circumstances. Two pilots said that they preferred a different control system type for the final approach than for the initial approach. However, they had opposing views. While subject 2 said he would prefer continuous control during the swing-over, subject 3 reported that continuous control only worked for him during initial approach. A very interesting comment was made by subject 5, who said he would change his preference towards on-off control if there was another task apart from flying. Subject 17 had difficulties with the deadzone of the sidestick in its continuous control configuration. He therefore indicated that his preference would rather be with continuous control if the deadzone was reduced. This comment shows that the inceptor characteristics of the continuous control system mismatched this particular pilot, who interestingly was the only subject with RPAS experience. Finally, subject 13 made an honest comment that is very valuable, because it reveals the mindset of some pilots: he said that he marked continuous control as his preferred type only because he was a pilot. On-off control, from his point of view, is only good for video games and not how airplanes ought to be flown. This attitude is comparable to that of the first astronauts in the 1950s and 1960s, who had been recruited from the pilot elite and wanted to fly spacecraft the same way they flew airplanes [152]. They nevertheless ended up landing on the moon not only with massive computer support, but also with incremental, pulse-type control of sink rate (cf. section 4.1). This very well illustrates that every new technology has to surmount not only technical, but also societal challenges.

More insight into pilot preferences and the suitability of either control system type is gained by the following evaluation of the subjects' free text comments. These comments have mostly been given in the form of bullet points, in German language and often in an informal way, sometimes not using the proper technical terms. Therefore, they have been rewritten for better readability, then categorized and listed in Table 6.22, Table 6.23, Table 6.24 and Table 6.25. Due to the fact that one single comment can be assigned to more than one of the following categories, some comments appear repeatedly, under multiple headlines. Identical comments within one category, however, stem from different subjects. Of course, all subjects did not always agree. Individual comments that differ from the opinion of the majority are distinguished by italic letters.

Table 6.22 – Rewritten pilot comments related to predictors and workload

In which situations do you think a continuous control system is more helpful or better suited than an on-off control system?	In which situations do you think an on-off control system is more helpful or better suited than a continuous control system?	Do you have any further remarks or suggestions for improvement?
Predictors		
<ul style="list-style-type: none"> ▪ In combination with predictors ▪ When a predictor is available ▪ When predictors are available ▪ When predictors are available 	<ul style="list-style-type: none"> ▪ <i>When predictors are available, on-off control is easier and more precise.</i> ▪ When predictors are not available 	<ul style="list-style-type: none"> ▪ Predictors are very helpful ▪ Predictors are extremely helpful ▪ Predictor is well suited for downwind and base leg, but annoying during final approach. ▪ Possibly show glide path and localizer instead of predictor ▪ Make the dots of the predictors larger (especially heading) ▪ Make turn rate predictor better readable (increase distance from turn rate indicator) ▪ Lateral predictor (turn) difficult to read. Suggestion: predictor above turn rate indicator, or as a laterally moving vertical bar ▪ Human-machine interface must be adapted (HUD and predictor symbols)
Workload		
<ul style="list-style-type: none"> ▪ When flying is the only task ▪ Was more convenient when controlling one axis 	<ul style="list-style-type: none"> ▪ Multiple simultaneous targets ▪ When there are other tasks than flying ▪ In more complex tasks ▪ Multiple axes simultaneously 	<ul style="list-style-type: none"> ▪ Flying is not the only task! (Payloads, taxi...)

First, Table 6.22 summarizes comments related to predictors and workload. It can be seen that generally, the continuous control system is preferred when predictors are available, when flying is the only task or when the flying task is sufficiently simple. The subjects' remarks show that the appearance of the predictors could be improved in many respects. Nonetheless, there is a general agreement that predictors are very helpful, which underscores the positive ratings shown in Figure 6.35.

Table 6.23 – Rewritten pilot comments related to latency, precision and flight phase

In which situations do you think a continuous control system is more helpful or better suited than an on-off control system?	In which situations do you think an on-off control system is more helpful or better suited than a continuous control system?
Latency	
<ul style="list-style-type: none"> ▪ Without time delay ▪ With little time delay 	<ul style="list-style-type: none"> ▪ With large latency, on-off control is more effective. ▪ When latencies are extreme (higher even than in the experiment)
Precision	
<ul style="list-style-type: none"> ▪ When fine-tracking needs to be performed ▪ Precise flight maneuvers ▪ During landing, to be able to make precise control inputs ▪ Precise flight maneuvers ▪ Generally better, because more fine corrections are possible ▪ <i>When less accurate and precise control inputs are required</i> ▪ Fine-tracking ▪ Precise flying ▪ For accurate guidance needing small corrections (taxi, payload piloting, air-to-air refueling, emergency landing) 	<ul style="list-style-type: none"> ▪ <i>When predictors are available, on-off control is easier and more precise.</i>
Flight Phase	
<ul style="list-style-type: none"> ▪ When small corrections are necessary (e.g., during landing) ▪ In “agile” situations (e.g., swing-over), where quick changes are required ▪ Flare ▪ During landing, to be able to make precise control inputs ▪ Approach 	<ul style="list-style-type: none"> ▪ “Simple” flight phases like straight flight or standard turns ▪ Turns, climb / descent ▪ Cruise flight / level flight ▪ <i>Final approach and landing</i>

Next, Table 6.23 lists comments related to latency, precision and flight phase. Several pilot comments appreciate the usefulness of on-off control in the presence of large time delays. Below, plenty of comments state that the continuous control system is better suited for precision maneuvers, whereas only two comments oppose this majority opinion. The quantitative performance metrics that led to the confirmation of hypothesis 3 in section 6.4.3 are in opposition to this general belief. Here again, some trained pilots seem to be biased against the new, unconventional type of control system. Acceptance for on-off control may not be high among airplane pilots. The last section of Table 6.23 lists the flight-phase dependent preferences expressed by some subjects. The majority of comments here favor continuous control in high-bandwidth flight phases, or consider on-off control more suitable for category C flight phases. This subjective impression can be neither supported nor opposed by objective measures. From the performance metrics analyzed in tasks C and D, however, it seems that there is indeed a difference between flight phases. While the on-off control system allowed better performance in some cases during initial approach, it seemed to be no different than the continuous control system during final approach (cf. section 6.4.3).

Table 6.24 – Rewritten pilot comments related to other aspects

In which situations do you think a continuous control system is more helpful or better suited than an on-off control system?	In which situations do you think an on-off control system is more helpful or better suited than a continuous control system?
Control Amplitudes	
<ul style="list-style-type: none"> ▪ When many small corrections are necessary (e.g., during landing) ▪ In “agile” situations (e.g., swing-over), where quick changes are required ▪ Reactions can be made quicker (e.g., evasive maneuvers) ▪ When very different amplitudes are required 	<ul style="list-style-type: none"> ▪ Large amplitudes ▪ When the pilot wants to follow a (target) trajectory without large control inputs (stationary flight)
Task and Target Type	
<ul style="list-style-type: none"> ▪ One-dimensional tracking of a slowly moving target ▪ Tracking tasks A, B ▪ Continuous tracking of continuous deviations 	<ul style="list-style-type: none"> ▪ Step-changes in target parameters ▪ Step-changes
General / Other	
<ul style="list-style-type: none"> ▪ Generally better, because finer corrections are possible 	<ul style="list-style-type: none"> ▪ In all situations except for when a predictor is available or in “agile” situations (e.g., swing-over) ▪ Virtually never ▪ Hard to say ▪ In situations prone to oversteering ▪ Most of all during the initial phase

All remaining categories of comments are listed in Table 6.24. Those comments related to control amplitudes are rather inconsistent. It seems that many different opinions exist about which control system type is better suited for large inputs or quick maneuvers. The statement that continuous control is preferable when different control input amplitudes are required is, of course, correct. In what situations they are required, however, is a question that remains unanswered. The fact that the theoretical minimum completion time of task A as described in section 6.4.1 is increased with on-off control shows that, depending on the actual control sensitivity, a continuous control system may indeed enable larger control amplitudes and thereby faster maneuvers.

Pilot comments categorized as related to task and target type show that continuous control is favored for (continuous) tracking tasks and on-off control when following target steps. This may be due to the fact that the ramp in task B's forcing function (cf. Figure 6.8) was more difficult to follow with $\dot{\gamma}$ fixed by the on-off control system. This is indeed a valid point. Most of the remaining comments in Table 6.24 express general preferences that are inconsistent. One noteworthy pilot comment states that on-off control may be better suited during the initial (training) phase.

Table 6.25 – Rewritten pilot remarks and suggestions

Do you have any further remarks or suggestions for improvements?
Training
<ul style="list-style-type: none"> ▪ Guess: continuous control requires more training, but then enables more precise control ▪ After some more training, continuous control will probably enable better performance, because on-off control requires more constant attention (counting)
Other Remarks
<ul style="list-style-type: none"> ▪ For both continuous and on-off control system, the control sensitivity has a large influence on handling. What sensitivity is appropriate depends on the situation. ▪ The (“haptic”) control feel of the continuous control system is more comfortable. ▪ Deadzone must be eliminated or reduced (stick) ▪ Apart from the final approach, I was satisfied with the run with continuous control system + predictor. ▪ Good way to go!
Suggestions
<ul style="list-style-type: none"> ▪ May on-off control with two reaction intensities make sense? ▪ On-off control with two intensities ▪ Wings-level button would be helpful ▪ Make it possible to affect longitudinal and lateral motion separately

Two of the further remarks and suggestions, listed in Table 6.25, express similar opinions. Indeed, the suspicion that on-off control brings the most advantage in the learning phase and becomes less beneficial as pilots learn to fly with large time delays is backed up by the quantitative evaluation of workload and performance from task A through task D.

Notable other remarks concern the suitability of control sensitivity levels, an issue that is explored in section 6.4.2, and the control feel of the inceptor, indicating that the on-off inceptor characteristics as implemented in the active sidestick can be improved. Furthermore, the deadzone in the continuous sidestick characteristics was too large for one subject, as a previous paragraph also mentions.

The subjects' suggestion to implement on-off control with more than one amplitude level shows that this idea, also presented in section 4.3.1, may have potential. The same paragraph in section 4.3.1 also proposes buttons that cause the airplane to return to straight and/or level flight – a concept that can be found again as a suggestion here in Table 6.25. The final comment about the possibility to separately control longitudinal and lateral motion was made, as the subject orally confirmed, because he involuntarily produced control inputs in one axis while he made a deliberate input in the other axis using the continuous control system. This problem had been observed in preliminary tests and the sidestick's dead zone had been increased as a consequence (cf. section 6.2.2). It seems, though, that this solution was not sufficient for this particular subject. Considering that another subject complained about the large deadzone, it can be concluded that involuntary cross-channel control inputs in the case of a continuous control system should not be prevented with a large deadzone. Instead, the inceptor position could be varied, so that the pilot's limb can easily perform pure lateral and pure longitudinal movements. Another option is to implement a noticeable breakout force. Incidentally, this would make the continuous control inceptor feel a little more like the on-off control inceptor.

6.5 Experimental Pilot Model Validation

In the final part of this chapter, recordings from the experiments on manual remote flight control are used to validate the dual-mode pursuit tracking pilot model presented in section 3.3.3 of this thesis. In section 6.5.1, the model is first applied to task A to showcase and evaluate some basic characteristics and the effect of parameter variations. Then, parameters are fitted to the experimental data from task A and the ability of the model to replicate the human control behavior in a pure pursuit tracking task is assessed. In section 6.5.2, the model is applied to task B and again fitted to experimental data to obtain more insight into the validity of the model for different types of tracking tasks and control sensitivities. Prior to any simulation or application, the pilot model was implemented in MATLAB, Simulink and Stateflow [153]. Interfacing with the airplane and task simulations, which had been implemented in the same environment, was therefore straightforward.

6.5.1 Pure Pursuit Tracking

For an initial model analysis, the two noises $n_{\dot{e}}$ and $n_{\dot{y}_{ss}}$ are suppressed. Hence, the only human imperfections modelled are the CNS's time delay and the neuromuscular system with its lags and noise. With this setting, the correct functioning of the state machine can be verified and an upper bound for task performance can be obtained. Then, each of the noises $n_{\dot{e}}$ and $n_{\dot{y}_{ss}}$ is activated separately to analyze their effects. The last steps consist in fitting the model to experimental data and assessing the validity of the model.

Figure 6.43 shows a simulation of the pilot model performing task A with the on-off control system, with both noises $n_{\dot{e}}$ and $n_{\dot{y}_{ss}}$ suppressed. The first plot shows system input and output and thereby illustrates tracking performance. The plot furthermore lists three relevant quantitative metrics of the task: completion time, normalized completion time and control energy. The values of these metrics are all smaller than those achieved by human subjects (cf. section 6.4.1). Interestingly, however, even with the noises $n_{\dot{e}}$ and $n_{\dot{y}_{ss}}$ inhibited, the pilot model does not achieve the theoretical minimum completion time. This can be explained by the fact that the model comprises additional time delays τ_{cns} and τ_{nm} that prolong task execution. Moreover, the computation of the move phase duration aims at exactly reaching the target, whereas task completion time could be further reduced by acquiring only the tolerance threshold. Generally, it can be seen that the model not only achieves stable target tracking, like a human pilot, but also correctly reproduces optimum performance.

The second plot shows the control action δ produced by the model. The qualitative appearance of the plot indicates that the model produces control actions that are achievable by a human pilot. Neither the time between control inputs nor the control inputs themselves are too short. Control activity is generally realistic. By comparing the first and the second plot, it can be seen that every target is acquired by one single control input. This is in line with the very small control energy produced and the overall good performance achieved by the model.

The third plot in Figure 6.43 reveals the behavior of the model's state machine by showing the state activity over time. Each line corresponds to one of the six states: Idle (I), Move (M), Modify Move (MM), Interrupt Wait (IW), Wait (W) and Closed-Loop Control (CL). State transitions can be recognized by grey vertical lines. On the right abscissa, the amount of time spent in each state during the entire simulation is indicated in percent. Note that the states Modify Move and Interrupt Wait did not occur at all in this simulation. This is in accordance with the design of task A, where the target only moves 5 s after the tolerance band has been reached (cf. section 6.3.1). As a result, the target only moves when the state machine is in the Idle state. Thus, transitions into the states Modify Move and Interrupt Wait cannot be triggered (cf. Figure 3.26). The wait phases in Figure 6.43 all have the same duration $t_w = 2.54$ s, because they are never interrupted. A final aspect to note in Figure 6.43 is that most targets are acquired using the move-and-wait strategy and that target acquisition in this case is almost flawless, with the exception of slight inaccuracies introduced by the neuromuscular system dynamics. When closed-loop control is performed, on the other hand, the model does not aim for zero error, but for the tolerance band, which is indeed acquired in an equally accurate manner. This minor difference between move-and-wait strategy and closed-loop control is only relevant for large values of e_{tol} and could then be corrected by increasing the value of K_p .

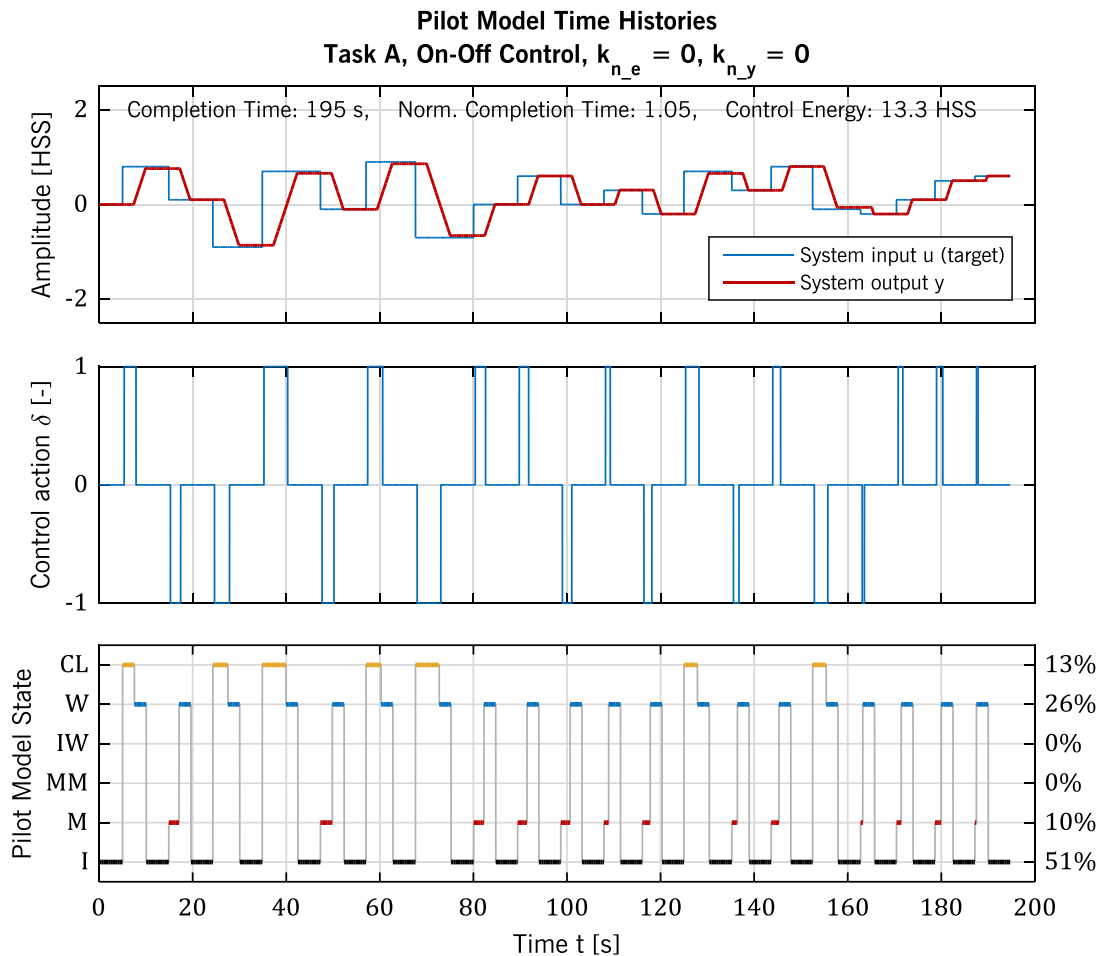


Figure 6.43 – Pilot model simulation: task A, on-off control, minimum noise

Next, Figure 6.44 shows a simulation of task A performed by the pilot model using a continuous control system and applying maximum input aggressiveness. Here, several new observations can be made. First, it is apparent that closed-loop control never occurs. This is due to the fact that, with $K_{agg} = 1$, the effective reaction magnitude \hat{y}_{ss} is so large that for every target step, $e \leq k_y \cdot \hat{y}_{ss} \cdot \tau_t$. Thus, the state machine cannot transition to the Closed-Loop Control state (cf. section 3.3.3). Since, in the simulation shown in Figure 6.44, every target is acquired using the move-and-wait strategy, the model aimed for zero error in those cases where, in the simulation shown in Figure 6.43, it only aimed for the tolerance band while performing closed-loop control. As a result, the value of control energy is slightly larger in Figure 6.44. Finally, the neuromuscular system dynamics, including the noise, can be recognized in the plot of control action of Figure 6.44.

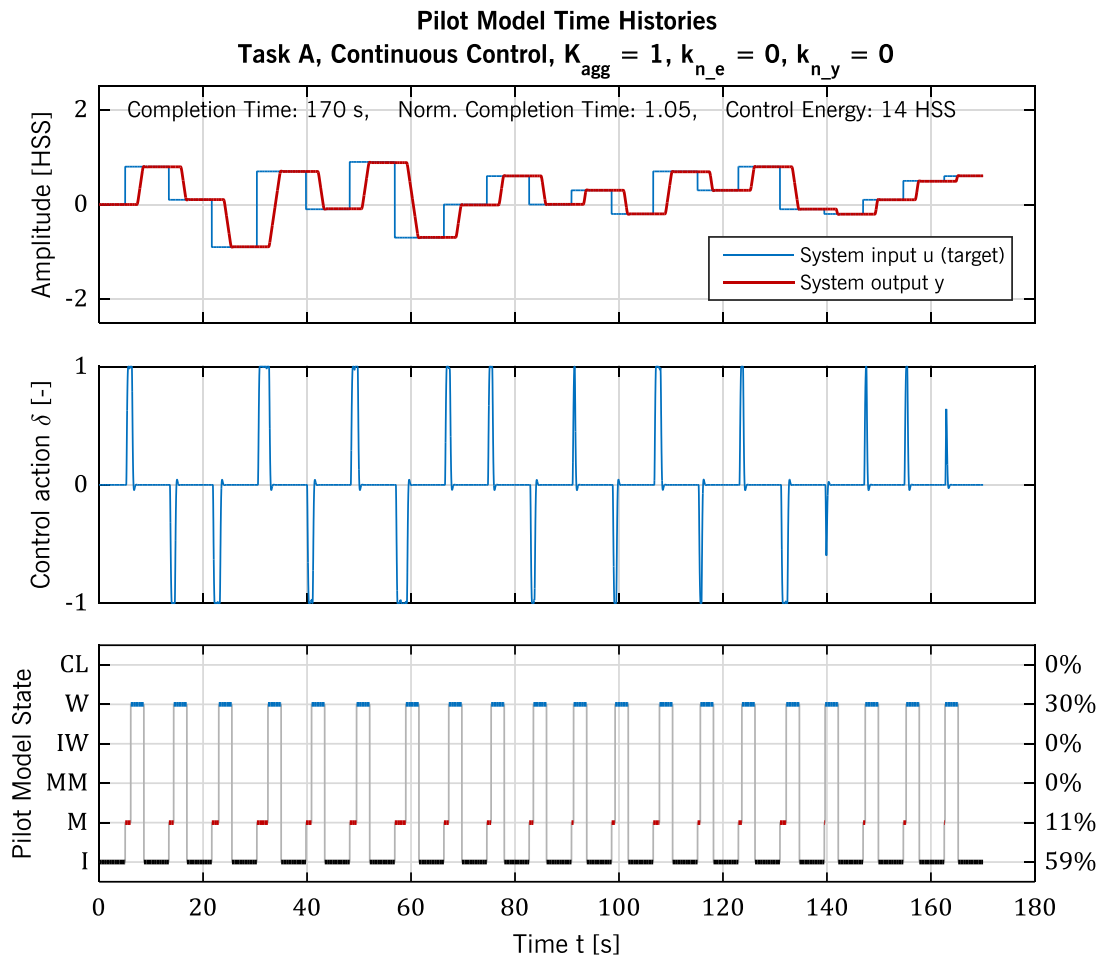


Figure 6.44 – Pilot model simulation: task A, continuous control, minimum noise

After the analysis of pilot model simulations without the noises n_e and n_y , the effect of each of these noises shall now be illustrated by simulations with extreme values of k_{n_e} and k_{n_y} . Figure 6.45 shows the simulation time histories of the pilot model in task A, using the continuous control system and applying an input aggressiveness $K_{agg} = 0.4$. The noise n_y is still suppressed, but k_{n_e} , on the other hand, is set to a value of 0.2. Due to the smaller input aggressiveness as compared to the simulation shown in Figure 6.44, closed-loop control does occur for larger target steps. Moreover, the neuromuscular noise is more clearly visible in Figure 6.45 than in Figure 6.44 and the completion time is prolonged. In fact, the value of K_{agg} here exactly cancels the difference in control sensitivity between the continuous control system and the on-off control system. As a result, the completion time would resemble that of the simulation shown in Figure 6.43 if n_e would be suppressed. Without the noise n_y , the move-and-wait strategy is flawlessly applied. Closed-loop control, on the other hand, is affected by the extreme noise n_e . Thus, under- and overshoots occur frequently, further prolonging the task completion time and increasing the control energy. Note that at $t = 183$ s, a control input is applied in the wrong direction, away from the target. This shows that the noise power is not only extreme, but already excessive.

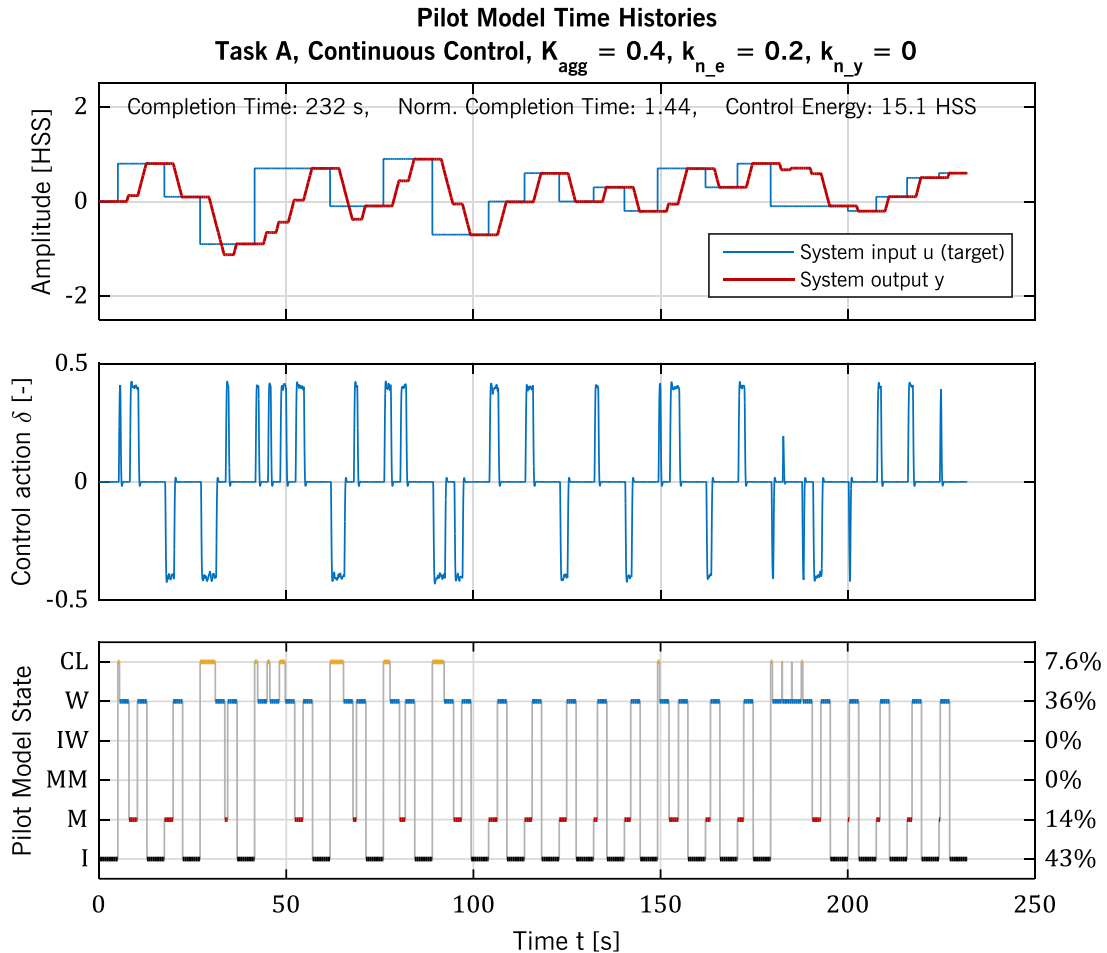


Figure 6.45 – Pilot model simulation: task A, continuous control, extreme noise n_y

Next, the effects of the noise n_y are illustrated. Figure 6.46 shows a simulation of the pilot model using on-off control and, again, performing task A. Here, n_e is suppressed, whereas $k_{n_y} = 0.1$ is chosen. The most obvious effect of the noise n_y is that large under- and overshoots occur when the move-and-wait strategy is applied. Another effect, which is more difficult to see in Figure 6.46, is that closed-loop control is sometimes not employed, even though the error would be large enough. This is the case at $t = 65$ s. Similarly, closed-loop control is sometimes erroneously attempted. This can be observed at $t = 115$ s and at $t = 152$ s, where the error is so small that the move-and-wait strategy would have to be applied. As a consequence, large overshoots occur. Note that in these cases the duration of the Closed-Loop Control state is exactly τ_t , because closed-loop control is not affected by noise and therefore flawlessly executed. As soon as the delayed system reaction is “perceived” by the model, the lead time constant causes the decision mapping element to switch (cf. Figure 3.28, Figure 3.31 and Figure 3.20) and thus, the transition to the Wait state is triggered. Finally, the large increases in tracking error that the model produces at $t = 155$ s and $t = 262$ s confirm that $k_{n_y} = 0.1$ is already an extreme value.

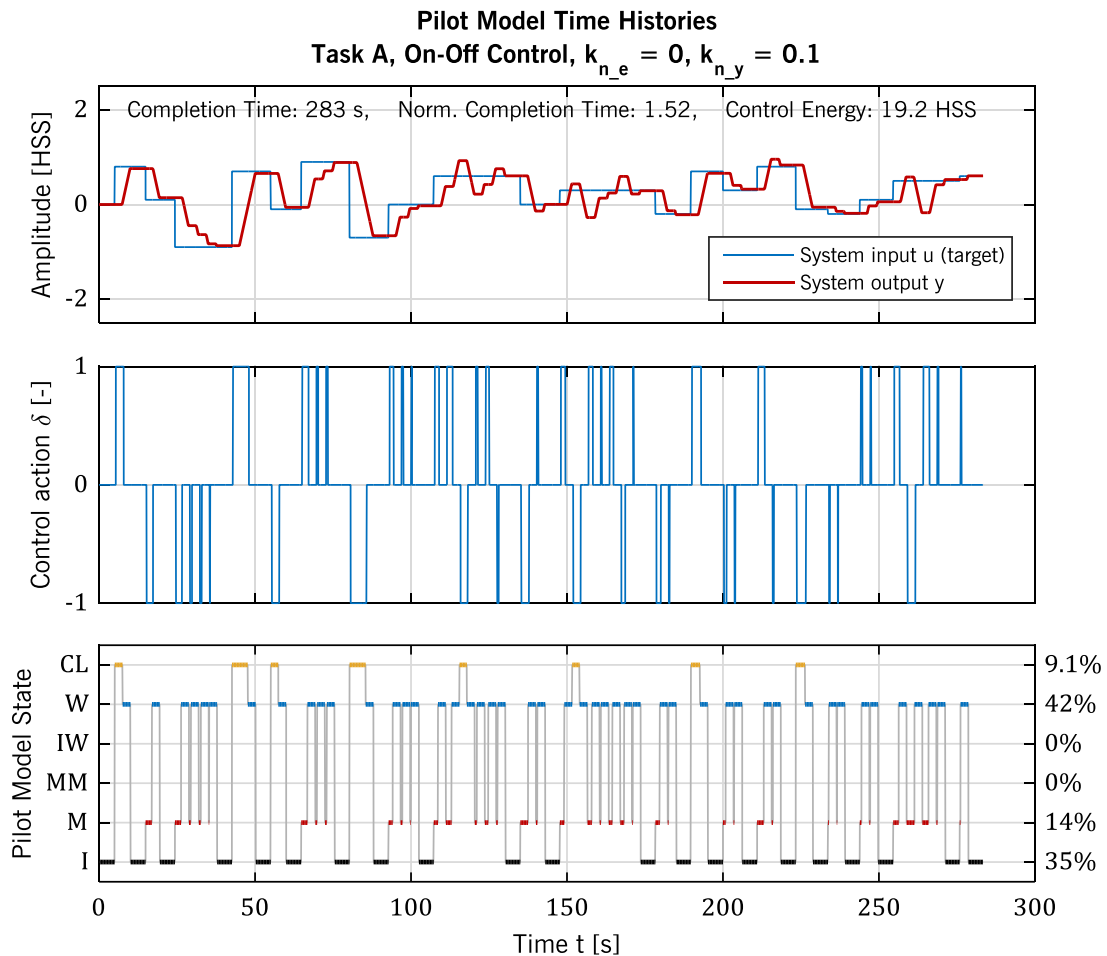


Figure 6.46 – Pilot model simulation: task A, on-off control, extreme noise n_e

The previous paragraphs have shown that the implementation of the pilot model behaves as expected and that the model successfully accomplishes task A with human-like control activity. Moreover, the effects of the noises n_e and n_y have been illustrated. In the following paragraphs, the model is fitted to experimental data to obtain suitable values for k_{n_e} , k_{n_y} and K_{agg} and to more thoroughly assess the validity of the model.

Since the model was not designed to describe learning, the second run of each subject, during which the change in control behavior due to learning was certainly less important than in the first run, shall serve as a reference. The process of fitting the three model parameters to the experimental data was chosen as follows. First, k_{n_e} and k_{n_y} are varied so that completion time and control energy of the pilot model simulation, using on-off control, are similar to the values achieved by the experiment subjects. Note that it is not necessary to take the normalized completion time parameter into account, since completion time and normalized completion time are equivalent if only one control system type is used. The resulting value of k_{n_e} can also be employed with the continuous control system. The parameter k_{n_y} , on the other hand, may differ between control system types, since the power of n_y is hypothesized to be larger in the case a continuous control system is used (cf. section 3.3.3). Hence, the second step consists in varying K_{agg} and k_{n_y} to

match completion time and control energy of the pilot model simulation, using continuous control, with the values achieved in the experiments.

Suitable values of k_{n_e} and k_{n_y} were expected to lie between 0 and the extreme values illustrated above, i.e., 0.2 for k_{n_e} and 0.1 for k_{n_y} . These ranges of values were discretized with a sample spacing of 0.01, resulting in 21 values of k_{n_e} and 11 values of k_{n_y} . It was planned to then perform pilot model simulations for all 231 parameter value combinations. However, a simulation with $k_{n_e} = 0.17$ did not terminate within a reasonable amount of time, which indicates that this parameter value is already excessive. With the range of possible k_{n_e} values reduced, 187 simulations were executed in total. The resulting values of completion time and control energy are illustrated by Figure 6.47.

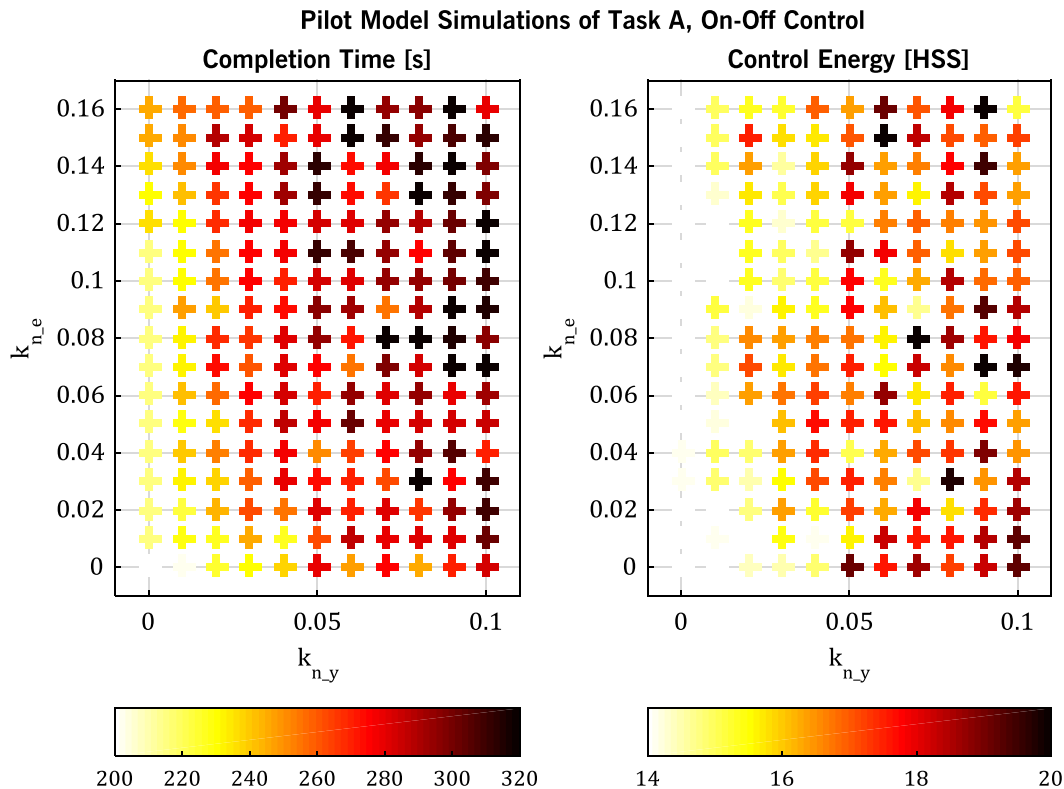


Figure 6.47 – Metrics of pilot model simulations, task A, on-off control

It can be seen that completion time increases with both parameters k_{n_e} and k_{n_y} . In Figure 6.47, it is therefore lowest for $k_{n_e}, k_{n_y} \approx 0$. Changes in completion time across both model parameters are quite smooth. Changes in control energy, on the other hand, are less smooth. This difference can be explained by the fact that both undershooting and overshooting the target equally prolongs the completion time, whereas only overshoots increase the control energy required to reach the target. Due to the nondeterministic nature of the noises, the model produces a different number (and size) of overshoots and thus a different amount of control energy in two different simulations with similar completion time, even if the same model parameter values are employed.

It can also be noted that control energy mainly varies with k_{n_y} or, in other words, that the value of k_{n_e} has little influence on control energy. This leads to the conclusion that, when

closed-loop control is applied, undershoots occur more frequently than overshoots. One possible reason for this imbalance is the shape of the noise spectrum S_{nn_e} . The noise has zero mean, so both increases and decreases of the perceived error rate by the noise are equally probable. A decrease causes a late transition to the Wait state and thereby an overshoot, whereas an increase causes premature transitioning. It thus seems that similar numbers of over- and undershoots should occur. However, if the noise spectrum contains too much high frequency components, the sign of n_e changes relatively often and, as a result, the perceived error rate is increased and decreased in quick succession. In a prolonged phase of closed-loop control, it is highly probable that the perceived error rate is increased at some moment, thus causing premature transitioning even if the error rate was decreased by the noise for most of the time. It can thus be concluded that the noise spectrum S_{nn_e} should have a lower cutoff frequency than the one chosen, so that it contains less high frequency components.

To identify suitable values of k_{n_e} and k_{n_y} despite the sudden changes in control energy between neighboring simulation data points, the data points are averaged. In Figure 6.48, every point indicates the average completion time or control energy of the respective $(k_{n_y}|k_{n_e})$ data point and the 8 neighboring data points. For instance, the completion time at point (0.02|0.02) in Figure 6.48 is the average completion time of the points (0.01|0.01), (0.01|0.02), (0.01|0.03), (0.02|0.01), (0.02|0.02), (0.02|0.03), (0.03|0.01), (0.03|0.02) and (0.03|0.03) of Figure 6.47. Figure 6.48 also shows contour lines, which are drawn at the 1st, 2nd and 3rd quartile level of the experimental data (cf. Figure 6.10 and Figure 6.11).

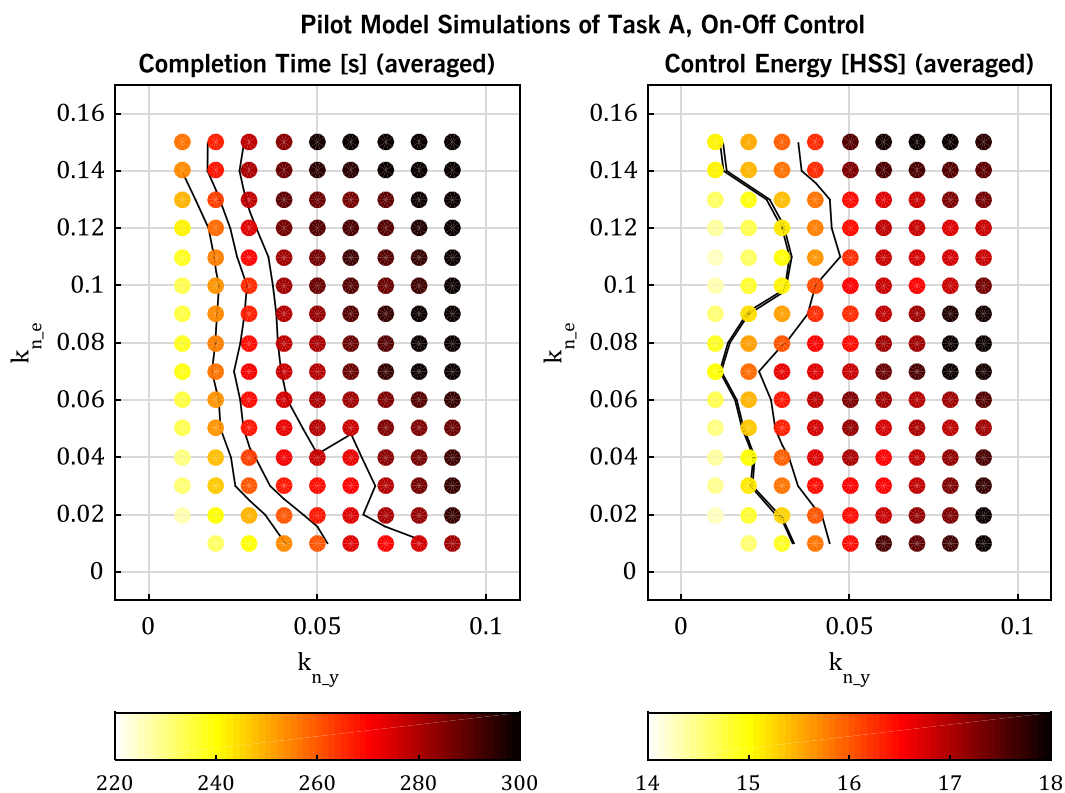


Figure 6.48 – Averaged metrics of pilot model simulations, task A, on-off control

Only few points lie well within both sets of contour lines. Considering that a simulation with $k_{n_e} = 0.17$ did not terminate, those points in the upper range of k_{n_e} values seem too extreme. In the range of moderate k_{n_e} values, the point that fits best to both sets of contour lines is (0.03|0.09). A comparison of experimental run Ao of subject 7, who achieved average completion time and control energy values, with a pilot model simulation with $k_{n_y} = 0.03$ and $k_{n_e} = 0.09$ is shown in Figure 6.49. The general appearance of both time history plots is very similar. This indicates that the model indeed well describes on-off control in task A. One notable difference, however, is that the tracking performance of subject 7 seems to improve along the run, whereas the model's performance is rather constant. This shows that subject 7 still learned and confirms again that the model does not describe learning.

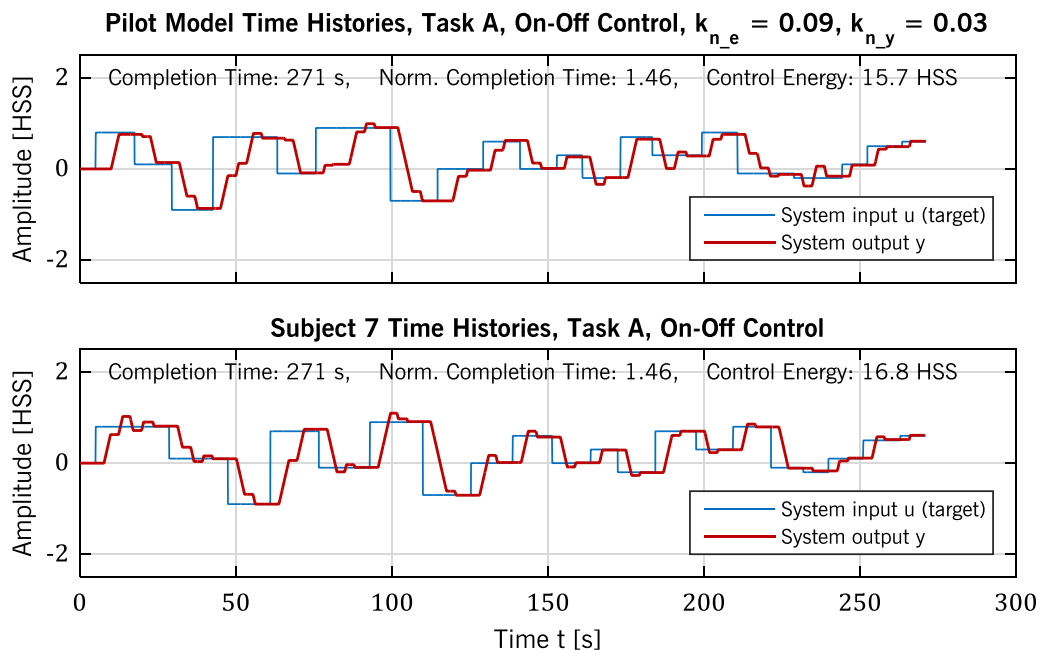


Figure 6.49 – Comparison of pilot model simulation and experimental run Ao

For the following analysis of continuous control during task A, the value of $k_{n_e} = 0.09$ remains unchanged. This time, however, K_{agg} and k_{n_y} are varied to match completion time and control energy of the pilot model simulation with the values achieved in the experiments. First simulations, which employed similar k_{n_y} values as above, produced very poor task performance, indicating an excessive n_y power. It was suspected that this was due to the factor K_a in the numerator of S_{nn_y} , which was 2.5 times as large for the continuous control system as compared to the on-off control system. It was thus decided to retry the simulations with a different definition of the noise spectrum S_{nn_y} . This definition, which is given by equation (6.6), only differs from the original definition (cf. equation (3.48)) in the additional factor K_{agg} for continuous control systems.

$$S_{nn_{\dot{y}}}(\omega) = \frac{k_{n_{\dot{y}}} \cdot \dot{y}_{ss}}{0.5j\omega + 1} = \begin{cases} \frac{k_{n_{\dot{y}}} \cdot K_a}{0.5j\omega + 1} & \text{for on-off control systems} \\ \frac{k_{n_{\dot{y}}} \cdot K_{agg} \cdot K_a}{0.5j\omega + 1} & \text{for continuous control systems} \end{cases} \quad (6.6)$$

Using the spectrum defined by equation (6.6), a total of 110 simulations were performed to identify suitable values of K_{agg} and $k_{n_{\dot{y}}}$. For $k_{n_{\dot{y}}}$, the same 11 values were selected as above for the on-off control system. For K_{agg} , 10 evenly spaced values between 0.1 and 1 were chosen. Figure 6.50 illustrates the simulation results of all parameter value combinations. In addition to the values of completion time and control energy resulting from each simulation, contour lines are shown like in Figure 6.48. These contour lines originate from the same averaging operation described above. They again indicate the 1st, 2nd and 3rd quartile level of the corresponding experimental data (cf. Figure 6.10 and Figure 6.11).

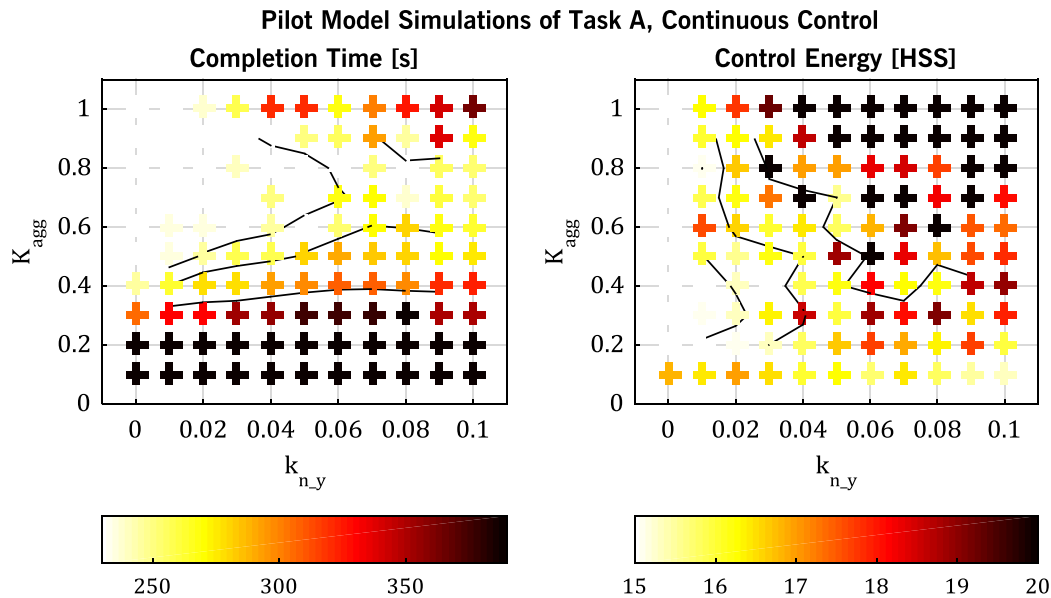


Figure 6.50 – Metrics of pilot model simulations, task A, continuous control

Here, it can be seen that completion time initially reduces with increasing input aggressiveness, which makes perfect sense given that a larger value of K_{agg} enables the model to reach every target more quickly. At high values of K_{agg} , however, completion time increases again due to the corresponding increase in $n_{\dot{y}}$ power. Likewise, control energy increases with K_{agg} , but also with $k_{n_{\dot{y}}}$, because both parameters are factors in the noise spectrum $S_{nn_{\dot{y}}}$. The selection of a suitable pair of parameter values is straightforward. The point that is closest to the intersection of both 2nd quartile contour lines is (0.04|0.5). Note that this value of K_{agg} almost exactly cancels the difference in control sensitivity between the continuous control system and the on-off control system. Equation (6.7) recapitulates the $n_{\dot{y}}$ noise spectra found suitable for task A. Note that the noise power is indeed larger if a continuous control system is employed instead of an on-off control system, as hypothesized in section 3.3.3.

$$S_{nn_y}(\omega) = \begin{cases} \frac{0.009}{0.5j\omega + 1} & \text{task A, on-off control system} \\ \frac{0.015}{0.5j\omega + 1} & \text{task A, continuous control system} \end{cases} \quad (6.7)$$

Figure 6.51 shows the time histories of a pilot model simulation with the selected parameter values next to those of an average experimental run, performed by subject 6. As expected, completion time and control energy of simulation and experiment are very similar. Beyond that, it can be seen that subject 6 often made larger but shorter control inputs than the model. This indicates that the K_{agg} value chosen is too small. Simply increasing this value, however, would not improve the match between model and reality. Subject 6 effectively varied K_{agg} between control inputs. As apparent from Figure 6.51, his strategy for target acquisition was to make a first input with high aggressiveness and then successively decrease K_{agg} to approach the target more and more cautiously. With this strategy, subject 6 produced few overshoots and little control energy, but required more time to acquire each target. The pilot model does not describe this strategy. Extending it by a model for variations in aggressiveness could solve this issue.

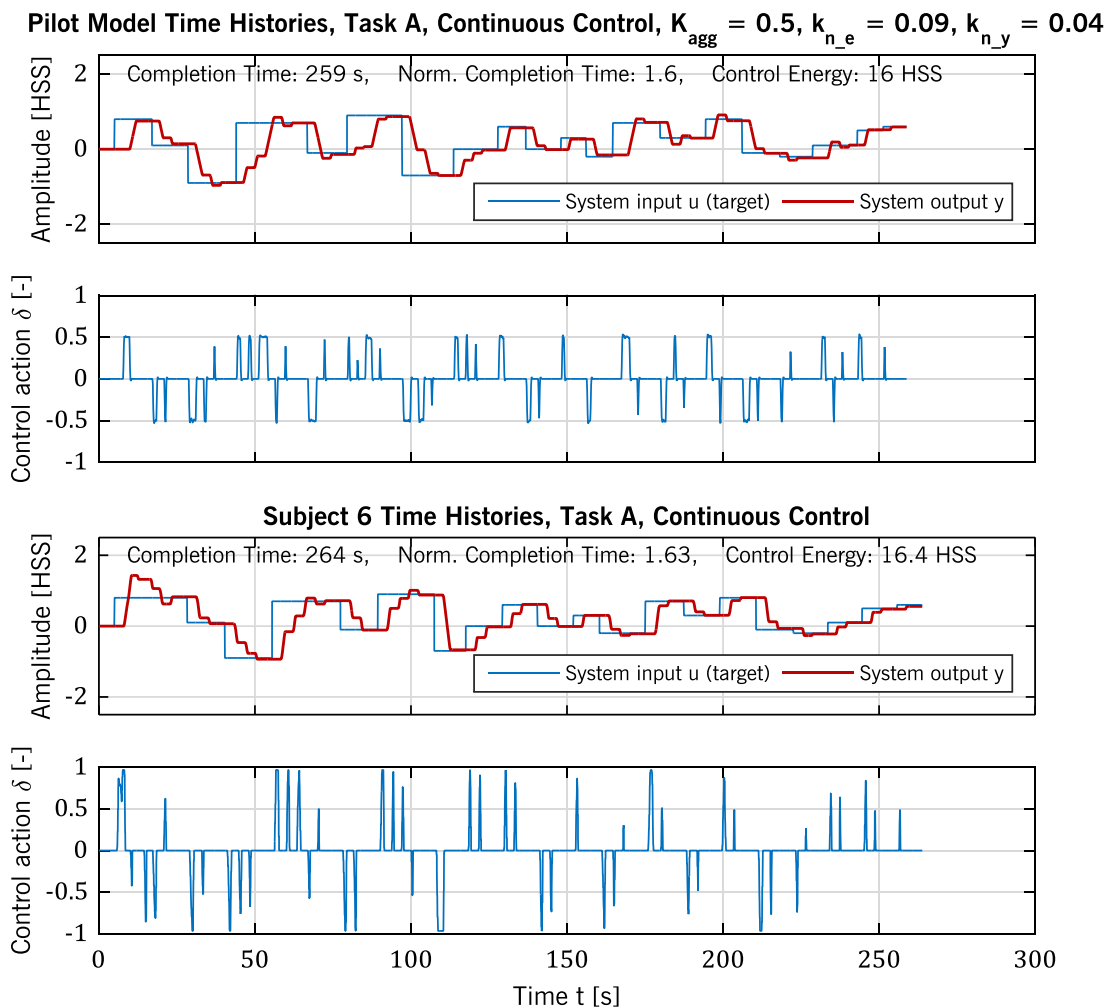


Figure 6.51 – Comparison of pilot model simulation and experimental run Ac

All in all, it can be said that the dual-mode pursuit tracking pilot model presented in section 3.3.3 well describes pure pursuit target tracking tasks like task A. In simulations, the model achieves similar performance and produces similar control activity like human subjects. Model fitting showed that the power of n_y is indeed higher if a continuous control system is employed instead of an on-off control system, thus validating the description of differences between control system types given in section 3.3.3. The initial definition of the noise spectrum S_{nn_y} was corrected to better describe changes of the noise power due to variations in control sensitivity and input aggressiveness. Remaining minor shortcomings of the proposed model, which can easily be corrected in the future, are the excessively high cutoff frequency of the noise spectrum S_{nn_e} and the inability to describe the strategy of approaching a target with decreasing input aggressiveness. Effects of time delay variations, most notably those on S_{nn_e} , could not be validated due to the absence of experimental data for τ_a values different from 2 s.

6.5.2 Pursuit and Pre-Cognitive Tracking

This section describes the application of the dual-mode pursuit tracking model proposed in section 3.3.3 to task B. This application is more explorative than pilot model simulations with task A, because task B is not a pure pursuit tracking task. To some degree, experiment subjects were able to perform pre-cognitive tracking in the sense that future tracking targets were predictable. This was, for instance, the case during the two ramps included in the forcing function (cf. Figure 6.8). Moreover, the fact that a Θ forcing function was low-pass filtered to obtain a γ forcing function meant that the initial rate of change $\dot{\gamma}_{tgt}$ following a step in the original Θ forcing function could be used to predict the steady-state target change $\Delta\gamma_{tgt,ss}$. The model, as it is described in section 3.3.3, was not designed to describe this kind of pre-cognitive tracking. It is therefore not expected to correctly describe all aspects of the experimental runs of task B.

First, the model is applied to on-off control of task B with sensitivity level S2, i.e., the baseline sensitivity level. Then, continuous control of the same task and sensitivity level is investigated. An outlook is then given on the application of the model to all other combinations of control system type and sensitivity level. Since a tolerable error was not defined for task B, the value of the model parameter e_{tol} is derived from equation (3.44). To obtain accurate comparisons between model and experiments, the model simulation was interfaced not only with the same task, but also with the same airplane and flight controller simulation model as employed in the experiments. The value of the parameter $\tau_{lags} \approx 0.8$ s can therefore be taken from section 4.2.3. Using equation (3.39), a total time delay $\tau_t = 3.14$ s can be computed.

As a first guess, the same values of the independent model parameters k_{n_e} , k_{n_y} and K_{agg} could be used as for task A. However, initial simulations of experimental run B2o found the resulting power of n_y to be excessive. Therefore, the range of k_{n_y} values considered was chosen one order of magnitude smaller than the range chosen for task A. Likewise, the range of values considered for k_{n_e} was enlarged, since it was uncertain whether the power of n_e really scaled with K_a , as assumed by equation (3.49). Figure 6.52 shows the

319 parameter value combinations considered and illustrates the values of RMSE, EVAR and control energy obtained from simulations with each combination. Again, contour lines indicate the 1st, 2nd and 3rd quartile level of the corresponding experimental data (cf. Figure 6.23, Figure 6.24 and Figure 6.25).

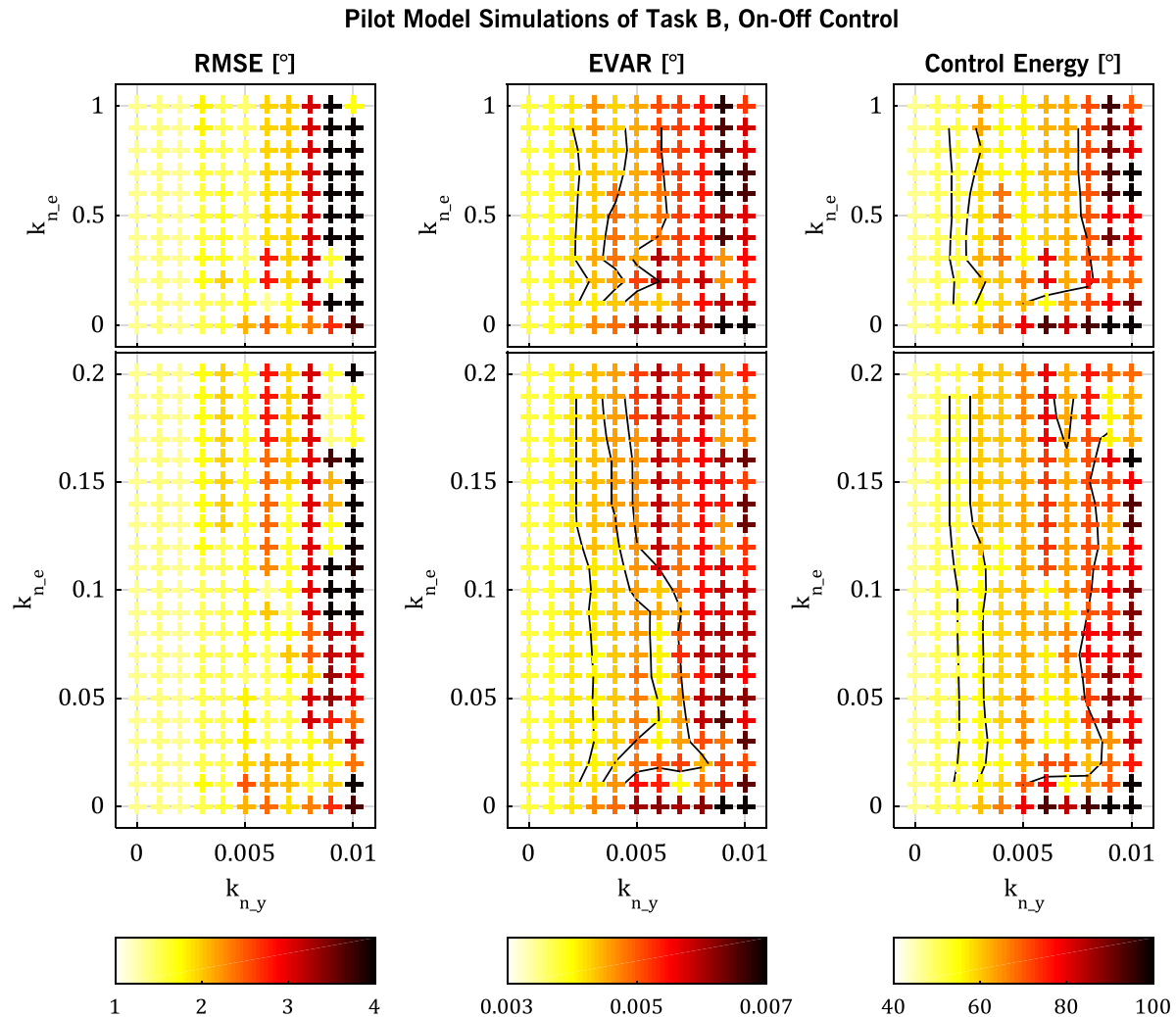


Figure 6.52 – Metrics of pilot model simulations, task B2, on-off control

First, it has to be noted that no contour lines are shown on the RMSE plot. This is due to the fact that all RMSE values obtained from simulations are higher than those obtained in experiments. Furthermore, it can be seen that, like for task A, the parameter k_{n_e} has little influence on the performance metrics, even though a much wider range of values was simulated here. One possible reason for this observation is described in the following paragraph. Regarding the contour plots of EVAR and control energy in Figure 6.52, it seems valid to employ the same k_{n_e} value for task B as for task A, namely 0.09 and to choose $k_{n_y} = 0.004$.

A comparison between a pilot model simulation with the parameter values selected above and the experimental run B2o of subject 8, who achieved average RMSE, EVAR and control energy values, is given by Figure 6.53. Although EVAR and control energy of simulation and experiment are similar, the RMSE value is much higher for the simulation.

During some phases of the task, simulation and experiment produced similar system outputs γ , although the simulation seems to generally lag behind the experiment. This can be explained by the fact that the human operator, as opposed to the pilot model, was able to act pre-cognitively. This can also explain the smaller RMSE achieved in the experiments. At some moments, the model produced control inputs that led the aircraft away from the target. Most of these hiccups can be explained by changes in γ_{tgt} during the 2 s simulated signal transmission time delay and could therefore have been produced by a human operator as well. The most extreme case at around $t = 81$ s occurs while the model is in the Closed-Loop Control state. This state is entered erroneously at this point due to the noise $n_{\dot{y}}$, since the minimum error required for transitioning into the Closed-Loop Control state is, according to equation (3.35), 6.28° . The fact that closed-loop control occurred only once erroneously explains why the value of k_{n_e} has not much influence on the performance metrics.

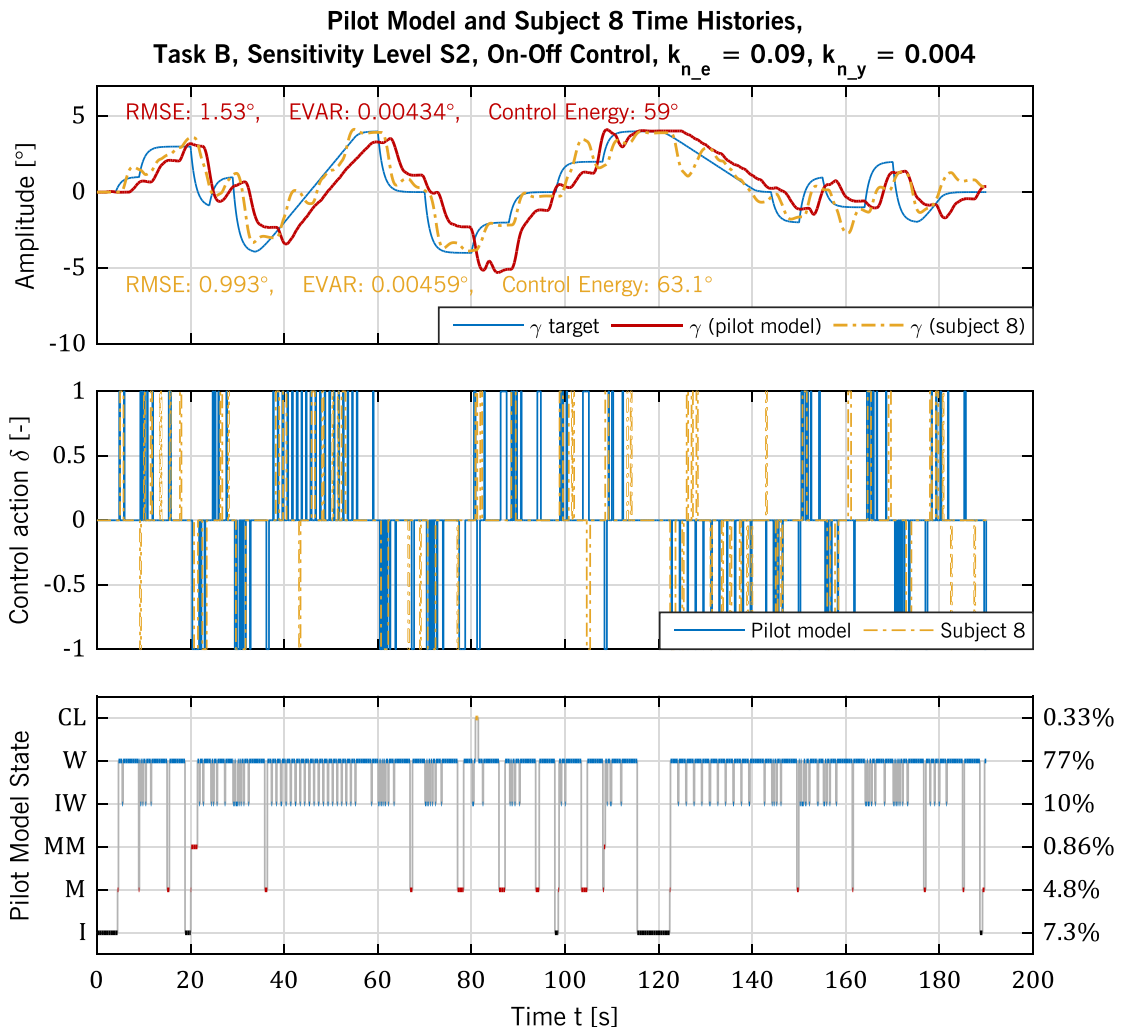


Figure 6.53 – Comparison of pilot model simulation and experimental run B2o

A major difference of the model behavior in run B2o as compared to its behavior when applied to task A is that the states Modify Move and Interrupt Wait are entered. In fact, the state machine spent more time in these states than in the Move state. The reason for this is that γ_{tgt} remained constant only for brief periods of time during task B. A varying

target may cause the pilot model to make a control input, transition to the Wait state and, as the target continues to move, transition to the Interrupt Wait state before entering the Wait state again. For rather slow but prolonged target variations, this cycle may be repeated many times. This behavior can be observed quite often in Figure 6.53, especially during the ramps of the forcing function. Repeated switching between the states Wait and Interrupt Wait can also be recognized by the pulsed appearance of control inputs. Some of these pulses are quite short, but they are never shorter than the minimum input duration $t_{m,min} = 0.15$ s assumed in section 3.3.3. The human subject generally did not employ pulsed control inputs, but many of his inputs are similar to the sum of the model's pulses and thus produce a similar system reaction. Interestingly, though, the pulse control strategy is applied by subject 8 during the target ramps, most notably between $t = 131$ s and $t = 141$ s. A major flaw associated with repeated switching between the states Wait and Interrupt Wait is that the model performs pure open-loop control during this time. Thus, tracking errors due to imprecise estimations \hat{y}_{ss} accumulate as the switching between Wait and Interrupt Wait continues, until the condition for a transition to the Closed-Loop Control state is satisfied (cf. Figure 3.26). During the simulation shown in Figure 6.53, however, the Move state is still entered often enough to prevent disproportionate tracking errors.

The fact that the k_{n_y} values suitable for run B2o are one order of magnitude smaller than those suitable for run Ao indicates that the numerator of the noise spectrum S_{nn_y} needs to be modified once again to describe how changes in control sensitivity affect the power of n_y . Instead of a linear variation with \dot{y}_{ss} , an exponential variation is proposed here. The numerator of S_{nn_y} thus reads $k'_{n_y} \cdot (\dot{y}_{ss})^k$, with an exponent k to be specified. This exponent k as well as the modified scaling factor k'_{n_y} can be derived from the system of equations (6.8), which is based on the values of k_{n_y} and K_a of the runs Ao and B2o.

$$\begin{aligned} k'_{n_y} \cdot (K_{a,Ao})^k &= k_{n_y,Ao} \cdot K_{a,Ao} \\ k'_{n_y} \cdot (K_{a,B2o})^k &= k_{n_y,B2o} \cdot K_{a,B2o} \end{aligned} \quad (6.8)$$

The system of equations (6.8) can easily be solved for both variables k and k'_{n_y} . The symbolic and numeric solutions are given by equation (6.9).

$$\begin{aligned} k &= \ln\left(\frac{k_{n_y,B2o} \cdot K_{a,B2o}}{k_{n_y,Ao} \cdot K_{a,Ao}}\right) \cdot \left(\ln\left(\frac{K_{a,B2o}}{K_{a,Ao}}\right)\right)^{-1} = 1.937 \\ k'_{n_y} &= k_{n_y,Ao} \cdot (K_{a,Ao})^{1-k} = 0.09266 \end{aligned} \quad (6.9)$$

The definition of the noise spectrum S_{nn_y} can now be corrected accordingly. Equation (6.10) provides the new definition. With this new definition, the above matching of the model with experimental data from task Ao and task B2o results in one single parameter value $k'_{n_y} = 0.09266$. Likewise, the corresponding value of k'_{n_y} for run Ac can be found to be 0.1002. For the following analyses, it is assumed that the definition of S_{nn_y} by equation

(6.10) correctly describes variations in noise power due to changes in control sensitivity and control input aggressiveness and that only a single value of k'_{n_y} can thus be used for each control system type. These values are summed up by equation (6.11).

$$S_{nn_y}(\omega) = \frac{k'_{n_y} \cdot (\dot{y}_{ss})^{1.937}}{0.5j\omega + 1} \tag{6.10}$$

$$k'_{n_y} = \begin{cases} 0.09266 & \text{for on-off control systems} \\ 0.1002 & \text{for continuous control systems} \end{cases} \tag{6.11}$$

Next, the pilot model's performance in run B2c is analyzed. Figure 6.54 shows a comparison between model simulation and experiment for this run.

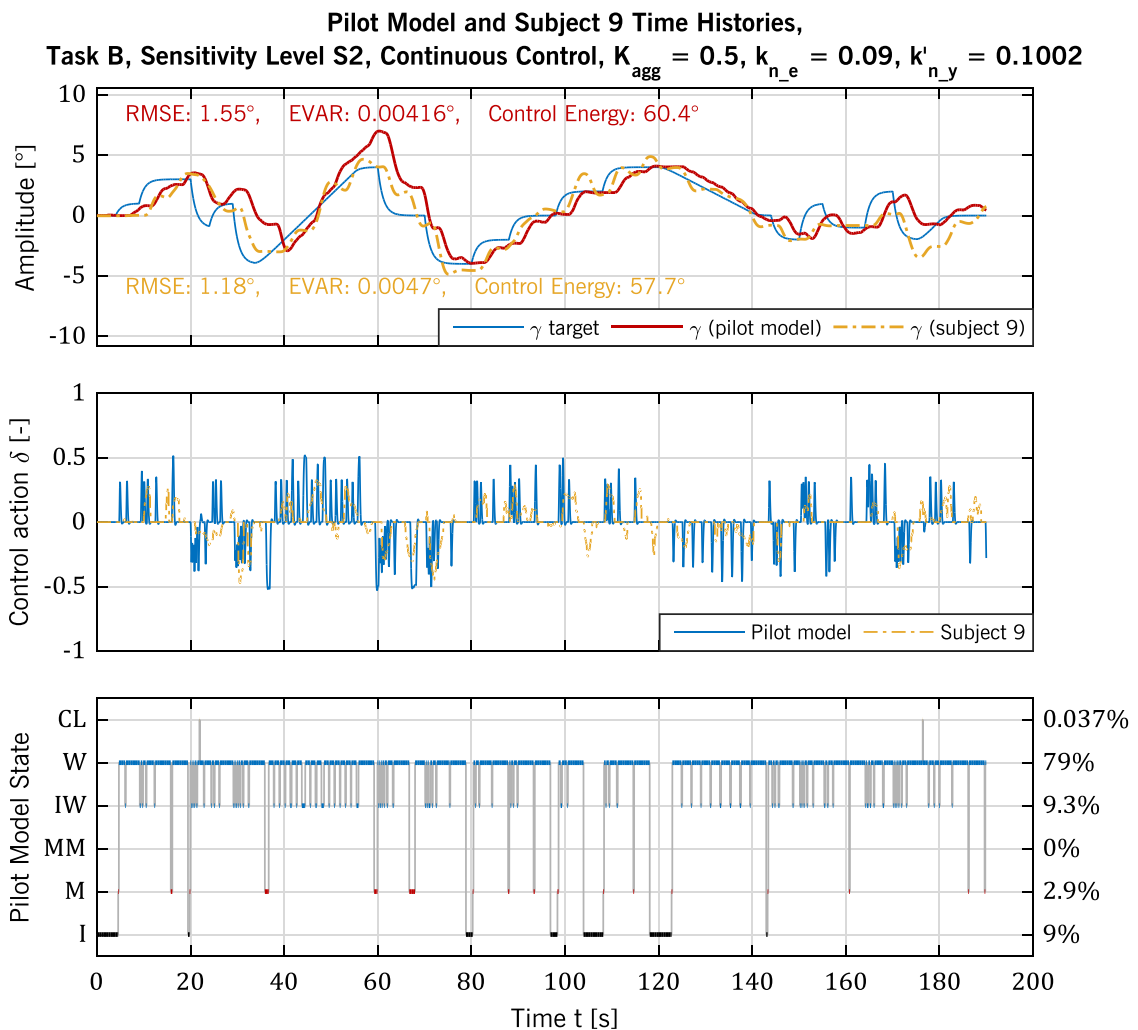


Figure 6.54 – Comparison of pilot model simulation and experimental run B2c

The same factor $K_{agg} = 0.5$ was used as for task A. This choice seems suitable, given that simulated and experimental control actions are similar in amplitude. The value of $k_{n_e} = 0.09$ was chosen to remain unchanged for all remaining analyses. In Figure 6.54, similar observations can be made as in Figure 6.53. Again, EVAR and control energy are comparable between simulation and experiment, but the RMSE is worse for the simulation.

The pulsed control inputs due to repeated switching between the states Wait and Interrupt Wait can be observed again. This time, however, a large error accumulated at the end of the first ramp, at around $t = 60$ s. According to equation (3.35), the minimum error required for transitioning into the CL state for this run and these model parameters is 7.85° . It is therefore no surprise that closed-loop control practically never occurred. In this case, the value of k_{n_e} indeed has no influence at all on tracking performance.

Based on the observations from the above simulations of task B with control sensitivity level S2, it can be expected that closed-loop control does not occur at all for control sensitivity levels S3 and S4. Indeed, the pilot model simulation of run B3o, which is compared to a representative experimental run in Figure 6.55, shows that the CL state was never entered. Apart from that, similar observations can be made as for the simulations of sensitivity level S2. Control energy and EVAR produced by the model are slightly smaller than the experimental values, whereas RMSE is much larger for the simulation. The model produces pulsed control inputs by repeatedly switching between the states Wait and Interrupt Wait. The γ output of simulation and experiment are similar in some phases, but the simulation tends to lag behind the experiment.

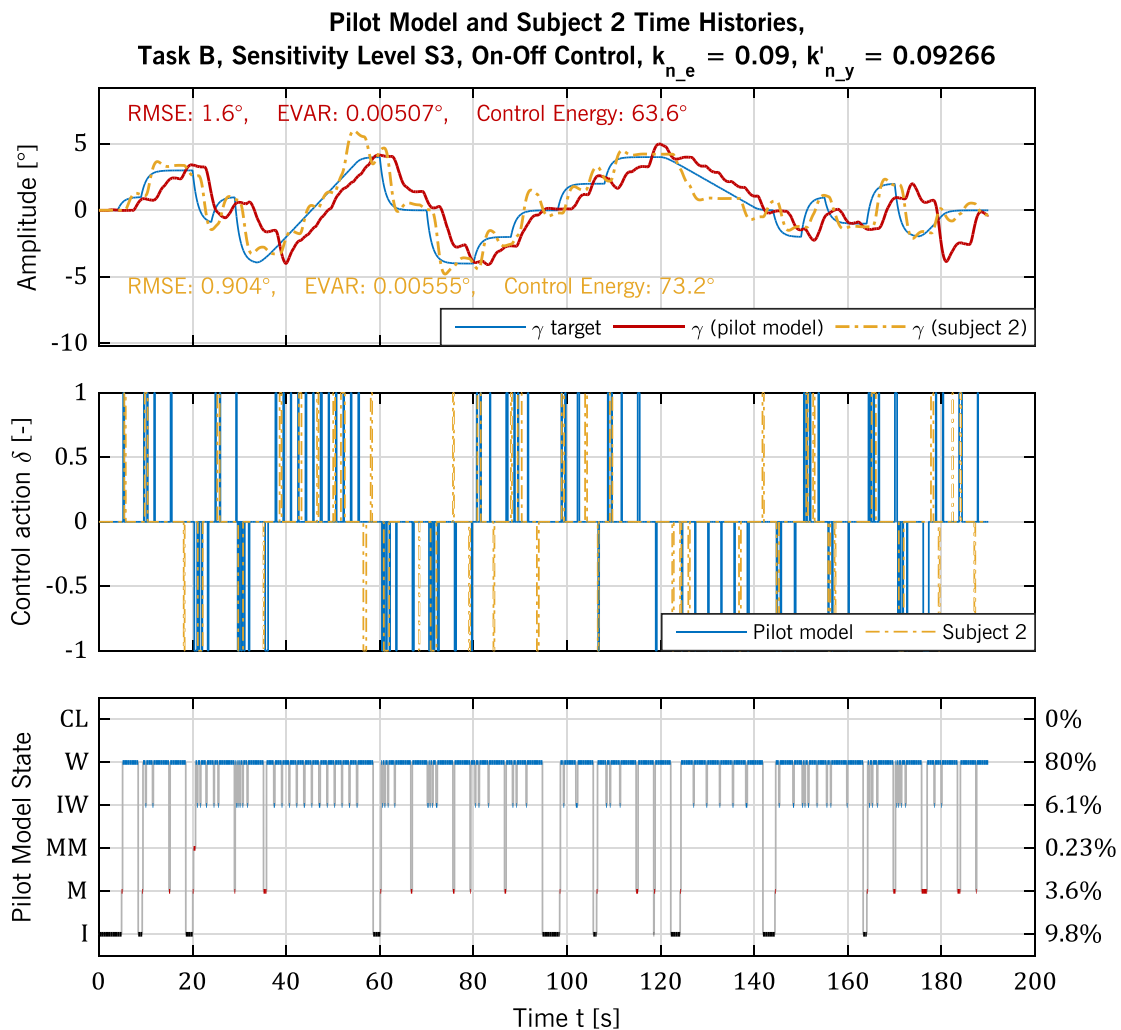


Figure 6.55 – Comparison of pilot model simulation and experimental run B3o

For the simulation of run B3c, which is illustrated in Figure 6.56, the same input aggressiveness $K_{agg} = 0.5$ was chosen as for all previous simulations. This choice seems suitable, given that the control actions of the pilot model and of subject 11 are similar in amplitude. As expected, the model did not enter the CL state in this run. In this run B3c, simulation and experiment exhibit similar RMSE values, but EVAR and control energy are smaller for the simulation. Subject 11 indeed produced large oscillations and thus large EVAR and control energy values between $t = 20$ s and $t = 40$ s. Generally, though, the same problem can be observed as in all above cases of task B: simulation and experiment never agree in all three performance metrics.

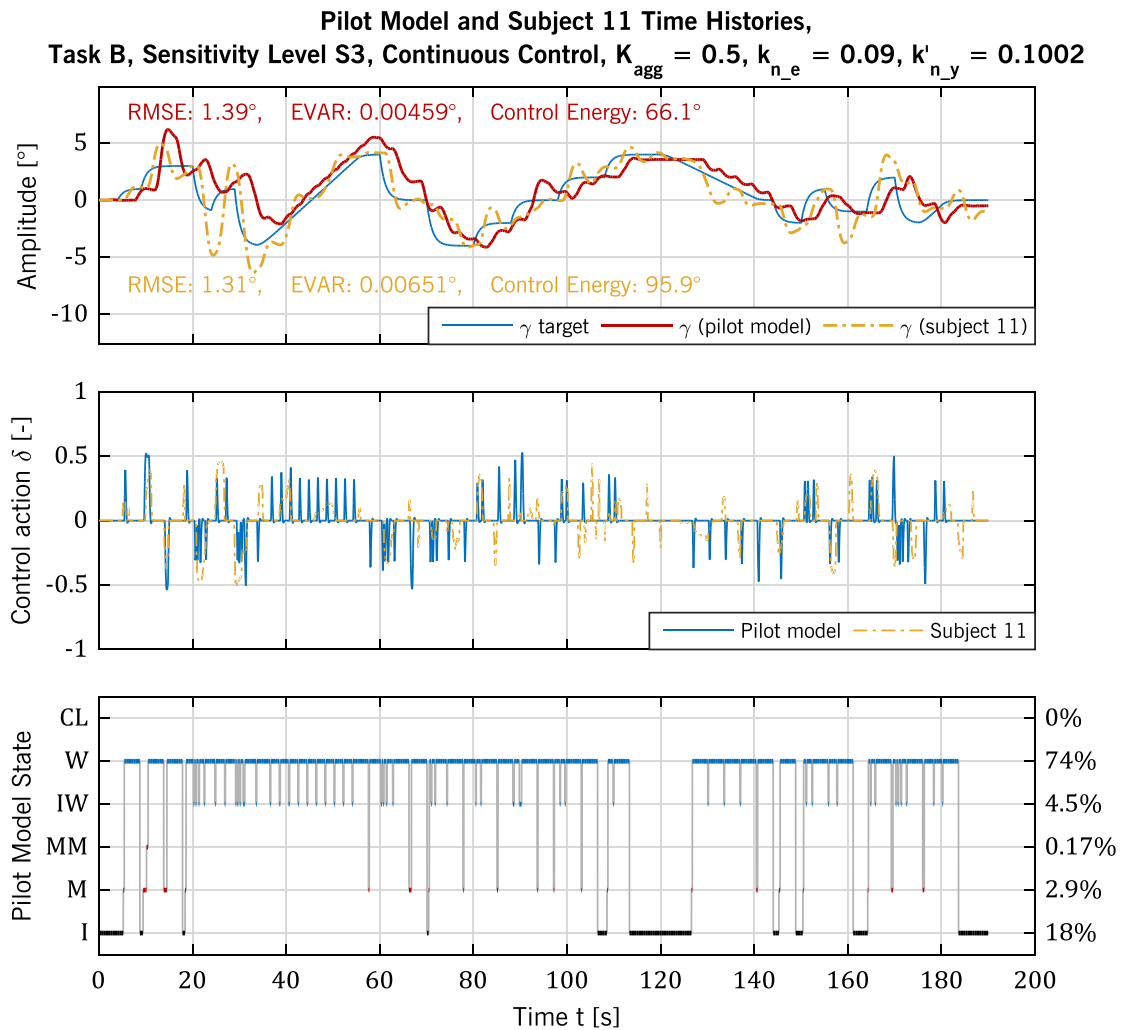


Figure 6.56 – Comparison of pilot model simulation and experimental run B3c

Figure 6.57 compares a model simulation and an average experimental run of task B with on-off control and the highest control sensitivity S4. Due to the high control sensitivity, control inputs are rare and brief. Here, none of the performance metrics matches between simulation and experiment. Similar to the cases above, the pilot model produces an excessive RMSE, but too little control energy and EVAR.

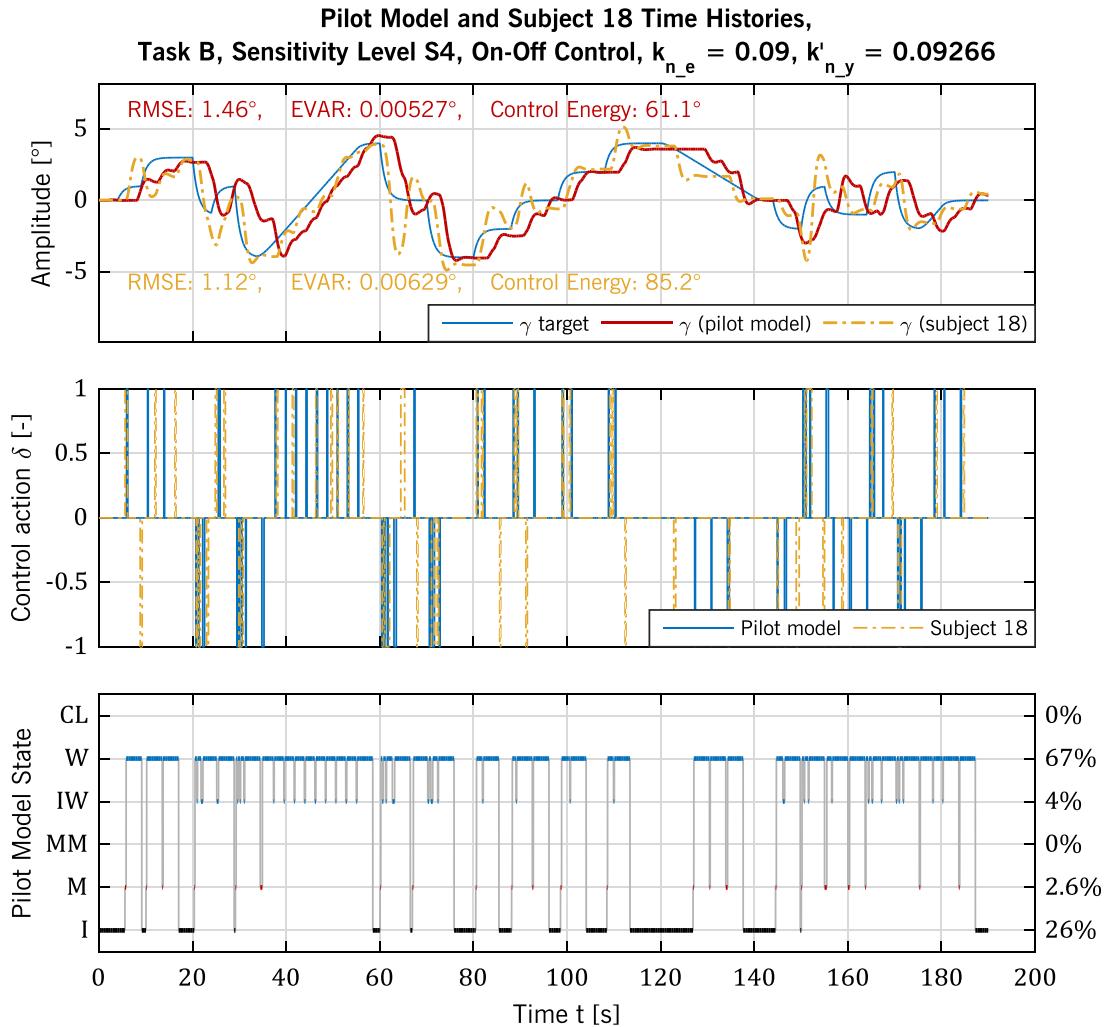


Figure 6.57 – Comparison of pilot model simulation and experimental run B4o

Next, Figure 6.58 shows time histories of a pilot model simulation and of subject 5's experimental run B4c. Instead of using the same K_{agg} value as in all previous simulations, $K_{agg} = 0.3$ was chosen for this high sensitivity level, based on the control inputs recorded during the experiment. Due to the reduced \dot{y}_{ss} , control inputs are a little more frequent here than in run B4o. Like in run B4o, the simulation's EVAR and control energy are smaller, but RMSE is higher than that of subject 5.

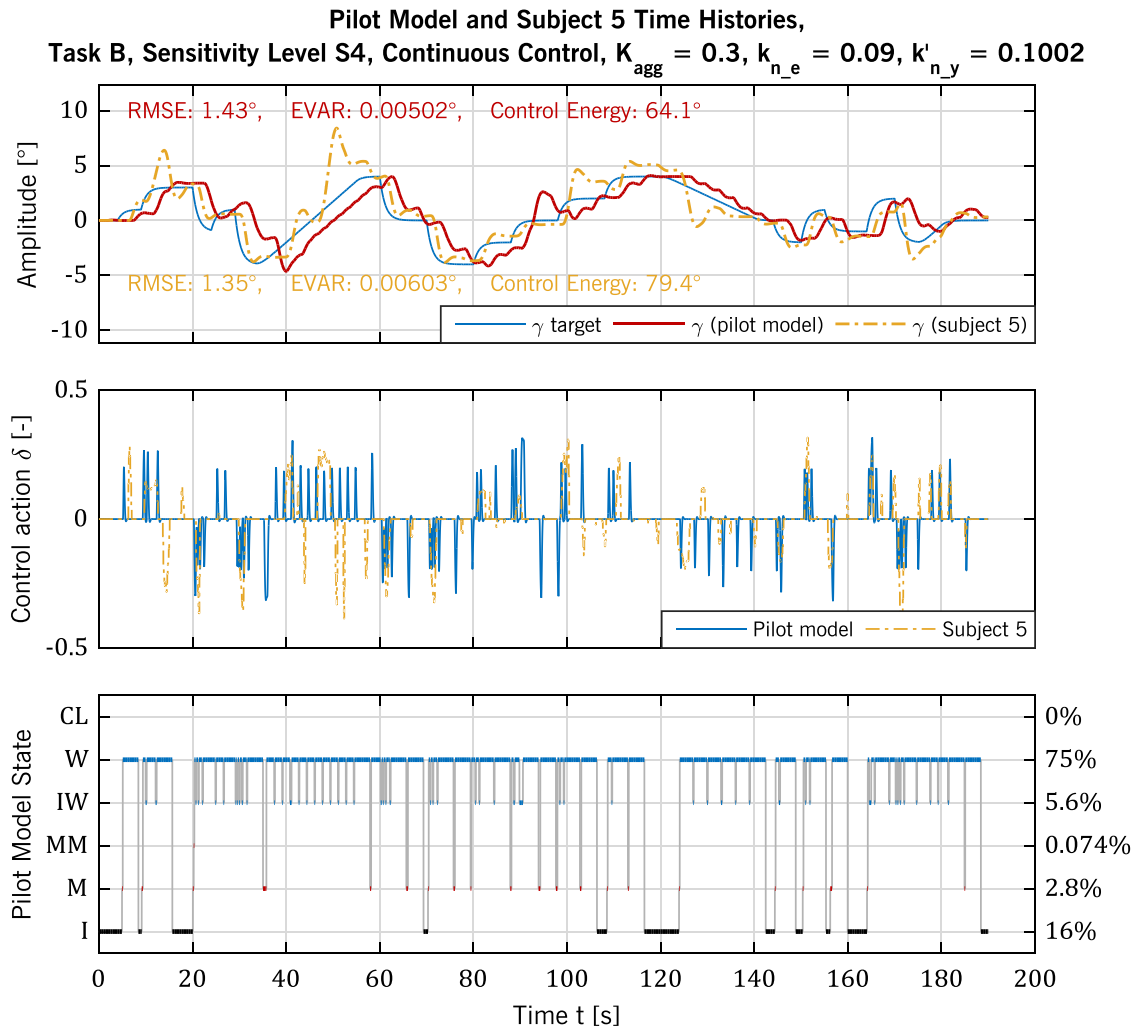


Figure 6.58 – Comparison of pilot model simulation and experimental run B4c

The final control sensitivity level to be investigated is S1. Time histories of both a model simulation and a representative experimental run B1o are shown in Figure 6.59. The model achieves a similar EVAR value as subject 14, but a lower control energy and a higher RMSE. Due to the small control sensitivity, closed-loop control appears more often than in any of the previous runs of task B. It has to be noted, though, that the Closed-Loop Control state is always entered from the Wait state, because the model spent remarkably little time, namely only the first couple of seconds, in the Idle state. This observation supports the interpretation of the lower control energies but worse TLX ratings of sensitivity level S1 as compared to sensitivity level S2 given in section 6.4.2. Figure 6.59 also uncovers another flaw of the model when applied to tasks that enable pre-cognitive tracking. The repeated switching between the states Wait and Interrupt Wait during the ramp in γ_{tgt} produces a smaller average $\dot{\gamma}_{ss}$ than if a constant control input would be applied. This effectively further reduces the ability to track the changes of γ_{tgt} . In general, the pilot model produces the most excessive tracking errors in this run of task B. This is mostly due to the fact that the phases of closed-loop control always ended prematurely, which indicates that the power of $n_{\dot{\epsilon}}$ was excessive.

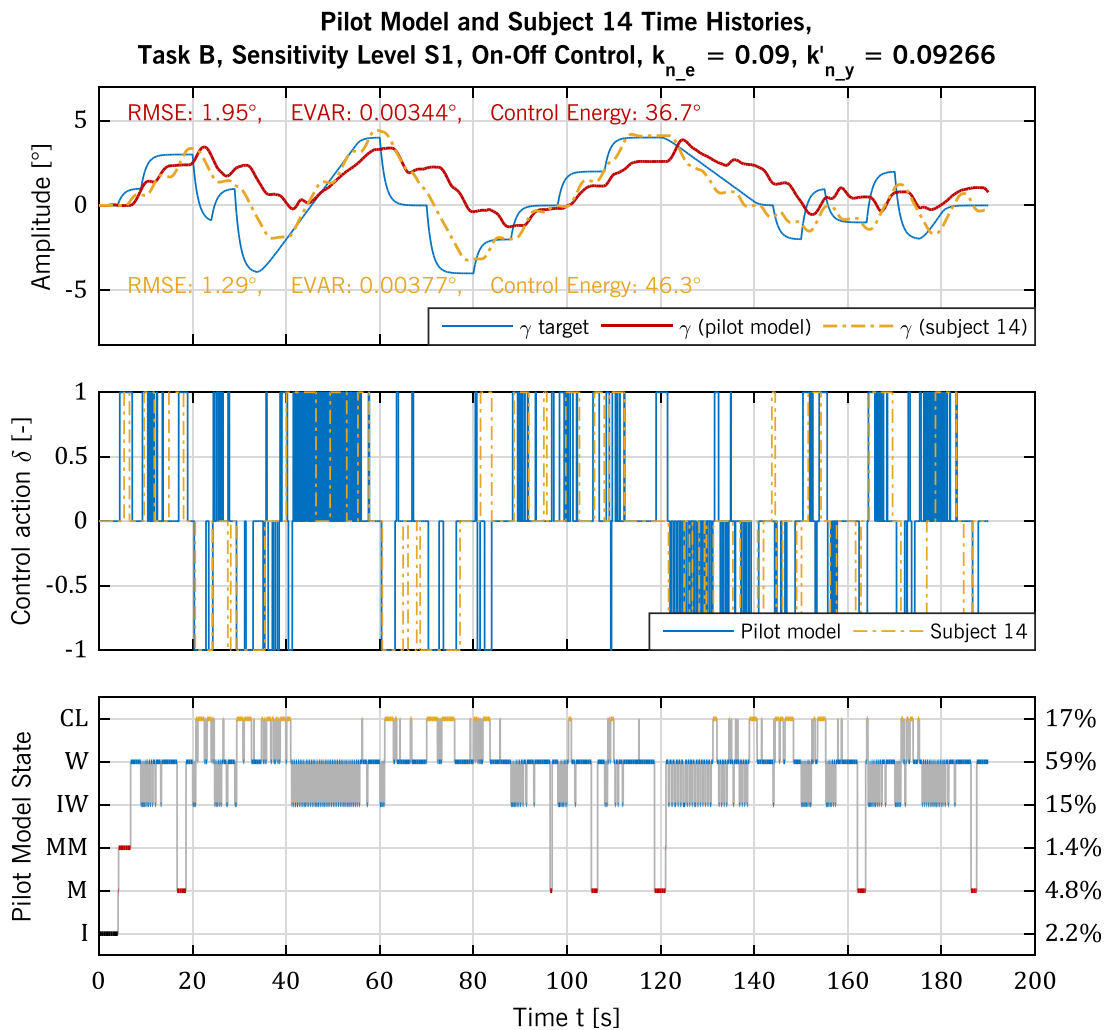


Figure 6.59 – Comparison of pilot model simulation and experimental run B1o

Given that the power of $n_{\dot{e}}$ with $k_{n_{\dot{e}}} = 0.09$ was excessive for run B1o, another simulation of this run was performed with $k_{n_{\dot{e}}} = 0.0033$. This value of $k_{n_{\dot{e}}}$ was obtained by assuming that, similar to the power of n_y , the power of $n_{\dot{e}}$ scales with $(K_a \tau_a)^{1.937}$. Figure 6.60 shows the corresponding simulation along with the representative run of subject 14. Here, model and experiment agree much better than in Figure 6.59, even though the same problems described for all previous runs persist. As a result, it can be suspected that $S_{nn_{\dot{e}}}$ follows equation (6.12), with a time constant T to be specified.

$$S_{nn_{\dot{e}}}(\omega) = \frac{0.1452 \cdot (K_a \tau_a)^{1.937}}{T \cdot j\omega + 1} \quad (6.12)$$

To more precisely define this noise spectrum, more experiments are required that let subjects (and the model) perform closed-loop control at different levels of control sensitivity and time delay.

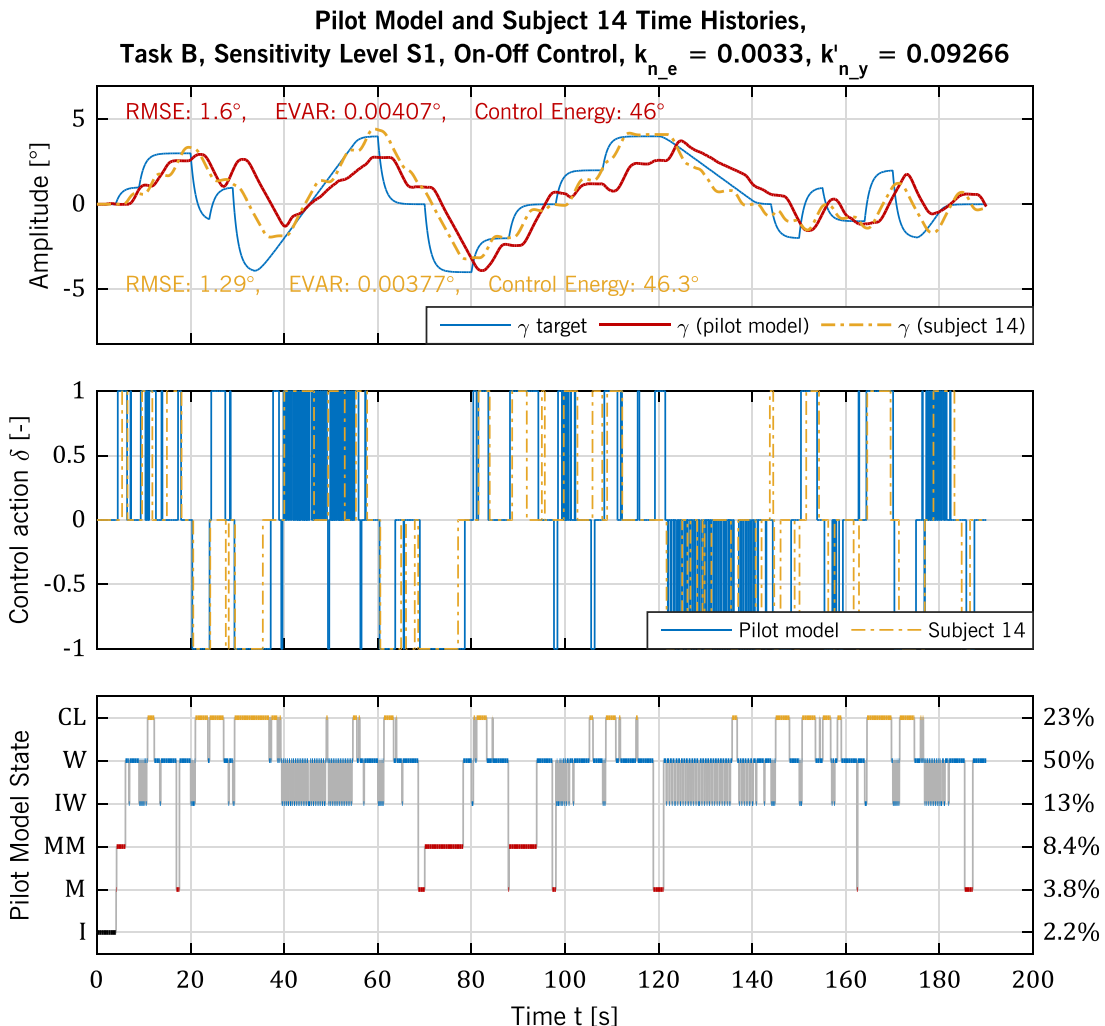


Figure 6.60 – Comparison of alternative model simulation and experimental run B1o

A comparison between model and experiment for the only remaining run of task B, namely B1c, is shown in Figure 6.61. Like for the run B4c, it was suspected that the control input aggressiveness would have to be adjusted for the extreme value of control sensitivity of

run B1c. Here, a value $K_{agg} = 1$ was chosen, based on the appearance of the subject's control inputs. Like in most of the runs discussed above, simulation and experiment produced similar EVAR and control energy values, the RMSE value resulting from the simulation is larger. However, the similarity between simulated and experimental system output γ , as well as between simulated and experimental control action δ is remarkable during some phases of the run. The high control aggressiveness causes $\dot{\gamma}_{ss}$ to be higher here than for run B1o, which is shown in Figure 6.59. As a result, closed-loop control appears less frequently and the original, excessive value of k_{n_e} does not adversely affect model performance.

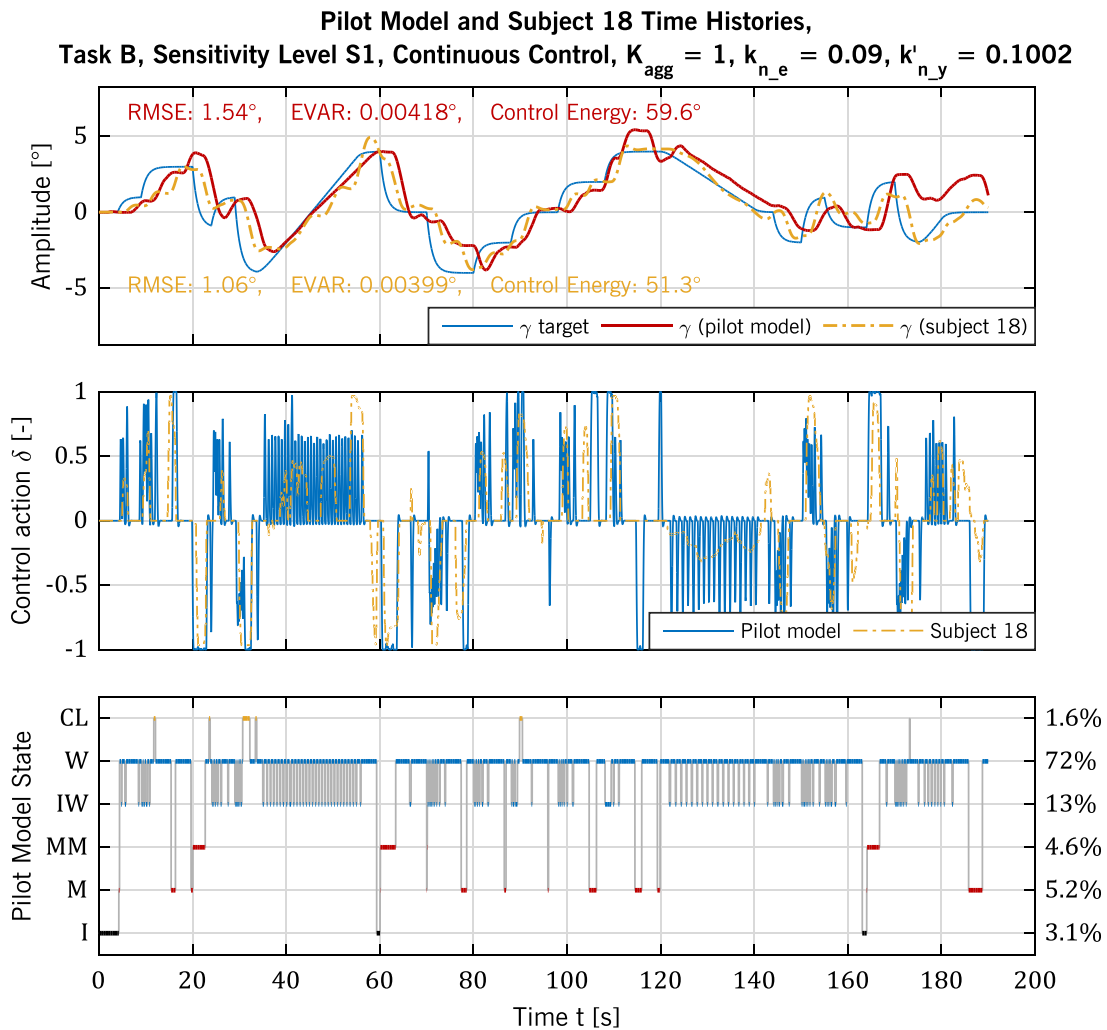


Figure 6.61 – Comparison of pilot model simulation and experimental run B1c

Summing up, it can be said that the dual-mode pursuit tracking pilot model presented in section 3.3.3 describes combined pursuit and pre-cognitive tracking with restricted validity. The model is able to accomplish task B using the same aircraft and flight controller as employed in the experiments without grossly excessive tracking errors for most of the four levels of sensitivity defined. Only in run B1o, large tracking errors occur due to an excessive power of n_e . The performance metrics resulting from the simulation generally never matched those from the experiments all at the same time. For most runs, similar values of control energy and EVAR could be achieved, but the RMSE value almost always

exceeded that of the corresponding experimental runs. This can be explained by the fact that the task design allowed subjects to predict future values of γ_{tgt} and to thereby perform pre-cognitive control, whereas the model is restricted to pursuit control by design.

The definition of the noise spectrum S_{nn_y} was modified once again to better describe changes of the noise power due to variations in control sensitivity. The final definition, given by equation (6.10), was derived from runs Ao and B2o. Corresponding values of k'_{n_y} , given by equation (6.11), were derived from runs Ao, Ac and B2o. The resulting noise spectra seemed to well describe not only the runs used to derive their definition, but also all remaining runs of task B.

A remaining major flaw of the model when applied to a combined pursuit and pre-cognitive tracking task is the repeated switching between states Wait and Interrupt Wait that often occurs. This behavior is rarely observed with human operators. Moreover, while switching between the states Wait and Interrupt Wait, the model performs pure open-loop control. During this time, tracking errors due to imprecise estimations \hat{y}_{ss} accumulate until the error threshold for transitioning to the Closed-Loop control state is reached. As a result, errors can grow excessively, which, for instance, is the case for the simulation of run B2c (cf. Figure 6.54). Like in task A, effects of time delay variations, most notably those on S_{nn_e} , could not be validated due to the absence of experimental data for τ_a values different from 2 s.

7 CONCLUSIONS AND PERSPECTIVE

The aim of the research leading up to this thesis was to make low level, closed-loop flight control by a human pilot in the presence of large time delays and with missing sensory feedback channels safer, more effective and more efficient (cf. section 1.3.1). To achieve these goals, human operator behavior during control of systems with large time delays was analyzed in a first step. Previous research on this matter was summed up and the findings of various researchers were related to each other to produce a holistic picture: large time delays in an unfamiliar system are tackled by applying the move-and-wait strategy, whereas the often co-occurring pulse-like control behavior is a form of low-frequency lead generation that, at the same time, makes the system response more predictable. Existing quasi-linear pilot models and models of pulse-like control behavior were presented, but found to be either inapplicable to or insufficient for the description of pulse-like control behavior associated with large time delays in the controlled system.

The novel representations of pulse-like pilot behavior derived and described in section 3.3 are therefore a major contribution of this thesis. The first model, describing compensatory tracking of a stationary target, allows an intuitive analysis of the nonlinear pilot-aircraft control loop in the phase plane. Using this model, the influence of desired tracking accuracy, control sensitivity, time delay and pilot lead on maneuverability and control loop stability were illustrated. Moreover, the idea to restrict control input amplitudes to three discrete levels by design was introduced and the expected differences between such an on-off control system and a continuous control system were described. The compensatory pilot model was then extended to describe dual-mode pursuit tracking, i.e., the hybrid open- / closed-loop move-and-wait strategy. As the central element of this second model, a state machine describes the pilot's choice when to move, when to wait and when to perform true closed-loop control. Most of the independent model parameters were fixed a priori, so that only three parameters remained to be determined empirically. This new model was also used to illustrate some of the differences between continuous control systems and on-off control systems.

Based on the insights into human operator behavior and handling qualities implications gained from previous research and the new pilot models (even though they had not been validated at this point), a flight control system was tailored to the problem of flight control

with large time delays and reduced sensory feedback. Summing up, the following features and design characteristics were proposed:

- An on-off control system derived from the pulse-like pilot behavior, which facilitates control of systems with large time delays by making the system response more predictable.
- For manual control, an inceptor force-deflection characteristic that reflects the on-off nature of the control system by discrete deflections and thus makes control inputs easily perceivable through the proprioceptive and the tactile channel.
- A choice of command variables that is adequate for conducting the reference flight mission and at the same time accounts for the reduced pilot-aircraft bandwidth.
- Protection mechanisms that re-establish an adequate level of safety in the case of missing sensory feedback channels.
- A visual predictor display that reduces the apparent time delay.
- Multimodal displays, possibly exploiting the tactile channel, that mitigate the problem of reduced sensory feedback.

Except for the multimodal displays, these design characteristics were implemented in a prototypical flight control system and in a flight simulator for subsequent experiments on manual remote flight control and on BMI controlled flight.

Concerning BMI control, which, like long-range RPA control, is affected by large time delays, it has to be noted that the BMI characteristics effectively prevent pulse-like control input characteristics: the noise present in the BMI control channel would heavily distort any pulse-like control intention. Furthermore, it is impossible to apply the move-and-wait strategy, because even in the absence of any control intention, i.e., when the BMI output should be zero, the noise is still present. The time delay introduced by BMI output filtering is quantified by equation (3.63) for the particular case of an SMA filter. One subject of the experiments presented in chapter 5 faced a filtering time delay of approximately 1 s. Like the similarly large signal transmission time delays in manual remote flight control, this filtering delay requires pilots to anticipate the aircraft movements and to generate lead. However, the prediction of future system outputs is more difficult with BMI control due to the fact that a permanent noise prevents both the move-and-wait strategy and pulse-like control inputs. The high workload due to lead generation was indeed reported by the experiment subjects. Interestingly, it was even reported when no BMI output filtering was employed. This can be explained by the fact that in these cases, the BMI output spectrum was not white but exhibited low-pass characteristics, as described in section 5.5.

Speaking of noise when referring to unreliable BMI outputs is a concept that has already been presented elsewhere, but section 3.4.2 additionally identifies the SNR as a performance metric of the subject-BMI system, which is related to the STR. Experimental data obtained with two different types of BMIs is used in section 5.5 to confirm that BMI outputs can indeed be described by a Gaussian noise of constant variance, whose mean value changes with the user intention. The validity of this simple BMI is, however, compromised when the STR is close to or even below chance (50%), which is the case for subjects who do not (yet) have control. Moreover, the model does not describe time-varying BMI characteristics and biases towards one user intention. Unfortunately, the

BMI model also cannot be used to predict BMI output characteristics of a given subject-BMI combination. Instead, the values of the model parameters must be derived from experimental data. However, reference values from past experiments can be used to get an idea of possible BMI control performance. This information is valuable when a control system is to be adapted or when the suitability of closed-loop BMI control for a given task has to be assessed. Possible future improvements of the BMI output model include the description of biases and of the time-varying nature of BMI characteristics. The model's quantification of BMI control performance could also be used to derive a model for learning or, more exactly, for the subject-BMI adaptation over time.

The explorative experiments on BMI control presented in chapter 5 investigated closed-loop BMI control with two different types of BMIs. In an approach unusual for BMI research, methods of handling qualities evaluation established in the aerospace domain were applied in the course of experiment set up, implementation and evaluation. This application-driven approach yielded realistic and operationally relevant tasks and a highly realistic experimental environment. The experiment results are therefore more relevant for actual BMI application than if they had been obtained in a laboratory environment with artificial tasks. Designing realistic tasks for the experiments on BMI controlled flight was a challenge due to the fact that control performance was uncertain and expected to be a lot poorer than with manual control. The fact that the easiest task was readily accomplished by several subjects, whereas the most difficult task was barely accomplishable even for the best performing subjects shows that a suitable range of difficulties was presented. Another distinctive feature of the experiments are the tuning efforts described in section 5.3, during which special attention was given to subjective comments of the experiment participants. These efforts aimed at identifying suitable dynamic plant characteristics and suitable filtering and mapping functions for each subject. These efforts, as well as the subsequent comparison of different control system configurations confirm that controllability and handling not only depend on the BMI characteristics, but are also influenced by the plant dynamics.

The way the experiments were set up, conducted and evaluated can serve as an example for similar studies in the future. Moreover, the experiment results reported in this thesis, including the description of both suitable and unsuitable configurations, can provide guidance for future BMI control system designs. Section 5.4.2 notes that control of a single pure integrator is easier and allows more precise tracking than control of a double pure integrator. Generally, agility can be traded off against stability. A control system configuration that enables fast changes of the controlled parameter makes it difficult to keep this same parameter constant. However, controllability requires sufficiently reliable BMI outputs in the first place. Hence, some subjects did not have control at all. Others were able to perform closed-loop BMI control of the horizontal airplane motion with acceptable accuracy, using the flight control system described in chapter 4. As expected, however, the performance of manual control was not matched by far. Moreover, subjects reported that BMI control produces an extreme mental workload. The following list sums up the major challenges for BMI application identified.

- Significant improvements in BMI reliability are required for closed-loop BMI control.
- Biases and variations of BMI control performance between sessions, runs and within a run must be minimized.
- The mental effort needed to generate the required brain activity must be reduced.
- The amount of attention that is dedicated to the (visual) BMI feedback must be reduced to free up resources for the high-level task and possible secondary tasks.
- Generation of brain signals must be intuitive. For instance, imagining feet movements to turn left is unacceptable.

Finally, an effective means to substitute the undelayed cues of proprioceptive feedback still has to be found, since the simple visual display proved unsatisfactory.

In another experimental campaign, the flight control system designed and implemented was applied to remote manual flight control with a time delay of 2 s. With a total of 18 subject pilots, these experiments were large in comparison to other handling qualities studies. The design of this campaign mainly aimed at comparing the on-off with the continuous control system type and at investigating the initial learning phase when controlling systems with large time delays. However, it also allowed to assess the suitability of different levels of control sensitivity and to obtain insights into the strengths and weaknesses of some of the proposed flight control system concepts. Six a-priori hypotheses were formulated in section 6.1, which were all confirmed by the subsequent experiments. It can thus be said that

- pilots naïve to flight control with large time delays find an appropriate control strategy quicker with an on-off control system than with a continuous control system

and that, as long as pilots have not yet accumulated a lot of experience in controlling systems with large time delays,

- workload is less with an on off control system as compared to a continuous control system,
- performance with an on-off control system is comparable or better than performance with a continuous control system and
- visual predictor displays reduce workload and improve performance, but also bind a significant amount of visual attention.

Increasing familiarity with the controlled system, including the time delay, is expected to weaken the positive effects of on-off control, so that continuous control ultimately becomes preferable. It has to be noted, however, that increased familiarity can only be achieved by frequent exposure to lower-level manual flight control with large time delays, either in a simulated training scenario or in actual flight operations. The experiments also showed that, although the inceptor characteristics implemented in the simulator's sidestick were not optimal, the general concept of reflecting the on-off nature of the control system by discrete inceptor deflections is suitable. In the case of a continuous control system, it was found that involuntary cross-channel control inputs can easily occur in the presence of large time delays. To prevent such cross-channel inputs, a larger breakout force of the inceptor is better suited than a larger deadzone in each axis, because it provides an

immediate tactile/proprioceptive cue to the pilot. The position and orientation of the inceptor with respect to the pilot can also be optimized in this respect. Finally, the protection mechanisms proved helpful in preventing extreme flight conditions and the proposed flight controller functions, namely Altitude Hold, Path Straightener and Standard Rate Turn Hold, were generally rated helpful.

The flight control system as presented in chapter 4 and flown in the experiments comprises feedback control algorithms and thus effectively establishes a higher level of automation as compared to unaugmented aircraft, with the associated drawbacks (cf. section 1.2). However, being located approximately in the middle of the spectrum of automation shown in Figure 1.3, it still involves the pilot to a considerable degree. The experiments have shown that, with a round-trip delay of 2 s, this concept may be adequate for nonterminal flight phases, but that landings have a low success rate. Other schemes of UAV control therefore seem more promising. Indeed, automation should be employed in situations where pilot errors significantly reduce operational performance or easily result in accidents (cf. section 1.2). In the case of unanticipated events like automation failures or evasive maneuvers, however, remote operators may need to take over control on a lower level of automation. At this moment (where predictors may also not be available), the beneficial effects of on-off control are most pronounced, because pilots are hardly familiar with control on this lower, non-normal level of automation. Moreover, the advantages of on-off control over continuous control can be expected to be effective at many different levels of automation, i.e., with many different command variables. Such an on-off control system for non-normal operations may not enable picture-perfect landings, but it helps preventing loss of control in flight. If, for landing, attempts to re-establish a suitable degree of automation or to transfer control to a local pilot fail, the remote operator can at least end the flight in a desired area and thereby avoid harm to persons or damage to objects on the ground.

One concept that was outlined, but unfortunately could not be implemented and tested, is that of a tactile or multimodal display which conveys information of flight-control related variables. Such a display is hoped to increase the pilot's situational awareness and thereby free up mental resources that can then be allocated to coping with the reduced sensory feedback. Detailed design and implementation of such displays and, most of all, investigations into their effectiveness therefore constitute important goals for future work. Likewise, the amount of attention devoted by pilots to predictor displays should be quantified objectively, since the experiments presented in this thesis only relied on subjective pilot ratings in that respect. Some predictor display designs, possibly using a different stimulus dimension or even a different sensory channel than the one presented in this thesis, may require more pilot attention than others. Furthermore, the experiments did not comprise secondary tasks that concurred with the observation of the predictor symbols. Future investigations could provide better insights into the effectiveness of different predictor designs in operational environments.

This thesis discusses flight control with time delays in the range of 1...3 s, but the experiments on manual remote flight control only covered the single time delay value of 2 s. Although the findings of the experiments are valid for the considered range of time

delays and probably for larger values as well, it may be interesting to investigate, in a future study, how task performance and workload are affected by time delay variations. More importantly, additional research is required on human operator behavior and possible control system concepts for time delay values smaller than 1 s, i.e., in a grey area between negligible time delays and large time delays. For instance, neither the smallest time delay value at which pulse-like operator behavior first occurs, nor the minimum time delay for which on-off control has advantages over continuous control are known at this point. It is also imaginable that altogether different concepts are better suited for this range of time delay values.

For the large time delay values considered in this thesis, the concept of a pulse control system, which is presented in section 4.1, may also be suitable, but due to the rather unconventional handling characteristics of such a system, an on-off control system was preferred for implementation and testing. Interestingly, however, some subjects of the experiments presented in chapter 6 applied pulsed inputs with the on-off control system. To assess whether further improvements in workload and controllability can be achieved by implementing a pulse control system, a similar study could be performed in the future that compares a pulse control system with a continuous control system and/or an on-off control system.

The experimental data from the human subject study presented in chapter 6 of this thesis was also used to validate the novel pilot models proposed in section 3.3. It was confirmed that the new compensatory tracking model correctly predicts the period and maximum amplitude of possibly occurring limit cycles, regardless of the control system type employed. This new model can thereby contribute to estimating the worst case of PIO in a given system. For validation of the novel dual-mode pursuit tracking model, suitable values of the three remaining independent model parameters were determined by matching the quantitative performance metrics of model simulations with results from the experiments. It was shown that the model well describes pure pursuit tracking like the tracking of stationary targets in task A, but that it has several shortcomings in describing combined pursuit and pre-cognitive tracking as in task B. In task A, the model achieves a similar performance and produces similar control activity like human subjects. In task B, on the other hand, the performance metrics resulting from the simulation generally never match those from the experiments all at the same time. In most cases, the simulation seems to lag behind the experiment and thus, the tracking error is larger. This can be explained by the fact that the task design allowed subjects to predict future target values and to thereby perform pre-cognitive control, whereas the model is restricted to pursuit control by design. Another flaw of the model when applied to a combined pursuit and pre-cognitive tracking task is that prolonged phases of pure open-loop control can occur, during which pulsed control inputs are made.

The assumption made in section 3.3.3 that the power of n_y is higher if a continuous control system is employed instead of an on-off control system was validated by model fitting to task A. This fact provides an explanation for the advantage of on-off control over continuous control, at least for subjects with little training. The initial definition of the noise spectrum S_{nn_y} was modified twice during model validation to more accurately

describe changes of the noise power due to variations in control sensitivity. The final definition seemed to well describe a variety of control sensitivity settings.

Remaining shortcomings of the proposed dual-mode pursuit tracking model are the excessively high cutoff frequency of the noise spectrum S_{nn_e} and the model's inability to describe the strategy of approaching a target with decreasing input aggressiveness. To find a suitable definition of S_{nn_e} , more data on closed-loop control with large time delays needs to be gathered in additional experiments that not only vary the system's control sensitivity, but also its time delay. Data from the same experiments could also be used to assess whether the final form of S_{nn_y} presented in this thesis is indeed valid. Moreover, the dual-mode pursuit tracking pilot model should be extended by a model that describes variations in input aggressiveness. Possible future work also includes the validation of the proposed model against a pure pursuit tracking task with a continuously moving target, like task 2 of the experiments on BMI control. Furthermore, an attempt at extending the model to describe pre-cognitive tracking as well is imaginable. The ultimate goal would be to derive a handling qualities metric from the model, which predicts the suitability of a given combination of control system type, augmented aircraft dynamics and time delay for a certain task. The description and evaluation of the pilot model in this thesis constitutes a first, large step in this direction.

Summing up, it can be said that important progress was made towards the research goals of improving safety, effectiveness and efficiency of flight control with large time delays and reduced sensory feedback (cf. section 1.3.1). In the case of BMI control, more application-driven research and development was promoted. Safety, effectiveness and efficiency of BMI control are still far too inadequate for most applications, but some means of improvement have been identified, such as suitable dynamic plant characteristics or protection mechanisms. Concerning RPAS operations, the proposed flight control concepts can contribute to a safe continuation of the flight after adverse events. Admittedly, a lot of PIOs occurred in the experiments, but on-off control, possibly combined with protection mechanisms or even predictors, promotes controlled flight. Effectiveness may be improved in that minor system failures do not require a precautionary termination of the mission. If, for instance, a UAV needs to revert to some lower-level remote flight control law, the improvements in safety described above may allow the human operator to resume the mission with an acceptable risk. At the same time, the human operator's workload in this situation is reduced by the concepts presented in this thesis and thus, mission efficiency is improved. Finally, the novel models of pilot dynamic behavior developed and presented in this thesis provide a thorough explanation of human operator behavior during control of systems with large time delays and thereby lay the foundation for further progress towards optimal controllability and handling of such systems.

REFERENCES

- [1] C. M. Cotting, "Evolution of Flying Qualities Analysis: Problems for a New Generation of Aircraft," Dissertation, Virginia Polytechnic Institute and State University, Blacksburg, Virginia, USA, 2010.
- [2] A. J. Thurling, "Improving UAV Handling Qualities Using Time Delay Compensation," Master's Thesis, Air Force Institute of Technology, Wright-Patterson Air Force Base, Ohio, USA, 2000.
- [3] J. S. McCarley and C. D. Wickens, "Human Factors Implications of UAVs in the National Airspace," 2005.
- [4] K. W. Williams, *A Summary of Unmanned Aircraft Accident/Incident Data: Human Factors Implications: DOT/FAA/AM-04/24*. Washington D.C., USA: U.S. Department of Transportation, Federal Aviation Administration, 2004.
- [5] S. K. Sarrafian, *Simulator Evaluation of a Remotely Piloted Vehicle Lateral Landing Task Using a Visual Display*. NASA TM-85903. Edwards, California, USA: National Aeronautics and Space Administration, 1984.
- [6] J. T. Hing and P. Y. Oh, "Development of an Unmanned Aerial Vehicle Piloting System with Integrated Motion Cueing for Training and Pilot Evaluation," *Journal of Intelligent and Robotic Systems*, vol. 54, no. 1, pp. 3–19, 2009.
- [7] S. C. de Vries, *UAVs and Control Delays*, 3rd ed. Soesterberg, The Netherlands: Nederlandse Organisatie voor Toegepast Natuurwetenschappelijk Onderzoek (TNO), 2005.
- [8] M. Mouloua, R. Gilson, E. Daskarolis-Kring, J. Kring, and P. Hancock, "Ergonomics of UAV/UCAV Mission Success: Considerations for Data Link, Control, and Display Issues," in *Proceedings of the Human Factors and Ergonomics Society 45th Annual Meeting*, 2001.
- [9] T. B. Sheridan, "Space Teleoperation Through Time Delay: Review and Prognosis," *IEEE Transactions on Robotics and Automation*, vol. 9, no. 5, 1993.
- [10] J. R. Rice, J. P. Yorchak, and C. S. Hartley, "Planning for Unanticipated Satellite Servicing Teleoperations," in *Proceedings of the Human Factors Society - 30th Annual Meeting*, 1986.
- [11] Direction Générale de l'Armement, *Le SIDM (système intérimaire de drones de moyenne altitude longue endurance)*. [Online] Available: www.defense.gouv.fr/dga/equipement/missiles-et-drones/le-sidm-systeme-interimaire-de-drones-de-moyenne-altitude-longue-endurance. Accessed on: Mar. 24 2016.
- [12] K. W. Williams, *Human Factors Implications of Unmanned Aircraft Accidents: Flight-Control Problems: DOT/FAA/AM-06/8*. Washington D.C., USA: U.S. Department of Transportation, Federal Aviation Administration, 2006.
- [13] Champalimaud Foundation, Tekever, EagleScience, and Technical University of Munich, *BRAINFLIGHT CONOPS*. [Online] Available: <http://www.fp7->

- brainflight.eu/wp-content/uploads/2014/06/BRAINFLIGHT-308914-D2.1-CONOPS-V1.pdf. Accessed on: May 25 2016.
- [14] T. Fricke and F. Holzapfel, "Applying Brain Machine Interfaces to Aircraft Control - Potentials and Challenges," in *Der Mensch zwischen Automatisierung, Kompetenz und Verantwortung: 56. Fachausschusssitzung Anthropotechnik der Deutschen Gesellschaft für Luft- und Raumfahrt - Lilienthal-Oberth e.V.*, M. Grandt and S. Schmerwitz, Eds., Bonn: DGLR, 2014, pp. 207–214.
- [15] F. O. Flemisch, J. Kelsch, C. Löper, A. Schieben, and J. Schindler, "Automation spectrum, inner / outer compatibility and other potentially useful human factors concepts for assistance and automation," in *Human Factors for assistance and automation*, D. de Waard, F. O. Flemisch, B. Lorenz, H. Oberheid, and K. A. Brookhuis, Eds., Maastricht, the Netherlands: Shaker Publishing, 2008, pp. 1–16.
- [16] S. Wood, *Flight Crew Reliance on Automation: CAA PAPER 2004/10*: Civil Aviation Authority, 2004.
- [17] M. Ebbatson, "The Loss of Manual Flying Skills in Pilots of Highly Automated Airliners," PhD Thesis, Cranfield University, Cranfield, 2009.
- [18] *DO-304: Guidance Material and Considerations for Unmanned Aircraft Systems*. Washington D.C., USA: RTCA, Inc., 2007.
- [19] D. W.-K. Ng, Y.-W. Soh, and S.-Y. Goh, "Development of an Autonomous BCI Wheelchair," in *CIBCI 2014: 2014 IEEE Symposium on Computational Intelligence in Brain Computer Interfaces : proceedings*, 2014.
- [20] R. E. Smith, "Training + Automation = A Winning Combination," Garching, Germany, Jun. 18 2015.
- [21] S. Hirche and M. Buss, "Human-Oriented Control for Haptic Teleoperation," *Proceedings of the IEEE*, vol. 100, no. 3, pp. 623–647, 2012.
- [22] P. F. Hokayem and M. W. Spong, "Bilateral teleoperation: An historical survey," *Automatica*, vol. 42, no. 12, pp. 2035–2057, 2006.
- [23] T. B. Sheridan and W. R. Ferrell, "Remote Manipulative Control with Transmission Delay," *IEEE Transactions on Human Factors in Electronics*, vol. 4, no. 1, pp. 25–29, 1963.
- [24] W. R. Ferrell, "Remote Manipulation with Transmission Delay," *IEEE Transactions on Human Factors in Electronics*, vol. 6, no. 1, pp. 24–32, 1965.
- [25] L. Stark *et al.*, "Telerobotics: Display, Control, and Communication Problems," *IEEE Journal of Robotics and Automation*, vol. 3, no. 1, 1987.
- [26] G. Hirzinger, J. Heindl, and K. Landzettel, "Predictive and Knowledge-Based Telerobotic Control Concepts," in *IEEE International Conference on Robotics and Automation*, 1989, pp. 1768–1777.
- [27] F. T. Buzan and T. B. Sheridan, "A Model-Based Predictive Operator Aid for Telemanipulators with Time Delay," in *IEEE International Conference on Systems, Man and Cybernetics*, 1989, pp. 138–143.

-
- [28] A. K. Bejczy and W. S. Kim, "Predictive Displays and Shared Compliance Control for Time-Delayed Telemanipulation," in *IEEE International Workshop on Intelligent Robots and Systems, Towards a New Frontier of Applications*, Jul. 1990, pp. 407–412.
- [29] T. Sato and S. Hirai, "Language-Aided Robotic Teleoperation System (LARTS) for Advanced Teleoperation," *IEEE Journal of Robotics and Automation*, vol. 3, no. 5, 1987.
- [30] N. Diolaiti and C. Melchiorri, "Tele-Operation of a Mobile Robot Through Haptic Feedback," in *HAVE 2002: Proceedings*, Piscataway, New Jersey, USA: IEEE, 2002.
- [31] D. Lee, O. Martinez-Palafox, and M. W. Spong, "Bilateral Teleoperation of a Wheeled Mobile Robot over Delayed Communication Network," in *Proceedings of the 2006 IEEE International Conference on Robotics and Automation*, 2006.
- [32] S. M. Alaimo, L. Pollini, J.-P. Bresciani, and H. H. Bühlhoff, "A Comparison of Direct and Indirect Haptic Aiding for Remotely Piloted Vehicles," in *Proceedings of the 19th IEEE International Symposium on Robot and Human Interactive Communication*, 2010.
- [33] S. M. Alaimo, L. Pollini, M. Innocenti, J.-P. Bresciani, and H. H. Bühlhoff, "Experimental Comparison of Direct and Indirect Haptic Aids in Support of Obstacle Avoidance for Remotely Piloted Vehicles," *Journal of Mechanics Engineering and Automation*, vol. 2, no. 10, pp. 628–637, 2012.
- [34] C. F. Prosser and C. D. Wiler, *RPV Flying Qualities Design Criteria: AFFDL-TR-76-125*. Wright-Patterson Air Force Base, Ohio, USA: Air Force Flight Dynamics Laboratory, 1976.
- [35] T. Foster and J. Bowman, "Dynamic Stability and Handling Qualities of Small Unmanned-Aerial-Vehicles," in *43rd AIAA Aerospace Sciences Meeting and Exhibit*
- [36] J. Zhou, Z. Jiang, and G. Tang, "A new approach for teleoperation rendezvous and docking with time delay," *Science China Physics, Mechanics and Astronomy*, vol. 55, no. 2, pp. 339–346, 2012.
- [37] J. Zhou, J. Zhou, Z. Jiang, and H. Li, "Investigation into Pilot Handling Qualities in Teleoperation Rendezvous and Docking with Time Delay," *Chinese Journal of Aeronautics*, vol. 25, no. 4, pp. 622–630, 2012.
- [38] G. Sachs, "Perspective Predictor/Flight-Path Display with Minimum Pilot Compensation," *Journal of Guidance, Control, and Dynamics*, vol. 23, no. 3, pp. 420–429, 2000.
- [39] G. Sachs and K. Dobler, "Predictor/Flight-Path Display for Manual Longitudinal Control Improvement," *Journal of Guidance, Control, and Dynamics*, vol. 25, no. 3, pp. 494–501, 2002.
- [40] C. D. Wickens, S. E. Gordon, Y. Liu, and J. Lee, *An Introduction to Human Factors Engineering*. Harlow: Pearson Education Limited, 2014.

- [41] F. Zhang, T. Fricke, and F. Holzapfel, "Integrated Control and Display Augmentation for Manual Remote Flight Control in the Presence of Large Latency," in *AIAA Guidance, Navigation, and Control Conference: American Institute of Aeronautics and Astronautics*, 2016.
- [42] R. Stich, G. Sachs, and T. H. Cox, "Path-Attitude Decoupling Problems of Aerospace Craft," in *9th International Space Planes and Hypersonic Systems and Technologies Conference*, 1999.
- [43] R. Stich, G. Sachs, and T. H. Cox, "Path-Attitude Inconsonance in High Speed Flight and Related Path Control Issues," in *22nd Congress of International Council of the Aeronautical Sciences*, 2000.
- [44] G. Sachs and C. Moravszki, "Predictive Tunnel Display for Hypersonic Flight Path Control," in *AIAA Guidance, Navigation, and Control Conference and Exhibit*, 2006.
- [45] C. S. Hartley, D. J. Cwynar, K. D. Garcia, and R. A. Schein, "Capture of Satellites Having Rotational Motion," in *Proceedings of the Human Factors Society - 30th Annual Meeting*, 1986.
- [46] C. S. Hartley, D. J. Cwynar, L. Ray, and K. D. Garcia, "Ground Control Considerations for Remotely Piloted Spacecraft," in *Proceedings of the Human Factors Society - 28th Annual Meeting*, 1984.
- [47] A. H. Rupert, F. E. Guedry, and M. F. Reschke, "The Use of a Tactile Interface to Convey Position and Motion Perceptions," in *AGARD Conference Proceedings*, vol. 541, *Virtual Interfaces: Research and Application*, Neuilly-sur-Seine, France: North Atlantic Treaty Organization, Advisory Group for Aerospace Research & Development, 1994.
- [48] B. J. McGrath, *Tactile Instrument for Aviation: NAMRL Monograph 49*. Pensacola, Florida, USA: Naval Aerospace Medical Research Laboratory, 2000.
- [49] J. van Erp, J. A. Veltman, H. van Veen, and A. B. Oving, "Tactile Torso Display as Countermeasure to Reduce Night Vision Goggles Induced Drift," in *RTO meeting proceedings*, vol. 86, *Spatial Disorientation in Military Vehicles: Causes, Consequences and Cures*, Neuilly-sur-Seine, France: North Atlantic Treaty Organization, Research and Technology Organization, 2003.
- [50] C. Jansen, A. Wennemers, W. Vos, and E. Groen, "FlyTact: A Tactile Display Improves a Helicopter Pilot's Landing Performance in Degraded Visual Environments," in *Lecture Notes in Computer Science, Haptics: Perception, Devices and Scenarios*, M. Ferre, Ed.: Springer Berlin Heidelberg, 2008, pp. 867–875.
- [51] J. van Erp and B.P. Self, Eds., *Tactile Displays for Orientation, Navigation and Communication in Air, Sea and Land Environments*. Neuilly-sur-Seine, France: North Atlantic Treaty Organization, Research and Technology Organization, 2008.
- [52] B. Graimann, B. Allison, and G. Pfurtscheller, "Brain-Computer Interfaces: A Gentle Introduction," in *The Frontiers collection, Brain-Computer Interfaces*:

- Revolutionizing Human-Computer Interaction*, B. Graimann, B. Allison, and G. Pfurtscheller, Eds., Berlin, Heidelberg: Springer, 2010, pp. 1–27.
- [53] Autonomos Labs, *BrainDriver*. [Online] Available: <http://www.autonomos.inf.fu-berlin.de/subprojects/braindriver>. Accessed on: May 22 2014.
- [54] J. Pan, Y. Li, Z. Gu, and Z. Yu, “A comparison study of two P300 speller paradigms for brain-computer interface,” *Cognitive neurodynamics*, vol. 7, no. 6, pp. 523–529, 2013.
- [55] K. LaFleur *et al.*, “Quadcopter control in three-dimensional space using a noninvasive motor imagery-based brain-computer interface,” *Journal of Neural Engineering*, vol. 10, no. 4, p. 46003, 2013.
- [56] A. Akce, M. Johnson, and T. Bretl, “Remote Teleoperation of an Unmanned Aircraft with a Brain-Machine Interface: Theory and Preliminary Results,” in *IEEE International Conference on Robotics*, 2010.
- [57] A. Akce, M. Johnson, O. Dantsker, and T. Bretl, “A Brain-Machine Interface to Navigate a Mobile Robot in a Planar Workspace: Enabling Humans to Fly Simulated Aircraft With EEG,” *IEEE Transactions on Neural Systems and Rehabilitation Engineering*, vol. 21, no. 2, pp. 306–318, 2013.
- [58] E. Cooper and R. Harper, *The use of pilot rating in the evaluation of aircraft handling qualities*. NASA TN D-5153. Washington D.C., USA: National Aeronautics and Space Administration, 1969.
- [59] P. Jackson, Ed., *IHS Jane's All the World's Aircraft: Development & Production, 2014-2015*. Couldson, Surrey, UK: IHS Jane's.
- [60] *Certification Specifications for Normal, Utility, Aerobatic, and Commuter Category Aeroplanes, CS-23*, 3rd ed. Köln: European Aviation Safety Agency, 2012.
- [61] Aurora Flight Sciences, Ed., “Centaur Optionally-Piloted Aircraft,” [Online] Available: http://www.aurora.aero/wp-content/uploads/2015/10/Centaur-Brochure_web_X1.pdf. Accessed on: Jul. 03 2016.
- [62] The MathWorks, *MATLAB*. [Online] Available: <http://www.mathworks.com/products/matlab/>. Accessed on: May 25 2016.
- [63] The MathWorks, *Simulink*. [Online] Available: <http://www.mathworks.com/products/simulink/>. Accessed on: May 25 2016.
- [64] Diamond Aircraft Industries, “DA 42 NG Airplane Maintenance Manual,” Oct. 2009.
- [65] Garmin, *G1000*. [Online] Available: <https://buy.garmin.com/en-US/US/in-the-air/general-aviation/flight-decks/g1000-/prod6420.html>. Accessed on: Aug. 22 2016.
- [66] R. Brockhaus, W. Alles, and R. Luckner, *Flugregelung*, 3rd ed. Berlin: Springer Berlin, 2010.
- [67] *MIL-HDBK-1797: Flying Qualities of Piloted Airplanes*. Military Handbook succeeding MIL-STD-1797A. Washington D.C., USA: Department of Defense, 1997.

- [68] B. Etkin and L. D. Reid, *Dynamics of flight: Stability and control*, 3rd ed. New York: Wiley, 1996.
- [69] B. L. Stevens and F. L. Lewis, *Aircraft control and simulation*, 2nd ed. Hoboken, N.J.: J. Wiley, 2003.
- [70] F. Schuck, "Ein integriertes Auslegungskonzept zur Sicherstellung exzellenter Handling Qualities für Kleinflugzeuge," Dissertation, Technical University of Munich, Garching, Germany, 2013.
- [71] J. C. Gibson, *Development of a methodology for excellence in handling qualities design for fly wire aircraft*. Delft: University Press, 1999.
- [72] Diamond Aircraft Industries, "DA 42 NG Airplane Flight Manual," Feb. 2009.
- [73] T. Fricke, "Handling Qualities Requirements for Brain Controlled Flight of a Light Aeroplane," Diploma Thesis, Institute of Flight System Dynamics, Technical University of Munich, Garching, Germany, 2013.
- [74] A. Degani, M. Shafto, and A. Kirlik, "Mode Usage in Automated Cockpits: Some Initial Observations," in *Proceedings of the International Federation of Automatic Control Man Machine Systems (IFAC-MMS) Conference*, T. B. Sheridan, Ed., 1995.
- [75] Airbus, *The Unique Benefits of Airbus Commonality*. [Online] Available: <http://www.airbus.com/innovation/proven-concepts/in-design/commonality/>. Accessed on: Oct. 07 2015.
- [76] W. Langewiesche and L. H. Collins, *Stick and rudder: An explanation of the art of flying*. New York: McGraw-Hill, 1972.
- [77] U.S. Department of Transportation, Ed., *Airplane Flying Handbook*. Oklahoma City, Oklahoma, USA: U.S. Department of Transportation, Federal Aviation Administration, 2004.
- [78] T. Fricke and F. Holzapfel, "Strategies for Manual Landing of Remotely Piloted Airplanes with Large Time Delay," in *30th Congress of the International Council of the Aeronautical Sciences*, 2016.
- [79] J. Hodgkinson, *Aircraft handling qualities*. Oxford: Blackwell Science, 1999.
- [80] J. Wood and J. Hodgkinson, *Definition of Acceptable Levels of Mismatch for Equivalent Systems of Augmented CTOL Aircraft*. MDC A6792. Saint Louis, Missouri, USA: McDonnell Douglas Corporation, 1980.
- [81] R. E. Smith and S. K. Sarrafian, *Effect of time delay on flying qualities: an update*. NASA TM-88264. Washington D.C., USA: National Aeronautics and Space Administration, 1986.
- [82] D. T. McRuer, *Pilot Induced Oscillations and Human Dynamic Behaviour*. CR-4683. Washington D.C., USA: National Aeronautics and Space Administration, 1995.
- [83] D. G. Mitchell and D. Klyde, "A critical examination of PIO prediction criteria," in *23rd Atmospheric Flight Mechanics Conference*, Aug. 1998 - Aug. 1998.

- [84] D. T. McRuer and E. S. Krendel, *Human Pilot Dynamics in Compensatory Systems: AFFDL-TR-65-15*. Wright-Patterson Air Force Base, Ohio, USA: Air Force Flight Dynamics Laboratory, 1965.
- [85] D. T. McRuer and E. S. Krendel, *Mathematical Models of Human Pilot Behavior: AGARDograph No. 188*. Neuilly-sur-Seine, France: North Atlantic Treaty Organization, Advisory Group for Aerospace Research & Development, 1974.
- [86] R. A. Hess, "Structural Model of the Adaptive Human Pilot," *Journal of Guidance, Control, and Dynamics*, vol. 3, no. 5, pp. 416–423, 1980.
- [87] M. S. Sanders and E. J. McCormick, *Human factors in engineering and design*, 6th ed. New York: McGraw-Hill, 1987.
- [88] D. T. McRuer et al., *New Approaches to Human-Pilot/Vehicle Dynamic Analysis: AFFDL-TR-67-150*. Wright-Patterson Air Force Base, Ohio, USA: Air Force Flight Dynamics Laboratory, 1968.
- [89] *Safety Information Bulletin 2013-02: Stall and Stick Pusher Training*. Köln: European Aviation Safety Agency, 2013.
- [90] R. A. Hess, "Obtaining Multi-Loop Pursuit-Control Pilot Models From Computer Simulation," in *45th AIAA Aerospace Sciences Meeting and Exhibit*
- [91] E. S. Krendel and D. T. McRuer, "Psychological and Physiological Skill Development - A Control Engineering Model," in *Proceedings of the 4th Annual Conference on Manual Control*, Washington D.C., USA, 1969, pp. 275–288.
- [92] T. P. Neal and R. E. Smith, *An In-Flight Investigation to Develop Control System Design Criteria for Fighter Airplanes: AFFDL-TR-70-74*. Wright-Patterson Air Force Base, Ohio, USA: Air Force Flight Dynamics Laboratory, 1970.
- [93] H. A. Mooij, *Criteria for low-speed longitudinal handling qualities of transport aircraft with closed-loop flight control systems*. Dordrecht, The Netherlands: M. Nijhoff for Nationaal Lucht- en Ruimtevaartlaboratorium (NLR), 1984.
- [94] R. A. Hess, "Unified Theory for Aircraft Handling Qualities and Adverse Aircraft-Pilot Coupling," *Journal of Guidance, Control, and Dynamics*, vol. 20, no. 6, pp. 1141–1148, 1997.
- [95] R. A. Hess, "Effects of Time Delays on Systems Subject to Manual Control," *Journal of Guidance, Control, and Dynamics*, vol. 7, no. 4, pp. 416–421, 1984.
- [96] L. Young and J. Meiry, "Bang-Bang Aspects of Manual Control in High-Order Systems," *IEEE Transactions on Automatic Control*, vol. 10, no. 3, pp. 336–341, 1965.
- [97] R. A. Hess, "A Rationale for Human Operator Pulsive Control Behavior," *Journal of Guidance, Control, and Dynamics*, vol. 2, no. 3, pp. 221–227, 1979.
- [98] J. J. Potter and W. E. Singhose, "Effects of Input Shaping on Manual Control of Flexible and Time-Delayed Systems," *Human Factors: The Journal of the Human Factors and Ergonomics Society*, vol. 56, no. 7, pp. 1284–1295, 2014.
- [99] R. A. Hess, "Dual-Loop Model of the Human Controller," *Journal of Guidance, Control, and Dynamics*, vol. 1, no. 4, pp. 254–260, 1978.

- [100] D. Graham and D. T. McRuer, *Analysis of Nonlinear Control Systems*. New York: John Wiley & Sons, 1961.
- [101] F. M. Drop, D. M. Pool, H. J. Damveld, van Paassen, Marinus M, and M. Mulder, "Identification of the feedforward component in manual control with predictable target signals," *IEEE Transactions on Cybernetics*, vol. 43, no. 6, pp. 1936–1949, 2013.
- [102] R. A. Hess and W. Siwakosit, "Assessment of Flight Simulator Fidelity in Multiaxis Tasks Including Visual Cue Quality," *Journal of Aircraft*, vol. 38, no. 4, pp. 607–614, 2001.
- [103] C. M. Harris and D. M. Wolpert, "Signal-dependent noise determines motor planning," *Nature*, vol. 394, no. 6695, pp. 780–784, 1998.
- [104] W. Levison, S. Baron, and D. Kleinman, "A Model for Human Controller Remnant," *IEEE Transactions on Man Machine Systems*, vol. 10, no. 4, pp. 101–108, 1969.
- [105] G. Pfurtscheller, C. Guger, G. Müller, G. Krausz, and C. Neuper, "Brain Oscillations Control Hand Orthosis in a Tetraplegic," *Neuroscience Letters*, vol. 292, no. 3, pp. 211–214, 2000.
- [106] G. R. Müller-Putz, R. Scherer, G. Pfurtscheller, and R. Rupp, "EEG-Based Neuroprosthesis Control: A Step Towards Clinical Practice," *Neuroscience Letters*, vol. 382, no. 1-2, pp. 169–174, 2005.
- [107] T. Fricke, T. O. Zander, K. Gramann, and F. Holzapfel, "First Pilot-in-the-loop Experiments on Brain Control of Horizontal Aircraft Motion," in *Deutscher Luft- und Raumfahrtkongress, Augsburg, 16.09.-18.09.14*, 2014.
- [108] F. Popescu, S. Fazli, Y. Badower, B. Blankertz, and K.-R. Müller, "Single Trial Classification of Motor Imagination Using 6 Dry EEG Electrodes," *PLoS ONE*, vol. 2, no. 7, e637, 2007.
- [109] NeuroSky, "MindWave User Guide," Jul. 2011.
- [110] Emotiv, "Emotiv EPOC & Testbench Specifications," 2014.
- [111] G. Pfurtscheller, C. Brunner, A. Schlögl, and Lopes da Silva, F.H., "Mu rhythm (de)synchronization and EEG Single-Trial Classification of Different Motor Imagery Tasks," *Neuroimage*, vol. 31, no. 1, pp. 153–159, 2006.
- [112] L. F. Nicolas-Alonso and J. Gomez-Gil, "Brain computer interfaces, a review," *Sensors (Basel, Switzerland)*, vol. 12, no. 2, pp. 1211–1279, 2012.
- [113] J. Kronegg, T. Alecu, and T. Pun, "Information theoretic bit-rate optimization for average trial protocol Brain-Computer Interfaces," in *HCI International 2003*, 2003.
- [114] M. Sahin, "Noise tolerance as a measure of channel discrimination for multi-channel neural interfaces," in *2001 23rd Annual International Conference of the IEEE Engineering n Medicine and Biology Society*, Oct. 2001, pp. 704–706.
- [115] J. Kronegg, S. Voloshynovskiy, and T. Pun, *Brain-Machine Interface Model: Upper-Capacity Bound, Signal-to-Noise Ratio Estimation, and Optimal Number of Symbols*. [Online] Available: <http://archive-ouverte.unige.ch/unige:48014>.

- [116] P. M. Fitts, "The Information Capacity of the Human Motor System in Controlling the Amplitude of Movement," *Journal of Experimental Psychology*, vol. 47, no. 6, pp. 381–391, 1954.
- [117] T. Fricke, "Scenarios and Requirements for a System for Brain Controlled Aircraft Flight," Semester thesis, Institute of Flight System Dynamics, Technical University of Munich, Garching, Germany, 2012.
- [118] T. Fricke and F. Holzapfel, "An Approach to Flight Control with Large Time Delays Derived from a Pulsive Human Control Strategy," in *AIAA Atmospheric Flight Mechanics Conference: American Institute of Aeronautics and Astronautics*, 2016.
- [119] R. B. Voas, "Manual control of the Mercury spacecraft," *Astronautics*, no. March, pp. 18–38, 1962.
- [120] National Aeronautics and Space Administration, "Project Gemini familiarization manual," Sep. 1965.
- [121] R. F. Stengel, "Manual Attitude Control of the Lunar Module," *Journal of Spacecraft and Rockets*, vol. 7, no. 8, pp. 941–948, 1970.
- [122] D. Eyles, "Apollo LM Guidance Computer Software for the Final Lunar Descent," *Automatica*, vol. 9, pp. 243–250, 1973.
- [123] E. Mueller, K. D. Bilimoria, and C. Frost, "Dynamic Coupling and Control Response Effects on Spacecraft Handling Qualities During Docking," *Journal of Spacecraft and Rockets*, vol. 46, no. 6, pp. 1288–1297, 2009.
- [124] D. C. Cheatham and C. T. Hackler, "Handling Qualities for Pilot Control of Apollo Lunar-Landing Spacecraft," *Journal of Spacecraft and Rockets*, vol. 3, no. 5, pp. 632–638, <http://dx.doi.org/10.2514/3.28506>, 1966.
- [125] D. Eyles, *Tales from the Lunar Module Guidance Computer*. [Online] Available: <http://www.doneyles.com/LM/Tales.html>. Accessed on: May 18 2016.
- [126] R. E. Bailey *et al.*, "Investigation of Reaction Control System Design on Spacecraft Handling Qualities for Docking," *Journal of Guidance, Control, and Dynamics*, vol. 32, no. 6, pp. 1723–1735, 2009.
- [127] Federal Government of the United States, "Special Conditions: Airbus Model A380-800 Airplane; Dynamic Braking, Interaction of Systems And Structures, Limit Pilot Forces, Side Stick Controllers, Dive Speed Definition, Electronic Flight Control System-Lateral-Directional Stability, Longitudinal Stability, And Low Energy Awareness, Electronic Flight Control System-Control Surface Awareness, Electronic Flight Control System-Flight Characteristics Compliance Via the Handling Qualities Rating Method, Flight Envelope Protection-General Limiting Requirements, Flight Envelope Protection-Normal Load Factor (G) Limiting, Flight Envelope Protection-High Speed Limiting, Flight Envelope Protection-Pitch And Roll Limiting, Flight Envelope Protection-High Incidence Protection and Alpha-Floor Systems, High Intensity Radiated Fields (HIRF) Protection, and Operation Without Normal Electrical Power," *Federal Register*, vol. 71, no. 69, 2006.

- [128] Federal Government of the United States, "Special Conditions: Airbus Model A350–900 Series Airplane; Electronic Flight-Control System: Lateral-Directional and Longitudinal Stability, and Low-Energy Awareness," *Federal Register*, vol. 79, no. 143, 2014.
- [129] van der Geest, P.J., A. Nieuwpoort, and J. Borger, "A Simulator Evaluation of Various Manual Control Concepts for Fly-By-Wire Transport Aircraft," in *Guidance, Navigation and Control Conference: American Institute of Aeronautics and Astronautics*, 1992.
- [130] F. Holzapfel, F. Schuck, L. Höcht, and G. Sachs, "Flight Dynamics Aspects of Path Control," in *AIAA Guidance, Navigation and Control Conference and Exhibit*, 2007.
- [131] Wittenstein AG, *Wittenstein*. [Online] Available: <http://www.wittenstein.de>. Accessed on: May 25 2016.
- [132] S. R. Sturmer, "Pitch rate sensitivity criterion for category C flight phases - Class IV aircraft," in *Astrodynamics Conference*, Aug. 1986 - Aug. 1986.
- [133] *MIL-STD-1472G: Human Engineering*. Washington D.C., USA: Department of Defense, 2012.
- [134] J. Verspay *et al.*, "Simulator evaluation on control and display issues for a future regional aircraft," in *21st Atmospheric Flight Mechanics Conference: American Institute of Aeronautics and Astronautics*, 1996.
- [135] T. O. Zander, T. Fricke, F. Holzapfel, and K. Gramann, "Applying active BCIs out of the lab - Piloting a plane with motor imagery.," in *6th International Brain-Computer Interface Conference, Graz, 16.09.-19.09.14*, 2014, pp. 384–387.
- [136] T. Fricke, V. Paixão, N. Loureiro, R. M. Costa, and F. Holzapfel, "Brain Control of Horizontal Airplane Motion - A Comparison of Two Approaches," in *AIAA Atmospheric Flight Mechanics Conference: American Institute of Aeronautics and Astronautics*, 2015.
- [137] Panavia Aircraft GmbH, *Tornado Aircraft*. [Online] Available: <http://www.panavia.de/aircraft/>. Accessed on: Sep. 12 2016.
- [138] Federal Aviation Administration, "Flight Simulation Training Device Initial and Continuing Qualification and Use," *Code of Federal Regulations, 14 CFR Part 60*, 2016.
- [139] Joint Aviation Authorities, "Joint Aviation Requirements - Flight Crew Licensing (Aeroplane)," *JAR-FCL 1 Amendment 7*, 2006.
- [140] H. W. Lilliefors, "On the Kolmogorov-Smirnov Test for Normality with Mean and Variance Unknown," *Journal of the American Statistical Association*, vol. 62, no. 318, pp. 399–402, 1967.
- [141] Israel Aerospace Industries, *Hunter*. [Online] Available: www.iai.co.il/2013/36718-16401-en/BusinessAreas_UnmannedAirSystems.aspx. Accessed on: Apr. 08 2016.

-
- [142] Airbus Defence and Space, *Tracker - Unmanned Aircraft System UAS*. [Online] Available: <http://militaryaircraft-airbusds.com/Aircraft/UAV/Tracker.aspx>. Accessed on: Apr. 08 2016.
- [143] D. J. Alvarez, D. H. Klyde, M. Lotterio, and T. Lambregts, "Fixed-Base Piloted Simulation Evaluation of Pitch Axis Fly-By-Wire Flight Control System Characteristics," in *AIAA Atmospheric Flight Mechanics Conference*
- [144] S. G. Hart and L. E. Staveland, "Development of NASA-TLX (Task Load Index): Results of Empirical and Theoretical Research," in *Human Mental Workload*, P. A. Hancock and N. Meshkati, Eds., Amsterdam, The Netherlands: North Holland Press, 1988.
- [145] Human Performance Research Group, NASA Ames Research Center, *NASA Task Load Index (TLX): Paper and Pencil Package*.
- [146] C. Pfendler, *Vergleichende Bewertung der NASA-TLX-Skala und der Zeis-Skala bei der Erfassung von Lernprozessen*. Wachtberg, Germany: Forschungsinstitut für Anthropotechnik, Forschungsgesellschaft für Angewandte Naturwissenschaften e.V., 1991.
- [147] Microsoft, *Excel*. [Online] Available: <https://office.microsoft.com/excel>. Accessed on: May 25 2016.
- [148] IBM, *SPSS*. [Online] Available: <http://www.ibm.com/software/analytics/spss/>. Accessed on: Jun. 07 2016.
- [149] R. G. O'Brien, "A Simple Test for Variance Effects in Experimental Designs," *Psychological Bulletin*, vol. 89, no. 3, pp. 570–574, 1981.
- [150] S. W. Greenhouse and S. Geisser, "On Methods in the Analysis of Profile Data," *Psychometrika*, vol. 24, no. 2, pp. 95–112, 1959.
- [151] H. Huynh and L. S. Feldt, "Estimation of the Box Correction for Degrees of Freedom from Sample Data in Randomized Block and Split-Plot Designs," *Journal of Educational Statistics*, vol. 1, no. 1, pp. 69–82, 1976.
- [152] D. A. Mindell, *Digital Apollo: Human and machine in spaceflight*. Cambridge, MA: MIT Press, 2008.
- [153] The MathWorks, *Stateflow*. [Online] Available: <http://www.mathworks.com/products/stateflow/>. Accessed on: May 25 2016.

APPENDIX

A. FLIGHT CONTROLLER LAYOUT

The structure of the prototypical flight controller presented in chapter 4, which is illustrated by the following figures, can be divided into three parts: longitudinal controller, autothrottle and lateral controller. These controllers are comprised of cascaded feedback loops and the following descriptions go from the outermost loop to the innermost loop. Starting with the longitudinal controller, Figure A.1 shows the feedback loops and switching structure of the Altitude Hold mode. If the control input δ_{lon} is larger than a threshold set to ± 0.05 , the Altitude Hold mode is inactive and δ_{lon} is multiplied by the longitudinal control sensitivity $K_{a,lon}$ to obtain the reference value of the longitudinal command variable $C_{lon,dem}$. If, on the other hand, $|\delta_{lon}| < 0.05$ and, at the same time, $|\dot{h}| < 0.508 \text{ m/s}$ (i.e., 100 ft/min), the vertical speed loop and the altitude loop are closed, so that the reference altitude is maintained. Upon switching, a setpoint altitude value is generated that can be reached aperiodically.

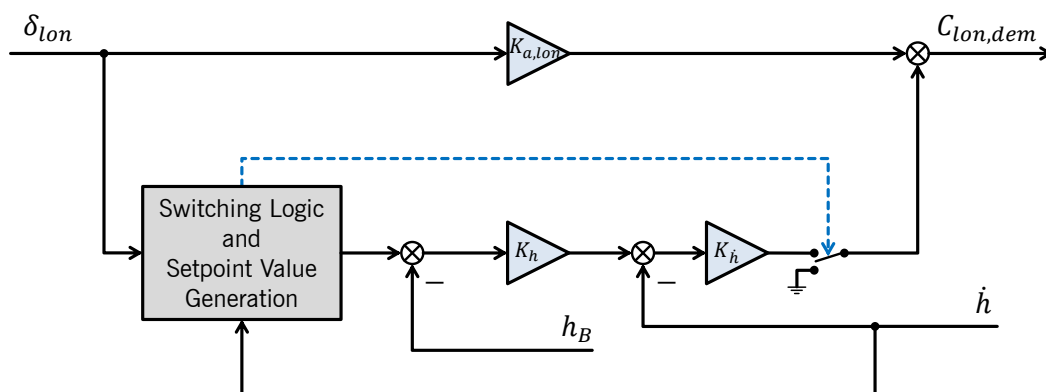


Figure A.1 – Altitude hold mode structure

Next, Figure A.2 shows the outer control loop of the longitudinal controller. Before comparison of nominal and actual value, the command variable is integrated. A feedforward gain h_{lon} accelerates the system response. Note that the limitations of θ and γ (cf. section 4.2.2) are implemented in this loop. Since these saturation-type nonlinearities are located downstream of an integrator, an anti-windup structure with gain K_{AW} is set up. The outcome of the longitudinal outer loop is a command in load factor change $\Delta n_{z,cmd}$.

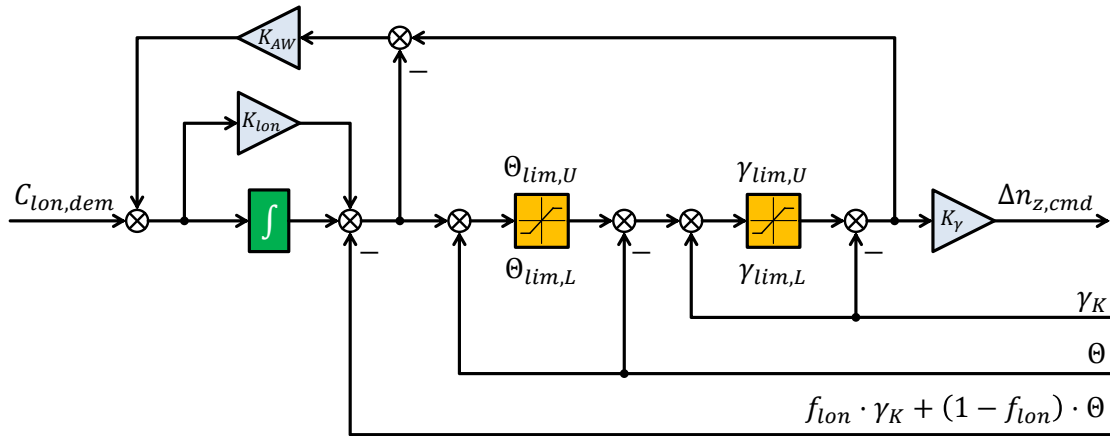


Figure A.2 – Longitudinal outer control loop structure

The commanded load factor change $\Delta n_{z,cmd}$ is the input of the longitudinal inner loop, whose structure is shown in Figure A.3. The feedback Δn_z follows equation (A.1), where $1/\cos \Phi$ approximates the load factor required in a steady-state turn [66].

$$\Delta n_z = (n_z)_B - 1/\cos \Phi \tag{A.1}$$

$$\dot{\Theta} = q \cdot \cos \Phi - r \cdot \sin \Phi \tag{A.2}$$

Given that the longitudinal controller does not control the airplane's motion in its plane of symmetry, but the motion in the vertical plane, $\dot{\Theta}$ is fed back instead of q . The value of $\dot{\Theta}$ can be computed from q , r and Φ as shown by equation (A.2) [66].

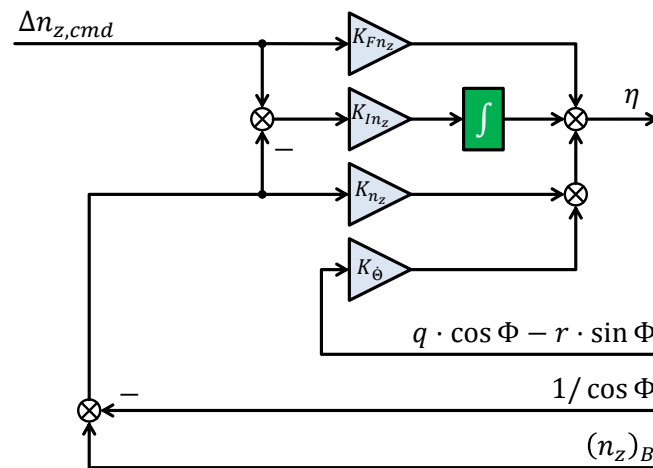


Figure A.3 – Longitudinal inner control loop structure

It may be noted that the controller layout propagates steps from longitudinal pilot inputs to the elevator actuator. However, the actuator model prevented actual step deflections of the control surface and beyond that, the controller gains were tuned such that the steps commanded at the actuator level were rather small. In the final configuration, they were always smaller than 0.77° .

Figure A.4 shows the structure of the autothrottle control loop. A proportional-integral controller acts on the error between demanded and measured IAS and generates a reference longitudinal load factor. Thrust lever commands are restricted and an anti-windup feedback K_{AW} prevents integrator windup.

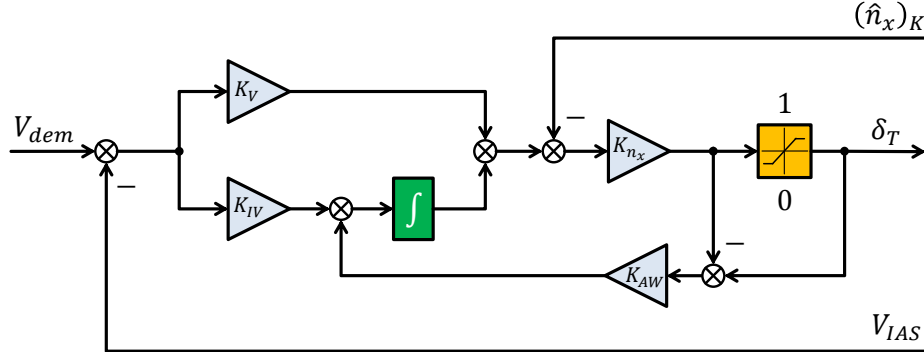


Figure A.4 – Autothrottle structure

Continuing with the lateral controller, Figure A.5 shows the structure of the turn rate hold mode. If the control input δ_{lat} is larger than a threshold set to ± 0.05 , the turn rate hold mode is inactive and δ_{lat} is multiplied by the lateral control sensitivity $K_{a,lat}$ to obtain the longitudinal command variable C_{lat} . This variable is then integrated and subsequently limited to the upper and lower turn rate limits (cf. equation (4.12)), so that the integrated lateral command variable $C_{lat,int}$ is obtained, which can be seen as a commanded turn rate. Integrator windup is prevented by a feedback structure with anti-windup gain k_{AW} . Moreover, a bank angle feedback with a deadband of $\pm\pi/6$ introduces spiral stability for bank angles beyond $\pm 30^\circ$. The bank angle limitation gain K_{BAL} follows equation (A.3) and thereby effectively restricts bank angles to the permissible attitude range $[-\Phi_{max,att}, \Phi_{max,att}]$.

$$K_{BAL} = \frac{1}{\Phi_{max,att} - \pi/6} \quad (A.3)$$

If equation (A.4) is satisfied, i.e., if both control input and commanded turn rate are small, the upper switch in the structure of Figure A.5 is closed and as a result, zero turn rate is established and maintained. If, on the other hand, equation (A.5) is satisfied, i.e., if the control input is small and the commanded turn rate is approximately standard turn rate ($\pi/60s$) in either direction, both switches in Figure A.5 are closed to maintain standard turn rate. To achieve this, the value of the factor K_{ST} equals the standard turn rate.

$$\begin{cases} |\delta_{lat}| < 0.05 \\ |C_{lat,int}| < \pi/360s \end{cases} \quad (A.4)$$

$$\begin{cases} |\delta_{lat}| < 0.05 \\ \left| |C_{lat,int}| - \pi/60s \right| < \pi/360s \end{cases} \quad (A.5)$$

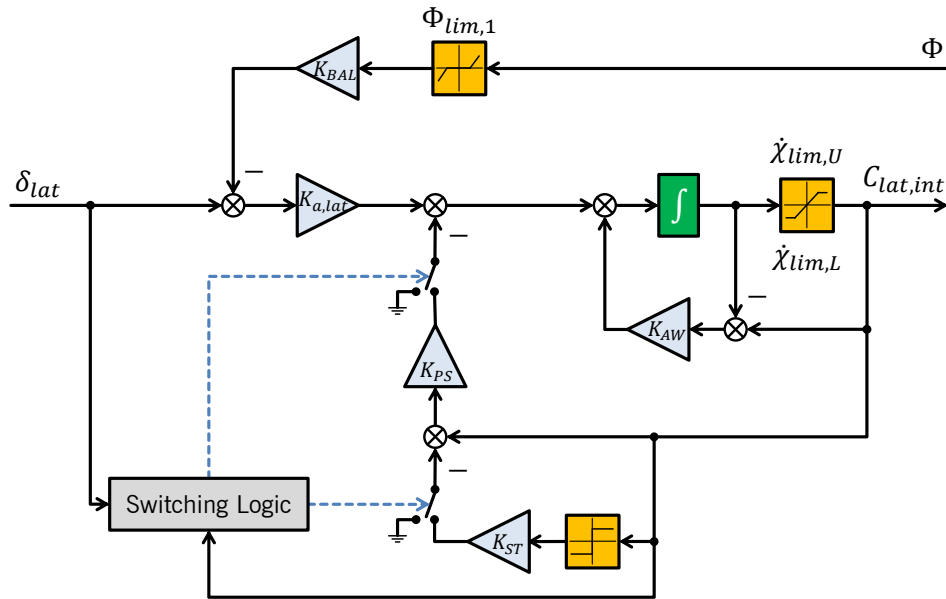


Figure A.5 – Turn rate hold mode structure

Next, Figure A.6 shows the structure of the lateral outer control loop. Since a bank angle command is generated for the inner loop, the bank angle limits from equation (4.11) are enforced here. However, no anti-windup scheme is needed, because the bank angle limitation is already implicitly applied by the bank angle feedback and the turn rate limitation in the structure of Figure A.5.

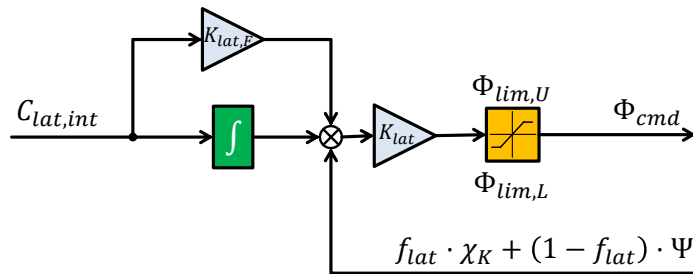


Figure A.6 – Lateral outer control loop structure

The lateral inner control loops structure is shown in Figure A.7. A proportional bank angle controller generates a roll rate command, which is fed to a proportional-integral roll rate controller. The feedback of yaw rate aims at canceling L_r .

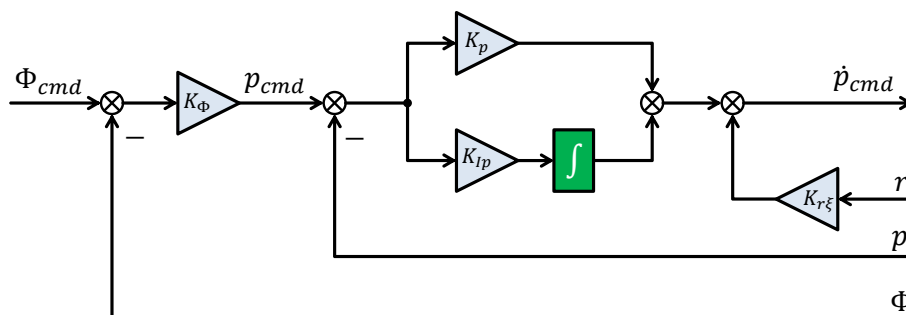


Figure A.7 – Lateral inner control loops structure

Figure A.8 shows the structure of the directional inner control loops, which is similar to that of the lateral inner control loops. Remember that, according to the design goals formulated in section 4.1, $n_{y,cmd} = 0$. A proportional n_y controller generates a yaw rate command, which is fed to a proportional-integral yaw rate controller.

$$r_{\dot{\Psi}} \approx \dot{\Psi} \cdot \cos \Phi \cdot \cos \Theta = \frac{g}{V_K} \cdot \sin \Phi \cdot \cos \Theta \quad (\text{A.6})$$

To prevent the yaw rate controller from interfering with turning flight, an estimation of the turn-induced yaw rate is fed back as well. According to [66], yaw rate during a turn with $\dot{\Theta} = 0$ can be approximated as in equation (A.6). The feedback of roll rate aims at canceling N_p .

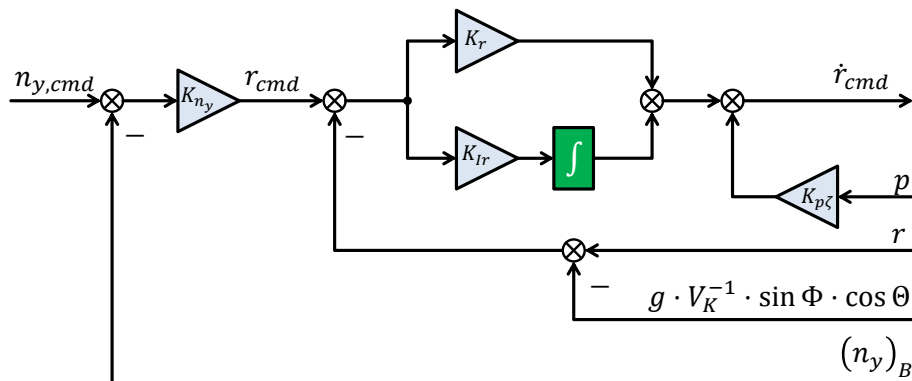


Figure A.8 – Directional inner control loops structure

Finally, the lateral-directional control allocation is shown in Figure A.9. It accounts for the cross-coupling effects N_{ξ} and L_{ζ} and derives appropriate aileron and rudder deflections to generate the commanded rate accelerations.

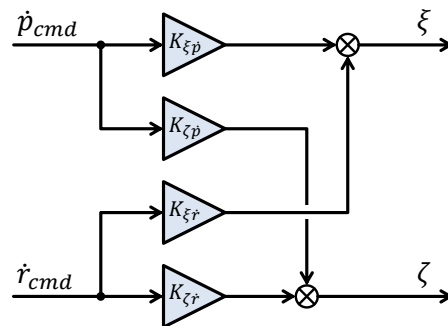


Figure A.9 – Lateral-directional control allocation structure

B. HANDBOOK FOR EXPERIMENTS ON MANUAL REMOTE FLIGHT CONTROL

The following pages show the English version of the experimental handbook that was used during the experiments on manual remote flight control. An equivalent German version, which is not shown here, had been compiled for German subjects. The handbook was handed out to each subject in four parts. The first part, comprising pages 1 through 7, introduced the subjects to the experiments in general, demanded some personal information that subjects agreed to provide and presented the TLX rating scale. Then, a description of task A was provided, followed by the associated rating scales. The second part, namely pages 8 through 17, started with a debriefing on task A that familiarized the subject pilots with possible control strategies to make sure that everyone had the same information for the following tasks. After that, task B was introduced and the TLX rating scales for all runs of task B were provided. The third part comprised pages 18 through 21 and contained the information and rating scales related to task C. The fourth and last part, ranging from page 22 to page 26, then provided the same content for task D and additionally concluded the session with some final questions.

Participant number:

Experiment Handbook – Introduction

Dear Participant,

Thank you for supporting me in my research activities! By your participation in these experiments, you contribute to investigations that may be valuable in tailoring future flight control systems to the pilots' needs.

Your participation is voluntary. You can quit at any moment without justification.

This document guides you through the experimental session. It contains information, instructions and questionnaires. If questions should arise, you can ask them at any time. This handbook is divided into 4 parts that will be handed out successively to give you the information you need for each part of the experimental session.

Aim

One issue with **remote flight control of unmanned aerial vehicles** over large distances is the latency or time delay introduced by signal transmission. The reaction of the aircraft to a control input as seen in the ground control station can be delayed by more than a second.

In these experiments, the suitability of different control system concepts for flight control with large latency will be investigated. The latency in these experiments is constant and in the order of seconds.

Note: This study investigates the performance of different flight control concepts, not your performance as a pilot. The questionnaires aim at capturing your subjective opinion.

Personal Information and Experience

To help me gain insight into your personal experience which may affect the experiments, kindly provide the following information about yourself.

Age: _____

Piloting experience [hours]: _____

Pilot licenses
(current and former): _____

Class and type ratings
(current and former): _____

Last flight (month/year): _____

Have you ever experienced large
latencies in (flight) control tasks? _____

Aircraft / Control System

Flight dynamics and flight control system differ in each part of the experiment and will be explained in detail elsewhere in this document. Here, some common features will be explained.

Participant number:

You control the airplane's movement in the pitch axis and in the roll axis. A sidestick is used as control inceptor. The pedals have no function. You can have your feet rested on the ground. Yaw axis control is automated. Moreover, speed is maintained by an autothrottle system. The throttle levers therefore have no function. All other controls in the cockpit, including gear and flap lever, should not be operated either. Please also do not press any buttons on the sidestick. Should you happen to press one of those buttons, please indicate this while continuing to fly!

In short: you only control pitching and rolling motion. You only use the sidestick.

All the different control configurations that you will fly can be categorized into two types: those with continuous control and those with on-off control. Continuous control is the conventional form of flight control, where control inputs of varying amplitude can be generated. A greater deflection of the sidestick results in an equally greater reaction of the airplane.

With on-off control, you can choose three distinct sidestick deflections in each axis. The neutral position is identical to the neutral position in the case of continuous control. From this position, the stick can be forced to "snap" into two opposing positions along each axis. It may be more vivid to call those positions "up" and "down" in the longitudinal axis and "left" and "right" in the lateral axis. This means that with on-off control, the control input amplitude and therefore the amplitude of the airplane's reaction is fixed and cannot be influenced by the pilot.

Whether you will be flying with continuous or on-off control will be announced prior to each run. Prior to the first run with on-off control you will have the opportunity to try how the sidestick feels and behaves with this type of control.

Plan

The experimental session will take about 2.5 hours.

Welcome and Information	
Part A	Introduction
	2x Generic Tracking Task
	Debriefing
Part B	Introduction
	8x Flying Task 1 – Tracking
Break	
Part C	Introduction
	2x Flying Task 2 – Approach
Part D	Introduction
	2x Flying Task 2 – Approach with Predictor
Debriefing	

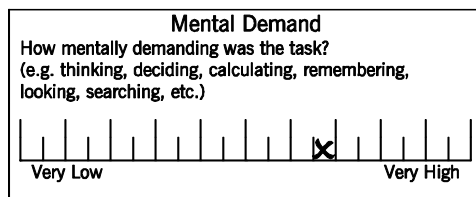
Participant number:

Pilot Rating: Introduction to the NASA-TLX

Each run is to be rated using the NASA Task Load Index (NASA-TLX), an index which quantifies your subjective impression of work load. The NASA-TLX defines six sources of workload:

- **Mental Demand**
How mentally demanding was the task?
(e.g. thinking, deciding, calculating, remembering, looking, searching, etc.)
- **Physical Demand**
How physically demanding was the task?
(e.g. pushing, pulling, turning, controlling, activating, etc.)
- **Temporal Demand**
How hurried or rushed was the pace of the task?
How much time pressure did you feel?
- **Performance**
How successful were you in accomplishing what you were asked to do?
How satisfied were you with your performance?
- **Effort**
How hard did you have to work (mentally and physically)
to accomplish your level of performance?
- **Frustration**
How insecure, discouraged, irritated, stressed and annoyed versus
secure, gratified, content, relaxed and complacent did you feel during the task?

After each run, the workload in each of these dimensions is to be rated on a 20 point scale, like shown in the following example.



After the last run of each task, the sources of workload are to be compared against each other. For every one of the 15 pairs presented, mark that source of workload that was more important for the total workload perceived. In the following example, the physical demand is marked as more important than frustration.

Frustration
 Physical Demand

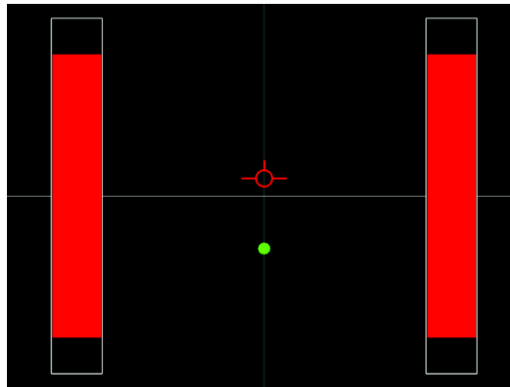
Participant number:

Experiment Handbook – Part A

Dynamics / Displays

In Part A, no specific flight simulation is implemented. Instead, the reactions to your control inputs follow generic, airplane-like dynamics. You only control the longitudinal motion (“up and down”).

The display is comprised of a stationary cross for orientation in the background, an airplane symbol, a target ball and two large, vertical bars. The **color** of airplane symbol and bars changes with the offset between airplane symbol and target ball. **Red** indicates a large offset, **yellow** a medium offset and **green** a small offset.



The airplane symbol on the display behaves similarly to the flight path of a real airplane at high speeds. Pulling on the sidestick moves the symbol up on the display. Pushing the sidestick moves the symbol down on the display. With the sidestick in its neutral position, the symbol remains at its present position. Remember that the display reaction here and in all other parts of the experimental session is delayed by latency!

Task

Align airplane symbol and target ball! During the run, the target ball jumps to different positions on the vertical axis and waits there until you have followed him before jumping anew. Follow as quickly as possible to lose as few points as possible. Your score is represented by the **height** of the two bars. Your score continuously decreases as long as airplane symbol and bars are red or yellow. When airplane symbol and target ball are nearly aligned (green color), your score does not change. In this situation, no further corrections are required and after a few seconds the target ball jumps to the next position.

Prior to 1st run

Move the sidestick in all directions to familiarize with its characteristics.

Participant number:

After 1st run

Describe the entire 1st run in the following ratings!

<p style="text-align: center;">Mental Demand</p> <p>How mentally demanding was the task? (e.g., thinking, deciding, calculating, remembering, looking, searching, etc.)</p> <p style="text-align: center;">Very Low Very High</p>	<p style="text-align: center;">Performance</p> <p>How successful were you in accomplishing what you were asked to do? How satisfied were you with your performance?</p> <p style="text-align: center;">Perfect Failure</p>
<p style="text-align: center;">Physical Demand</p> <p>How physically demanding was the task? (e.g., pushing, pulling, turning, controlling, activating, etc.)</p> <p style="text-align: center;">Very Low Very High</p>	<p style="text-align: center;">Effort</p> <p>How hard did you have to work (mentally and physically) to accomplish your level of performance?</p> <p style="text-align: center;">Very Low Very High</p>
<p style="text-align: center;">Temporal Demand</p> <p>How hurried or rushed was the pace of the task? How much time pressure did you feel?</p> <p style="text-align: center;">Very Low Very High</p>	<p style="text-align: center;">Frustration</p> <p>How insecure, discouraged, irritated, stressed and annoyed versus secure, gratified, content, relaxed and complacent did you feel?</p> <p style="text-align: center;">Very Low Very High</p>

When during the run did you develop a strategy to cope with the latency?

right at the beginning
 near the end
 not at all

If you have found a strategy, did the control system rather support you or hinder you?

rather hindered
 rather supported

When during the run did you acquire a feeling for the amount of latency?

right at the beginning
 near the end
 not at all

Prior to 2nd run

Move the sidestick in all directions to familiarize with its characteristics.

Participant number:

After 2nd run

Describe the entire 2nd run in the following ratings!

<p style="text-align: center;">Mental Demand</p> <p>How mentally demanding was the task? (e.g., thinking, deciding, calculating, remembering, looking, searching, etc.)</p> <p style="text-align: center;">Very Low Very High</p>	<p style="text-align: center;">Performance</p> <p>How successful were you in accomplishing what you were asked to do? How satisfied were you with your performance?</p> <p style="text-align: center;">Perfect Failure</p>
<p style="text-align: center;">Physical Demand</p> <p>How physically demanding was the task? (e.g., pushing, pulling, turning, controlling, activating, etc.)</p> <p style="text-align: center;">Very Low Very High</p>	<p style="text-align: center;">Effort</p> <p>How hard did you have to work (mentally and physically) to accomplish your level of performance?</p> <p style="text-align: center;">Very Low Very High</p>
<p style="text-align: center;">Temporal Demand</p> <p>How hurried or rushed was the pace of the task? How much time pressure did you feel?</p> <p style="text-align: center;">Very Low Very High</p>	<p style="text-align: center;">Frustration</p> <p>How insecure, discouraged, irritated, stressed and annoyed versus secure, gratified, content, relaxed and complacent did you feel?</p> <p style="text-align: center;">Very Low Very High</p>

Physical Demand	□	□	Temporal Demand	□	□	Frustration
Effort	□	□	Mental Demand	□	□	Effort
Frustration	□	□	Physical Demand	□	□	Temporal Demand
Effort	□	□	Frustration	□	□	Performance
Mental Demand	□	□	Temporal Demand	□	□	Physical Demand
Physical Demand	□	□	Effort	□	□	Performance
Temporal Demand	□	□	Performance	□	□	Physical Demand
Frustration	□	□	Mental Demand			

Please also fill out the next page >>>

Participant number:

When during the run did you develop a strategy to cope with the latency?

right at the beginning near the end not at all

If you have found a strategy, did the control system rather support you or hinder you?

rather hindered rather supported

When during the run did you acquire a feeling for the amount of latency?

right at the beginning near the end not at all

Participant number:

Debriefing Part A

The results from part A will be used to investigate how people react to the problem of flight control with large latency. The colors and the score aimed at generating stress. Since each participant may have found a different strategy to cope with the problem, this debriefing provides background information to establish a common understanding of all participants for the remainder of the experimental session.

The familiar art of (flight) control with a continuous control system is done by continuous changes in sidestick deflection. In the case of control with large latency, however, operators often make pulse-like inputs. They abruptly bring the stick from its neutral position to a certain deflection, hold it there for a certain amount of time and then bring it back to neutral. Thereby, the following exemplary strategies, formulated from the point of view of the pilot, can be pursued.

- "From my experience I know that I need to pull the stick full aft for two seconds to raise the nose by 2°."
- "I currently hold the stick at a constant deflection. From my experience, the latency amounts to about 3 seconds. To point the nose onto the target, I therefore need to bring the stick back to neutral about 3 seconds before reaching the target."
(Estimating time delay and velocity of movement)
- "I currently hold the stick at a constant deflection. My experience has shown me that the airplane's nose continues to move about 1° after I bring the stick back to neutral. To point the nose onto the target, I therefore need to bring the stick back to neutral about 1° before the target."
(Estimating distance on the display)

You are not required to apply these strategies, but you may do so. Pulse-like control inputs can be made with both continuous and on-off control systems.

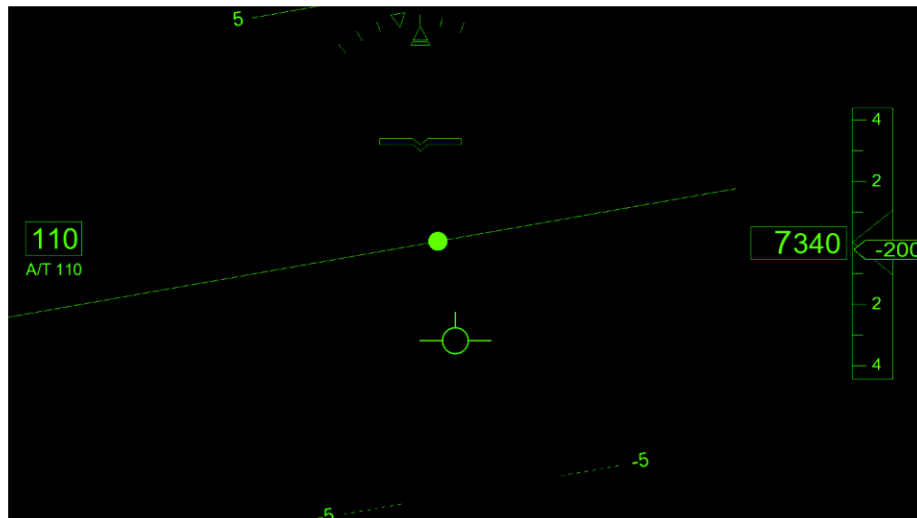
Participant number:

Experiment Handbook – Part B

Dynamics / Displays

In this part, you will fly the light twin-engine airplane Diamond DA42 (class MEP). **Again, you only control the longitudinal motion** („up and down“). You control the airplane through a flight control computer. Sidestick inputs correspond to a demand to change the flight path climb angle. By pulling the sidestick, you make the flight path go up. By pushing, you make it go down more and more towards the ground. Without control input, the current flight path climb angle is maintained. Thus, the flight dynamics are very similar to the dynamics known from part A. If the flight path climb angle should reach extreme values, control authority may be restricted by the flight control computer to prevent a departure from the flight envelope.

The display of part A is replaced by a head-up display (HUD), which is conform to the forward view from the airplane shown during the experiment. The same airplane symbol that you controlled in part A is controlled again here, because it symbolizes the flight path climb angle. The target ball as well is known from part A. In the background of the HUD, you can see a horizon line and a pitch/climb angle scale with steps of 5°. The horizontal bar with a bend represents the pitch angle. The curved scale on top shows 5°, 10° and 15° bank angle. Altitude and vertical speed are shown on the right and airspeed and autothrottle target speed are shown on the left.



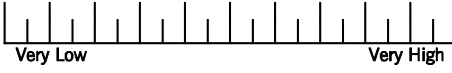



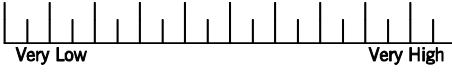

Task

Follow the target flight path, represented by the target ball, as accurately as possible! The target path jumps and wanders in this task without waiting for you. There are no colors and no score.

The first two jumps allow you to familiarize with the current configuration. After these two jumps, the airplane returns to level flight on its own while ignoring your control inputs. Only then, the actual experimental run starts.

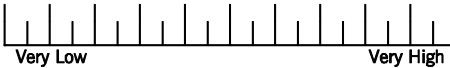

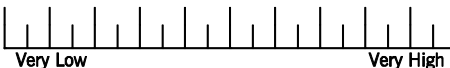

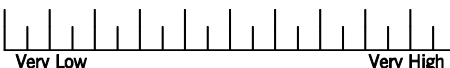
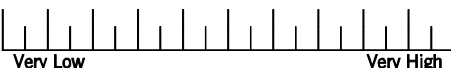
Participant number:

After the 1st run

<p style="text-align: center;">Mental Demand</p> <p>How mentally demanding was the task? (e.g., thinking, deciding, calculating, remembering, looking, searching, etc.)</p>  <p style="display: flex; justify-content: space-between;">Very LowVery High</p>	<p style="text-align: center;">Performance</p> <p>How successful were you in accomplishing what you were asked to do? How satisfied were you with your performance?</p>  <p style="display: flex; justify-content: space-between;">PerfectFailure</p>
<p style="text-align: center;">Physical Demand</p> <p>How physically demanding was the task? (e.g., pushing, pulling, turning, controlling, activating, etc.)</p>  <p style="display: flex; justify-content: space-between;">Very LowVery High</p>	<p style="text-align: center;">Effort</p> <p>How hard did you have to work (mentally and physically) to accomplish your level of performance?</p>  <p style="display: flex; justify-content: space-between;">Very LowVery High</p>
<p style="text-align: center;">Temporal Demand</p> <p>How hurried or rushed was the pace of the task? How much time pressure did you feel?</p>  <p style="display: flex; justify-content: space-between;">Very LowVery High</p>	<p style="text-align: center;">Frustration</p> <p>How insecure, discouraged, irritated, stressed and annoyed versus secure, gratified, content, relaxed and complacent did you feel?</p>  <p style="display: flex; justify-content: space-between;">Very LowVery High</p>

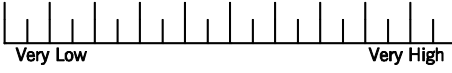

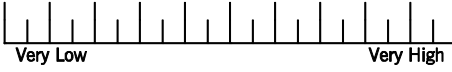



Participant number:

After the 2nd run

<p>Mental Demand How mentally demanding was the task? (e.g., thinking, deciding, calculating, remembering, looking, searching, etc.)</p>  <p>Very Low Very High</p>	<p>Performance How successful were you in accomplishing what you were asked to do? How satisfied were you with your performance?</p>  <p>Perfect Failure</p>
<p>Physical Demand How physically demanding was the task? (e.g., pushing, pulling, turning, controlling, activating, etc.)</p>  <p>Very Low Very High</p>	<p>Effort How hard did you have to work (mentally and physically) to accomplish your level of performance?</p>  <p>Very Low Very High</p>
<p>Temporal Demand How hurried or rushed was the pace of the task? How much time pressure did you feel?</p>  <p>Very Low Very High</p>	<p>Frustration How insecure, discouraged, irritated, stressed and annoyed versus secure, gratified, content, relaxed and complacent did you feel?</p>  <p>Very Low Very High</p>

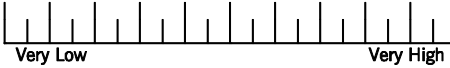

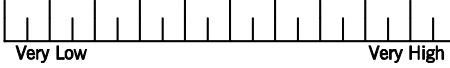

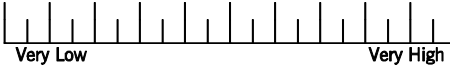

Participant number:

After the 3rd run

<p>Mental Demand How mentally demanding was the task? (e.g., thinking, deciding, calculating, remembering, looking, searching, etc.)</p>  <p>Very Low Very High</p>	<p>Performance How successful were you in accomplishing what you were asked to do? How satisfied were you with your performance?</p>  <p>Perfect Failure</p>
<p>Physical Demand How physically demanding was the task? (e.g., pushing, pulling, turning, controlling, activating, etc.)</p>  <p>Very Low Very High</p>	<p>Effort How hard did you have to work (mentally and physically) to accomplish your level of performance?</p>  <p>Very Low Very High</p>
<p>Temporal Demand How hurried or rushed was the pace of the task? How much time pressure did you feel?</p>  <p>Very Low Very High</p>	<p>Frustration How insecure, discouraged, irritated, stressed and annoyed versus secure, gratified, content, relaxed and complacent did you feel?</p>  <p>Very Low Very High</p>

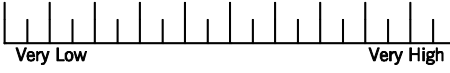

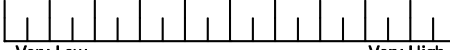

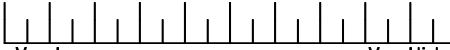
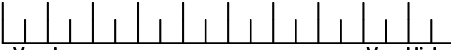
Participant number:

After the 4th run

<p style="text-align: center;">Mental Demand</p> <p>How mentally demanding was the task? (e.g., thinking, deciding, calculating, remembering, looking, searching, etc.)</p>  <p style="display: flex; justify-content: space-between;">Very LowVery High</p>	<p style="text-align: center;">Performance</p> <p>How successful were you in accomplishing what you were asked to do? How satisfied were you with your performance?</p>  <p style="display: flex; justify-content: space-between;">PerfectFailure</p>
<p style="text-align: center;">Physical Demand</p> <p>How physically demanding was the task? (e.g., pushing, pulling, turning, controlling, activating, etc.)</p>  <p style="display: flex; justify-content: space-between;">Very LowVery High</p>	<p style="text-align: center;">Effort</p> <p>How hard did you have to work (mentally and physically) to accomplish your level of performance?</p>  <p style="display: flex; justify-content: space-between;">Very LowVery High</p>
<p style="text-align: center;">Temporal Demand</p> <p>How hurried or rushed was the pace of the task? How much time pressure did you feel?</p>  <p style="display: flex; justify-content: space-between;">Very LowVery High</p>	<p style="text-align: center;">Frustration</p> <p>How insecure, discouraged, irritated, stressed and annoyed versus secure, gratified, content, relaxed and complacent did you feel?</p>  <p style="display: flex; justify-content: space-between;">Very LowVery High</p>

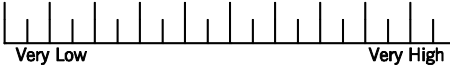

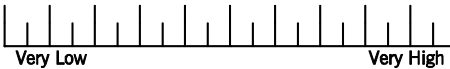

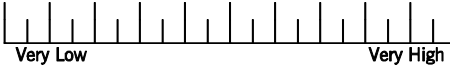

Participant number:

After the 5th run

<p style="text-align: center;">Mental Demand</p> <p>How mentally demanding was the task? (e.g., thinking, deciding, calculating, remembering, looking, searching, etc.)</p>  <p style="text-align: center;">Very Low Very High</p>	<p style="text-align: center;">Performance</p> <p>How successful were you in accomplishing what you were asked to do? How satisfied were you with your performance?</p>  <p style="text-align: center;">Perfect Failure</p>
<p style="text-align: center;">Physical Demand</p> <p>How physically demanding was the task? (e.g., pushing, pulling, turning, controlling, activating, etc.)</p>  <p style="text-align: center;">Very Low Very High</p>	<p style="text-align: center;">Effort</p> <p>How hard did you have to work (mentally and physically) to accomplish your level of performance?</p>  <p style="text-align: center;">Very Low Very High</p>
<p style="text-align: center;">Temporal Demand</p> <p>How hurried or rushed was the pace of the task? How much time pressure did you feel?</p>  <p style="text-align: center;">Very Low Very High</p>	<p style="text-align: center;">Frustration</p> <p>How insecure, discouraged, irritated, stressed and annoyed versus secure, gratified, content, relaxed and complacent did you feel?</p>  <p style="text-align: center;">Very Low Very High</p>

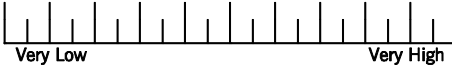

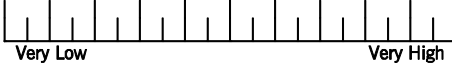

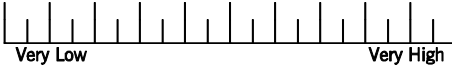

Participant number:

After the 6th run

<p>Mental Demand How mentally demanding was the task? (e.g., thinking, deciding, calculating, remembering, looking, searching, etc.)</p>  <p>Very Low Very High</p>	<p>Performance How successful were you in accomplishing what you were asked to do? How satisfied were you with your performance?</p>  <p>Perfect Failure</p>
<p>Physical Demand How physically demanding was the task? (e.g., pushing, pulling, turning, controlling, activating, etc.)</p>  <p>Very Low Very High</p>	<p>Effort How hard did you have to work (mentally and physically) to accomplish your level of performance?</p>  <p>Very Low Very High</p>
<p>Temporal Demand How hurried or rushed was the pace of the task? How much time pressure did you feel?</p>  <p>Very Low Very High</p>	<p>Frustration How insecure, discouraged, irritated, stressed and annoyed versus secure, gratified, content, relaxed and complacent did you feel?</p>  <p>Very Low Very High</p>

Participant number:

After the 7th run

<p style="text-align: center;">Mental Demand</p> <p>How mentally demanding was the task? (e.g., thinking, deciding, calculating, remembering, looking, searching, etc.)</p>  <p style="text-align: center;">Very Low Very High</p>	<p style="text-align: center;">Performance</p> <p>How successful were you in accomplishing what you were asked to do? How satisfied were you with your performance?</p>  <p style="text-align: center;">Perfect Failure</p>
<p style="text-align: center;">Physical Demand</p> <p>How physically demanding was the task? (e.g., pushing, pulling, turning, controlling, activating, etc.)</p>  <p style="text-align: center;">Very Low Very High</p>	<p style="text-align: center;">Effort</p> <p>How hard did you have to work (mentally and physically) to accomplish your level of performance?</p>  <p style="text-align: center;">Very Low Very High</p>
<p style="text-align: center;">Temporal Demand</p> <p>How hurried or rushed was the pace of the task? How much time pressure did you feel?</p>  <p style="text-align: center;">Very Low Very High</p>	<p style="text-align: center;">Frustration</p> <p>How insecure, discouraged, irritated, stressed and annoyed versus secure, gratified, content, relaxed and complacent did you feel?</p>  <p style="text-align: center;">Very Low Very High</p>

Participant number:

After the 8th run

<p style="text-align: center;">Mental Demand</p> <p>How mentally demanding was the task? (e.g., thinking, deciding, calculating, remembering, looking, searching, etc.)</p> <p style="text-align: center;">Very Low Very High</p>	<p style="text-align: center;">Performance</p> <p>How successful were you in accomplishing what you were asked to do? How satisfied were you with your performance?</p> <p style="text-align: center;">Perfect Failure</p>
<p style="text-align: center;">Physical Demand</p> <p>How physically demanding was the task? (e.g., pushing, pulling, turning, controlling, activating, etc.)</p> <p style="text-align: center;">Very Low Very High</p>	<p style="text-align: center;">Effort</p> <p>How hard did you have to work (mentally and physically) to accomplish your level of performance?</p> <p style="text-align: center;">Very Low Very High</p>
<p style="text-align: center;">Temporal Demand</p> <p>How hurried or rushed was the pace of the task? How much time pressure did you feel?</p> <p style="text-align: center;">Very Low Very High</p>	<p style="text-align: center;">Frustration</p> <p>How insecure, discouraged, irritated, stressed and annoyed versus secure, gratified, content, relaxed and complacent did you feel?</p> <p style="text-align: center;">Very Low Very High</p>

Physical Demand	□	□	Temporal Demand	□	□	Frustration
Effort	□	□	Mental Demand	□	□	Effort
Frustration	□	□	Physical Demand	□	□	Temporal Demand
Effort	□	□	Frustration	□	□	Performance
Mental Demand	□	□	Temporal Demand	□	□	Physical Demand
Physical Demand	□	□	Effort	□	□	Performance
Temporal Demand	□	□	Performance	□	□	Physical Demand
Frustration	□	□	Mental Demand	□	□	Physical Demand

Participant number:

Experiment Handbook – Part C

Dynamics / Displays

In this part of the experiment you fly the same airplane with the same flight controller as in the previous part. This time, however, **you control the trajectory both vertically and horizontally**. During a sideways deflection of the sidestick, a turn rate into the desired direction is built up. Without lateral sidestick input, the current turn rate is maintained. If in this case the current turn rate is approximately zero, the airplane automatically returns to straight flight (“wings leveler”). If the current turn rate approximately equals standard turn rate and no control input is made, the airplane automatically turns at standard turn rate (“standard rate turn hold”). Similarly, the altitude is maintained as soon as the flight path climb angle is approximately zero and no longitudinal control input is made (“altitude hold”).

Bank and pitch angle are limited. Furthermore, excessively high and low speeds are prevented through a variable limit of the flight path climb angle (“protections”).

Control sensitivity is neither extremely high nor extremely low. It is comparable to the moderate sensitivities of the previous part of the experimental session.

A compass rose is introduced into the HUD, which otherwise you are already familiar with. An arc along the compass rose’s circumference indicates the current turn rate. Two large radial marks intersect this arc at standard turn rate. A triangle inside the compass rose indicates the target heading and a box near the altitude indication shows the target altitude.



Task

You will fly an approach to Düsseldorf airport, as illustrated by the following sketch. The atmosphere is calm with light turbulences. Fly all maneuvers in a manner appropriate for the simulated airplane type.

Participant number:

Initial position
2500 ft
230°

3 NM

4 NM

30°

05L

05R

NOT TO SCALE!

Note that you will start relatively far away from the airport and then fly a rather wide circuit. The approach is to be flown according to given announcements that have been prerecorded and that will be played on positions 1 through 6:

- 1) „Descend 1500 ft!“
- 2) „Turn left heading 140!“
- 3) „Turn left heading 080! Descend 1200 ft!“
- 4) „Turn left, runway heading 053! Cleared visual approach runway 05L!“
- 5) „Start descent!“
- 6) „Swing over runway 05R! Cleared to land runway 05R!“

Each announcement initiates the respective maneuver. Target altitude and heading will also be shown in the HUD. Between position 4 and position 5, only lateral guidance is to be performed visually. **Maintain altitude**, as indicated in the HUD! Only at point 5, an announcement initiates your descent to the runway. At the same time, the ball (which is **not** a target here) appears and falls several times through the HUD. Aim for a landing on runway 05L until reaching position 6, where a swing over is commanded. The ball appears again, flashing several times inside the flight path symbol.

The simulation is stopped several meters above ground. You should nevertheless start the flare at your own discretion. In this case, the flare should result in level flight slightly above ground level.

Participant number:

After the 1st run

How much attention did you pay to the head-up display?

very little a lot none

<p style="text-align: center;">Mental Demand</p> <p>How mentally demanding was the task? (e.g., thinking, deciding, calculating, remembering, looking, searching, etc.)</p> <p style="display: flex; justify-content: space-between;">Very LowVery High</p>	<p style="text-align: center;">Performance</p> <p>How successful were you in accomplishing what you were asked to do? How satisfied were you with your performance?</p> <p style="display: flex; justify-content: space-between;">PerfectFailure</p>
<p style="text-align: center;">Physical Demand</p> <p>How physically demanding was the task? (e.g., pushing, pulling, turning, controlling, activating, etc.)</p> <p style="display: flex; justify-content: space-between;">Very LowVery High</p>	<p style="text-align: center;">Effort</p> <p>How hard did you have to work (mentally and physically) to accomplish your level of performance?</p> <p style="display: flex; justify-content: space-between;">Very LowVery High</p>
<p style="text-align: center;">Temporal Demand</p> <p>How hurried or rushed was the pace of the task? How much time pressure did you feel?</p> <p style="display: flex; justify-content: space-between;">Very LowVery High</p>	<p style="text-align: center;">Frustration</p> <p>How insecure, discouraged, irritated, stressed and annoyed versus secure, gratified, content, relaxed and complacent did you feel?</p> <p style="display: flex; justify-content: space-between;">Very LowVery High</p>

Please rate the following functions:

Altitude Hold

very annoying very helpful Function was not observed or was not active

Wings Leveler

very annoying very helpful Function was not observed or was not active

Standard Rate Turn Hold

very annoying very helpful Function was not observed or was not active

Protections (pitch angle, climb angle, bank angle)

very annoying very helpful Function was not observed or was not active

Participant number:

After the 2nd run

How much attention did you pay to the head-up display?

very little a lot none

Which configuration do you prefer?

- The configuration of the 1st run
- The configuration of the 2nd run

<p style="text-align: center;">Mental Demand</p> <p>How mentally demanding was the task? (e.g., thinking, deciding, calculating, remembering, looking, searching, etc.)</p> <p style="text-align: center;">Very Low Very High</p>	<p style="text-align: center;">Performance</p> <p>How successful were you in accomplishing what you were asked to do? How satisfied were you with your performance?</p> <p style="text-align: center;">Perfect Failure</p>
<p style="text-align: center;">Physical Demand</p> <p>How physically demanding was the task? (e.g., pushing, pulling, turning, controlling, activating, etc.)</p> <p style="text-align: center;">Very Low Very High</p>	<p style="text-align: center;">Effort</p> <p>How hard did you have to work (mentally and physically) to accomplish your level of performance?</p> <p style="text-align: center;">Very Low Very High</p>
<p style="text-align: center;">Temporal Demand</p> <p>How hurried or rushed was the pace of the task? How much time pressure did you feel?</p> <p style="text-align: center;">Very Low Very High</p>	<p style="text-align: center;">Frustration</p> <p>How insecure, discouraged, irritated, stressed and annoyed versus secure, gratified, content, relaxed and complacent did you feel?</p> <p style="text-align: center;">Very Low Very High</p>

Please rate the following functions:

Altitude Hold

very annoying very helpful Function was not observed or was not active

Wings Leveler

very annoying very helpful Function was not observed or was not active

Standard Rate Turn Hold

very annoying very helpful Function was not observed or was not active

Protections (pitch angle, climb angle, bank angle)

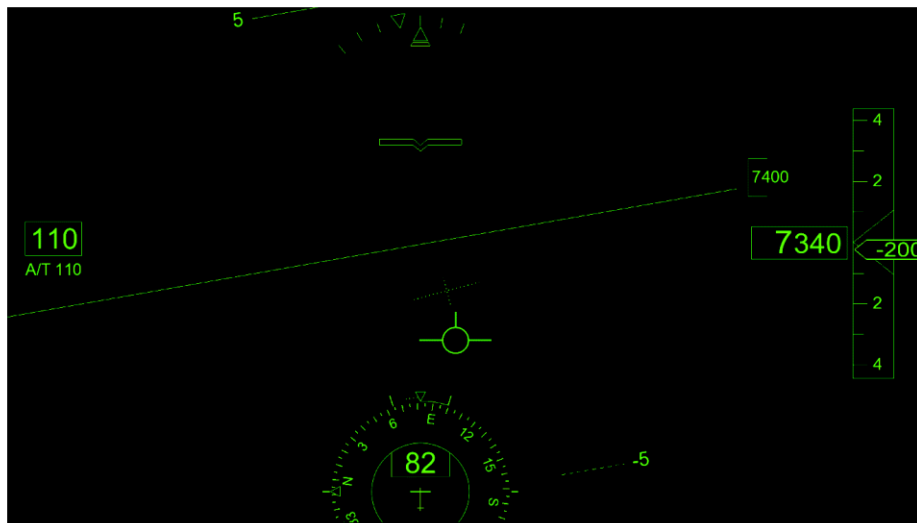
very annoying very helpful Function was not observed or was not active

Participant number:

Experiment Handbook – Part D

Dynamics / Displays

Airplane and flight controller are the same as in the previous part. The HUD is complemented by two predictors. They indicate flight path climb angle, bank angle and turn rate without delay. The dotted cross can be understood as predicted position (flight path climb angle) and attitude (bank angle) of the airplane symbol. The dotted arc around the compass rose corresponds to the predicted turn rate.



Task

The task is the same as in the previous part.

Participant number:

After the 1st run

How much attention did you pay to the head-up display with predictor?

very little a lot none

<p style="text-align: center;">Mental Demand</p> <p>How mentally demanding was the task? (e.g., thinking, deciding, calculating, remembering, looking, searching, etc.)</p> <p style="display: flex; justify-content: space-between;">Very LowVery High</p>	<p style="text-align: center;">Performance</p> <p>How successful were you in accomplishing what you were asked to do? How satisfied were you with your performance?</p> <p style="display: flex; justify-content: space-between;">PerfectFailure</p>
<p style="text-align: center;">Physical Demand</p> <p>How physically demanding was the task? (e.g., pushing, pulling, turning, controlling, activating, etc.)</p> <p style="display: flex; justify-content: space-between;">Very LowVery High</p>	<p style="text-align: center;">Effort</p> <p>How hard did you have to work (mentally and physically) to accomplish your level of performance?</p> <p style="display: flex; justify-content: space-between;">Very LowVery High</p>
<p style="text-align: center;">Temporal Demand</p> <p>How hurried or rushed was the pace of the task? How much time pressure did you feel?</p> <p style="display: flex; justify-content: space-between;">Very LowVery High</p>	<p style="text-align: center;">Frustration</p> <p>How insecure, discouraged, irritated, stressed and annoyed versus secure, gratified, content, relaxed and complacent did you feel?</p> <p style="display: flex; justify-content: space-between;">Very LowVery High</p>

Please rate the following functions:

Predictors

very annoying very helpful Function was not observed or was not active

Altitude Hold

very annoying very helpful Function was not observed or was not active

Wings Leveler

very annoying very helpful Function was not observed or was not active

Standard Rate Turn Hold

very annoying very helpful Function was not observed or was not active

Protections (pitch angle, climb angle, bank angle)

very annoying very helpful Function was not observed or was not active

Participant number:

After the 2nd run

How much attention did you pay to the head-up display with predictor?

very little a lot none

Which configuration do you prefer?

- The configuration of the 1st run
- The configuration of the 2nd run

<p style="text-align: center;">Mental Demand</p> <p>How mentally demanding was the task? (e.g., thinking, deciding, calculating, remembering, looking, searching, etc.)</p> <p style="display: flex; justify-content: space-between;">Very LowVery High</p>	<p style="text-align: center;">Performance</p> <p>How successful were you in accomplishing what you were asked to do? How satisfied were you with your performance?</p> <p style="display: flex; justify-content: space-between;">PerfectFailure</p>
<p style="text-align: center;">Physical Demand</p> <p>How physically demanding was the task? (e.g., pushing, pulling, turning, controlling, activating, etc.)</p> <p style="display: flex; justify-content: space-between;">Very LowVery High</p>	<p style="text-align: center;">Effort</p> <p>How hard did you have to work (mentally and physically) to accomplish your level of performance?</p> <p style="display: flex; justify-content: space-between;">Very LowVery High</p>
<p style="text-align: center;">Temporal Demand</p> <p>How hurried or rushed was the pace of the task? How much time pressure did you feel?</p> <p style="display: flex; justify-content: space-between;">Very LowVery High</p>	<p style="text-align: center;">Frustration</p> <p>How insecure, discouraged, irritated, stressed and annoyed versus secure, gratified, content, relaxed and complacent did you feel?</p> <p style="display: flex; justify-content: space-between;">Very LowVery High</p>

Please also fill out the next page >>>

Participant number:							
Physical Demand	<input type="checkbox"/>	<input type="checkbox"/>	Temporal Demand	Temporal Demand	<input type="checkbox"/>	<input type="checkbox"/>	Frustration
Effort	<input type="checkbox"/>	<input type="checkbox"/>	Mental Demand	Performance	<input type="checkbox"/>	<input type="checkbox"/>	Effort
Frustration	<input type="checkbox"/>	<input type="checkbox"/>	Physical Demand	Effort	<input type="checkbox"/>	<input type="checkbox"/>	Temporal Demand
Effort	<input type="checkbox"/>	<input type="checkbox"/>	Frustration	Frustration	<input type="checkbox"/>	<input type="checkbox"/>	Performance
Mental Demand	<input type="checkbox"/>	<input type="checkbox"/>	Temporal Demand	Performance	<input type="checkbox"/>	<input type="checkbox"/>	Physical Demand
Physical Demand	<input type="checkbox"/>	<input type="checkbox"/>	Effort	Mental Demand	<input type="checkbox"/>	<input type="checkbox"/>	Performance
Temporal Demand	<input type="checkbox"/>	<input type="checkbox"/>	Performance	Mental Demand	<input type="checkbox"/>	<input type="checkbox"/>	Physical Demand
Frustration	<input type="checkbox"/>	<input type="checkbox"/>	Mental Demand				

Please rate the following functions:

Predictors

	very annoying	<input type="checkbox"/>	<input type="checkbox"/>	<input type="checkbox"/>	<input type="checkbox"/>	<input type="checkbox"/>	very helpful		<input type="checkbox"/>
Altitude Hold								Function was not observed or was not active	
	very annoying	<input type="checkbox"/>	<input type="checkbox"/>	<input type="checkbox"/>	<input type="checkbox"/>	<input type="checkbox"/>	very helpful		<input type="checkbox"/>
Wings Leveler								Function was not observed or was not active	
	very annoying	<input type="checkbox"/>	<input type="checkbox"/>	<input type="checkbox"/>	<input type="checkbox"/>	<input type="checkbox"/>	very helpful		<input type="checkbox"/>
Standard Rate Turn Hold								Function was not observed or was not active	
	very annoying	<input type="checkbox"/>	<input type="checkbox"/>	<input type="checkbox"/>	<input type="checkbox"/>	<input type="checkbox"/>	very helpful		<input type="checkbox"/>
Protections (pitch angle, climb angle, bank angle)								Function was not observed or was not active	
	very annoying	<input type="checkbox"/>	<input type="checkbox"/>	<input type="checkbox"/>	<input type="checkbox"/>	<input type="checkbox"/>	very helpful		<input type="checkbox"/>

- 25 -

Participant number:

Concluding Questions

Which of the two types of control systems, on-off or continuous, do you generally prefer?

- Continuous control system
- On-off control system

In which situations do you think a continuous control system is more helpful or better suited than an on-off control system?

In which situations do you think an on-off control system is more helpful or better suited than a continuous control system?

Do you have any further remarks or suggestions for improvements?

Thank you very much for your participation!

- 26 -